Linear to Nonlinear Rheology of Bread Dough and its Constituents

By

Trevor Shen Kuan Ng

B.A., Engineering, University of Cambridge (2001)
M.Eng., Engineering, University of Cambridge (2001)
S.M., Mechanical Engineering, MIT (2006)

Submitted to the Department of Mechanical Engineering
in Partial Fulfillment of the Requirements for the Degree of
Doctor of Philosophy in Mechanical Engineering
at the

Massachusetts Institute of Technology
[September 2007]
Aug 2007

Signature of Author.....
Department of Mechanical Engineering
August 16th, 2007

Certified by.....
Gareth H. McKinley
Professor of Mechanical Engineering
Thesis Supervisor

Accepted by.....
Lallit Anand
Chairman, Department Committee on Graduate Students

Linear to Nonlinear Rheology of Bread Dough and its Constituents

by

Trevor S. K. Ng

Submitted to the Department of Mechanical Engineering

in Partial Fulfillment of the Requirements for the Degree of

Doctor of Philosophy in Mechanical Engineering

Summary

There are many practical reasons for studying the deformational behavior or rheological properties of a dough system. The mass production of bread has led to a need of machines that are able to handle and process large volumes of dough. An understanding of the deformational properties can aid in designing machines of this kind. Less obviously, the texture of the bread we eat is governed by the mechanical properties of the dough from which it is proofed and baked from. During the bread making process, large non-linear deformations feature prominently. In mixing and kneading, dough is stretched and sheared by hand or by specially designed mixing devices, while in proofing and baking, the expansion of gas cells causes significant extensional strain on the surrounding dough. Other than directly affecting the moduli of the fibers and membranes in the solid phase of bread, a link between the rheology of dough and the baked loaf volume has also been established.

In this thesis, we first develop consistent and accurate techniques for measuring the rheological properties of the dough. Good experimental techniques and protocols are essential for studying the mechanical properties of such a sticky, visco-elasto-plastic, time-dependent material. We modify some of the standard rheometric hardware and protocols to accommodate this unusual material. Special attention is given to nonlinear deformations such as uniaxial extensional flows and large amplitude oscillatory shear flows (LAOS).

We use the new techniques to probe the microstructure of dough and its constituents from a mechanical viewpoint. The strongly nonlinear rheological properties of dough arise from the interactions of a protein matrix and a high filler concentration consisting of hydrated starch particles. We demonstrate that the gluten protein that imbues the dough with its characteristic viscoelasticity should be considered as a *transient network* that is interconnected by finitely extensible biopolymer segments (~20nm mesh size) and held together by hydrogen bonds and/or hydrophilic interactions.

Using this renewed understanding of the microstructure, we construct appropriately frame-invariant constitutive equations (*generalized gel equation* and a multi-mode *FENE network model*) that describe the rheology of gluten gels with a minimal number of parameters. The behavior of gluten gels can then be related

to prototypical flour-water doughs by the effects of the starch filler using the concept of *strain amplification*.

Finally, this general framework of microstructure and rheological properties of gluten gels and flour-water dough are applied to practical situations. We discuss the utility of this work in context to some specific case studies of rheological aging, the effects of water content and flour-type variations.

Thesis supervisor: Gareth H. McKinley
Professor
Mechanical Engineering

Acknowledgements

I will like to give my sincerest thanks to my thesis advisor Professor Gareth H. McKinley for his support, for guiding this student from course 16 with little experience in non-Newtonian fluid mechanics. His enthusiasm and extensive knowledge in rheology and many other areas of science has greatly aided my own development. My committee members, Prof Boyce and Prof. Hosoi have been incredibly helpful, they provided a refreshing perspective to the whole project with insightful suggestions. Also special thanks must go to my family, especially my parents for instilling a love of science and engineering, and for providing such perfect role models. I will like to thank Dr. Mahesh Padmanabhan and Dr. Yong Woo Inn of Kraft Foods for the many interesting discussions and financial support. Finally, I will also like to express my gratitude to my colleagues at the Non-Newtonian Fluids group for their friendship over the last few years. Especially Randy Ewoldt who developed the framework and software for LAOS analysis without which a large part of this thesis would not be possible; Dr. Christopher Pipe and Giorgia Bettin who have made my graduate school experience extremely enjoyable.

1. Introduction

The wheat grown worldwide these days originally descended from a wild eikorn grass in the Karacadag Mountains of South Eastern Turkey. During the period of agricultural revolution, humans replanted the seeds and began the long symbiotic relationship with the plant. The prehistoric man mixed the ground up grains of wheat with water to form a dough, and possibly cooked it under the sun or on a fire to form bread. Since then, the global production of wheat (626 million metric tones in 2005) and consumption of bread (60 loaves per North American in 2007) has increased rapidly. The industry has also recovered healthily from the fashion of low-carb diets and gluten allergies.

As a result of this huge demand, a large amount of research has been conducted on the subject of breadmaking. The focus of these works ranges from agricultural techniques to processing and baking. This science of food production and preparation has also entered the public's imagination over the last decade through the term molecular gastronomy. The term was coined by the Hungarian physicist Nicholas Kurti and French chemist Hervé This. It is loosely defined as the application of scientific principles to understand and improve the art of preparing food. In this thesis, we will concentrate on one particular aspect of the multi-disciplinary subject of food preparation and discuss an intermediate step in the process of bread making, namely the mechanical properties or rheology of dough.

Dough is the name given to the state in which the flour has been mixed with water but before the application of heat has gelatinized the starch. There are many practical reasons for studying the rheological properties of a dough system. First of all, the mass production of bread has led to a need of machines that are able to handle and process large volumes of dough. An understanding of the deformational properties can hugely aid in designing devices of this kind.

Perhaps less obviously, the texture of the bread that we eat is governed by the mechanical properties of the dough from which it is proofed and baked from. During the bread making process, large non-linear deformation feature prominently. In mixing and kneading, dough is stretched and sheared by hand

or by specially designed mixing machines, while in proofing and baking, the expansion of gas cells cause significant extensional strain on the surrounding dough. Other than directly affecting the moduli or "chewiness" of the fibers and membranes in the solid phase of the finished product [1], the composition and rheology of the dough can also affect the "airiness" or loaf volume of the bread [2-5]. So it has long been the objective of food scientist to characterize the rheological behavior of dough and relate it to particular baking qualities.

Bloksma [6] outlined two rheological requirements for producing high quality loaves: "1) the dough must have sufficiently large viscosity to prevent the ascent of gas cells, and 2) it must remain extensible for a long enough time during baking to avoid premature rupture of membranes between gas cells." The performance of a dough with respect to these requirements are known as its *functionality*. There are a number of studies that formally connect (through mathematical modeling) or make plausible (through experiments) the link between functionality and baking qualities [7-9].

The unique ability of wheat flour doughs to satisfy these requirements arise from the complex multi-scale structures comprising the dough. To the naked eye, ($O > 10^{-3} m$), the dough appear to be a continuum. But upon closer inspection under the microscope ($O < 10^{-3} m$), voids or gas cells become visible. While at even higher magnification ($O \sim 10^{-4} m$), one begin to distinguish the individual starch granules and an aqueous protein phase which binds them together. With the help of atomic force microscopy or environmental SEM, the structure of the protein phase can be seen ($O < 10^{-5} m$).

The resulting rheological behavior of such a multi-scale system is extremely complex and non-linear. Existing techniques of measurements might not be able to capture the important features relevant to breadmaking.

The objective of this thesis can be summarized in the following points:

1. *Develop consistent and accurate techniques for measuring the rheological properties of the dough.* Since the beginning of the subject, rheologists have agreed that good experimental techniques and protocols are essential for

studying the mechanical properties of such a complex material. The sticky, viscous nature of the materials in question makes forming samples suitable for testing on a conventional rheometer extremely difficult. To this end, we will modify some of the standard hardware to accommodate this unusual material. Dough and its constituents also typically exhibit thixotropy, aging and other time and history dependent effects. Thus it is critical to maintain a rigid set of protocols in order to create a standardized base point.

2. *Develop a methodology for distinguishing dough of different functional qualities.* Once we have identified the methods and protocols, a theoretical and mathematical framework is needed to interpret the results collected. We will next ask the questions: What are the material functions that best illustrate the functionality of a dough? Which are the parameters that mathematically characterize these functions? We will show how by using the appropriate material functions we can clearly demonstrate trends and differentiate dough of different "functionality".

3. *Understand the underlying micro-structure of the dough which gives it the unique rheological properties.* We explore the origin of these mechanical properties and investigate the properties of gluten. We will demonstrate a suitable molecular model and show how the implication of this model can lead us to an accurate description of the mechanical properties of the gluten gel. We then show how the gluten gel is the basis of the mechanical properties of the complete dough by considering the starch granules as filler particles.

1.1. Outline of the thesis

In spite of its universality, the rheology of breadmaking does not enjoy the reputation of being a very scientific subject and, generally speaking, the problems are attacked on a case-by-case basis. From a theoretical standpoint, the entire problem appears to be complex and unwieldy, and there is no idealized starting picture for analysis; from an applied viewpoint, it is easy to get lost in

the complexities of particular cases without ever seeing the structure of the entire subject.

Thus in this thesis, we will first identify a suitable starting point, in terms of previous work (Chapter 2), experimental technique (Chapter 3) and general dough behavior in both linear and nonlinear deformations (Chapter 4). The reader will gain a feel of the difficulties and general behavior of dough through these chapters.

The discussion then shifts gear and focuses on the origins of the mechanical behavior in dough. In chapter 5, we discuss in detail the general rheological behavior of the gluten gel which is believed to be primarily responsible for the viscoelastic nature of a dough The rheological evidence will point us towards a consistent microstructural model of the gluten gel. This idealized picture will in turn lead us to a more sophisticated constitutive model that is able to describe the linear to nonlinear rheology of the gluten gel (Chapter 6). Finally, we show, how the properties of gluten are reflected in a real dough when the primary effects of starch granule filler material are included (Chapter 7).

In the conclusion (Chapter 8), we take this general framework of microstructure and rheological properties of gluten gels and dough, and apply it to practical situations in which we outline how this work can explain and predict many of the specific observations discussed in the Chapter 2 and 4.

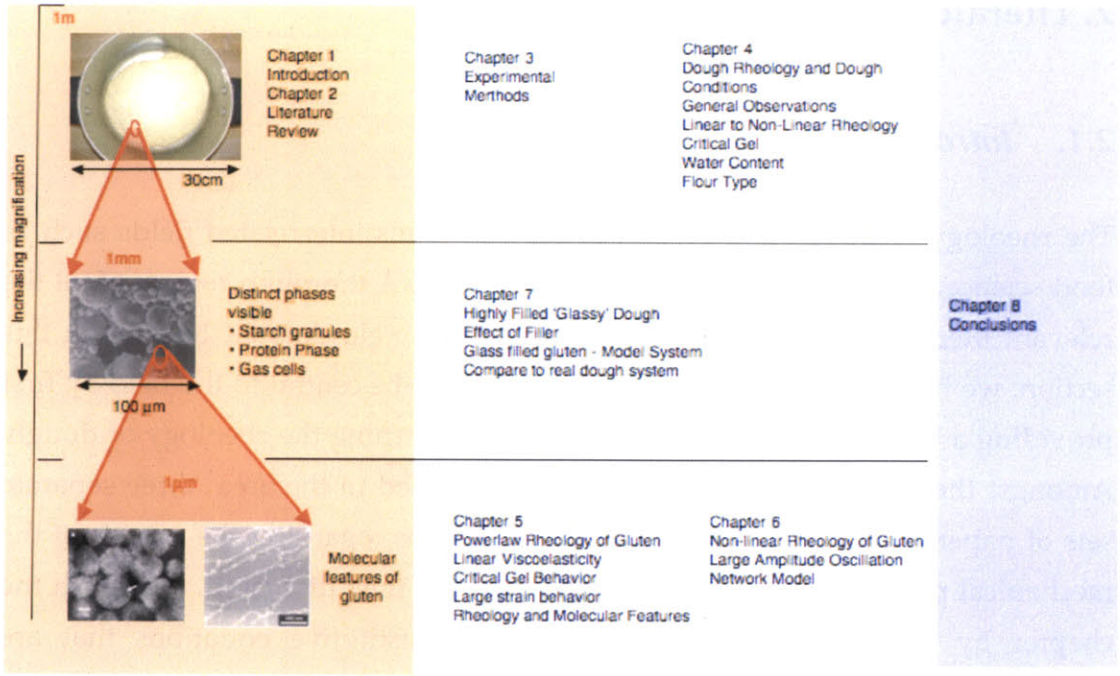

Figure 1 Outline of thesis

2. Literature review

2.1. Introduction

The rheology of dough is a broad subject that spans interrelated fields such as food science, chemistry and continuum mechanics. A thorough review of all the relevant literature will be beyond the scope of a single chapter. Instead, in this section, we highlight some ideas that we believe to be central to the field by first providing a brief overview of the early work concerning the rheology of dough. Amongst the copious amount of research performed in the area, three separate sets of papers stand out in particular. Current ideas regarding the origins of the mechanical properties and molecular structure are then discussed. We finish the chapter by a survey of common or useful constitutive equations that are commonly associated to dough systems. More detailed literature review on individual subjects will be presented at the beginning of the subsequent chapters.

2.2. Early Work 1932-1970

Today, when a rheologist desires to demonstrate "*the relationship between viscosity, elasticity and plastic strength of a soft material*", he or she will probably choose a well studied polymer solution or melt, perhaps a high molecular weight linear polystyrene for which the structure and properties have been thoroughly characterized. Such model systems were not available to the early rheologists and instead, a pair of researchers in the 1930s provided a beautiful illustrations of their thoughts on the "*... plastic strength of a soft material*" by discussing the mechanical properties of flour dough through a series of four papers in the Proceedings of the Royal Society of London [10-13]. To our best knowledge, this is the first systematic study on the rheology of dough; Schofield and Scott-Blair certainly made some prescient remarks that remain central to work in this field. First of all, they understood that dough is an extremely non-linear material. They began by extending the concept of a simple Maxwell fluid by considering a situation in which the relaxation time is not a constant but instead varies

according to stress [10]. This led to the construction of a constitutive equation [11, 12] in the form:

$$\tau + \lambda(\tau)\frac{d\tau}{dt} = \eta(\gamma,\tau)\frac{d\gamma}{dt} \tag{2.1}$$

Equation (2.1) is non-linear in both stress and strain: using it to make predictions on the rheological behavior of dough is difficult, especially in the 1930s when personal computers and Matlab were not readily available. However, we will point out in a later chapter that for a specific choice of viscosity η and relaxation λ functions, equation (2.1) can in fact be related to the critical gel equation, which is a surprisingly accurate description to many aspects of dough rheology.

Secondly, Schofield and Scott-Blair recognized the network nature of the gluten that imparts the distinct viscoelasticity to the dough: "In relating these deductions to the known structure of the dough one may safely identify the elastic elements with the protein part of the flour. That the elements form a connected structure is confirmed by the fact that the starch and other constituents of the flour can be washed out of the dough without breaking up the gluten." They also understood the transient nature of this network: "it is evident that the elements, though connected, are not joined securely, but slide past one another whenever a sufficient stress is operative." The chemical nature of the network was also probed by applying hydrocholoric acid and thus destroying the strength of the gluten. They suggested electrostatic attraction between oppositely charged groups in the neighboring molecules is an important factor in the strength of the network.

Their work must also be admired for the range of ingenious devices used in teasing out the material functions of dough. One must remember that at that time, not only did the researchers not have access to synthetic polymers or computers, rheometers as we know them today have not come into existence yet. Instead Schofield and Scott-Blair relied on a variety of machines, two notable examples are depicted in Figure 2 and Figure 3

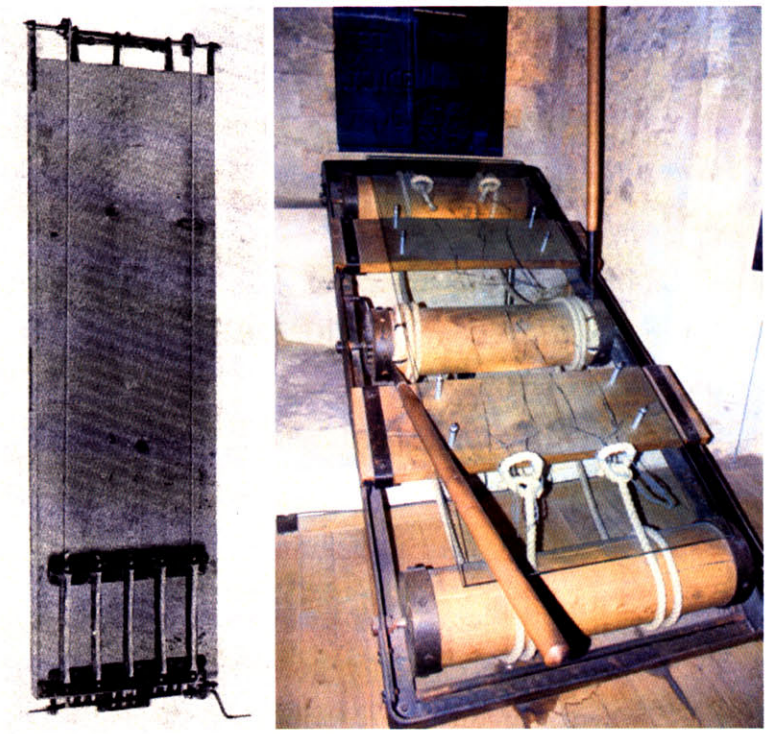

a. b.

Figure 2. a. The rack devised by Schofield and Scott-Blair. Controlled extension and recoil experiments were measured on this set-up. b. A torture rack photographed from the Tower of London, England, image by D. Bjorgen - http://en.wikipedia.org/wiki/Image:A_Torture_Rack.jpg

An instrument which they referred to as "the rack" is shown on Figure 2a. The name was given for its superficial resemblance to an ancient instrument of torture[1]. Multiple samples are attached to the rack with one end fixed by pressing it round a screw while the other end is attached to a thin strand of rubber by the extension of which the stress on the dough can be observed. The other end of the rubber strand is secured to a thread which could be wound up on a small winch.

---

[1] Incidentally, the author of this thesis finds rheology to be not unlike torture. In controlled stress torture/rheology, information is extracted from the victim/sample by application of strain, in such a way that they are under a state of stress; and vice versa for the controlled strain case.

Material functions in creep and stress relaxation in extension can be measured with this equipment.

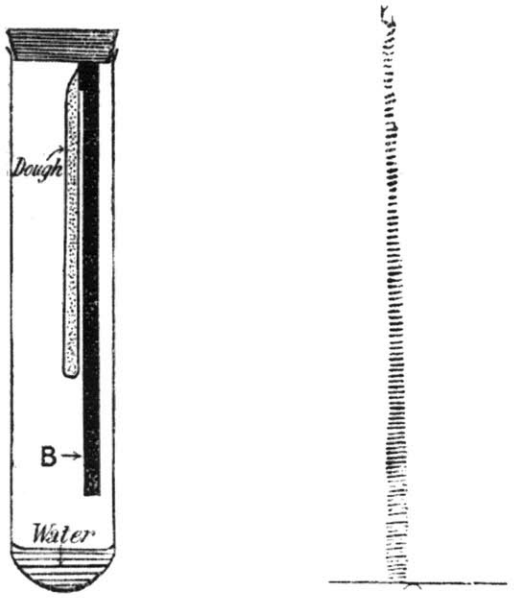

Figure 3 a. Rheogram experiment. An extruded cylinder of dough is marked with ink at 1mm intervals and is hung from the top of a sealed tube. The force of gravity acting on the dough itself elongates the sample. After a measured amount of time, the ink marks can be printed off to a sheet of paper and is referred to as a rheogram. The prints can be made while the sample is hanging vertically in the tube so as to measure instantaneous deformation, or while lying horizontally so as to measure the deformation in the recoiled state.

A slightly more sophisticated method is the rheogram illustrated in Figure 3. An extruded cylinder of dough is marked with ink at 1mm intervals and is hung from the top of a sealed tube. The force of gravity acting on the dough itself elongates the sample. After a measured amount of time, the ink marks can be printed off to a sheet of paper and is referred to as a rheogram. The prints can be made while the sample is hanging vertically in the tube so as to measure instantaneous deformation, or while lying vertically so as to measure the deformation in the recoiled state.

The rheogram can be analyzed by considering the force balance along different sections of the dough. The sample is assumed to be incompressible. Through this analysis, mean stress, viscosity, strain and strain rate can be calculated with the following expressions:

$$\begin{aligned} \sigma_{shear} &= \frac{1}{6} g \rho L_0 \left(1 + l/l_0\right) \\ \varepsilon_{mean} &= \ln\left(l/l_0\right) \\ \dot{\varepsilon}_{mean} &= \varepsilon/t \\ \eta_{mean} &= \sigma/\dot{\varepsilon} \end{aligned} \tag{2.2}$$

Crude, these experiments might be, they are nevertheless an excellent demonstration of the non-linear dependence of relaxation time and viscosity to strain and stress. Though limited in terms of quantitative predictions, Schofield and Scott-Blair showed an uncanny understanding of the physical and chemical nature of dough. Their work was extremely rich in ideas (strain-stiffening, Mullins effect, aging and the influence of filler material [13]) and is an excellent qualitative framework for subsequent generations of dough rheologist.

Hibberd et al also wrote a series of papers that had an important impact on the field [14-17]. In the first of the series, they discussed the linear aspects of dough rheology, concentrating on the dynamic moduli (see chapter 3). They recognized the small linear range of dough and quoted a value of $\gamma^* = 4.4 \times 10^{-3}$ as the critical strain, beyond which an anomalous softening became evident. They noted that this softening effect could be partially reversed by allowing the dough to rest. This effect was quantitatively demonstrated by performing a time sweep dynamic test. The amplitude of the test was alternated between values below ($\gamma_0 = 2.6 \times 10^{-3}$) and above ($\gamma_0 = 6.9 \times 10^{-2}$) the linear range. The results of this experiment are plotted in Figure 4. After the application of a large amplitude, the sample shows immediate softening that continued at a slower rate until the amplitude is returned to below the linear range. An immediate partial recovery was observed which was still incomplete after a further 60 minutes.

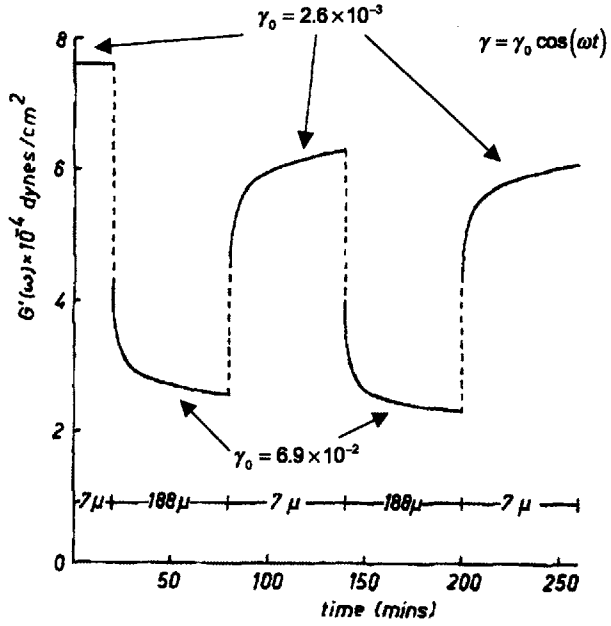

Figure 4 Dynamic time sweep to demonstrate aging and reformation of structure for a flour water dough [17]. Amplitudes that are below ($\gamma_0 = 2.6\times10^{-3}$) and above ($\gamma_0 = 6.9\times10^{-2}$) the linear range were applied alternately. After the application of a large amplitude, the sample shows immediate softening that continued at a slower rate until the amplitude was returned to below the linear range. An immediate partial recovery was observed which was still incomplete after a further 60 minutes.

This phenomenon was explained by considering the chain segments formed by the interaction of the protein filaments that connect adjacent starch molecules. Under deformation, the starch particles are likely to move apart, stretching out the protein chains. The chains are assumed to have a distribution of lengths such that some will be more stretched than others, with the shorter change breaking off at smaller strains. As the strain amplitude is increased, progressively longer chains are broken, thus causing a decreasing in modulus. The time dependence of this softening is interpreted as a gradual diffusion of the chains to a new equilibrium position that provides a more equitable distribution of the loads. This is also consistent with the gradual but incomplete recovery observed.

Having defined the linear region, the discussion in the second paper turns to the effect of water content in the said regime. Hibberd et al observed the lost tangent

of dough to be independent of the water content, and therefore suggested a simple superposition principle which is illustrated in Figure 5: a vertical shift factor is used to collapse small amplitude dynamic moduli onto a single master curve:

$$G^*(\omega,W)=G_0^*(\omega)\times Q(W-W_0) \tag{2.3}$$

Where W_0 is a reference water content, $G_0^*(\omega)$ is the complex modulus measured at W_0 and $Q(W-W_0)$ is the required function for shifting complex moduli from different water content onto the reference curve of $G_0^*(\omega)$.

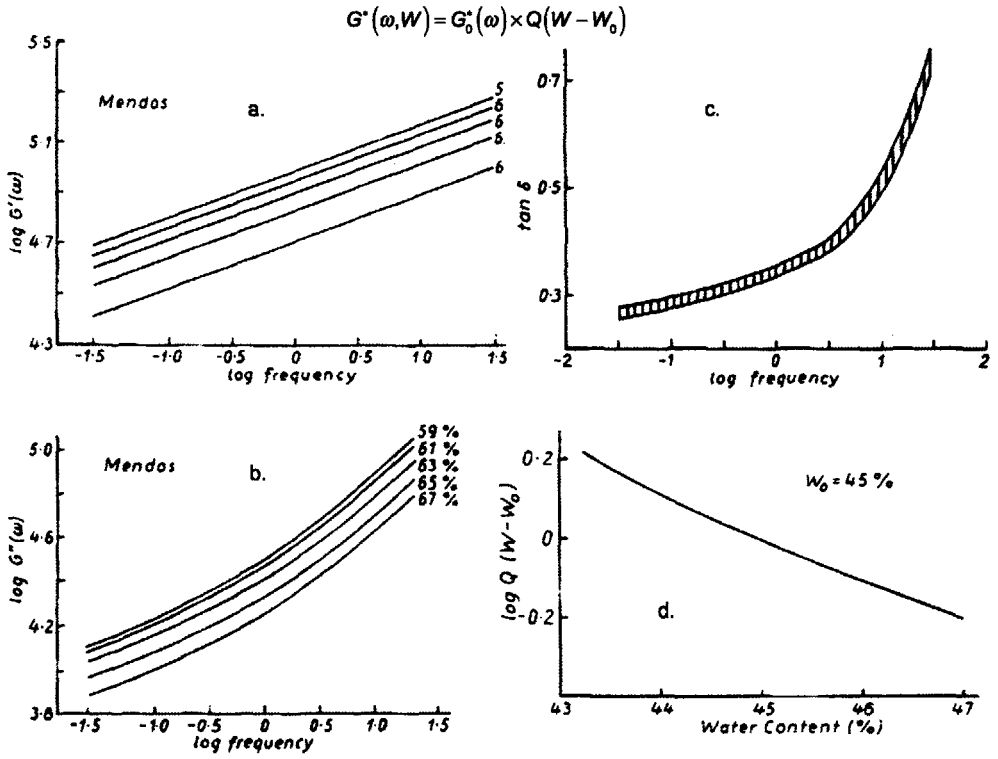

Figure 5 An example of using the principle of corresponding water contents. a.,b. Dynamic moduli of dough at different water content. c. The loss tangent varies with frequency, but is independent of water content. d. Proposed shift factor to reduce dynamic moduli to a reference curve.

The shape of the reference curve is still dependent on flour variety. However, Hibberd went on to suggest that it might be possible to factor out an additional

varietal dependence, i.e. $G_0^*(w, \text{Variety}) = G_{0,V}^*(w) \times C(\text{Variety})$: doughs prepared from different wheat flour varieties (V_a and V_b) can yield identical linear viscoelastic behavior if appropriate corresponding water contents (W_a and W_b) are used, or in terms of equation (2.3):

$$G^*(V_a, \omega, W_a) = G^*(V_b, \omega, W_b)$$
$$\text{if} \tag{2.4}$$
$$C(V_a)Q(W_a - W_0) = C(V_b)Q(W_b - W_0)$$

In view of the complexity of a dough system, the applicability of such a simple superposition principle is surprising. Hibberd suggested that within the linear region, experiments can only probe the short range interactions and it is reasonable to regard the degree of difference to be rather small for different flour varieties. A brief search on available databases shows that no further work has been performed to conclusively validate or disprove this result; and most researchers will certainly agree, that small amplitude shear deformations are not sufficient to distinguish between doughs [18].

Hibberd attributed the existence of these simple superposition functions to the similarity of protein-to-starch (*P/S*) ratios in typical wheat flours. To test this hypothesis, he performed experiments with a larger parameter space by preparing doughs of vastly different *P/S* ratios. He found that under this greater range of P/S ratio, the moduli cannot be superimposed onto each other; a separate water correspondence function and reference modulus function is required for each *P/S* ratio:

$$G^*(\omega, W, P/S) = G_0^*(\omega, P/S) \times Q(W - W_0, P/S) \tag{2.5}$$

For the purpose of qualitative comparison, an arbitrary frequency ω_0 was chosen as a reference point, so that:

$$\Phi(w, P/S) = \frac{G(w, W, P/S)}{G(w_0, W, P/S)} \tag{2.6}$$

$\Phi(\omega, P/S)$ is a dimensionless function that is independent of water content. The variation of Φ is plotted on Figure 6.

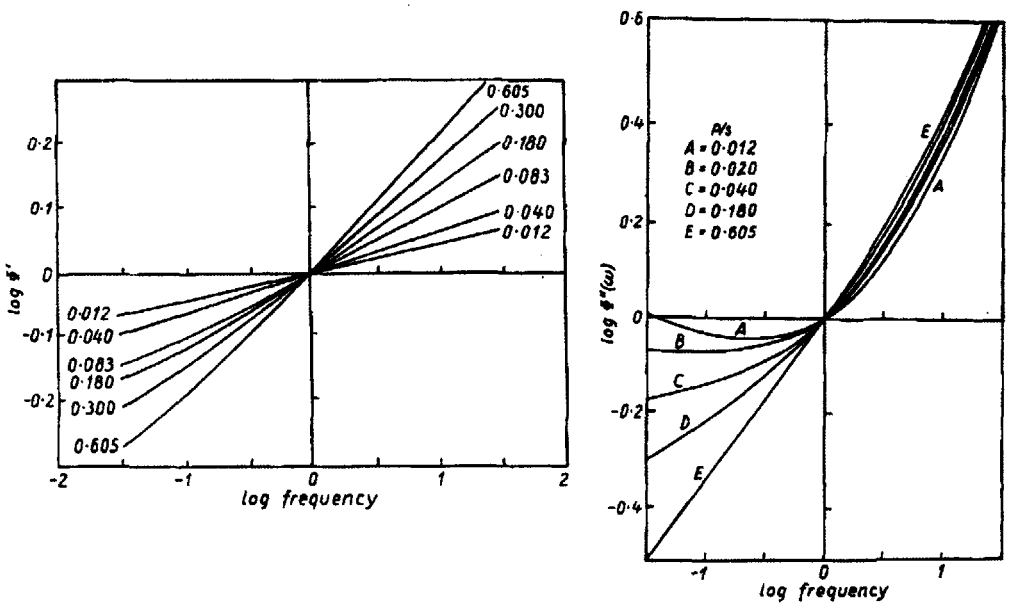

Figure 6 Influence of P/S ratio on the frequency dependent reduced moduli Φ', Φ''.

Φ' behaves as a power-law when plotted against frequency, the power-law index decreases with decreasing *P/S* ratio. Φ'' exhibits more dramatic qualitative differences: a local minimum develops as *P/S* ratio is decreased. Hibberd interpreted this result by comparing it with linear viscoelastic data collected for high molecular weight polymers. He suggested that the protein starch interactions play a role that is equivalent to entanglements in reptation models: the increase in starch concentration decreases the average length of the chain segments, thus shifting features such as the observed minimum to a lower frequency outside the observable range.

Other than these useful superposition principles, one of the most important contributions of Hibberd's work was that he brought to attention the importance of defining the linear viscoelastic domain. In the last paper of the series, he outlines yet another simple principle for the dynamic response of dough under

finite strains of $\gamma(t)=\gamma_0\cos(\omega t)$. He proposed a simple softening function, similar in form to a time-strain separable relaxation modulus:

$$G(\omega,\gamma_0)=G(\omega)\times\Psi(\gamma_0) \tag{2.7}$$

Where the softening function $\Psi(\gamma_0)$ can be thought of to be analogous to the damping function under step strain relaxation. This result is perhaps even more surprising than the superposition principles discussed in the first three papers of the series. Subsequent researchers have shown that the non-linearity of dough under oscillation cannot be easily factorized into a strain and frequency dependent components. We suspect the reason that the factorizability appeared to be valid for the results presented by Hibberd et al is due to the relative small amplitude of their finite strains ($\gamma_0<0.1$), as evident by the near sinusoidal response reported.

To conclude our review of seminal works on dough rheology performed from 1930s to 70s, We would like to direct the reader to a final set of four papers published by Tschoegl et al [19-22]. Force transducer and motor technology has certainly come a long way since Scott Blair's time of racks and rheograms, as a result, rheologist such as Tschoegl and co-workers were able to construct an experiment that reliably measures the extensional properties of wheat flour doughs. Their design is illustrated in Figure 7.

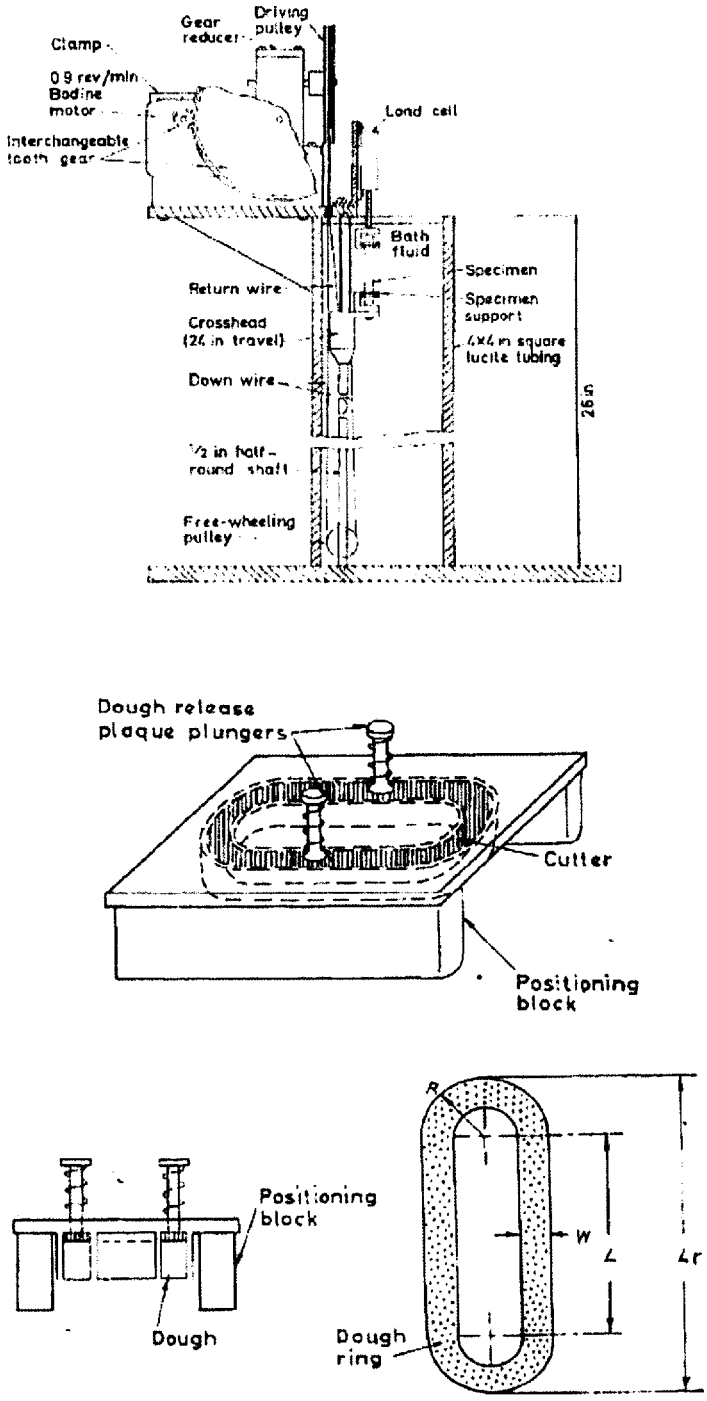

Figure 7 a. Schematic of Tschoegl's apparatus to test dough rings under uniaxial deformation. b. Sample preparation: dough ring mold and cutter.

Tschoegl et al were motivated by the fact that most industrial dough testing were performed on set-ups with outputs that are usually in the form of arbitrary units (Brabender Extensigraph, Chopin Alveographs etc...) and cannot be easily interpreted in terms of stress and strain. Therefore they set out to design an apparatus that maintains a well defined geometry. Their approach was inspired by a similar procedure that is used to measure extensional properties in elastomers. Two ends of a ring shaped sample were attached to supports. The upper support remains stationary and is attached to a load cell, while the lower support is driven by a motor-pulley system to stretch the sample at a nominally constant rate. Tschoegl et al noted that forming consistent samples was absolutely critical to obtaining reproducible results. To this end, they designed a mold and cutting fixture depicted in Figure 7b to create "race-track-ring" shaped samples.

Another interesting feature of their apparatus was the fluid bath. During the experiment, the samples were submerged in a mixture of mineral oil and Freon TF. This mixture was selected to provide a barrier against sample drying of the sample and to maintain a neutrally buoyant environment so that gravitational sagging was eliminated.

By assuming the deformation to be largely confined to the straight sections of the ring, they calculated the stress and strain sustained by the sample:

$$\sigma = \frac{F}{2WT}, \varepsilon = \ln\frac{L}{L_0}$$

F = tensile force

W, T = width and thickness of specimen (2.8)

L = length of specimen

L_0 = initial length of specimen

Though their design was a huge improvement from the typical industrial measurements, the deformation is still far from a uniform uniaxial elongation: the strain in the inside circumference is larger than the outside and the relative slip conditions at the end supports are ill-defined. Nevertheless, they concluded a carefully calculated correction factor can be used to take into account of these

effects. As we shall see in the next chapter, the difficulty in achieving ideal kinematics still remains one of the most intractable problem faced by dough rheologists.

Using this set-up, Tschoegl et al investigated the large deformation and rupture behavior of a variety of doughs under different temperature, mixing time and water absorption levels. Unfortunately, this wealth of information is somewhat obscured by the researchers unnecessarily complicated use of material functions based on engineering stresses and strains.

In the same series of paper, the issue of shear rheology was also investigated [19]. The set-up was essentially similar to the design of Hibberd et al [17] that we have discussed earlier and Tschoegl and co-workers essentially arrived at the same conclusions regarding linearity/non-linearity and thixotropic characteristics. But one observation was particularly interesting. They noted under some circumstances, the dynamic moduli of gluten or flour water doughs exhibit a power-law relationship with frequency. This is probably the first observation of power-law like behavior in these dough systems and in this thesis we will show that it is in fact a surprisingly accurate description of the rheology resulting from their microstructural composition.

Important ideas gained from the early work

This brief survey of representative early literature has provided us with a comprehensive outline of the different aspects of dough rheology. We summarize the significant ideas that the reader should keep in mind:

1. Performing experiments on dough is difficult – often specialized equipment or modifications to existing techniques are required. Extreme care has to be taken to ensure results that are consistent and free from artifacts.
2. Time dependence – dough exhibits both strong thixotropy and aging. A rigorous schedule have to be devised and adhered to for consistent results.

3. Large number of variables – the mechanical properties of dough are strongly affected by water content, mixing conditions etc... Simple scaling and superposition rules are invaluable in reducing the large amount of data.
4. Non-linear – small linear range, strong non-linear behavior.
5. Constitutive modeling – Schofield and Scott Blair were the first to attempt to describe the non-linearity mathematically. Many subsequent attempts have been made to model the mechanical behavior of dough, but yet no single equation can describe the response of dough under the range of typical deformation it experiences.
6. Power-law – Tschoegl et al were the first to report a power-law behavior in material functions under deformations within the linear range. Subsequent workers have also observed this curious behavior. In this thesis we will discuss how this observation can form the basis of a surprisingly accurate constitutive equation.
7. Gluten backbone – Schofield and Scott-Blair made a prescient remark in which they noted the insoluble protein phase or gluten forms a network structure that provides a dough with its distinct viscoelasticity. Following this, many workers have realized that an appreciation of the structure and rheology of this network is critical to understanding the mechanical behavior of the overall system. As a result, there has been a number of studies concerning gluten network isolated from the native dough. The microstructure of this network is still hotly debated, and a significant portion of this thesis will be dedicated towards this discussion.

2.3. *Dough functionality and microstructure*

It has been more than 250 years since Jacopo Bartolomeo Becarri Professor of Chemistry at the University of Bologna showed that wheat flour can be divided into two fractions [23]. By gently massaging a flour-water dough under a thin stream of running water, he showed that the starch can be washed off leaving an elastic network of proteins which he referred to as *glutenis*. Since then, the

microstructure of the dough is an area that is under intense debate. In this thesis, we will concentrate on the two main components of the dough, namely, starch and gluten.

Wheat flour starch mixed with water at concentrations simulating typical dough will form a thick paste that shows extreme shear-thickening behavior. The response is plotted in Figure 8. The viscosity increases abruptly at $\dot{\gamma} \sim 10\ s^{-1}$; the stresses beyond this critical strain rate is so high that measurements are no longer possible on the rheometer. This type of behavior is typical of highly charged colloidal particles that flocculate under large hydrodynamic forces [24, 25]. Another interesting observation on the starch solution is its time-dependent behavior: the viscosity increased by close to an order in magnitude overnight. Starch particles when submerged in water swells over time [26], this swelling leads to an increase in filler volume fraction and the filler stiffness, which in turn affects the viscosity. This time dependency is also present in dough systems and is a major bugbear to rheologists.

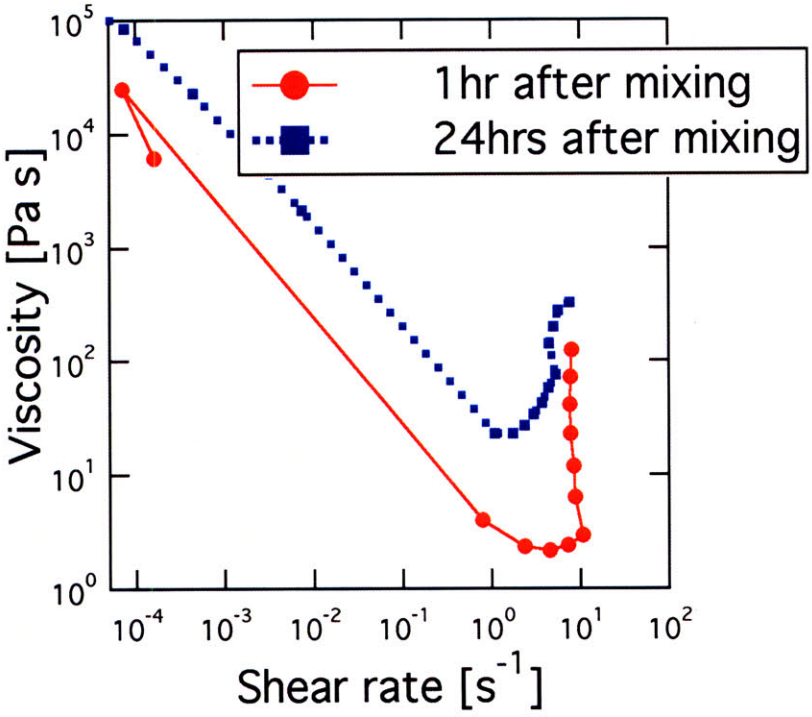

Figure 8 Viscosity of starch paste at 45% water content. Note the dramatic shear-thickening behavior, i.e. increase in viscosity at $\dot{\gamma} \sim 10\ s^{-1}$. The data is also compared to another set collected from the same sample but has been left to sit on the rheometer over night. The viscosity of the over night sample is approximately an order of magnitude greater than the fresh sample over most strain rates.

The mechanical properties of the starch solution is dramatically transformed if a small amount of gluten is mixed in with it, i.e. in a wheat flour dough. The shear-thickening behavior is no longer noticeable while the dough takes on some distinct viscoelastic properties (see chapter 4).

Starch granules has been suggested to act as an inert filler in the continuous protein matrix of the dough [27], while others described the dough as a bi-continuous network of starch granules and protein [28]. There are also suggestions that the rheological behavior can be influenced by the specific

properties of the starch granule surface [29]. Due to its size (typically > 10 μm) and high viscosity of the surrounding matrix ($> 10^3$ Pa s), it is unlikely that the starch forms a colloidal network within the dough [30].

The structure of gluten is even less well understood. Field-flow fractionation shows that gluten are the largest protein molecules in nature and their suitability of wheat flour for breadmaking may depend on the enormous size of these polymers [31]. The notable "springiness" of gluten doughs owes itself to the entropic elasticity common to molecules of this size.

Proteins are commonly classified by their solubility by a system introduced by Osborne [32]. The proteins are extracted sequentially with a series of solvents. This classification does not necessarily divide the proteins according to its bio-chemical properties or physical functionality, however, due to its convenience it is still widely used to separate the constituents into broad functional groups such as gliadin and glutenin. The non-gluten proteins (typically 15 – 20% of total proteins content) play only a minor role in bread-making, they occur mostly in the outer layers of the wheat kernel. While the gluten proteins (80 – 85%), mostly from the endosperm, has significant contribution to the properties relevant to the bread-making process. In view of this functionality, more attention will be paid to the gluten proteins in this article.

Osborne fraction	Solubility behavior	Composition	Biological role	Functional role
Albumin	Water	Non-gluten proteins (mainly monomeric)	Metabolic and structural proteins	Variable/ insignificant
Globulin	Dilute salt solution	Non-gluten proteins (mainly monomeric)	Metabolic and structural proteins	Variable/ insignificant
Gliadin	Aqueous alcohol	Gluten proteins	Prolamin-type seed storage proteins	Dough viscosity/plasticity
Glutenin	Dilute acetic acid	Gluten proteins	Prolamin-type seed storage proteins	Dough elasticity/strength
Residue	Unextractable	Gluten proteins	Prolamin-type seed storage proteins	Variable

Table 1 Different groups of protein, as defined by Osborne (1924)

Gluten can be further sub-divided into glutenin and gliadin, which are present in roughly equal amounts.

Glutenin – a heterogeneous mix of high molecular weight polymers (Mw – 8 x 10^4 to 10^6). They are one of the largest proteins found in nature [31]. Due to its insolubility, the structure of glutenin remains largely unknown until recent years where new techniques such as light, X-ray and electron scattering, NMR, AFM etc... [33-41] were made available. During mixing glutenin forms a continuous network throughout the dough, giving it the distinct elastic property.

Gliadin – a highly polymorphic group of monomeric polymers. (Mw – 3 x 10^4 to 10^6).

Gluten functionality arise largely from glutenin. Gliadin are thought to act as plasticizers on the glutenin network, increasing its viscous (liquid-like) behavior.

The distinctive feature which makes wheat flour dough uniquely suitable for bread-making is its ability to resist rupture of the gas cells during proofing and baking. Air is included into the dough during mixing in tiny pockets (~ 10^{-5} to 10^{-}

^{4} in diameter) dispersed throughout the dough, constituting approximately 10-15% of total dough volume. Leavening agents release gas into these cells further increasing the size. They undergo yet another expansion during baking through heating and release of dissolved alcohol/CO2 previously dissolved in the dough [6, 42]. The dough walls surrounding the gas cells are stretched and becomes thinner. It is believed that a "weak" dough with insufficient elasticity/strain-hardening will form dough walls which will rupture under these conditions. Van Vliet et al [9] provides a qualitative theory on how elasticity and strain-hardening can lead to a more stable dough wall under stretching. Their argument is essentially a linear stability analysis considering the effect of a small defect on a uniform sheet of dough under extension. Through this analysis they arrive at criterion which is equivalent to the Considère criterion, stating that rupture will occur when the rate of increase of stress with respect to strain falls below a certain value. A number of studies have been performed and seem to provide experimental justification for this hypothesis [4, 7, 43-46].

We next ask the question of what distinct feature of wheat flour gives rise to these properties? Experimental evidence point towards the gluten fraction of wheat proteins. Various researchers have come to the consensus that the glutenin macropolymer forms a three-dimensional network throughout the dough. The initially distinct glutenin molecules in the flour swells in size due to hydration and begin to interact with neighbouring glutenin molecules in the process of mixing/working. The large molecular weight of the glutenin macroplymers is essential to form a critical number of interactions in order to achieve a sample spanning structure which gives elasticity. Covalent disulphide bonds and non-covalent hydrogen/hydrophobic interactions both play an important role in the formation of this network, but their exact nature and properties imparted to this network is still unclear [27].

Létang et al [47] suggested a model that is depicted in Figure 9 consists essentially of linear polymer chains that are linked end to end by the di-sulphide bonds while the non-covalent bonds form interchain interactions. This model is also extremely similar to the linear glutenin model proposed by Ewart [8].

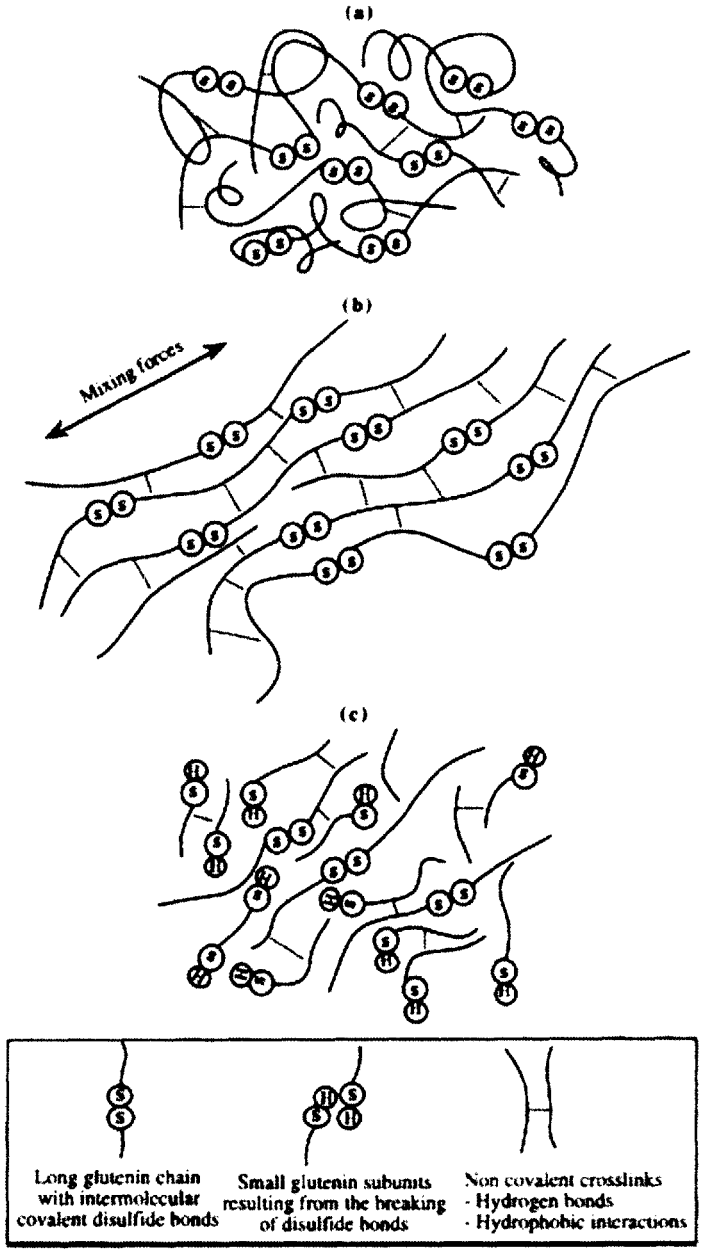

Figure 9 Letang's molecular interpretation of the gluten development (a) beginning of mixing, (b) optimum development, (c) overmixing.

He explains the development of the dough during mixing in terms of this molecular picture. At the beginning of dough mixing, the gluten molecules are folded. Some interactions between the molecules exist but the overall contributions of these forces is small because of the random orientation of the chains (Figure 9 (a)). As mixing progresses, the molecules are stretched and aligned, thus allowing a greater possibility of interaction between neighbouring chains. This increase in interaction "strengthens" the dough and is reflected in the increase in torque on the mixograph (see Chapter 3). Excessively long mixing time leads to the breaking of di-sulphide bonds along the ends of the molecules, thus decreasing its effective molecule size. The torque also decreases accompanied by an increase in the viscous nature of the dough as indicated by an increase in tan δ.

Belton's model [48] was also extremely similar, with the idea of alignment and orientation formalized in his loops and train model.

Singh and MacRitchie [49] took a view similar to that of Letang and Belton, but they also suggested that the mechanical properties could be understood in terms of rubber elasticity and in the context of polymer science. They hypothesized that entanglements between the giant gluten molecules play a role in forming inter-chain interactions. Dobraszyk et al suggested that the glutenin molecule is of a branched form. They felt that pinning at the branched points in the entangled gluten gel is the cause of the strain-hardening typically associated with dough [4].

On the other hand, Don et al [50, 51] cite microscopy evidence to show that the gluten gel is of a particulate nature. The gluten molecules form tight globules that flocculate to form a network through a mixture of covalent and non-covalent interactions. This particulate view of gluten networks has also been independently suggested by Lefebvre et al [52]. However, it has also been suggested that the presence of these particles under microscopy could be an artifact due to the use of SDS in extracting them [53].

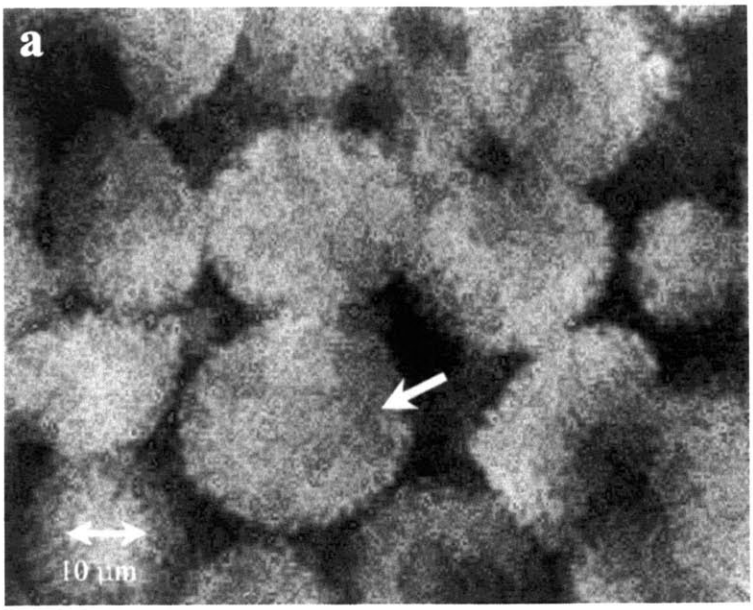

Figure 10 Microscope images of gluten molecules [54].

Other than microscopic evidence, Domenek et al [55] published results on gluten gels formed with a range of gel fraction. They concluded that the behavior of elastic modulus is consistent with a particulate system. However, insufficient evidence was given to discount the possibility of the rheology being also consistent with a polymeric gel system described by Letang. In fact, in Figure 11 we showed that the data is consistent with the picture of a physical polymeric gel system by comparing the divergence of modulus with the well known percolation result given by Flory [56, 57]. What it also shows is that gluten mixed at room temperature with typical dough like water fraction and without any additional heat treatment is indeed close to the critical point where the modulus diverges (Figure 11). i.e. a critical gel! (see Critical gels - Powerlaw model).

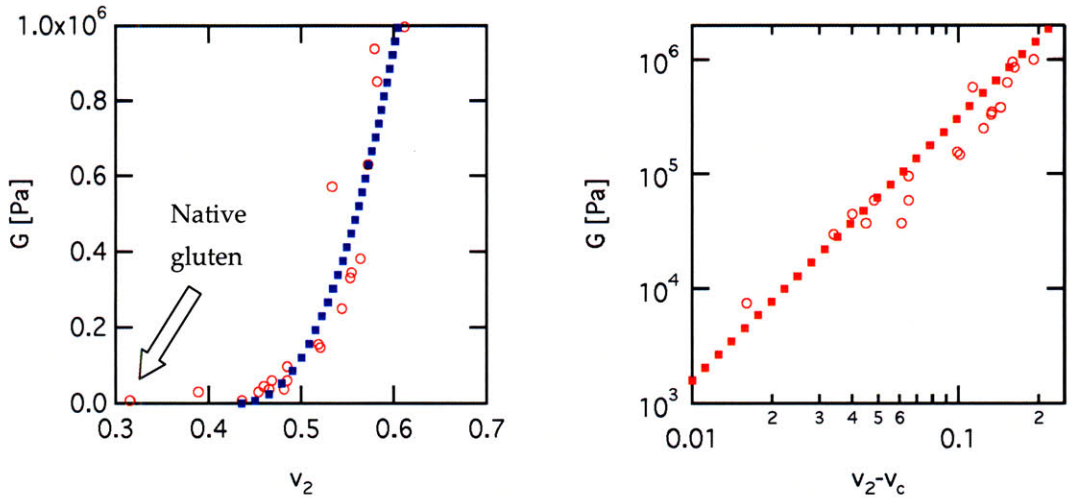

Figure 11 Modulus for gluten gelled by heat to various levels, data taken from Domenek et al [55]. A typical gluten dough formed by mixing at room temperature with a typical dough like water content is close to the critical point will have a gelled volume fraction ~ v_c = 0.43 and p ~ 2.3. Dotted lines are fitted lines to Flory's gelation theory $G \sim (v_2 - v_c)^p$.

Overall, there are an abundance of articles in the literature that provide a range of good ideas in terms of modeling and also plenty of heated discussion on the subject [53, 58]. However, we feel that none of the published works provide sufficient rheological evidence to support their chosen structural models. There is very limited rheological data presented in these works that definitively link the supposed functionality arising from the model to actual mechanical behavior. As a result, the constitutive modeling comprise of mostly empirical equations that seek to describe the deformation behavior of specific systems rather than general rheological features that arise from microstructural changes.

2.4. *Consititutive modeling of dough*

The constitutive models serve as a framework for discussing how material parameters can vary with different dough conditions such as mixing time, water content and base flour type.

A constitutive equation relates the state of stress σ in a fluid element in terms of its deformation history $\dot{\gamma}(t,t')$. It is a framework for relating the two typical raw data of forces and deformation obtained in dough rheology. Such equations provide us with a quantitative method in evaluating and comparing quality of the dough. Provided a suitable form of material function is selected, the effects of each ingredient and additive or molecular features should become apparent through changes in the parameters such as relaxation time and modulus. Knowledge of the appropriate material functions can also improve accuracy for calculations in process engineering leading to better efficiency.

Rheological modeling of dough borrows heavily from the related field of polymer science. Most studies have focused on dynamic oscillatory response using the dynamic moduli as a starting point for building a spectrum of modes. Relatively little work has been done on the mathematical description of extensional behavior. Under such strong flows, many phenomena that cannot be probed by small amplitude shearing will become apparent. These include finite extensibility and strain-hardening which are both important in the context of functionality.

Which leads us to the point of functional requirements when designing a constitutive model for dough. A good model, will not only allow us to make predictive calculations on the material behavior, but also teach us something about the physics of the system. Therefore it is important to choose a level of complexity that is just sufficient to illustrate the important ideas without encumbering it with too many details. One can of course use a large number of parameters and equations to make an extremely accurate description of a system, but it teaches us nothing! The reader is strongly encouraged to keep these ideas in mind when assessing the merits of a proposed constitutive equation for dough.

Upper Convected Maxwell and Oldroyd-B model

The upper convected Maxwell (U.C.M.) model and its close relative Oldroyd-B are natural starting points for this discussion. They are amongst the simplest

visco-elatic model used to describe behavior of dough in. The U.C.M. contains only two variables:

$$\sigma + \lambda \sigma_{(1)} = \eta \dot{\gamma}_{(1)} \tag{2.9}$$

Where η is a polymeric viscosity, λ is the relaxation time and the subscript (1) is the upper-convected derivative operator:

$$\sigma_{(1)} = \frac{D\sigma}{Dt} - \left[(\nabla v)^T \cdot \sigma + \sigma \cdot (\nabla v) \right] \tag{2.10}$$

The equation can be thought of as a description of a polymer modeled as a Hookean spring with a particular relaxation response.

A simple extension to the U.C.M. is to add a solvent contribution to the stress. Such a model is known as the upper-convected Jeffrey's or Oldroyd-B model:

$$\begin{aligned} \sigma &= \sigma_p + \sigma_s \\ \sigma_p + \lambda \sigma_{p(1)} &= \eta_p \dot{\gamma}_{(1)} \\ \sigma_s &= \eta_s \dot{\gamma}_{(1)} \end{aligned} \tag{2.11}$$

For both of these models, steady state will not be reached if $De \geq 0.5$. Above this critical Deborah number, the stress increases without bounds. From a physical point of view, this is unrealistic because a finite extensibility limit will be reached where the polymer has reached its maximum extension.

The use of these simple models illustrates the viscoelastic nature of doughs. Bagley et al claimed that the U.C.M. is able to describe with reasonable success the deformation of a dough under uniaxial compression [59]. However, they did concede that the range of relaxation time can vary dramatically.

Another short-coming of these models is that they are single modes. Published data on the dynamic oscillation response show a wide relaxation spectrum, indicating the highly poly-disperse nature of dough, a mode generalized form containing multiple modes will be required to fully describe this behavior [60].

Phan-Thien Model

The Phan-Thein model [61] is able to address many of the features which are not well described by the simple models in the previous section. It is a phenomenological model which describes the stress tensor $\boldsymbol{\sigma}$ as a combination of a hyper-elastic term ($\boldsymbol{\sigma}_E$ representing the glutenin/cross-linked network) and a visco-elastic contribution ($\boldsymbol{\sigma}_V$ representing the suspension of starch globules and gliadin components).

$$\boldsymbol{\sigma} = \boldsymbol{\sigma}_E + \boldsymbol{\sigma}_V \tag{2.12}$$

$$\boldsymbol{\sigma}_E = \frac{G_E}{1+a} f(\gamma)\left(\boldsymbol{B} - a\boldsymbol{B}^{-1}\right) \tag{2.13}$$

G_E is the elastic modulus, $\boldsymbol{B}$ is the relative Cauchy strain tensor.

The visco-elastic contribution is expressed as a summation of distinct modes with constant relaxation times λ_j and viscosities η_j.

$$\begin{aligned} \boldsymbol{\sigma}_V &= f(\gamma)\sum_{j=1}^{N}\boldsymbol{\sigma}^{(j)} \\ \boldsymbol{\sigma}^{(j)} &+ \lambda_j \boldsymbol{\sigma}^{(j)}_{(1)} = \eta_j \dot{\boldsymbol{\gamma}} \end{aligned} \tag{2.14}$$

G_E, λ_j and η_j are not arbitrary constants. They are determined from the oscillatory data:

$$\begin{aligned} G^*(\omega) &= G_E + \sum_j \frac{i\omega\eta_j}{1+i\lambda_j\omega} \\ \eta^*(\omega) &= \frac{G_E}{i\omega} + \sum_j \frac{\eta_j}{1+i\lambda_j\omega} \end{aligned} \tag{2.15}$$

The remaining parameters a and $f(\gamma)$ are determined from start-up of steady shear flow experiments. Phan-Thien et al observed the shear stress to increase with time to a peak value and then decrease continuously afterwards with a

"conspicuous" absence of steady state response. They believed that the peak value corresponds to a "rupture" or partial "breakdown" of the elastic network. This behavior is modeled through the strain-softening function $f(\gamma)$:

$$f(\gamma)=\frac{1}{\left(1+\gamma/\gamma_s\right)^{(1-m)/2}}\exp\left\{-\left(\frac{\gamma}{\gamma_p}\right)^4\right\} \tag{2.16}$$

where γ is the equivalent strain $\gamma=\left(Tr\underline{\underline{B}}-3\right)^{1/2}$, γ_s represents the strain at which shear-thinning occurs in the manner of the Carreau viscosity model with exponent m, and γ_p is the strain at which "rupture" occurs.

The predicted stress for a range of strain rates was compared to experimental data on start-up of steady shear flow and dynamic oscillation. They showed reasonable agreement, which is not at all surprising, since the constants are fitted from these data. This illustrates an important point in evaluating a constitutive equation: how will the predictions fair when compared to data obtained under different kinematic conditions? Since in the case of doughs, extensional behavior seems to be of most practical interest, the natural question to pose is whether a model can predict extensional rheological response. Rock [62] performed a numerical study on the predicted response of the model under bi-axial extension in the bubble inflation technique, but unfortunately no attempt has been made to compare the predictions with extensional data yet.

The greatest drawback for the Phan-Thien model is that it requires an unusually large number of parameters, making it unwieldy in performing qualitative analysis such as kinematic failure. It is also difficult to compare relative functionality of different dough. Fitting the strain-softening function is also extremely empirical, it is difficult to relate stress development to the molecular structure of the gluten network.

Pom-Pom model

The Pom-Pom model [63, 64] has a feature particularly appealing to rheologist studying dough: it describes the effect of branching on large deformation rheology. Micrographs of the glutenin network seem to show the molecules to have a highly branched structure [4].

The Pom-Pom model is an extension to reptation theory [65], where polymers are modeled as composing a backbone with branched ends, this is illustrated in Figure 12.

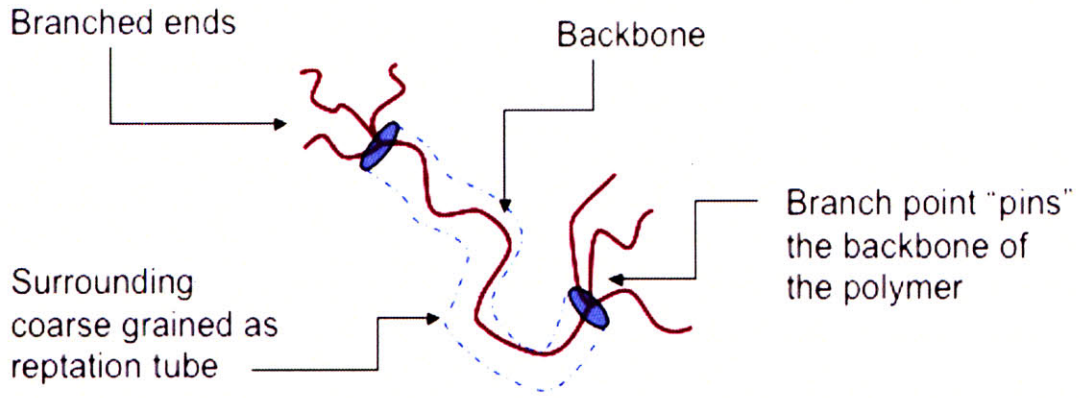

Figure 12 The Pom-Pom model

Branch point acts as a constraint "pinning" the ends of the polymer backbone to deform affinely with the flow. However, this "pinning" effect is not permanent and will release allowing the branched points to retract into the reptation tube if the backbone is stretched to a certain limit. The resulting constitutive equations are:

$$\begin{aligned} \boldsymbol{\sigma} &= G\phi^2 \boldsymbol{S} \\ \boldsymbol{A}_{(1)} &= \frac{1}{\lambda_b}\left(\boldsymbol{A} - \frac{1}{3}\boldsymbol{I}\right) \\ \boldsymbol{S} &= \frac{\boldsymbol{A}}{Tr(A)} \\ \frac{D\phi}{Dt} &= \phi(\nabla \boldsymbol{v} : \boldsymbol{S}) - \frac{1}{\lambda_s}(\phi - 1) \quad \text{for } \phi < q \end{aligned} \tag{2.17}$$

Where G is the modulus, S is the orientation tensor and ϕ is a measure of backbone stretching. The backbone relaxation occurs at a characteristic stretch relaxation time-scale λ_s while the orientation can also relax separately at a time-scale of λ_b. Branched point retraction bounds the stress growth providing a mechanism of finite extensibility to the model.

A natural extension to the Pom-Pom model is to include a spectrum of mode shapes to capture the dynamic shear response, however this will again increase its complexity because we will need to specify a q value for every single mode. There are currently no published results that compares the prediction of this model to measured rheological data.

Others

The equations discussed here are by no means a comprehensive study of the different approaches in building a constitutive equation for dough. Other examples include K-BKZ [66], Bird Carreau [67] model etc... Most models require a large number of constants reflecting the complex composition of the dough. All are able to describe particular aspects of dough rheology with varying degrees of success. In this work, we are most interested in the response under large nonlinear deformation and will be willing to sacrifice some accuracy in order to capture the important physics behind mechanism of strain-stiffening, nonlinear softening, finite extensibility and rupture discussed in the introduction.

Critical gels - Powerlaw model

In our review of early work, we saw that dough often exhibit a powerlaw type response in their linear viscoelastic material functions [15, 19, 61, 68]: relaxation modulus and creep compliance varies as a powerlaw with time, while the dynamic moduli are power law functions of oscillation frequency. Gabriele and co-workers [69] were the first to notice the similarity between powerlaw behavior of dough and the response of a class of materials called critical gels.

Critical gels refer to materials that lie on the ill-defined boundary between liquid and solid state. They can be best understood by considering the formation of them. Here, we use the example of a perfectly cooked egg yolk within a soft boiled egg as an example [70].

An egg yolk consists essentially of two phases: aqueous phase and globular protein phase. In Figure 13 we plot the dynamic moduli of an egg yolk as the temperature is increased. In the uncooked state, there is little interaction between neighboring globular proteins, and the yolk can be considered as a simple suspension that is predominantly of fluid nature, this is evident from the relative magnitudes of the dynamic moduli. As the temperature is raised, there is an increased level of interactions between neighboring protein globules, they begin to bond, the structure formed in this manner is able to span the entire sample thus turning the yolk from a fluid to solid state. The point at which this sample spanning structure first develops is the critical gel point. Since the bonding events occur randomly in space, the structures formed will be of a fractal nature, giving a critical gel its characteristic power law like behavior [71, 72].

Incidentally, the critical gel state is close to what epicureans consider a perfectly cooked egg yolk: "the yolk suspended between raw and cooked, ... freed from the slight rubberiness... a sexy egg" [73].

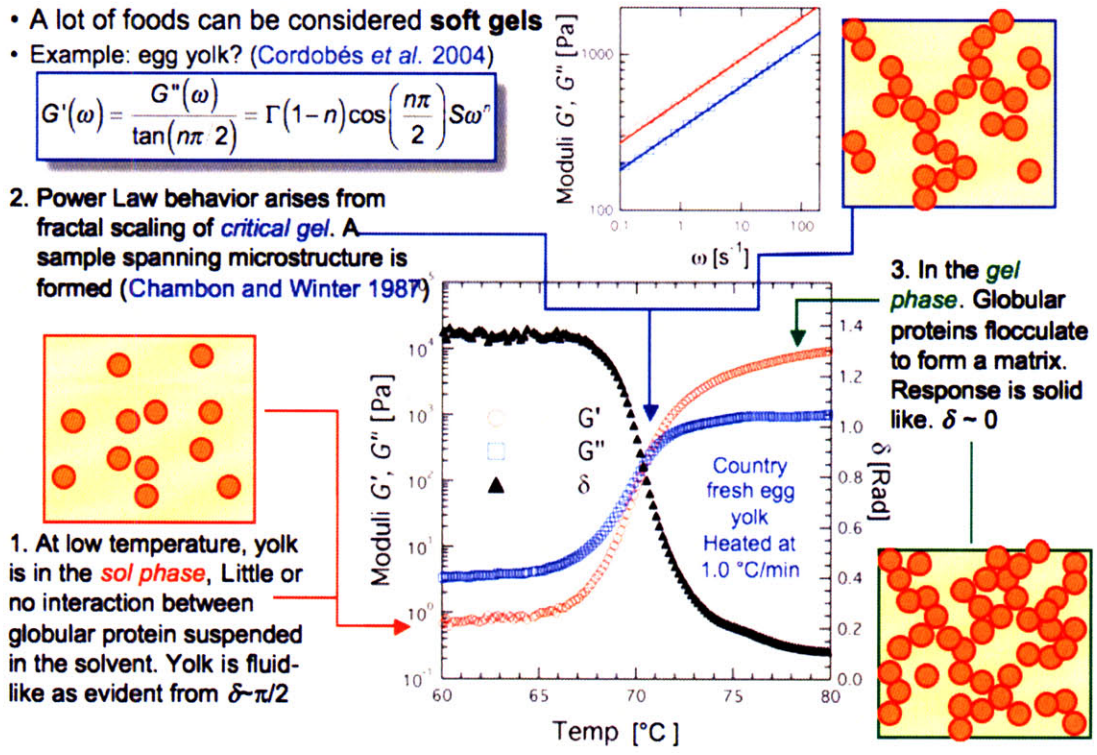

Figure 13 Mechanical properties of various stages of gelation illustrated by the cooking of an egg yolk.

The mechanical properties of a critical gel have been well documented [74-77]. It suffices here to note that the relaxation modulus shows is well known to show a powerlaw decay in time

$$G(t) = St^{-n} \tag{2.18}$$

where S is known as the gel strength and n is referred to as a gel index. Other linear viscoelastic material functions can be obtained by considering suitable transforms of equation (2.18) while an extension to include finite strain deformations will be discussed in the next chapter. Detailed treatment of the experimental and mathematical framework will appear later in this thesis, where we will compare theoretical predictions with experimental data obtained from gluten gels: a material with much simpler rheological behavior.

The fact that doughs also show a critical gel like response should not be surprising, after all, there are many other foodstuffs that also show this sort of powerlaw behavior [70, 78, 79]. However, exactly which components within the dough give rise to this critical gel behavior is an unanswered question and will be considered in turn later in the thesis.

2.5. *Conclusions*

The rheological study of dough has had a long and distinguished history, and we have spent this chapter discussing articles originating from a period that spans the best part of the last century. Through this discussion, we have highlighted a few important ideas that are central to dough rheology.

First of all, we learnt that good experimental technique is absolutely critical. Dough typically exhibit strongly non-linear rheological behavior and are time dependent/thixotropic, thus it is important to keep track of all the variables.

We also surveyed some proposed theories for the microstructure of dough. We showed that hydrated starch is on its own an extremely time dependent material. For the gluten part, we noted that they can be broadly classified into two schools of thought, with one school believing the proteins exists in a tightly bounded particulate form (particulate gels) and another believe that the proteins exists as long filaments (branched or linear) and behave more like typical long chain polymers (polymeric gels). Both schools are in agreement that there are strong interactions between neighbouring proteins that form a sample spanning network.

We also surveyed some common constitutive equations and assessed the "pros and cons" of using them. Of particular interest is the critical gel model that seems to be able to describe the linear viscoelastic properties with a surprising small number of parameters (gel strength S and gel index n). The material functions predicted are in agreement with the "powerlaw rheology" often observed in dough. In the next few chapters, we will build upon this mountain of previous work and hopefully shed light on some of the unanswered questions still remaining.

3. Equipment, Experiments and Sample Preparation

The ultimate goal of dough rheology is to directly measure or otherwise indirectly obtain its material functions, which can then be used to describe the functional properties of the dough. A general discussion of each of the following rheometric tests are provided by Bird et al. [60]. In this chapter, we will briefly sketch out the techniques and discuss their merits and shortfalls with regards to dough rheology. Detailed discussions of the specific geometries, procedures and results will follow in the subsequent chapters.

Bagely [80] outlined the range of difficulties encountered by rheologist attempting to characterize the mechanical response of dough. Firstly, there is the difficulty in obtaining repeatable data. He found that other than over-mixed dough, samples were so heterogeneous that even samples from the same mixing batch displayed significant variations. He also noted that these heterogeneities can be eliminated by over-mixing the dough, but over-mixed dough are of little practical interest. Short of over-mixing, the only solution is to be extra careful and consistent in preparing the sample, and to perform a large number of experiments to obtain a statistical mean.

Secondly, the interpretation of raw data is often extremely challenging, since very few experiments allow us to directly measure the material functions. After performing the tests, how should the rheologist interpret the raw data (force/pressure/displacement/Brabender Units etc...), and is it possible to form a basis for comparing different doughs? How do we compare the results from say the extensigraph test to the Alveograph or dynamic shear test? These are questions which we will consider for each of these tests.

Most of these are well developed techniques and are documented in detail in other works [60, 81-83], it suffices here to provide a very brief list and description of the "arsenal" available to the dough rheologist to attack the problems at hand.

3.1. *Mixing*

Mixing is the very first step towards forming a cohesive dough, whether for baking or for rheological testing. Obviously, the quality and proportion of ingredients will have an impact on the baking and rheological properties of the mixed dough; however, less obviously, the manner in which mechanical work is imparted onto the dough during mixing can have an effect too.

During the mixing process, the respective constituents are dispersed and the application of mechanical energy "forms" the dough by changing its molecular structure as described in [6, 27, 84].

Mechanical mixers come in various forms, industrial mixers are designed to handle large quantities of dough, some examples are agitator arms, dough hooks, spindle and planetary mixers etc... In the laboratory, dough is produced in much smaller quantities, and the mixers are used to produce samples of consistent properties for testing. Some mixers also monitor the properties of the dough during mixing and hence can be considered as a crude form of rheometer or indexer. Z-blade and pin mixers are the most commonly used for dough applications. In our laboratory, a pin type mixer [85] is used to prepare the dough samples.

The layout and typical output of the pin-type mixograph is illustrated in Figure 14 (a) and (b). The motion of the rotating pins causes the mixture to stretch and fold around the stationary pins. The resistance of the dough is reflected in the deflection of the torque spring. This deflection is recorded on a mechanical strip chart. Newer models of the mixograph come with the option of electronic torque measurement and analysis capability. In our lab, we instrumented our mixograph with a simple string potentiometer that outputs the deformation signal to a Labview data acquisition and analysis system.

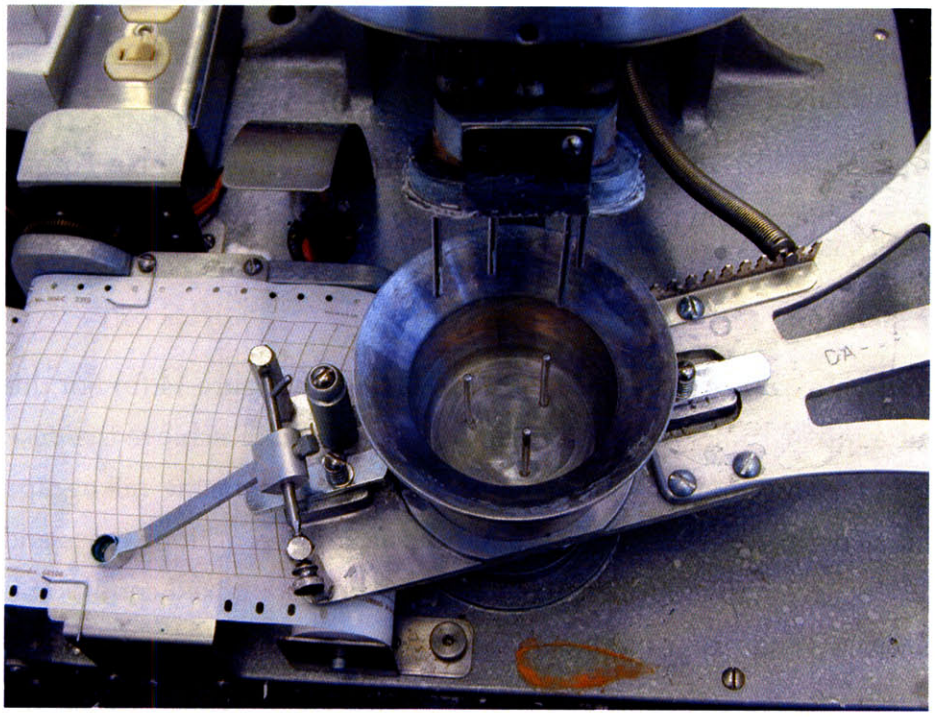

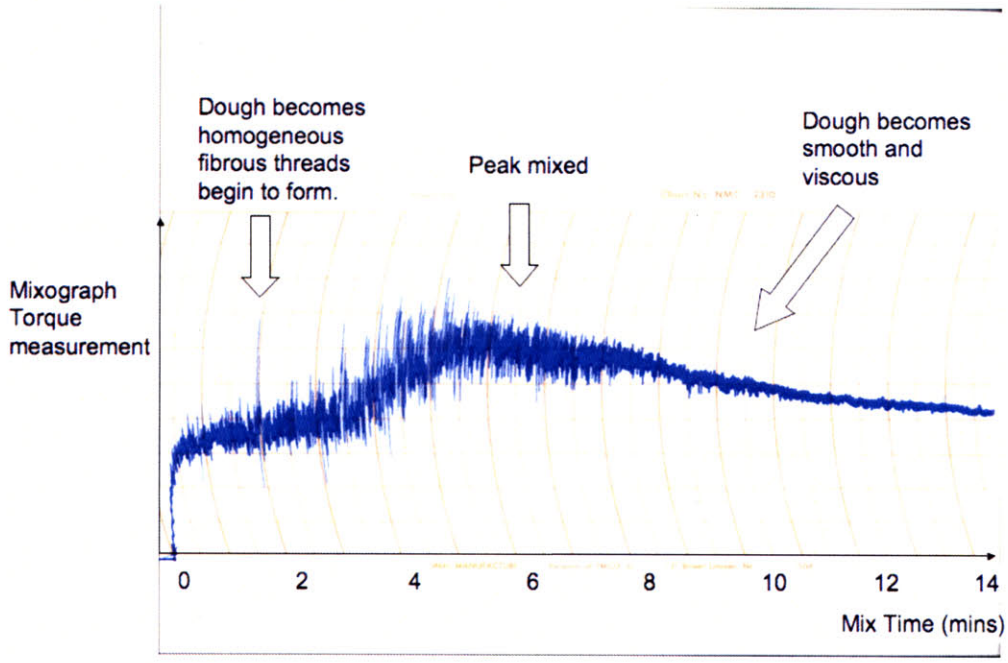

Figure 14 Mixograph and typical output

The shape of the mixograph varies with flour type, protein and water content, but several general features are usually present:

Under-mixed regime (typically 0-1.5mins): The dough is not homogeneous if mixed for less than 1.5 mins. Between 0 and 1.5 mins, the torque increases rapidly from 0 to 3 mixograph units.

First plateau region (1.5 to 3 mins): Only observable for strong doughs. Torque reaches a plateau and remains approximately constant at 3.5 mixograph units. During this period, the sample becomes homogeneous and fibrous threads are formed by the stretching action of the mixograph pins.

Peak-mixed (2-10 mins): Torque begins to increase again. In Figure 14 (b) For this particular flour a mixing time of seven minutes was required to achieve the peak mixed condition (i.e. the time at which the torque output from the mixograph was at maximum) but can vary by up to ± 5 minutes for different flour types and water content. The period of increasing torque up till the peak mixed condition is usually associated with the development of dough protein structure.

Over-mixed (after the dough was peak mixed): additional energy causes the breakdown of this structure, and the torque decreases. Visual inspection of the dough shows that it has become smooth and viscous, and can be described as "creamy".

The impact of mixing on the rheology [86-88] and bread making qualities [89, 90] of dough has been the subject of intense study [91]. The general idea is that the mechanical energy imparted by the mixing method causes dramatic microstructural changes: through gluten development/breakdown [92, 93], starch swelling/breakdown [94]. There also some studies that deal with the distribution of constituents in dough mixed to different levels of development [95, 96].

3.2. General Mechanical Testing

After the dough is mixed to the required consistency, mechanical testing can be performed on it. In the context of mechanical testing, scientists and engineers have found wheat flour dough a difficult substance to work with. Equipments and analyses in this field of study can be broadly divided into two approaches.

The first approach centers on devices that were developed specifically for assessing dough. Included under this category are devices such as Extensigraphs and Alveograms. The Extensigraph [97] and Alveograph [98] measures the resistance against extension after the dough has been mixed to a specified amount of time. Such devices are well suited for testing dough; dough has a large relaxation time, the mechanical response is highly dependent on its deformation history. Therefore sample loading is usually simple, protocols for preparing specimens either minimize handling or ensure that all batches are treated with uniform deformation. In view of these advantages, the devices under this first category are widely adopted by the food industry as standards. Unfortunately, the outputs are usually given in terms of empirical units (Brabender units etc...). Since the deformations are not well understood, it is difficult to convert results to universal parameters such as stress and strain.

Another approach utilizes instruments known as rheometers. Rheometers are capable of measuring resistance (torque/force) and displacements to a high degree of accuracy. Within the classification of rheometers, we can further divide them into shear and extensional devices. The deformations experienced by dough in the bread-making process are predominantly extensional, therefore it is widely believed that properties measured in the extensional rheometer are more relevant for describing the quality of the dough [4, 80, 99]. Contrary to the devices mentioned in the previous paragraph, rheometers are not well suited to testing dough due to the difficulty in sample loading. But the kinematics of deformation of the sample within the instrument are well defined, this makes the analysis to translate resistance-deformation data to universal parameters relatively simple.

Over the last few decades, a number of studies have been made towards understanding the kinematics in devices of the first approach and to establish the link between their results from fundamental quantities measured on true rheometers. Bloksma [100] related the pressure and displacement measurements from an Alveograph to stress and strain by making specific assumptions on the mode of deformation. Charalambides and co-workers later investigated these

assumptions through experimental observations [101] and computer simulations [102].

3.3. Devices designed specifically for dough

Extensigraph

The extensigraph was developed by Brabender. Dough is rolled into a cylindrical sample and clamped at its two ends. A hook is moved perpendicularly across the sample, stretching it to a V-shape (Figure 15).

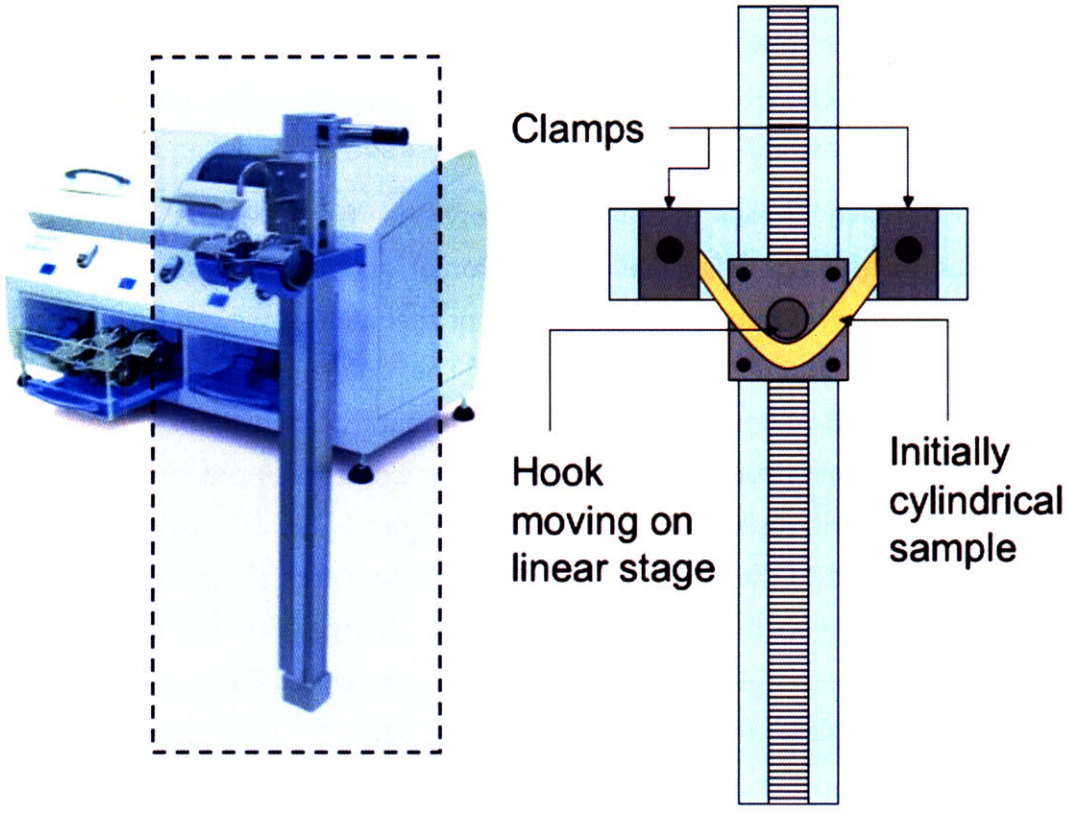

Figure 15 The extensigraph. Cylinders of dough are clamped at ends and stretched out by pushing a dough hook through the central portion.

The Brabender extensigraph outputs the resistance $R(t)$ that the hook experiences and the distance $E(t)$ which the hook has moved through. Resistance is measured in Brabender Units (BU), a typically arcane measurement favored by Brabender company, though it is not difficult to calibrate it to the more common S.I. units of

force measured in Newtons. From the outputs of the extensigraph, an empirical number which supposedly reflect the rheological properties can be computed:

$$\text{Ratio number} = Rn = \frac{R(t)}{E(t)} \tag{3.1}$$

A more useful measure is the extensibility E_{max}, which is simply the maximum length the dough can be stretched through before rupturing. Obviously, extensibility will have some direct relation to the dough volume as discussed in the previous chapter.

Bubble inflation technique

The bubble inflation technique is perhaps the most widely adopted method for performing extensional tests on dough. Its popularity might be partly due to the similarity in kinematics to the actual deformation during baking and proofing which is predominantly bi-axial. Furthermore, a set of accompanying equipment has been developed to form the initial sample conveniently and consistently with minimal handling. The Chopin Alveograph was one of the earliest development. Subsequent improvements and adaptations were made [7], but the underlying principle remains the same (Figure 16). A flat round disc of dough is clamped around its edges. A driven piston supplies a controlled flow of air, inflating the dough sheet into a bubble. Usually, only the volume and pressure of air are measured as raw data, a typical set of raw data is presented in Figure 17.

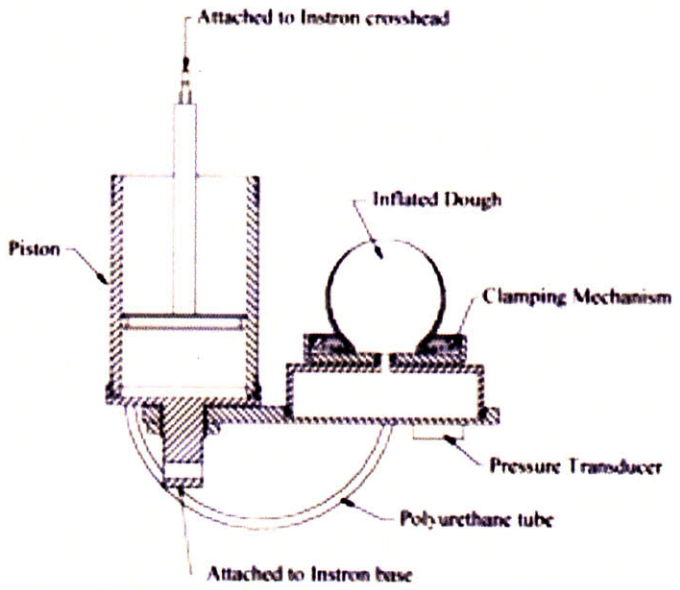

Figure 16 Schematic of bubble inflation set-up [102].

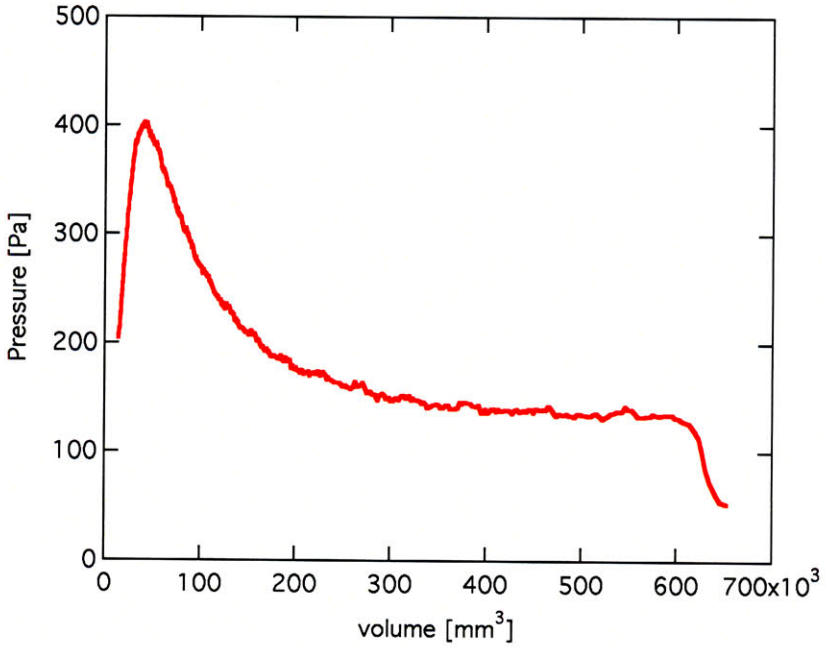

Figure 17 Typical raw data from bubble inflation test.

For a discussion on how the raw outputs of pressure and volume are interpreted, the reader should refer to the works of Hlynka [103], Bloksma [100] and Chalarambides [91, 101, 102].

3.4. Shear Rheology

Shear rheology is a convenient and well developed method of exploring the response of the viscoelastic materials. A rotational rheometer with good resolution in torque and angular displacement is relatively common. Unfortunately, a commonly encountered problem is slip. The large viscosity of dough generates large shear stresses at the interface between the sample and end-plates, which often leads to slip. Slip is usually eliminated by applying a roughened surface (usually sandpaper) on to the end-plate. As a result of this requirement, dough rheology is usually performed on parallel plates rather than cone and plate geometries, for it is easier to apply adhesive backed sand-paper onto a flat plate compared to cone geometries.

Typically, a "blob" of sample is placed on the lower rheometer plates, the top plate is then brought down to compress the sample to the required thickness. A large amount of normal force is generated in this process. This normal force limits the size of the plates, and a diameter between 20 and 40 mm is usually used for these experiments. After the dough is compressed to the desired gap size, excess dough is trimmed with a razor blade.

Stress relaxation

Stress relaxation is conceptually one of the simplest experiments to perform and understand on the rheometer (at least in the linear regime) [18]. Typically, a small shear strain of γ_0 is impulsively applied to the sample. The rheometer then monitors the shear stress $\sigma(t)$ required to maintain the sample in this deformation state. The material function obtained is the relaxation modulus:

$$G(t,\gamma_0)=\frac{\sigma(\gamma_0,t)}{\gamma_0} \tag{3.2}$$

which is typically a decaying function of time and is a measure of the "memory" in the material. The linear regime is defined as the region within which the relaxation modulus is independent of the step strain amplitude:

$$G(t) = \frac{\sigma(\gamma_0, t)}{\gamma_0} \tag{3.3}$$

The range of strain for which this is valid is surprisingly small for dough, typicall $\gamma_0^* < 10^{-3}$.

Unfortunately dough systems tend to have a long memory, therefore stresses incurred during sample loading can interfere with the actual relaxation of the experiment , especially at long times when the stress becomes diminishingly small. A discussion of this effect is given in a later chapter.

Steady shear experiment

In a steady shear experiment, a steady shear rate $\dot{\gamma}_0$ is applied on to the sample until the shear stress reaches a steady state is reached. The shear rate dependent viscosity $\eta(\dot{\gamma}_0)$ is defined as:

$$\tau_{yx}\Big|_{\text{steady state}} = \eta(\dot{\gamma}_0)\dot{\gamma} \tag{3.4}$$

Attempts to measure $\eta(\dot{\gamma})$ has not been successful because the shear stress does not reach a steady state [104]. For experiments conducted at relatively high rates, the sample tend to roll-out of the geometry. While at very slow strain rates, the stress can appear to approach a steady value and is sometimes extrapolated to give an estimate of a zero shear rate viscosity.

Start-up of steady shear

Effectively, the experiment is identical to the steady shear experiment discussed above but rather than just seeking a steady state viscosity, we instead monitor the transient changes in shear stress as the sample is deformed. Even though the

dough deviates from viscometric flows and "rolls out " of the gap at large strains, the transient shear stress leading up to this point can be monitored. The material function obtained from this test is the transient shear viscosity:

$$\tau_{yx}^{+} = \eta^{+}(\dot{\gamma}, t)\dot{\gamma}_{yx} \tag{3.5}$$

At very low rates, when the transient shear viscosity becomes independent of the strain rate, one can use the Gleissle's mirror [105] relationship to obtain an estimate of the steady shear viscosity [80]:

$$\eta(\dot{\gamma}) = \eta^{+}(t)\Big|_{t=1/\dot{\gamma}} \tag{3.6}$$

Creep

Creep is the stress-controlled analog of the start-up of steady shear flows. A constant shear stress σ_0 is applied to the sample and the resulting change in strain is measured. The material function obtained is the creep compliance given by:

$$J(t) = \frac{\gamma(t)}{\sigma_0} \tag{3.7}$$

Lefebvre et al conducted a series of comprehensive creep tests on a variety of wheat flour dough [30], he showed that the material behavior is similar to that observed in strain-controlled tests in which the sample is ejected from the gap at large strains. However, the creep experiment does have the advantage in that the directly measured function, the displacement, is an increasing function of time, thus making long time scale observations easier.

Oscillatory Shear Experiments

An alternative to stepped, transient and steady shear flows are oscillatory flows. Instead of a constant shear stress or rate, the deformation or torque are applied to the sample in a sinusoidal oscillating manner. In the linear viscoelastic regime,

(at very small strains $\gamma_0 < 10^{-2}$), the material functions are independent of the oscillation magnitude and is only a function of the frequency. Therefore we can simply focus on this frequency dependence and perform a sweep through the oscillation frequencies; this form of "mechanical spectroscopy", reflects the signature of microstructures at different length-scales in the frequency response. The material function is typically decomposed to an in-phase and out-of-phase component (relative to the imposed strain $\gamma(t) = \gamma_0 \sin(wt)$ or stress):

$$\sigma(t) = G'\gamma_0 \sin(\omega t) + G''\gamma_0 \cos(\omega t) \tag{3.8}$$

G' is referred to as the dynamic modulus and G'' the storage modulus. They are also sometimes expressed in equivalent terms of dynamic viscosities (!!!):

$$\sigma(t) = \eta''\dot{\gamma}_0 \sin(\omega t) + \eta'\dot{\gamma}_0 \cos(\omega t) \tag{3.9}$$

Since dough are composite materials that show a high degree of polydispersity and we expect its response to depend on a large range of time scales. Dynamic shear rheology can probe the behavior over this wide spectrum of time scales [68].

Phan-Thein et al [61] had reasonable success in using the oscillatory shear technique for characterizing dough behavior and obtained a relaxation spectrum for dough, the storage modulus and dynamic viscosity are plotted in Figure 18.

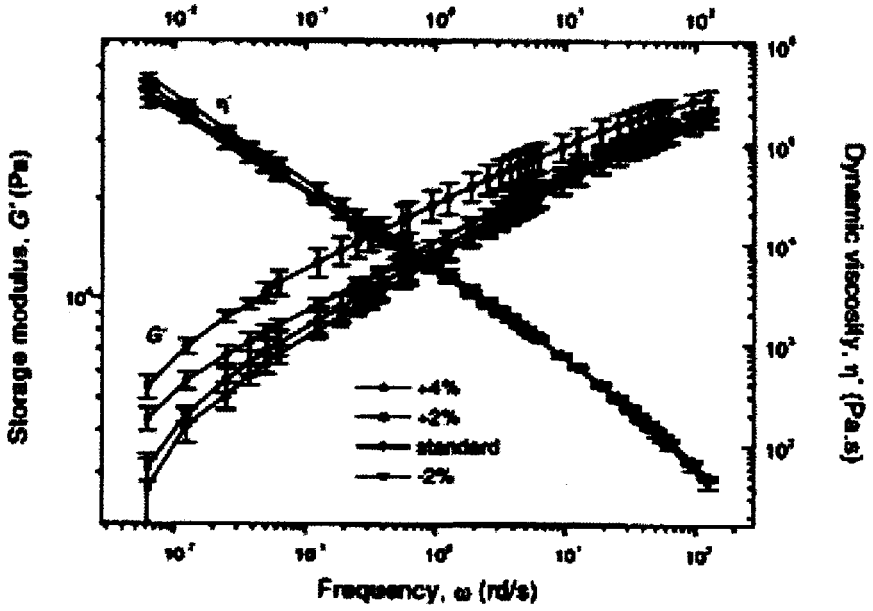

Figure 18 Typical frequency response from dynamic oscillatory shear data for wheat flour dough at various water concentrations [104].

To increase the accuracy of the spectrum, we need data from a wider range of frequencies. Time-temperature superposition is usually used to extend the range but is difficult to apply in this case, because change in temperature can alter the molecular/chemical structure significantly (gelling of starch, drying etc...) [17, 106].

It is important to remember that the analysis described above is only valid in the linear regime, in which the moduli are independent of strain amplitude. Thus, the first step towards dynamic shear rheology is to identify the linear range. We show typical variation in moduli over a strain sweep for a flou-water dough in Figure 19, the linear range of dough is surprisingly small (strains $\gamma \sim 10^{-3}$) and the manner in which the subsequent softening beyond the linear range is similar to other published data [107].

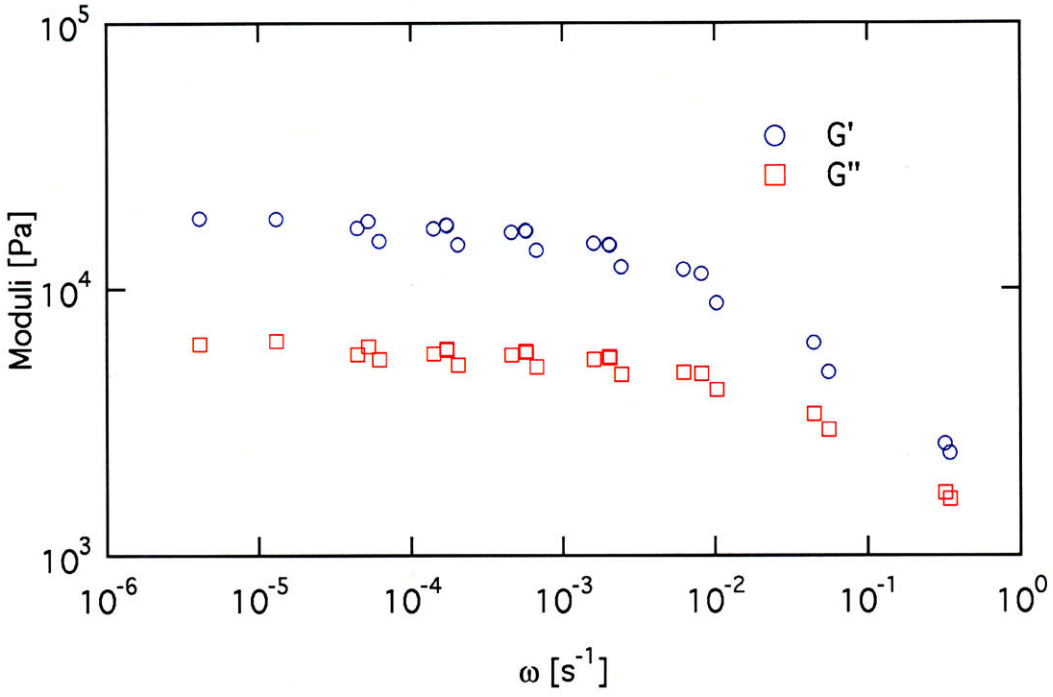

Figure 19 Strain sweep of HRS dough. Both moduli drop dramatically at strain of 5×10^{-3} which we define as the limit of linear range.

That is not to say that data collected beyond the linear range is not meaningful. But instead, more sophisticated techniques are required to understand the results [108-110]. More detailed discussion of such methods will be discussed in chapters 6 and 7.

Most commonly, the departure from linearity is signaled by a deviation from an sinusoidal response signal. The most obvious method for quantifying this deviation is by expressing the response as a series of Fourier harmonics [111] i.e.:

$$\frac{\sigma(t)}{\gamma_0} = \sum_{n=1,2...} G'_n(\omega,\gamma_0)\sin(n\omega t) + G''_n(\omega,\gamma_0)\cos(n\omega t) \qquad (3.10)$$

In the linear viscoelastic, the contribution of the higher harmonics tend to zero and we recover the simple harmonic response once again. The response can be paramterized by eliminating time and presented as Lissajous figures in which stress is plotted against strain. In the linear viscoelastic regime, the curves should

take on an elliptical shape (see chapter 6). These ellipses will become gradually distorted as the strain amplitude is increased beyond the linear range.

Some typical Lissajous figures of flour-water dough from the work of Phan-Thien et al are presented. The strongly nonlinear behavior of the flour-water dough is prominent from relatively small strains ($\gamma_0 \sim 0.01$) and becomes increasingly pronounced at larger strains.

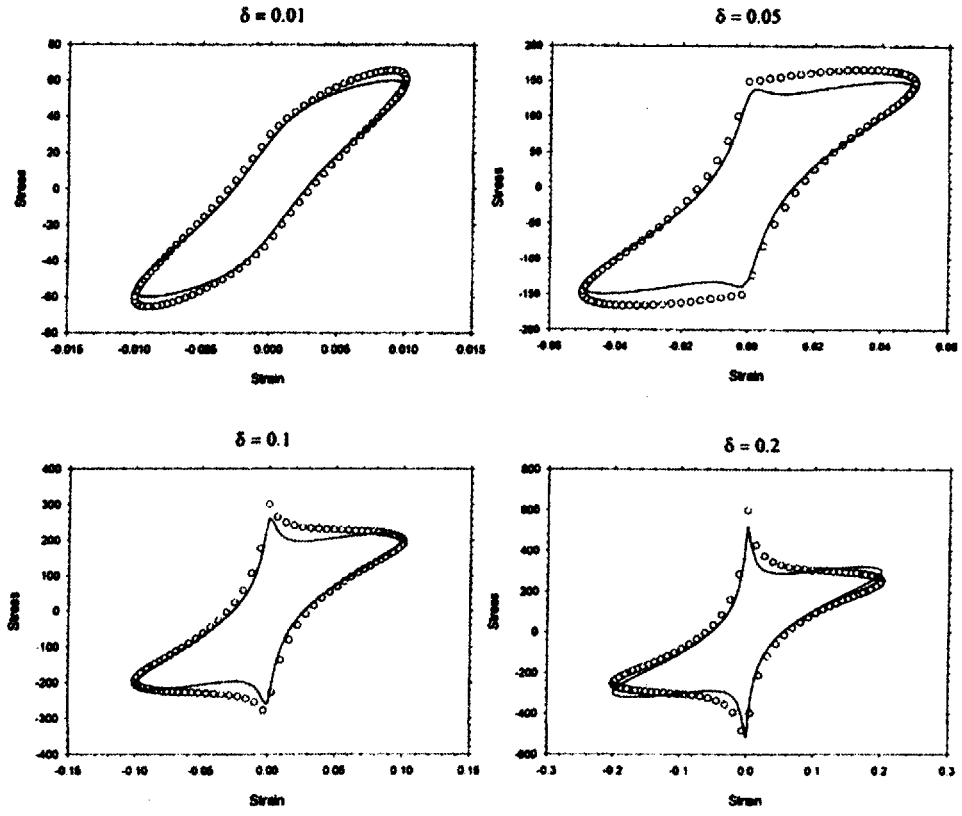

Figure 20. Lissajous figures of wheat-flour-water dough under oscillatory shear of amplitude δ.

Capillary Rheometry

Other than the typical rotational rheometer, a capillary rheometer is sometimes used [112]. Samples are extruded through a tube driven by a pressure difference Δp. We approximate the flow to be fully developed and therefore the pressure drops linearly and velocity profile does not change along the length of the tube.

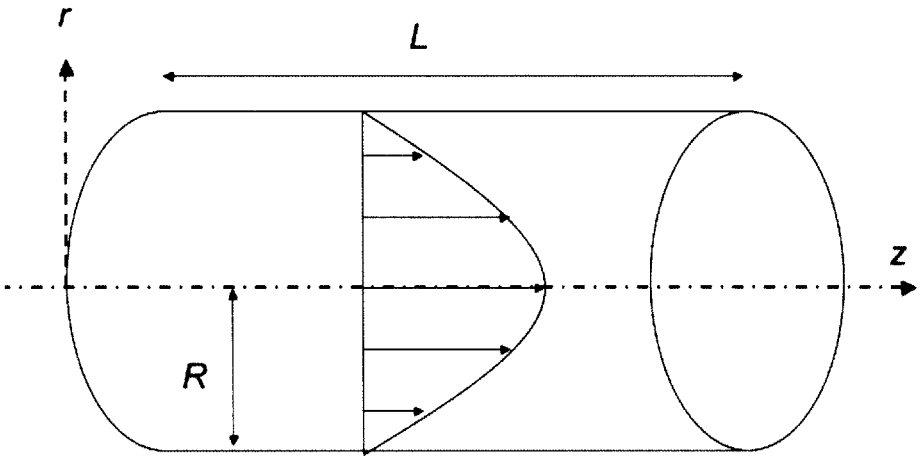

Figure 21 Fully developed flow in a capillary rheometer.

Shear stress in a fully developed flow is given by:

$$\tau = \frac{\Delta pR}{2(L+eR)} \tag{3.11}$$

Where e is an end correction factor. This end correction factor can be significantly large for dough, values of up to 200 are typical. It is therefore critical to have a large L/R ratio to mask the effect. We estimate an apparent strain rate at the wall by considering fully developed flow of a Newtonian fluid with parabolic velocity profile:

$$\dot{\gamma}_{\text{apparent}} = -\frac{\partial v_z}{\partial r} = \frac{4Q}{\pi R^3} \tag{3.12}$$

Where Q is the volume flow rate. An apparent viscosity can then be computed:

$$\eta_{apparent} = \frac{\Delta p \pi R^4}{8Q(L+eR)} \tag{3.13}$$

A variety of correction factors are typically required to account for the occurrence of slip, recirculation and other non-viscometric effects within the capillary [80].

Comparison between different methods of shear rheometry

Relatively few attempts have been made to compare the results obtained from different shear rheometry measurements. Bagley et al [80] presented results from capillary rheometer and start-up of steady shear in a cone and plate set-up. The two sets of data did not overlap each other, but it seems plausible that the shear-thinning behavior can be extrapolated from the cone and plate data to the capillary data.

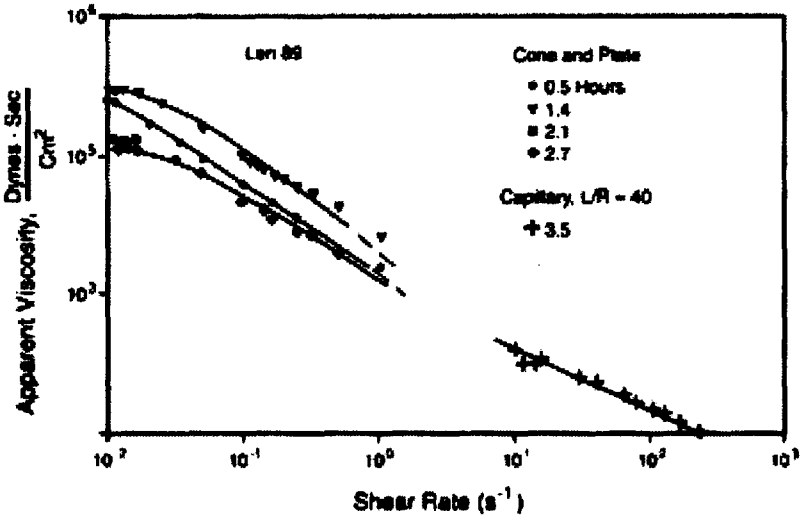

Figure 22 Apparent viscosity from a LEN 89 wheat flour. Values from start-up of steady shear in the cone and plate geometry was computed from the Gleissle rule. Capillary data was obtained through a pressure driven capillary rheometer. [80]

Another often cited result was published by Phan-Thein et al [104] in which they computed the relaxation spectrum from dynamic oscillatory data and step strain relaxation and found them to be in good agreement.

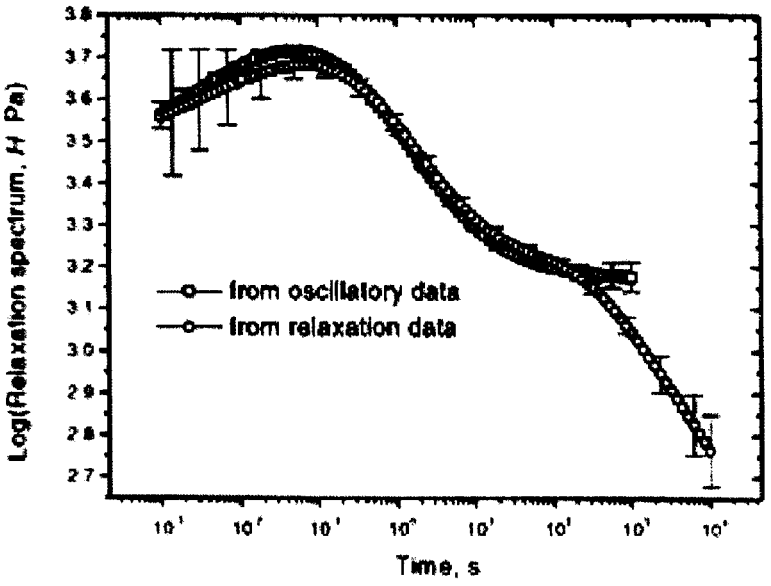

Figure 23 Comparison between relaxation spectra computed from dynamic oscillatory data and step-strain relaxation [104].

Such results are encouraging for they confirm the ability of the well-developed shear rheometry methods in measuring material functions accurately.

But shear rheometry alone is insufficient to characterize the functional properties relevant to bread-making. Since the deformations are in shear and usually of small amplitude, the results cannot be readily translated into properties relevant to the large extensional flows relevant to baking.

3.5. Extensional Rheology

Extensional rheology recently celebrated its hundredth birthday [113]. The study of extensional properties formally began when Trouton described his famous result in the Proceedings of the Royal Society [114]. Since then Schofield and Scott-Blair has developed a method to apply these ideas in a manner relevant to the measurement of "resistance" in bread doughs [10-13] [see chapter 2].

Uni-axial Compression

Uni-axial compression can be performed on instruments such as INSTRON and texture analyzer. A typically disc shaped sample is compressed along its axis of symmetry [59]. To generate a shear free flow, the end plates must be lubricated to allow perfect slip and the resulting deformation will be equivalent to bi-axial stretching. Unfortunately, maintaining perfect slip motion is perhaps more difficult than ensuring no-slip in a shear experiment. Consider the case where no-slip is occurring, The small aspect ratio ($\Lambda = L/R \ll 1$) suggests that a lubrication approximation should be appropriate. Performing the analysis will show that the pressure arising from extension scales like:

$$\tau_{ext} \sim \eta \frac{V}{L} \tag{3.14}$$

while pressure arising from shear:

$$p_{shear} \sim \eta \frac{V}{\Lambda L} \gg \tau_{ext} \tag{3.15}$$

We see that the lubrication pressure can overwhelm the force measured at the endplates; extracting extensional properties can be difficult. Furthermore, stick-slip situations are often observed, therefore generating a steady flow can be tricky.

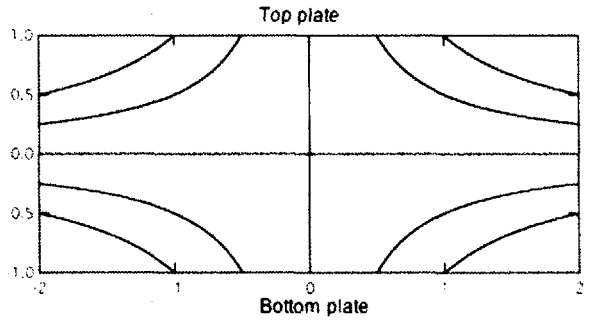

Perfect slip/potential flow

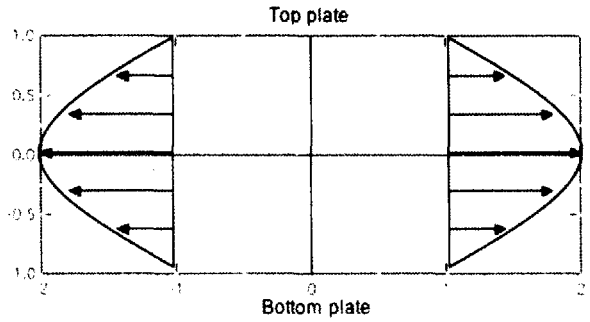

No-slip/lubrication flow

Figure 24 Two approximations of uni-axial compression streamlines.

Despite these difficulties, uni-axial compression has been performed on doughs and the response was found to approximate an upper convected Maxwell model with relaxation time in the range of 10 to 50s [59].

Filament stretching

Filament stretching is a technique more commonly associated with samples of lower viscosity range ($\eta^+_{Ext} \sim 1-100$ Pa s) [115-117], but can also be adapted to use for stretching dough systems which have viscosities in the range of $\eta^+_{Ext} \sim 10^4 - 10^6$ Pa s.

The Filament Stretching Rheometer, FiSER III, allows a large dynamic range (strain rates up to $0.001 \leq \dot{\varepsilon} \leq 5s^{-1}$ are possible), produces good accuracy in force measurements and is able to monitor in real-time the evolution of the mid-plane

diameter during the experiment. The last item is particularly important because under large strains the axial profile of the stretched filament is often not uniform. This extra piece of information gives us more accuracy in calculating rheological parameters such as true tensile stress and true Hencky strain. It also allows us to study the growth of non-uniformity that ultimately leads to rupture.

Figure 25 shows a schematic of the FiSER set-up.

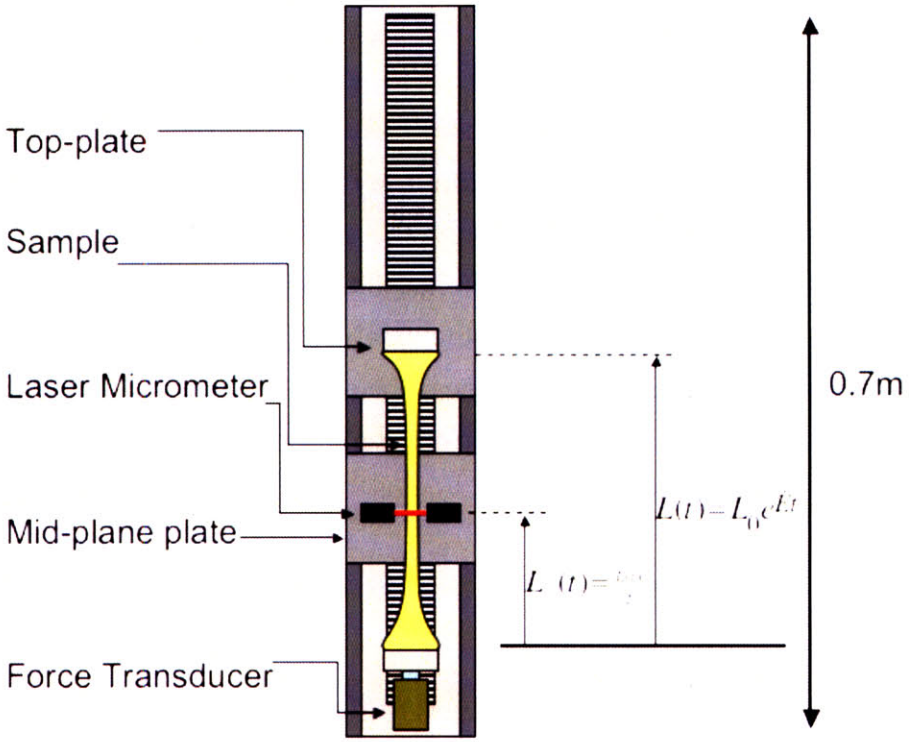

Figure 25 Schematic of Filament Stretching Rheometer

A sample of dough was attached between the top- and bottom-plates by means of sandpaper disks punched from a sheet of self-adhesive sandpaper. At the beginning of the test, the top-plate moved away from the stationary bottom plate at an exponential rate, stretching the dough at a nominally constant strain rate:

$$L = L_0 e^{\dot{E}t} \tag{3.16}$$

From this relationship, we define the nominal strain:

$$E = \dot{E}t = \ln\frac{L(t)}{L_0} \tag{3.17}$$

Mounted on the middle plate is a laser micrometer. This plate travels at half the velocity of the top-plate allowing the laser micrometer to monitor the evolution of the diameter at the mid-plane during the experiment. The laser micrometer was manufactured by OMRON (Z4LA), which measures diameters in the range of 50μm to 9mm with an accuracy of ±10μm.

$\dot{E}$, the axially-imposed or 'nominal' strain rate is based on the total length of the sample. In an ideal experiment for an incompressible material involving a fictional end-plate clamp which deforms accordingly so that the entire sample remain cylindrical, E will be the true strain everywhere in the sample. In practice, as a result of the no-slip condition at the end-plates, the filament shape is concave, and the true strain will vary along the axial length of the sample. The true strain experienced by the fluid elements near the axial mid-plane can also be calculated from the diameter measurements from the laser micrometer through the relationship

$$\varepsilon(t) = \int \dot{\varepsilon}(t)dt = -2\ln\frac{D_{mid}(t)}{D_0} \tag{3.18}$$

Where $D_{mid}(t)$ is the measured diameter from the laser micrometer and D_0 is the initial sample diameter. The local or effective strain rate can also be found from differentiation of this expression

$$\dot{\varepsilon}_{mid}(t) = \frac{d\varepsilon(t)}{dt} = -\frac{2}{D_{mid}(t)}\frac{dD_{mid}(t)}{dt} \tag{3.19}$$

In general, the relationship between the two strains has to be computed numerically.

A force transducer was mounted on the stationary bottom plate to monitor the tension within the dough filament. The force transducer was manufactured by Futek (L2338) and can measure forces up to 10N with an accuracy of ±0.05N. The force transducer has a characteristic time constant of 50 ms.

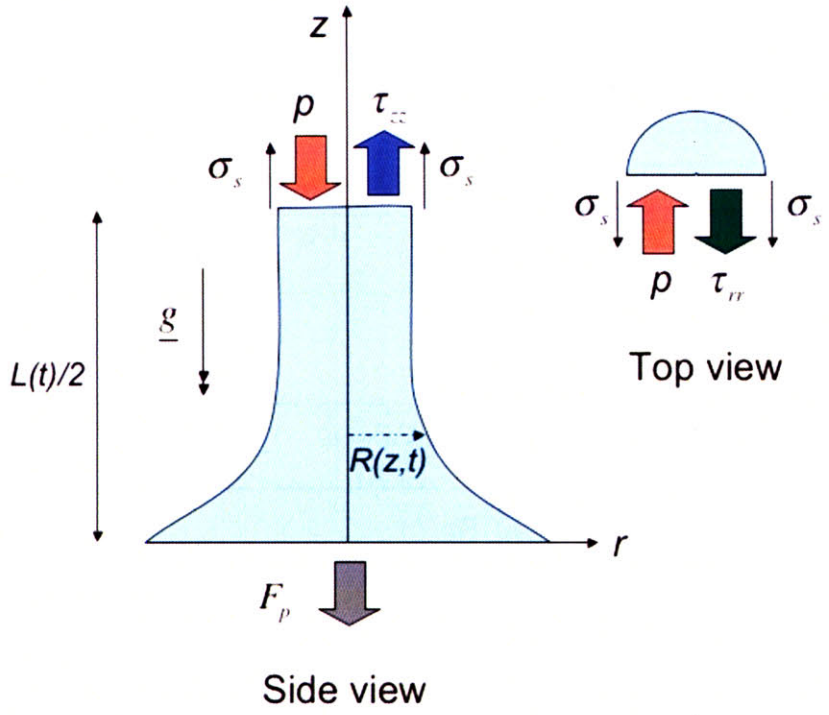

Figure 26 Force balance on a sample undergoing filament stretching

The stress within the sample can be found by performing a force balance at the mid-plane of the sample [118, 119].

$$p = \tau_{rr} + \frac{\sigma_s}{R} \tag{3.20}$$

$$F_p = (\tau_{zz} - p)\pi R_{mid}^2 + \sigma_s(2\pi R_{mid}) + \rho g \frac{V_0}{2} - \rho\pi \int_0^{L(t)/2} R^2(z,t)\frac{\partial v_z(z,t)}{\partial t} dz \tag{3.21}$$

Before writing out the explicit expression for computing stress evolution from FISER data, a few simplifications can be obtained by considering the relative contribution from each of the terms. We make an estimate of each of the terms:

$$\text{Extensional Stress difference} = \tau\pi R_{mid}^2 \sim \eta\dot{E}R_0^2 e^{-\dot{E}t}\pi$$

$$\text{Surface tension} = \sigma_s\left(2\pi R_{mid}\right) \sim \sigma_s R_0 e^{-\frac{1}{2}\dot{E}t}\pi$$

$$\text{Gravitational force} = \rho g\frac{V_0}{2} \sim \frac{\rho g}{2}R_0^2 L_0\pi \tag{3.22}$$

$$\text{Inertia} = \rho\pi\int_0^{L(t)/2} R^2(z,t)\frac{\partial v_z(z,t)}{\partial t}dz \sim \frac{\rho\pi R_0^2 L_0^2\dot{E}^2 e^{2\dot{E}t}}{4}$$

The characteristic size of experimental parameters:

Parameters	Typical Values
η	$10^4 Pas^{-1}$
$\dot{E}$	10^{-3} to $10^1 s^{-1}$
$\dot{E}t$	0 to 3
R_0	$10^{-3}m$
L_0	$10^{-3}m$
σ_s	$10^{-2}Nm^{-1}$
g	$10^1 ms^{-2}$

We can show that for the case of filament stretching of dough, all other terms can be considered negligible to the stress difference by evaluating their ratios:

$$\frac{\text{Surface tension}}{\text{Stress difference}} = \frac{\sigma_s R_0 e^{-\frac{1}{2}\dot{E}t}\pi}{\eta\dot{E}R_0^2 e^{-\dot{E}t}\pi} = \frac{\sigma_s e^{\frac{1}{2}\dot{E}t}}{\eta\dot{E}R_0} \sim 10^{-4} = Ca^{-1}$$

$$\frac{\text{Gravitational force}}{\text{Stress difference}} = \frac{\rho g R_0^2 L_0\pi}{2\eta\dot{E}R_0^2 e^{-\dot{E}t}\pi} = \frac{\rho g L_0 e^{\dot{E}t}}{2\eta\dot{E}} \sim 10^{-2} = \frac{Bo}{Ca} \tag{3.23}$$

$$\frac{\text{Inertia}}{\text{Stress difference}} = \frac{\rho\pi R_0^2 L_0^2\dot{E}^2 e^{2\dot{E}t}}{4\eta\dot{E}R_0^2 e^{-\dot{E}t}\pi} = \frac{\rho L_0^2\dot{E}e^{3\dot{E}t}}{4\eta} \sim 10^{-4} = \text{Re}$$

We conclude that capillary, gravitational and inertia effects are insignificant compared to the visco-elastic forces within the dough under filament stretching

for strain rates investigated in these experiments. Thus the force balance simply results in the following relationship:

$$\tau_{zz}(t) - \tau_{rr}(t) = \frac{F_p(t)}{\pi R_{mid}^2(t)} = \frac{4F_p(t)}{\pi D_{mid}^2(t)} \tag{3.24}$$

Initially, some crude filament stretching experiments were performed on the Texture Analyzer TA.XT2, we identified the need to improve on the systematic handling and loading of samples, especially during the mounting procedures. For this purpose, we designed and built a specialized end-plate assembly. Using this assembly, the sample could be mounted, pressed to the required thickness and cut into the required diameter, then allowed to relax without further deformation before mounting onto the FISER for testing. The design is illustrated below in Figure 27.

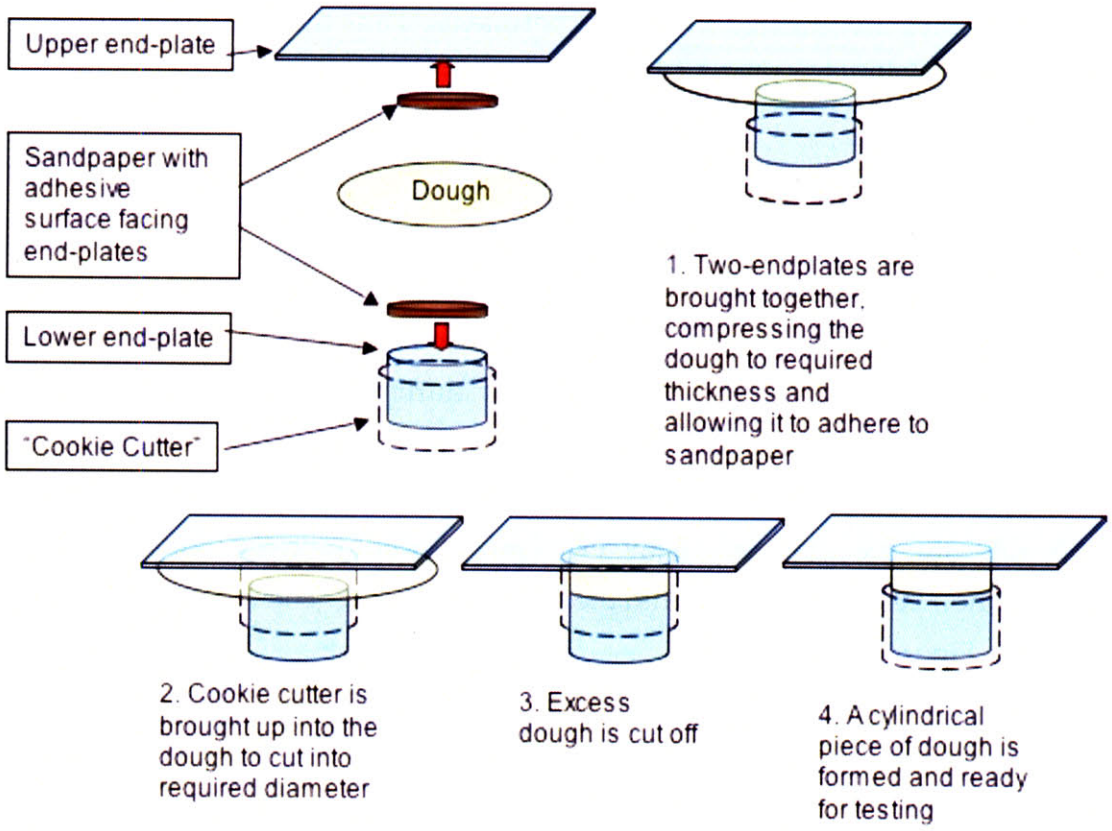

Figure 27 Procedures for preparing dough samples

Self-adhesive sandpaper was attached onto each end of the custom built end-plates. A sample of dough was then placed between them and pressed to the required thickness. The cookie cutter was then used to cut the sample into a cylindrical shape of the same diameter as the lower end-plate.

Dough sample of approximately 5g were mounted on to the customized end-plates. They are compressed to a thickness of 2.5mm then cut into a disc shape with radius 19.05mm. Next, a pre-stretch was performed so that the disc of dough was elongated to a cylinder of height 7.5mm and diameter of approximately 7.5mm, which is an initial aspect ratio Λ_0 of 2. The sample was painted with a thin film of silicone oil and left to relax for 30 mins before testing.

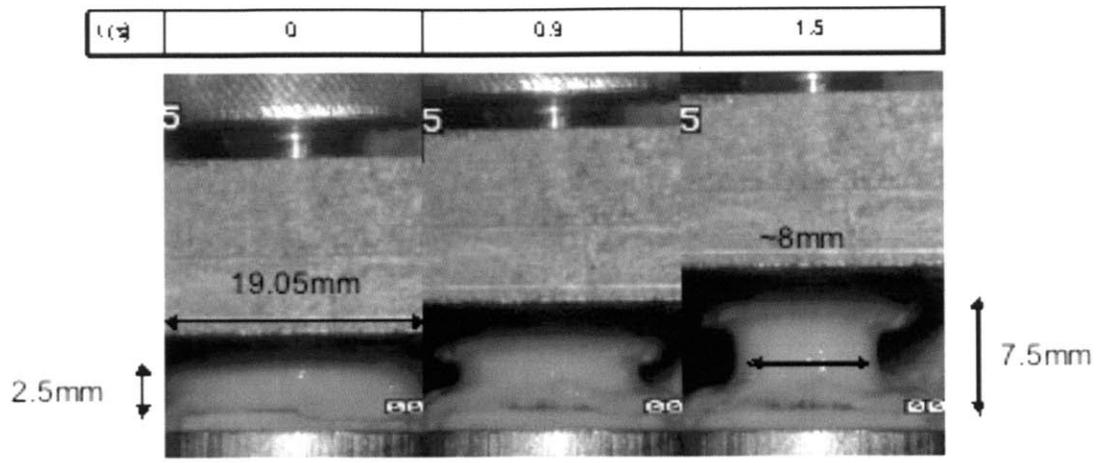

Figure 28 Pre-stretch of sample

The purpose of the pre-stretch is two-fold. Firstly, it increases the aspect ratio, by-passing the initial "lubrication" flow regime. The filament can be considered as almost cylindrical through most of the experiment. This greatly simplify the kinematics as discussed in the previous section. Secondly, the cross-sectional area is reduced, thus reducing the adhesive load required at the end-plates.

The thin film of silicone oil prevents excessive drying of sample. Vegetable oil and glycerol is not used because we found that the dough can absorb some of this coating fluid. The silicone oil used has viscosity 100 Pa s. This viscosity was selected so that it the oil is thick enough to resist draining by gravity yet not provide any significant contribution to the force balance in equation (3.21).

During the 30 minutes of relaxation, the force drops from 10^{-1} to 10^{-2} N. The length of relaxation was established through trial and error; experiments with shorter period of relaxation showed poor repeatability.

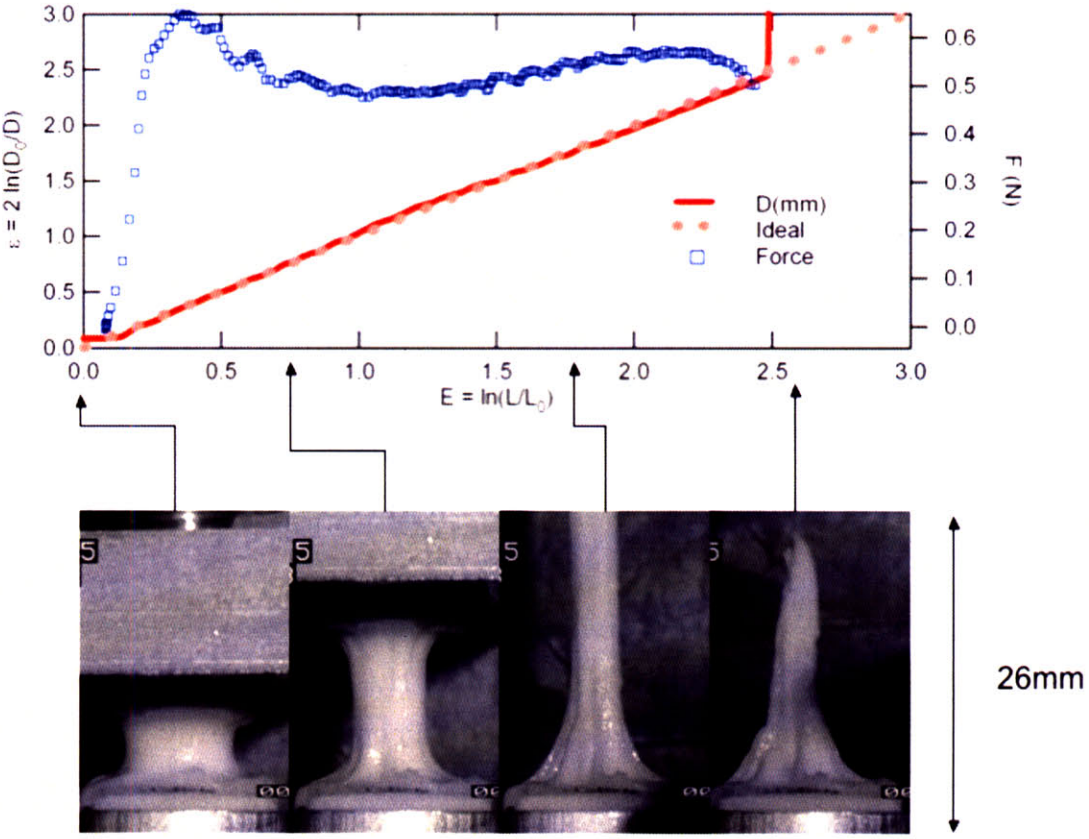

Figure 29 Typical Force/Diameter vs time data from FISER

Presented in Figure 29 are typical results obtained from filament stretching experiments. The diameter decreases exponentially (straight line on a log-linear scale), corresponding to a linear increase of strain in time. The profile of the stretched sample strongly resembles a cylinder because of reasons discussed in the previous section and the extreme care in ensuring a uniform initial condition. We note that over most of the experiment, $\varepsilon = E$, i.e. uniform uni-axial extension.

SER Method

More recently, Sentmanat et al developed a technique (Sentmanat Extensional Rheometer or SER) that is well-suited for materials with high viscosity range [120-122]. Compared to the specialized techniques of filament stretching (see previous) and other extensional rheometers [123], the greatest advantage of this

system is that it is a simple extension to the conventional rotational rheometer technique. Samples are prepared by pressing and cutting the dough into rectangular sheets of known initial dimensions. The sheets were coated with a layer of silicone oil to prevent drying and mounted onto two cylindrical drums as shown in Figure 30. The two drums are interconnected with a gearing system [120-122] to counter-rotate and stretch the sample.

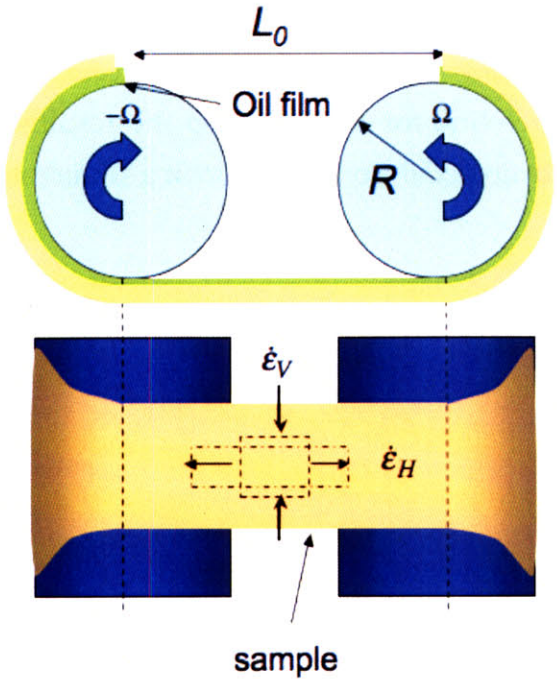

Figure 30 Schematic of the Sentmanat Extensional Rheometer. Sample is stretched between two counter rotating cylindrical drums.

The tension F within the sample can be inferred from the torque T acting on the drums.

$$F \simeq T/2R \qquad (3.25)$$

The nominal extensional strain rate in the horizontal direction (H) is given by:

$$\dot{E}_H = 2\Omega R/L_0 \quad (3.26)$$

In existing work with the SER, the deformation has always been assumed to be a purely affine uni-axial deformation such that $\dot{\varepsilon}_H = \dot{E}_H = -2\dot{\varepsilon}_V$ (where V is the vertical direction as shown in the figure). However the layer of low viscosity oil coating the dough can lead to partial slip between the sample and the drums. It is thus essential to directly measure the true deformation rate in the sample. Similar systematic differences between the imposed and actual deformation rates are well-known in other extensional rheometer designs that use strips of viscoelastic material [124]. As shown in Figure 31, we use an initially rectangular grid that is painted onto the dough to follow the homogeneity of deformation with high speed digital video. After correcting for the fluid slip the resulting strains were found to indeed approximate uni-axial elongation but at a strain rate 25% slower than the nominal rate.

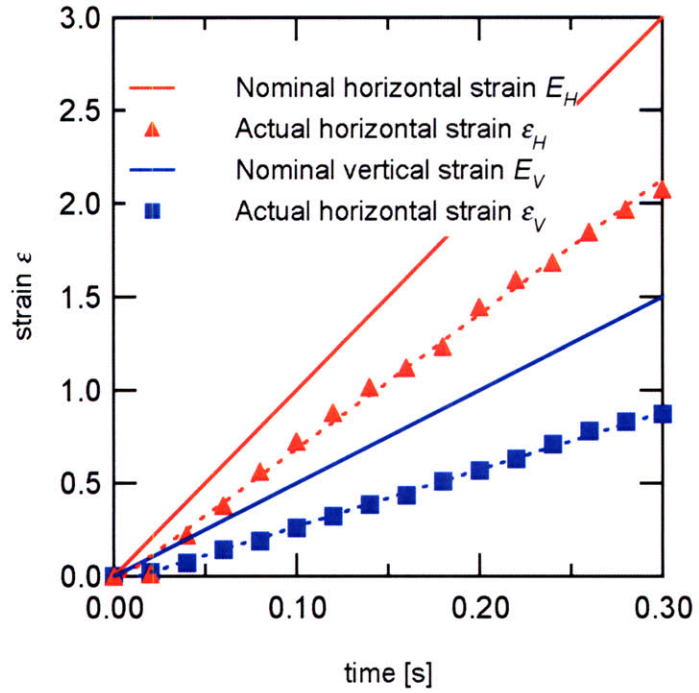

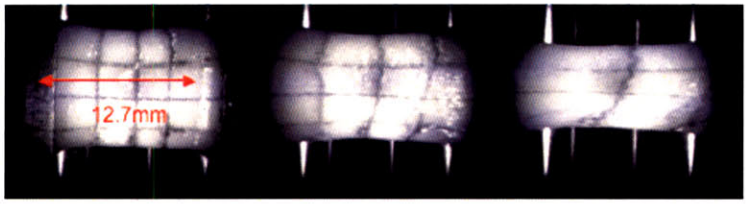

$\varepsilon = 0$ $\varepsilon = 0.6$ $\varepsilon = 2.1$

Figure 31 Deformation of a dough sample on the SER at $\dot{E} = 10s^{-1}$. Slip leads to an actaual deformation rate in the sample that is ~25% slower than the nominal imposed value; however the strains remain approximately uni-axial. True strains were calculated by measuring the change in length of material lines marked on the surface of the undeformed dough sample.

Results obtained from this method were found to be in good agreement to data from filament stretching (Figure 32).

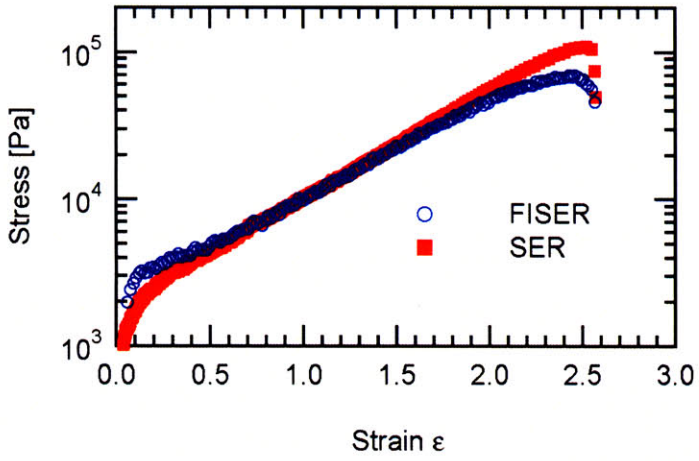

Figure 32 Comparison of extensional behavior of a wheat flour dough recorded on the FISER vs SER at $\dot{E} = 0.3s^{-1}$.

3.6. Conclusion

In this thesis, we focus on test methods described in the latter part of this section. The mixograph, extensigraph and alveograph suffer from a lack of control and information concerning the actual deformation of the dough. Furthermore, these experiments are usually performed at a constant rotation rate/inflation rate/cross-hair speed, rather than constant strain-rate. Achieving a constant strain-rate through a specific profile of inflation/cross-hair movement is not possible either, because the actual strains are not known. Controlling and understanding the kinematics of these tests is important; it allows us to translate the results to fundamental rheological quantities such as stress and strain; by controlling the rate of deformation so that the strain rate is constant, we can obtain true material functions such as transient extensional viscosities. Material functions serve to classify fluids, they are used to determine constants in non-Newtonian constitutive equations. By using the more well controlled techniques we can accurately reproduce the viscometric flows required to assess these material functions. We conclude by summarizing the relative deformation range

possible on these rheometric techniques and their relevance to dough baking performance in Figure 33.

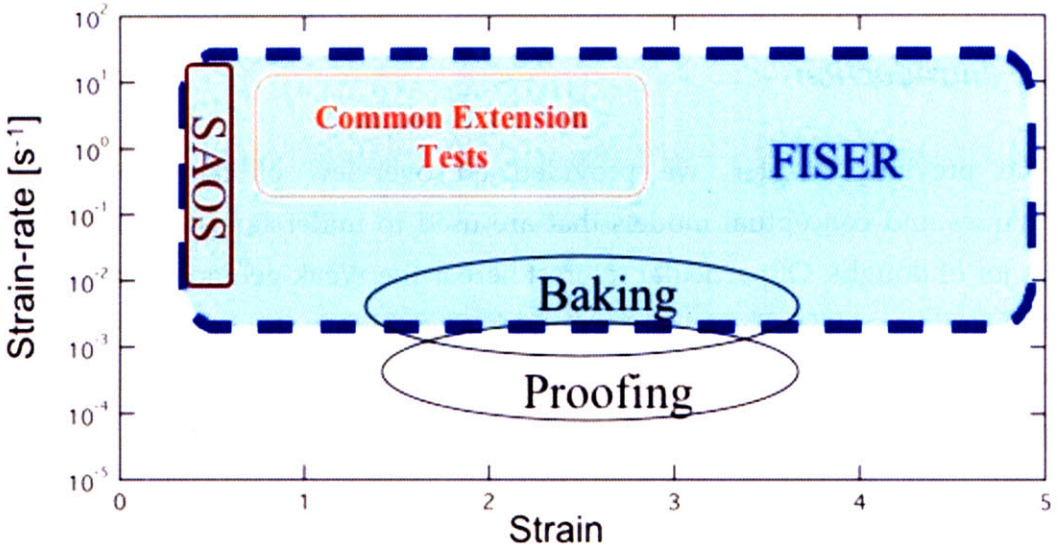

Figure 33 Operation chart of typical rheological tests on dough.

4. Power law rheology of doughs

4.1. Introduction

In the previous chapter, we provided an overview of the experimental techniques and conceptual models that are used to understand the mechanical behavior of doughs. Of particular interest here is the Weak-gel model introduced by de Cindio et al [69]. The advantage of this model lies in its simplicity: it is able to describe the rheology of a wide range of dough like materials with a surprising degree of accuracy.

We first ask the question: are current opinions on dough microstructure compatible with the idea of a critical gel like material? Various researchers have come to the consensus that the gluten macropolymer forms a three-dimensional network throughout the dough [8, 48, 49]. The initially distinct gluten molecules in the flour swell in size due to hydration and begin to interact with neighboring glutenin molecules in the process of mixing/working. The large molecular weight of the gluten macropolymer is essential to form a critical number of interactions. This gives rise to a sample-spanning structure that imbues the dough its elasticity. This process can be viewed as a form of physical gelation [77].

In this chapter, we present linear viscoelastic data that confirms the suitability of using the gel model as a basis for studying dough. Our investigation then moves to deformations of larger magnitudes and we will discuss the mechanical response of the dough under these different conditions in context of the gel model. Detailed mathematical derivations will be dealt with in a later chapter.

Linear Viscoelasticity of Dough

The linear viscoelastic properties of doughs have been well studied in the past and are known to contain a very broad spectrum of relaxation processes [17, 61,

125]. Recently it has been suggested by de Cindio and co-workers [69] that a simple way of describing the linear visco-elastic properties is through the critical gel model of Winter and Chambon [74, 76].

At the critical gel point, the stress relaxation modulus follows a power-law–like decay and is described by the gel equation:

$$G(t) = St^{-n} \tag{4.1}$$

Where S is the gel strength and n is the gel exponent. This behavior is illustrated in Figure 34 (a). Note that for small strains ($\gamma \sim 10^{-3}$), the relaxation modulus is roughly independent of strain amplitude, i.e. within the viscoelastic range.

With the appropriate Fourier transformation [74], one can show that the linear viscoelastic response in an oscillatory shear flow also behaves in a power-law fashion:

$$G' = \frac{G''}{\tan(n\pi/2)} = \Gamma(1-n)\cos(n\pi/2)S\omega^n \tag{4.2}$$

where $\Gamma(n)$ is the gamma function. This behavior is confirmed in Figure 36 (a). The gel parameters obtained by fitting to Figure 34 (a) (S = 6068 Pa s^n, n = 0.23) and Figure 36 (a) (S = 5060 Pa s^n, n = 0.21) are consistent, thus confirming the validity of using the critical gel model for describing the mechanical behavior of bread dough under small strain deformations. We will also show in the next section that the critical gel model is also a suitable constitutive model for doughs formed from a range of flour types, water content and mixing time.

Values of n are surprisingly similar for different dough varieties, they typically fall between the range $0.15 < n < 0.3$. The values for the gel strength S can vary by an order of magnitude ($10^3 < S < 10^4$ Pa s^n), and is extremely sensitive to factors such as water content, protein composition and mixing time (See next section).

The power law relaxation behavior persists throughout the range of time scales that can be practically studied on a conventional rheometer. There are some slight hints of a flattening out of the slopes at long time scales or low frequencies suggesting that the system is slightly to the gel side of the critical gel point (i.e.

solid like behavior). However we discuss in a later chapter how such measurements at long time scales are inherently inaccurate for a slowly relaxing powerlaw like system; effects of thixotropy and residual relaxation from the loading process are convoluted with the true relaxation resulting from the experimental deformation.

Large strain deformation of dough

The gel equation was initially developed to describe linear viscoelastic deformations. However, non-linear behavior becomes apparent in doughs even at relatively small strains ($\gamma \sim 10^{-3}$) and are depicted graphically in Figure 34 (a). We note a decrease in relaxation modulus as the strain amplitude of the step strain is increased. Since the slope on the log-log plot remains unchanged, we can conclude that this softening can be described as simply a decrease in the gel strength S with little change to the gel index n. We account for the decrease in modulus through a damping function $h(\gamma)$ as shown in Figure 34c. In Figure 34b, we show that the damping function is simply a vertical shift factor that collapses the data onto a single master curve and can be described by the following expression:

$$h(\gamma) = \frac{1}{1 + q\gamma^{2k}} \tag{4.3}$$

where q = 13.51, k = 0.2 are fitted constants. Through this expression, we can show quantitatively that the non-linearities begin at very small strains: $\gamma^* \sim q^{-1/(2k)} = 1.5 \times 10^{-3}$.

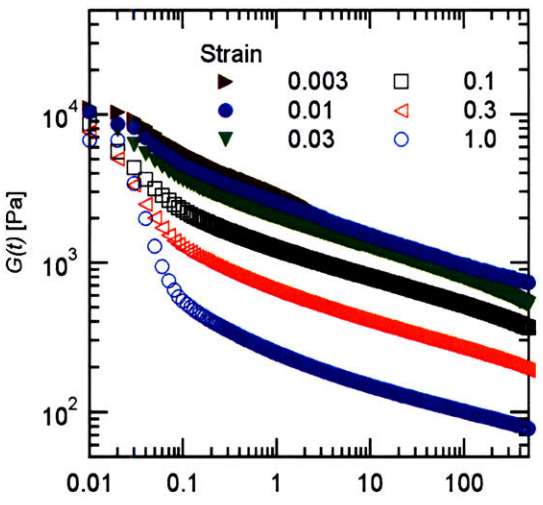

a.

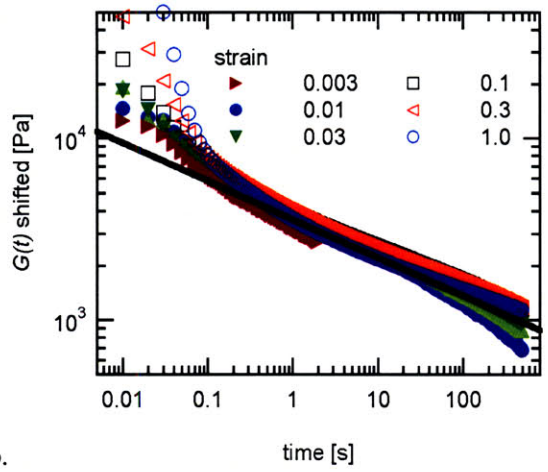

b.

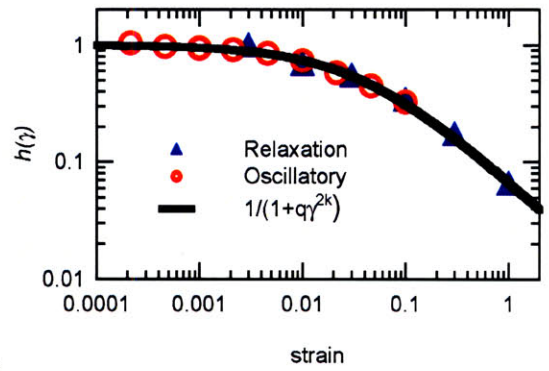

c.

Figure 34 a. Stress relaxation showing power-law–like behavior. b. Stress relaxation curves can be scaled to lie on a single curve through a damping function. c. The damping function $h(\gamma)$ as a function of the imposed strain amplitude. q =13.51, $k = 0.2$

To formally describe the corresponding non-linear properties in large straining deformations of dough, we construct a rheologically admissible constitutive

equation of Lodge rubber-like liquid form by combining the linear viscoelastic relaxation modulus of the critical gel with finite strain kinematics [126][2].

We first consider a simplified equation in which the dough behaves like a quasi-linear material. Mathematically, this is equivalent to setting the damping function $h(\gamma)$ to unity. This, as we have already showed, is far from the actual measured damping function (equation (4.3)), but will be a useful for considering the general form and behavior of the full constitutive equations. With the appropriate finite strain measure and using the Lodge Rubber-like Liquid description for the kinematics [75, 77], the constitutive equation can be written as:

$$\sigma(t) = -\int_{-\infty}^{t} G(t-t')h(\gamma)\gamma_{[1]}(t,t')dt' \tag{4.4}$$

$$\sigma(t) = -\int_{-\infty}^{t} G(t-t')\gamma_{[1]}(t,t')dt' \quad \text{for } h(\gamma) = 1 \tag{4.5}$$

Where $G(t)$ is the relaxation modulus from (4.1) and $\gamma_{[1]}$ is the finite strain rate tensor, defined by:

$$\gamma_{[1]}(t,t') = \frac{\partial}{\partial t'}\gamma_{[0]}(t,t') = -\frac{\partial}{\partial t'}C^{-1}(t,t') \tag{4.6}$$

and $\gamma_{[0]}$ is the finite strain tensor [60] and C^{-1} is the finger strain tensor.

---

[2] Tanner et al, also independently realized how the Lodge Rubber-like liquid formulation can be used to extend the useful range of the gel equation for describing nonlinear deformations of wheat flour doughs 127. Tanner, R.I., F. Qi, and S.-C. Dai, Bread Dough Rheology and Recoil I. Rheology. Journal of Non-Newtonian Fluid Mechanics, 2007. Accepted Manuscript..

Instead of a damping function, they used a damage function which records the amount of irreversible damage and softening accumulated by the dough i.e. The gel equation is multiplied by the damage function outside the integral.

The resulting set of equations (4.4) - (4.6) can be integrated for different kinematics to evaluate the stress in the dough at large strains.

We first discuss this in the context of start up of steady shear flows. The shear component of the rate of strain tensor for this flow is given by:

$$\gamma_{xy[1]} = \dot{\gamma}_0 \tag{4.7}$$

This strain rate is substituted into equation (4.5) to give an expression for the transient shear stress:

$$\begin{aligned} \sigma_{xy}^{+} &= \frac{S\dot{\gamma}_0}{1-n} t^{1-n} \\ &= \frac{S}{1-n} \dot{\gamma}_0^{n} \gamma^{1-n} \\ &= Sf(\dot{\gamma}_0)\Phi(\gamma) \end{aligned} \tag{4.8}$$

The expression predicts a power law growth in shear stress in time and strain. Furthermore, we note that the equation is of a time-strain separable form: the expression for stress can be written in terms of a rate dependent function $f(\dot{\gamma}_0) = \dot{\gamma}_0^{n}$ multiplied by a master strain function $\Phi(\gamma) = \gamma^{1-n}/1-n$.

In general, for $h(\gamma) \neq 1$, $\sigma_{xy}^{+} = Sf(\dot{\gamma}_0)\Phi(\gamma)$.

We compare these predictions to the actual experimental transient stress growth in Figure 35 (a) for a range of strain rates $\dot{\gamma}_0 = 0.01 - 10\ s^{-1}$. All the curves appear to follow a similar linear viscoelastic regime at small strains and short times and begin to deviate as the rate of increase in transient shear viscosity decreases. The curves also show an over shoot at large strains.

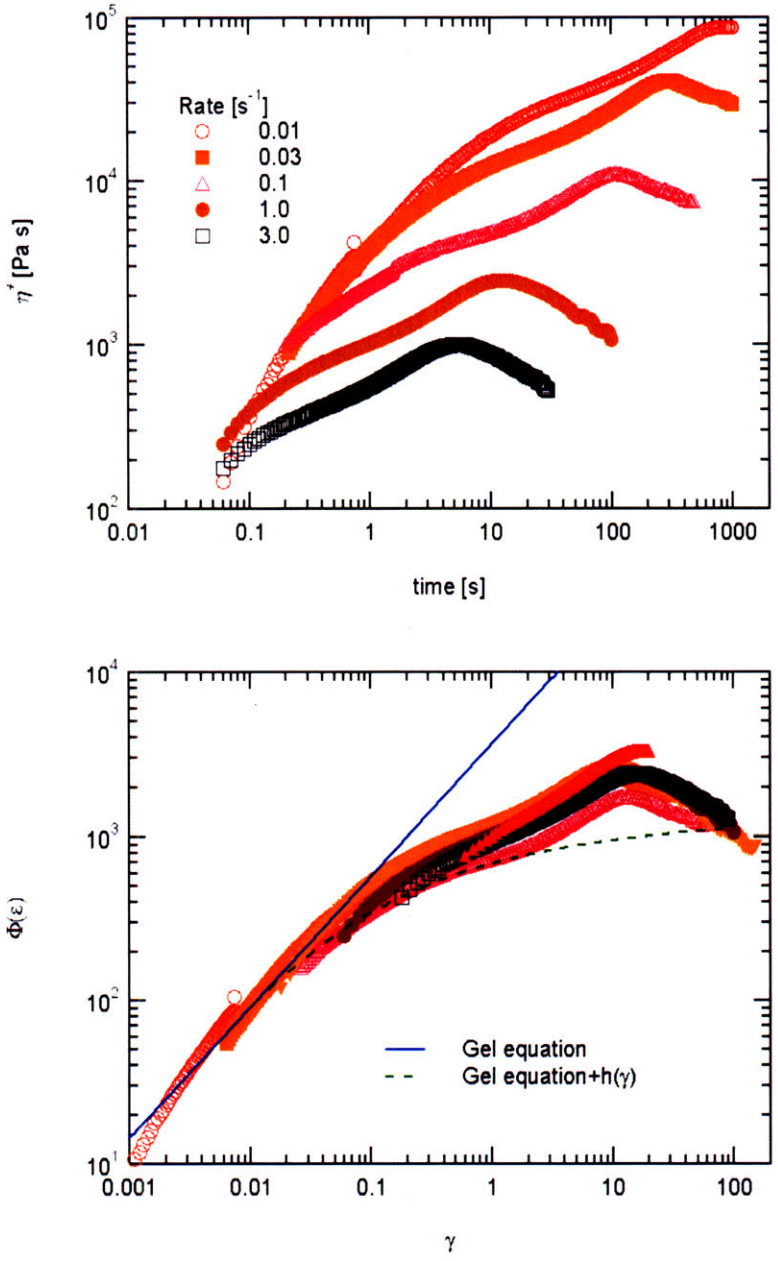

Figure 35 (a) Transient start-up of steady shear of a typical flour water dough. (b) Data can be collapsed onto a master strain function.

In Figure 35 (b) we show that a master strain function can indeed be obtained by dividing the transient shear stress by the rate dependent function $f(\dot{\gamma}_0) = \dot{\gamma}_0^n$. S = 6032 Pa s^n and n = 0.22 are obtained through linear viscoelastic measurements discussed in the previous section and we stress that there are no additional fitted

parameters. However, the master strain function $\Phi(\gamma)$ obtained from the experimental data is of a different form to that predicted by equation (4.8): it deviates from the power law growth $\sim\gamma^{1-n}$ (solid line) at small strains ($\gamma^* \sim 1.5\times10^{-3}$). This of course is not surprising, for we have neglected the damping function in the formulation of the simplified equation. Therefore to account for this softening, we reinsert the damping function and solve the equation numerically. This gives a much improved prediction that is valid up to $\gamma \sim 2$. The modified equation is still unable to predict the stress overshoot, and it is possible to further improve on the model by including strongly non-linear elastic terms in the manner of Phan-Thien et al [104]. However, we suspect that part of the reason for the failure of the constitutive model lies in the fact that the sample undergoes a viscometric instability: the strong normal stresses at these strains causes the edges of the sample to deform non-uniformly and eventually leads to it being completely ejected from the gap. Since, the flow ceases to be viscometric around this instability, we do not expect any constitutive model to give an accurate prediction of the shear stresses unless the full dynamic equations are solved together with the kinematics. This issue is discussed in greater detail in the section concerning gluten gels under the same deformation.

Nevertheless, the time-strain factorazibility is an interesting feature of the generalized gel equation and we shall see how it is also applicable to material functions in other start-up of steady flows.

Moving on, we next consider the case of transient uniaxial extension, the finite strain rate tensor takes the form:

$$\boldsymbol{\gamma}_{[1]} = \frac{\partial}{\partial t'}\boldsymbol{\gamma}_{[0]} = \dot{\varepsilon}_0\begin{bmatrix} -\exp\left[-\dot{\varepsilon}_0(t-t')\right] & 0 \\ 0 & 2\exp\left[2\dot{\varepsilon}_0(t-t')\right] \end{bmatrix} = \begin{bmatrix} -\lambda_r^2 & 0 \\ 0 & 2\lambda_z^2 \end{bmatrix} \qquad (4.9)$$

Substituting eq. (4.1) and eq. (4.9) into eq. (4.5) results in an integral equation for the stress field as a function of strain rate and elapsed time.

$$\sigma_{zz} - \sigma_{rr} = -\int_0^t S(t-t')^{-n}\left[2\dot{\varepsilon}_0\exp\left(2\dot{\varepsilon}_0\left[t-t'\right]\right) + \dot{\varepsilon}_0\exp\left(-\dot{\varepsilon}_0\left[t-t'\right]\right)\right]dt' \qquad (4.10)$$

First perform a change of variable such that

$$
\begin{aligned}
r &= t - t' \\
dt' &= -dr \\
t' = t &\rightarrow r = 0 \\
t' = 0 &\rightarrow r = t
\end{aligned}
$$

$$
\begin{aligned}
\sigma_{zz} - \sigma_{rr} &= S\int_{t}^{0} r^{-n}\left[2\dot{\varepsilon}_0 \exp\left(2\dot{\varepsilon}_0 r\right) + \dot{\varepsilon}_0 \exp\left(-\dot{\varepsilon}_0 r\right)\right]dr \\
&= -S\int_{0}^{t} r^{-n}\left[2\dot{\varepsilon}_0 \exp\left(2\dot{\varepsilon}_0 r\right) + \dot{\varepsilon}_0 \exp\left(-\dot{\varepsilon}_0 r\right)\right]dr
\end{aligned}
\tag{4.11}
$$

This integral expression can then be integrated by parts:

$$
\begin{aligned}
\frac{\sigma_{zz} - \sigma_{rr}}{-S} &= \int_{0}^{t} r^{-n}\left[2\dot{\varepsilon}_0 \exp\left(2\dot{\varepsilon}_0 r\right) + \dot{\varepsilon}_0 \exp\left(-\dot{\varepsilon}_0 r\right)\right]dr \\
&= \left[\frac{r^{1-n}}{1-n}\left[2\dot{\varepsilon}_0 \exp\left(2\dot{\varepsilon}_0 r\right) - \left(-\dot{\varepsilon}_0\right)\exp\left(-\dot{\varepsilon}_0 r\right)\right]\right]_0^t \\
&\quad - \int_{0}^{t} \frac{r^{1-n}}{1-n}\left[\left(2\dot{\varepsilon}_0\right)^2 \exp\left(2\dot{\varepsilon}_0 r\right) - \left(-\dot{\varepsilon}_0\right)^2 \exp\left(-\dot{\varepsilon}_0 r\right)\right]dr \\
&= \frac{t^{1-n}}{1-n}\left[2\dot{\varepsilon}_0 \exp\left(2\dot{\varepsilon}_0 t\right) - \left(-\dot{\varepsilon}_0\right)\exp\left(-\dot{\varepsilon}_0 t\right)\right] \\
&\quad - \left[\frac{r^{2-n}}{(2-n)(1-n)}\left[\left(2\dot{\varepsilon}_0\right)^2 \exp\left(2\dot{\varepsilon}_0 r\right) - \left(-\dot{\varepsilon}_0\right)^2 \exp\left(-\dot{\varepsilon}_0 r\right)\right]\right]_0^t \\
&\quad + \int_{0}^{t} \frac{r^{2-n}}{(2-n)(1-n)}\left[\left(2\dot{\varepsilon}_0\right)^3 \exp\left(2\dot{\varepsilon}_0 r\right) - \left(-\dot{\varepsilon}_0\right)^3 \exp\left(-\dot{\varepsilon}_0 r\right)\right]dr
\end{aligned}
$$

This process is applied repeatedly to yield a summation:

$$
-\frac{\sigma_{zz} - \sigma_{rr}}{S} = \sum_{m=1}^{\infty}(-1)^{m+1} \frac{t^{m-n}\left[\left(2\dot{\varepsilon}_0\right)^m \exp\left(2\dot{\varepsilon}_0 t\right) - \left(-\dot{\varepsilon}_0\right)^m \exp\left(-\dot{\varepsilon}_0 t\right)\right]}{(m-n)\ldots(1-n)}
\tag{4.12}
$$

Equation (4.12) can be simplified by recasting it in terms of the dimensionless variable Φ_{Ext}:

$$\Phi_{Ext} = -\frac{\sigma_{zz} - \sigma_{rr}}{S\dot{\varepsilon}_0^n}$$
$$= \sum_{m=1}^{\infty}(-1)^{m+1}\frac{\dot{\varepsilon}_0^{m-n}t^{m-n}\left[(2)^m\exp(2\dot{\varepsilon}_0 t) - (-1)^m\exp(-\dot{\varepsilon}_0 t)\right]}{(m-n)...(1-n)} \quad (4.13)$$

Substituting for $\varepsilon = \dot{\varepsilon}_0 t$ we arrive at the master strain function:

$$\Phi_{Ext} = \sum_{m=1}^{\infty}(-1)^{m+1}\frac{\varepsilon^{m-n}\left[(2)^m\exp(2\varepsilon) - (-1)^m\exp(-\varepsilon)\right]}{(m-n)...(1-n)} \quad (4.14)$$

The stress exhibits a power-law dependence on strain rate and a more complex dependence on strain. This expression is represented by the dotted lines in Figure 36b and c. We also note that Eq. (4.14) has an asymptotic limit in the form given by $(\sigma_{zz} - \sigma_{rr}) \sim \exp(2\varepsilon)$ at large strains, i.e. an affine scaling in strain. After the rate dependence is factored out by dividing the measured stress by the known power-law dependence on the strain rate (i.e. $f(\dot{\varepsilon}_0) = \dot{\varepsilon}_0^n$, experiments from a range of strain rates can be collapsed onto a single curve that defines a strain function $\Phi(\varepsilon)$ of the following form:

$$\Phi(\varepsilon) = (\sigma_{zz} - \sigma_{rr})/(S\dot{\varepsilon}^n) \quad (4.15)$$

The function $\Phi(\varepsilon)$ is shown Figure 36(c) and is of simple exponential form. This *factorizability* of the rate-dependence in dough rheology is a consequence of the power-law dependence of the relaxation modulus on time t (see eq. 6) and is applicable to both shearing and extensional deformations.

a.

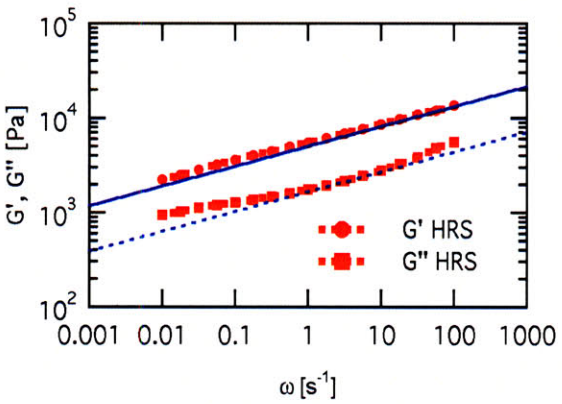

b.

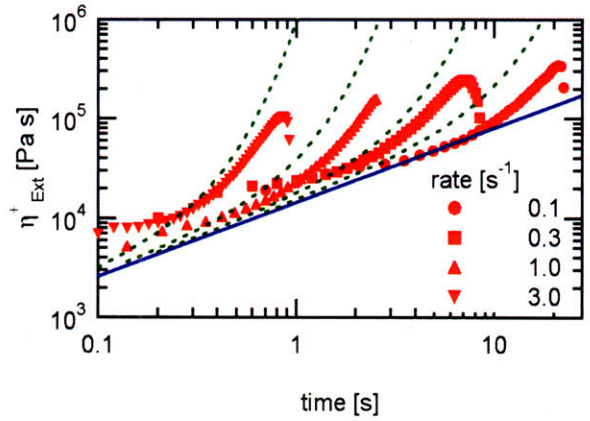

c.

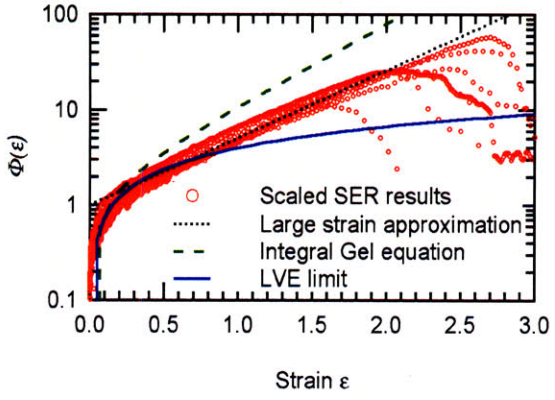

Figure 36. Critical gel-like behavior exhibited by dough: (a). in small amplitude oscillatory shear flows; solid lines are the fits to equation (4.2), S=5060 Pa.s^n, n=0.21; (b). in transient uniaxial extension. Dotted line represents predictions using a Lodge Rubber-like liquid constitutive relation with the relaxation modulus determined from (a). The solid line marks the linear viscoelastic limit. (c). Based on the gel equation scaling (equation (4.13)), we factor out the strain-rate dependence. The remaining strain-dependent function $\Phi(\varepsilon)$ is plotted on semilog axes. Experiments conducted at different strain rates now collapse onto a single curve.

Although this Rubber-Like Liquid model offers an improved description to the linear viscoelastic response (shown by the broken lines in Figure 36 (b) and (c)) it clearly over-predicts the experimentally measured response. This relative strain-softening (as compared to a purely affine strain response) is due presumably to changes in the network structure with the progressive deformation and disruption of the physical crosslinks between the glutenin molecules and starch granules. Similar to the case of shear flows, an appropriate strain-softening or *damping function* can be used to account for this phenomenon. At large strains the stress appears to tend toward a simple exponential function $\exp(k\varepsilon)$ as shown in Figure 36 (c) by the black dotted line. An estimate of this damping function can be calculated from the ratio of the large strain approximations to the asymptotic limit of the integral gel model of Eq. (4.14).

Conclusions

We observed striking similarity in the linear viscoelastic response between a critical gel and our model dough system that confirmed the suitability of using a powerlaw relaxation function to build up a constitutive equation. This led us to use the gel equation of Chambon and Winter as a starting point in formulating a rheologically admissible constitutive equation capable of describing finite deformations in shear (step strain) and elongation. The resulting predictions of the transient stress evolution in the deforming dough specimen are greatly improved; however the dough shows some additional strain softening at finite strains.

Thus to summarize, we find the generalized gel equation to be an appropriate description for the rheological behavior of dough:

$$\sigma(t) = -\int_{-\infty}^{t} S\left(t-t'\right)^{-n} h(\gamma)\gamma_{[1]}(t,t')dt' \qquad (4.16)$$

In this chapter, we have presented data from a single flour type at fixed water content and mixing time, thus the all the material parameters (S, n, $h(\gamma)$) are held constant. In effect, we have changed the functional form of $\gamma_{[1]}$ by utilizing

different rheological experiments to measure these material parameters. It is gratifying to see that the measured values are consistent between the tests, thus confirming the validity of the gel model and the generalized gel equation. The time-strain separable form ($\sigma(t) = S\dot{\gamma}_0^n \Phi(\gamma)$ for start-up of steady flows) predicted by this equation is confirmed and will be a useful way of collapsing data over a range of strain rates. In the next section, we see how each of the material parameters introduced here varies with different dough conditions.

4.2. *Rheological aging*

The difficulty of testing dough is compounded by the fact that freshly mixed dough sample shows rheological aging. The stiffness of a dough was found to increase gradually in time even when left undisturbed – presumably due to an evolution of the microstructure. This phenomena is first quantitatively reported by Hibberd et al [14] (see chapter 2). Samples left sitting undisturbed will show a gradual change of properties. This has important implications regarding experimental techniques, special procedures must be adhered to to ensure samples are tested at the same "age".[3]

Typically, a predetermined amount of rest time (~1hr) is set for the dough to rest after mixing and another period (~1hr) for the sample to rest after being mounted onto the rheometer [6]. But this can lead to many practical issues: to perform test on a dough at the same age, a new batch has to be mixed up and rested for every single test. Other than being wasteful, the variability introduced through each round of mixing and sample loading is greatly increased and will more often than not offset any potential gain in accuracy from the regimented resting procedure. A technique that allows the rheologists to use the same batch of mixed dough will greatly increase the efficiency and accuracy in testing.

---

[3] It is important to point out that in these experiments, the mass exchange between the surrounding environment and the samples are negligible since the samples are either coated or submerged in a bath of silicone oil.

Since the change in properties are associated with the evolution of microstructure, a possible way round the problem is to ensure a consistent state of microstructure at the beginning of each experiment. Such an idea has been routinely applied by scientists studying the rheological aging of other glassy gels such formed from laponite, bentonite etc... A high strain rate or stress (above the yield stress) is usually used to "breakdown" any structures within the sample, and tests are performed at a predetermined amount of time after the cessation of the high rate deformation [128].

In practice, the technique of high rate of shear over prolonged period is not suitable for breaking down structures within the dough because dough samples have the tendency to undergo a viscometric instability and roll out of gaps at shear strains of $\gamma \sim 10$. Therefore, as an alternative, a large amplitude oscillatory deformation is used. All samples are put through a few cycles (~5) cycles of oscillatory shear at strain amplitude of $\gamma_0 \sim 3$ immediately after loading, and tests are performed on the dough after a predetermined period (~1hr).

The validity of using this procedure to ensure consistent samples is illustrated in Figure 37. The magnitude and loss tangent of the dynamic modulus is plotted in the figure beginning from $t = 0$ corresponding to the cessation of the initial large amplitude oscillatory shear. From $0 < t < 3000$ s, the dynamic moduli is measured by applying a small amplitude oscillatory strain to the sample. The amplitude of this oscillation is small ($\gamma_0 = 10^{-3}$), so that the deformation does not interfere with the evolution of microstructure. Similar to the observations by Hibberd et al [17], the magnitude of the modulus gradually increases while the loss tangent remains constant. This growth in modulus is probably associated with a growth in microstructure. At $t = 3000$ s, a single cycle of oscillation at $\gamma_0 \sim 3$ is applied to breakdown this growing microstructure. A dramatic decrease in stiffness can be observed, but the growth resumes as soon as the large amplitude oscillation is ceased.

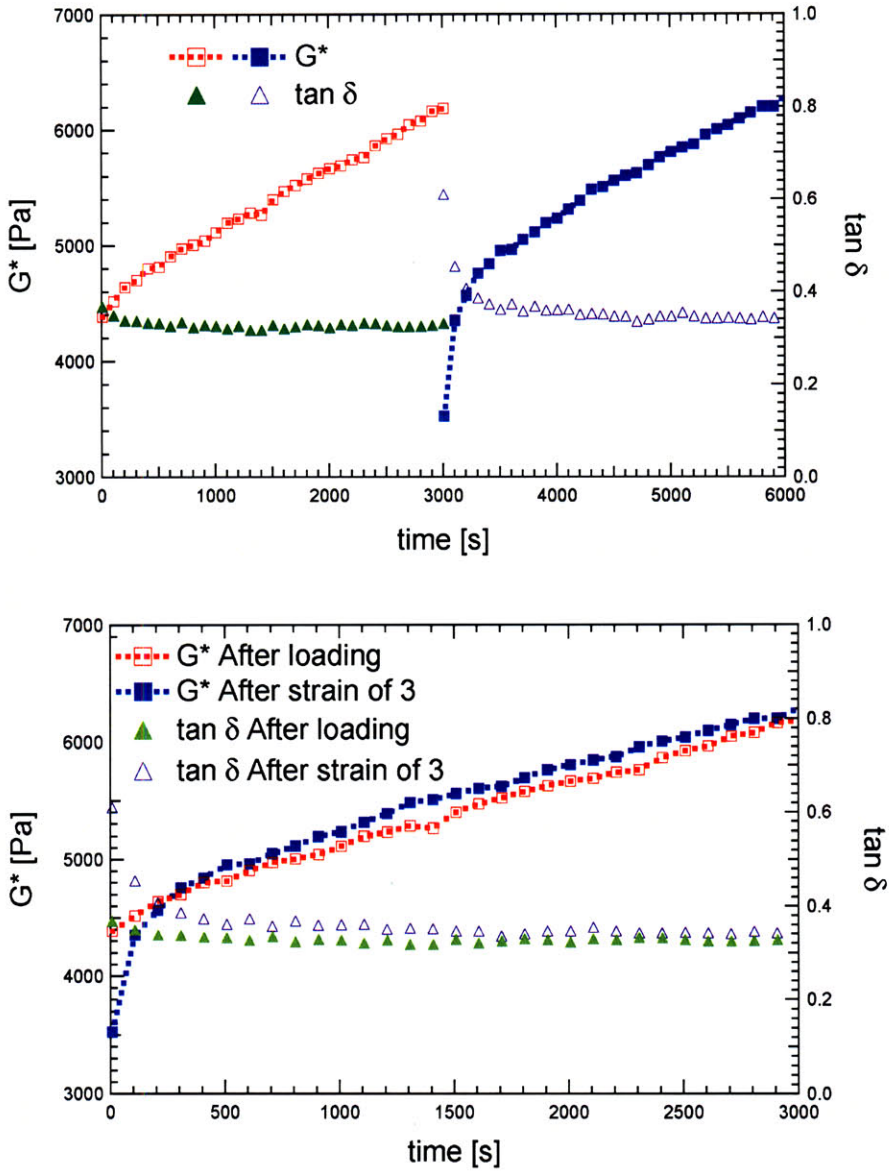

Figure 37 Magnitude and loss tangent of dynamic modulus of dough as a function of time. The amplitude of the oscillation is within the linear regime ($\gamma_0 = 10^{-3}$) and the temperature is held constant at 22°C so as to minimize/eliminate external disturbances that might affect the change in rheology/microstructure. At t = 3000 s, the amplitude of the oscillation is increased for one cycle to $\gamma_0 = 3$. A dramatic reduction in modulus can be observed which corresponds to a breakdown of microstructure. Upon the resumption of small amplitude oscillations, the modulus increases once again.

The manner of this growth is identical and is illustrated by overlaying the curves for $t < 3000$ s and $t > 3000$ s in Figure 37. This experiments confirms that samples can be brought to a consistent initial conditions by waiting for a predetermined amount of time after a large initial deformation. Furthermore, instead of discarding the dough sample after each tests, the sample can be used for further testing provided another round of large oscillatory shear is applied to it, and the same predetermined amount of time is allowed between the tests. It was found that by following these procedures, the repeatability and efficiency of doing rheological tests on dough can be greatly increased.

4.3. Effect of Water Content on Dough Rheology

The rheological reponse of dough depends on an extremely wide range of factors. A few obvious factors are flour formulation, water content, gluten content, glutenin/gliadin ratio and mixing time. Other less obvious factors which are difficult to control include ambient humidity and temperature, rest time etc. To gain an overall appreciation of the large amount of experimental results generated in the many studies conducted on such flour water systems and be able to view them in the correct context, it is essential to understand the consequence of varying each of these factors and how they are interlinked. In this document, we begin by studying the impact of water content in terms of its mixing properties, linear and non-linear rheology. We use a rheologically consistent methodology based on the gel equation and water moduli correspondence principle to quantify the respective effects.

The composition of the doughs used in the current study is reported in Table 2.

Flour	Added Water [g]	Total water content [Fraction]
HRS 30g 12% Initial moisture content	15	0.413
	16	0.426
	17	0.438
	18	0.450
	19	0.461
	20	0.472
	21	0.482
	22	0.492
	23	0.502
	24	0.511

Table 2 Composition of doughs used in current study. Water content of 0.45 was chosen as the reference condition (W_0)

Mixograph

30g of HRS flour and 19-23g of water was mixed in a National Mfg pin mixer for 600s. Assuming an initial moisture content of 12% within the flour, we estimate the mixture to have a water content fraction of 0.46-0.50. The resulting signal from the mixograph was plotted on Figure 38 as a function of time and water content. We found that a mixture containing less than 46% water required extremely high torque inputs from the mixograph. The lever arm for measuring torque was deflected all the way to the limiting stops. Therefore doughs with low water content were not included in Figure 38.

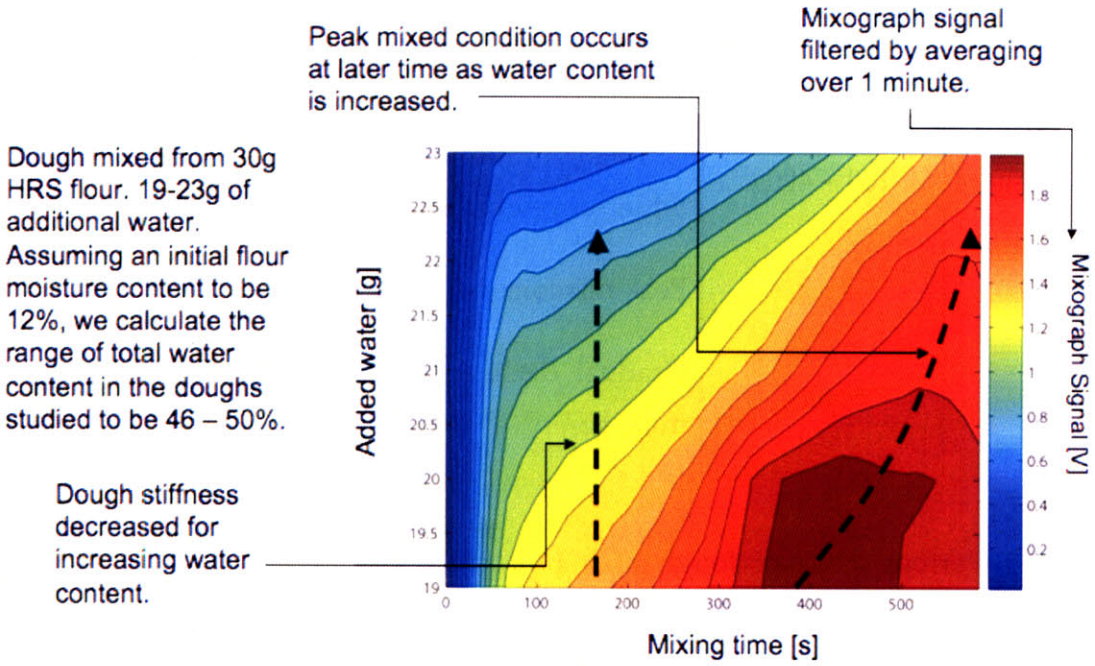

Figure 38 Mixograph torque input as a function of time and water content

In a chapter 3, we identified four key features for the slowly varying signal on a typical mixograph output strip-chart, these are summarized in Table 3.

Stage	Time	Feature
1	0 ~ < 100s	Rapid initial torque increase.
2	100 ~ 400s	Gradual torque increase. Usually associated with under-development.
3	420±20s	Peak mixed condition
4	> 400s	Gradual decline in torque. Referred to as over-mixing.

Table 3 Various stages of dough mixing.

We found the variation of water content has two significant impacts on the key features. First of all, increasing water content decreases the stiffness of the dough and the required mixograph torque. Secondly, the peak mixed condition was shifted progressively to longer times as the water content is increased.

Linear Viscoelasticity

The relaxation modulus of doughs can be reasonably well approximated over a significant time span (0 to 500s) as a power-law–like relaxation:

$$G(t) \simeq St^{-n} \tag{4.17}$$

where S [Pa s^n] is the gel strength (a measure of stiffness) and the dimensionless parameter n is the gel exponent which describes the rate of stress relaxation. This equation was found to successfully predict many aspects of linear visco-elasticity with only two parameters. The effect of water content on S and n for HRS doughs mixed for 360s are plotted in Figure 39.

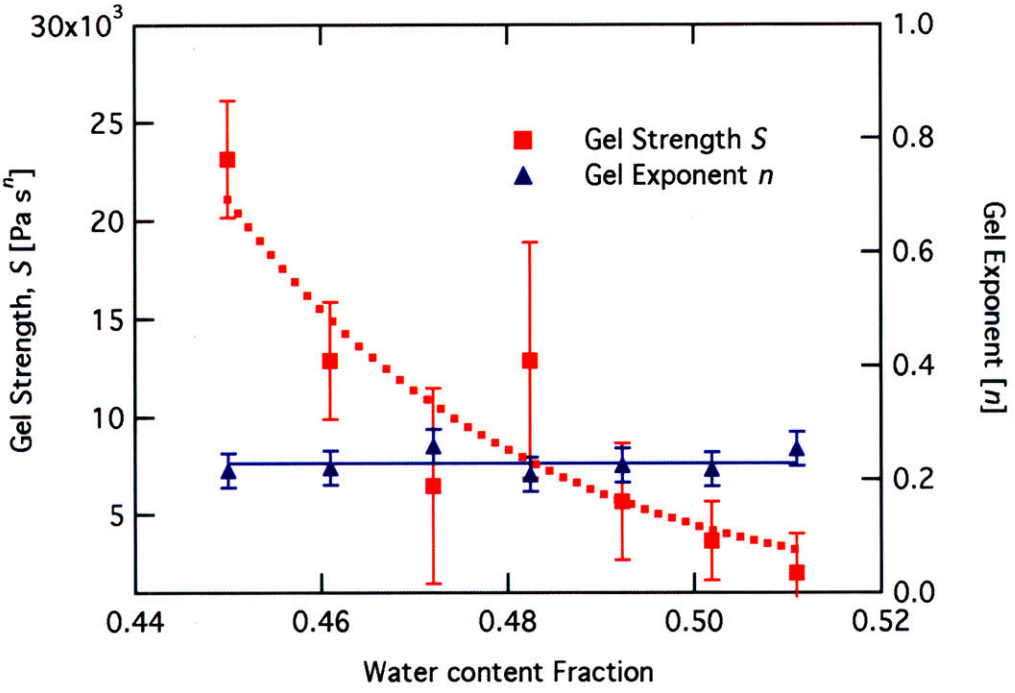

Figure 39 Effect of water content on linear visco-elastic properties. HRS flour, mixing time = 360s. Averaged between stress relaxation ($\gamma = 10^{-3}$), oscillation frequency sweep ($\gamma_0 = 10^{-3}, \omega = 10^{-2}$ to 10^{2}).

We find that the gel strength decreases with increasing water content, in a consistent manner predicted by the mixograph. While the gel exponent does not show significant changes as the water content is varied.

$$n \simeq 0.23 \pm 0.03 \tag{4.18}$$

Water content moduli correspondence

Figure 39 suggests that the variation in the relaxation modulus as water content is varied can be written in a self-consistent form:

$$G(t) = S(W - W_0)t^{-n} \tag{4.19}$$

where W_0 is an arbitrary reference water content . This observation is consistent with the water content moduli correspondence principle suggested by Hibberd et al [17]. A simplified form of the principle can be written as:

$$\begin{aligned} G'(\omega, W) &= G'(\omega, W_0).Q(W - W_0) \\ G''(\omega, W) &= G''(\omega, W_0).Q(W - W_0) \end{aligned} \tag{4.20}$$

where the function $Q(W - W_0)$ is only a function of the water content and not the frequency. In the original experiment, Hibberd studied doughs in small amplitude oscillatory shear experiments, since the principle concerns behavior in the linear viscoelastic regime, we can translate it to describe stress relaxation experiments.

$$G(W,t) = Q(W - W_0).G_0(t) \tag{4.21}$$

where $G_0(t)$ is the relaxation modulus at the reference water content $W = W_0$. Applying this to the particular case of gel-like behavior in doughs:

$$G(W,t) = Q(W - W_0)S_0 t^{-n} \tag{4.22}$$

where:

$$Q(W - W_0) = S(W - W_0) / S_0 \tag{4.23}$$

where S_0 is the gel strength at reference water content. The function $Q(W - W_0)$ for this particular dough formulation is plotted on Figure 40 and can be approximated by:

$$Q(W - W_0) \simeq \exp\left(-(W - W_0) / A\right) \tag{4.24}$$

with

$$A = 0.028 \tag{4.25}$$

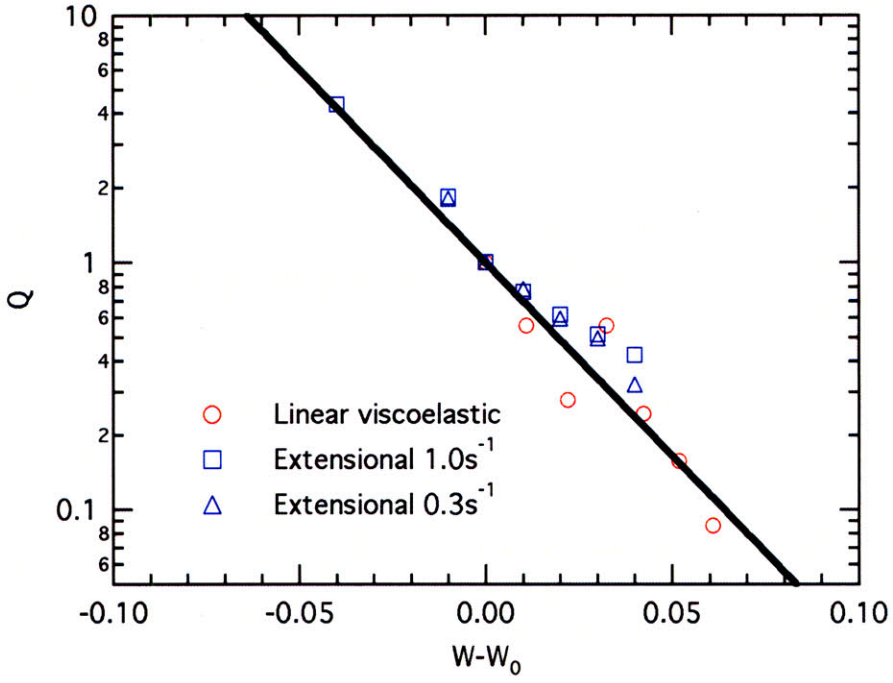

Figure 40 Water moduli correspondence function Q for HRS mixed for 420s with W_0=0.45. Solid line is best fit for $Q(W-W_0) \simeq \exp\left(-(W-W_0)/A\right), A = 0.028$.

The principle can be stated most succinctly as "the loss tangent is independent of water content", of course in the case of a critical gel, the loss tangent also happens to be independent of frequency!

It might seem surprising that a complex system such as dough can be reduced through such a simple principle, however, as Hibberd [15] correctly pointed out, within the linear region, rheological measurements reflect primarily the short range interactions which can be very similar for a wide range of doughs irrespective of gluten type or composition.

In general the water content function $Q(W-W_0)$ and gel strength S at reference content will also be a function of dough formulation parameters such as mixing time, starch content, functional gluten quality and quantity. Hibberd et al [14] performed a study on the effect of starch/protein ratio, they suggest the correspondence principle can be written in a more general form as:

$$G(t,W) = Q(W-W_0, P/S).G_0(t, P/S) \qquad (4.26)$$

where P/S is the protein-starch ratio (for the HRS system, P/S ~ 0.14). They found the correspondence principle to be valid for the range of protein-starch ratios studied, but the shift factor (and the reference values) are now a function of P/S ratios.

Non-linear Rheology

The non-linear rheology of doughs with varying water content was investigated through two extensional techniques: Filament stretching (FISER) and the SER. The response of doughs for various water contents is plotted on Figure 41.

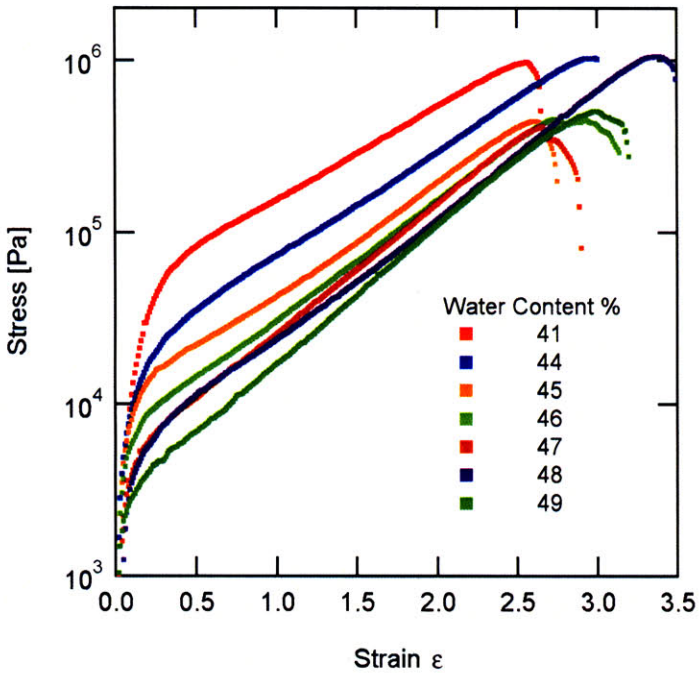

Figure 41 Stress extension data generated on the SER at $\dot{\varepsilon} = 1.0s^{-1}$. HRS, 360s mixing time.

In the previous section, we proposed a constitutive equation that can be constructed from a linear superposition principle of the stress relaxation modulus.

$$\sigma = \int_0^\infty S(t-t')^{-n}\gamma_{[1]}h(\gamma)dt' \tag{4.27}$$

S and n are the gel parameters extracted from linear viscoelastic measurements. $\gamma_{[1]}$ is the finite strain rate tensor. $h(\gamma)$ is a damping function that represents the non-linear softening observed in flour-water dough systems.

The damping function can be estimated by considering the asymptotic approximation of the integral (4.27) at large strains. If $h(\gamma)=1$, then the model is a form of the Lodge Rubber-like liquid and the tensile stress difference approaches the following function:

$$iff\ h(\gamma)=1,\quad \Delta\sigma \sim 2^n\Gamma(1-n)S\dot{\varepsilon}^n \exp(2\varepsilon) \tag{4.28}$$

While at large strains, the measured stress appears to take the form:

$$\Delta\sigma \sim K\dot{\varepsilon}^n \exp([2-\alpha]\varepsilon) \tag{4.29}$$

where $0<\alpha<2$. This suggests the use of a damping function in the form:

$$h(\gamma)=\exp(-\alpha\varepsilon) \tag{4.30}$$

where the large strain response will be:

$$\Delta\sigma \sim \frac{2^n}{2-\alpha}\Gamma(-n)S\dot{\varepsilon}^n \exp([2-\alpha]\varepsilon) \tag{4.31}$$

The damping function parameter α that characterizes the softening behavior and the gel strength prefactor K can be extracted by fitting equation (4.29) to the measured data. We compare the measured prefactors to the calculated values from equation (4.28) and (4.31) in Figure 42.

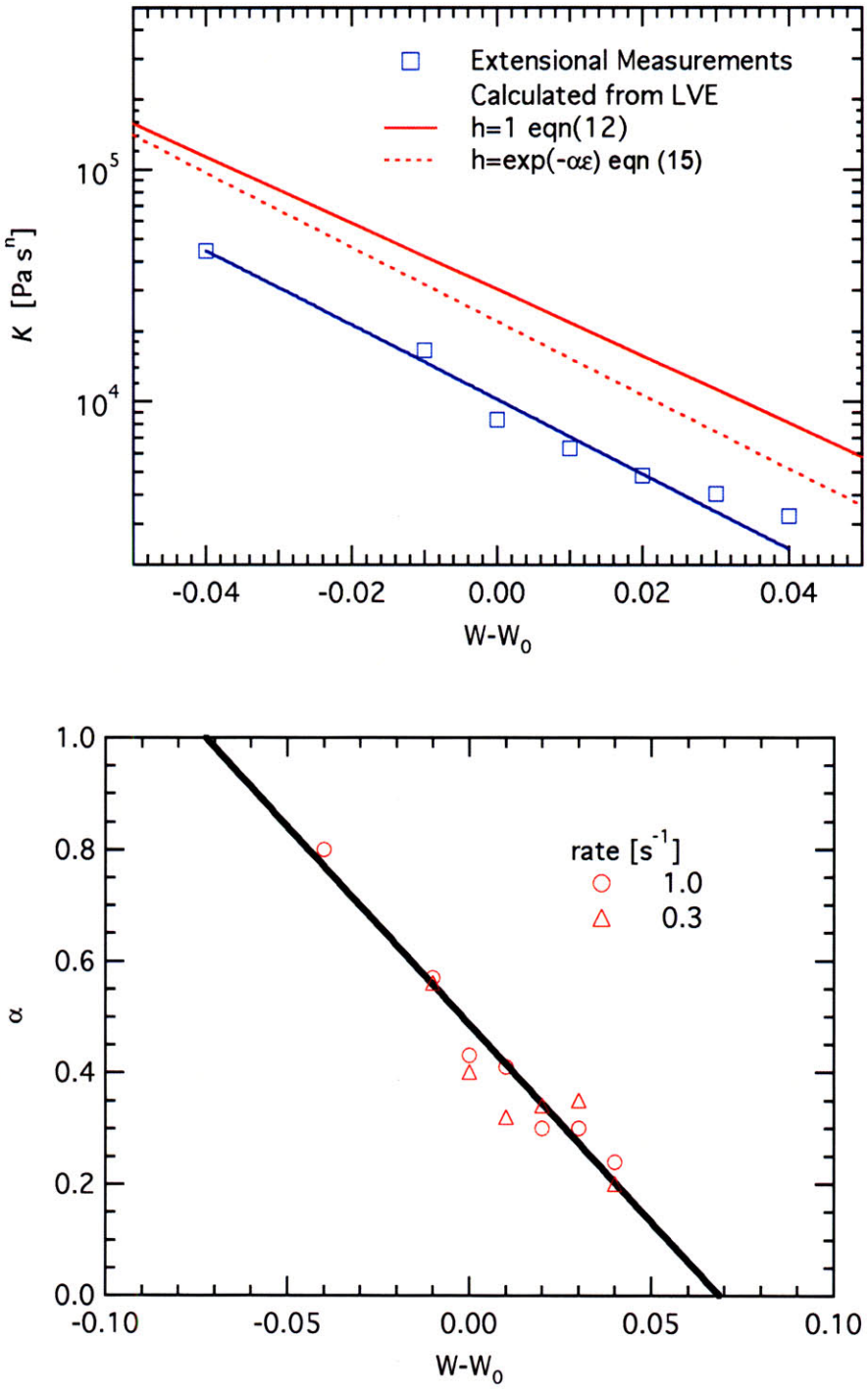

Figure 42 Strain softening exponent α and rate dependent prefactor K as a function of water content.

K was found to decrease with increasing water content in the same manner as a critical gel with an exponential damping function. The absolute values are slighty smaller, possibly due to different levels of rheological ageing between the linear viscolastic and extensional measurements. The calculated shift factors $Q(W-W_0)$ are also plotted on Figure 40 and was found to be well described by the same equation ((4.24) and (4.25)).

The damping exponent α obeyed a simple linear relationship:

$$\begin{aligned} &\alpha(W-W_0) \simeq 0.486 - 7.1(W-W_0) \\ &-0.21 < W-W_0 < 0.068 \end{aligned} \tag{4.32}$$

We see that the damping function decreases with increasing water content. Or in other words, a greater degree of strain-hardening is expected from doughs with higher water content. Generally speaking, the damping function is *dependent* on water content, $h = h(\gamma, W)$: non-linear rheology is *not* simply related through the water content moduli correspondence principle. An additional function is required to describe the dependence on water content. The role of water under non-linear rheology cannot be understood by simply performing linear viscoelastic measurements.

Perhaps a more consistent way of viewing this is through considering the stage of dough development under mixing. As seen in Figure 38, the peak-mixed condition occurs at later times for doughs with increasing water content, indicating that dough development under mixing is "retarded" by the addition of water. As reported in a separate document [129], the peak-mixed condition is not indicative of optimum dough development in terms of strain-hardening, in fact dough mixed for the shortest times exhibited the largest degree of strain-hardening. Following this line of argument, since the doughs presented in Figure 41 and Figure 42 are all mixed for the same amount of time (360s), one might conclude that doughs with lower water content are more "developed" and will thus show decreased strain-hardening capability.

Mixing and water content are intrinsically linked, the addition of water increases the time for a dough to reach a certain stage of development. The relationship between the two is still not well defined. The reason is that rheological ageing and day-to-day variability can change the response of a dough significantly, masking the effect of mixing and water content. To increase consistency among the results, we made every effort to perform experiments concerning a particular area on the same day with a single batch of dough. Such a requirement is in conflict with the need to perform experiments at a fixed time after mixing to avoid "contaminating" the results with rheological ageing (which requires a new batch of dough for every single experiment). The large number of experiments required for the water content study makes this unfeasible. Therefore it is difficult to view the large amount of data in context without an understanding the how such variability affect the results. In view of this, we recommend breaking down the system to its respective components and build up a more complete understanding of variability, rheological ageing and water content for each individual component beginning with the obvious: glutens and starches.

4.4. Effect of Flour Type on Dough Rheology

The quality of flour is one of the most obvious factors that can affect a dough's bread making properties. Bloksma [6] outlined two requirements for producing high quality loaves: "1) the dough must have sufficiently large viscosity to prevent the ascent of gas cells, and 2) it must remain extensible for a long enough time during baking to avoid premature rupture of membranes between gas cells." Bloksma concluded that the first condition is met by virtually all doughs while the second can serve as a discriminator for flours of different baking performance. Extensibility stems from the quality (or gluten functionality) and quantity of protein in the flour [7, 99]. Physically, large molecular weight protein molecules known as glutenin form an elastic network capable of strain-hardening under extension and gives stability under large extensional strain..

The three basic tests performed on the doughs are: step strain relaxation, step rate shear and SER extensional tests. The doughs used in the current studies are all mixed to a water content of 45%.

Step strain relaxation experiments

Step shear strain relaxation data was fitted to the critical gel model:

$$G(t) = St^{-n} \tag{4.33}$$

The fitted parameters from step strain relaxation experiments are presented in Table 4. Samples were rested for $t_w = 1200s$ before a step strain of $\gamma_0 = 10^{-3}$ was applied.

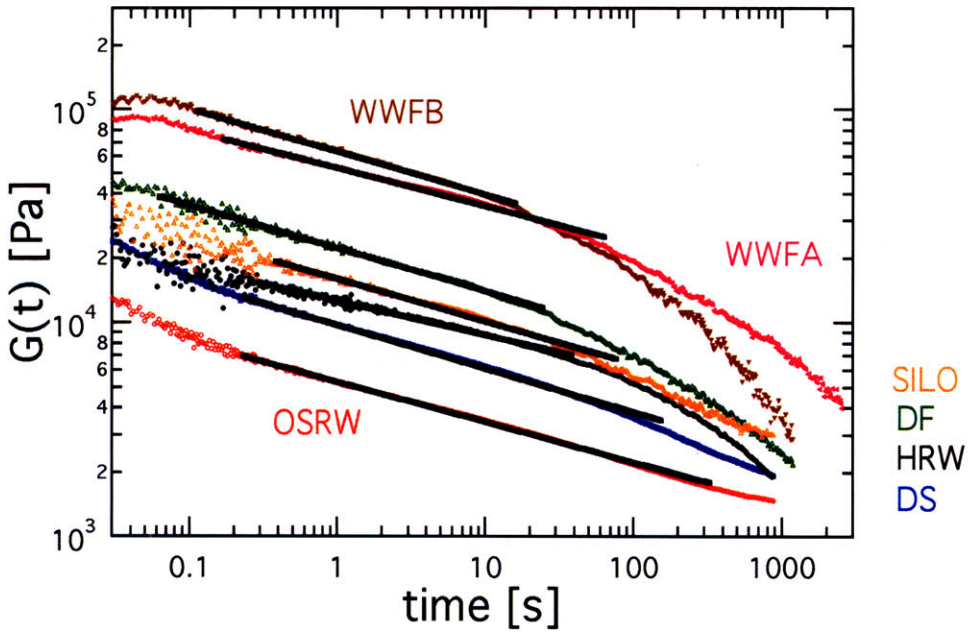

Figure 43 Stress Relaxation Data for wheat flour water doughs at 45% water content. All samples were mixed for 240s and rested for $t_w = 1200s$ before a step strain of $\gamma_0 = 10^{-3}$ was applied. Solid lines are best fit of equation (4.33) to the power law region.

The rest time allows the residual stress accumulated during loading to relax. The magnitude of the step strain was chosen to be within the usual quoted linear range of dough systems.

All doughs showed a prominent power-law relaxation regime from $t \sim 1$ to 100s. Deviations from this regime are noticeable at short times and long times. Short time deviation can be attributed to:

i. Rouse like relaxation at short time.

ii. Rheometer response – The AR G2 is a controlled stress device but is well optimized for viscous or material with large loss tangents. For elastic materials such as dough, coupling between the moment of inertia of the rheometer and springiness of the material leads to ringing.

At long times, the can roll off more rapidly than power law like or it may plateau out to a constant value, again two effects are at work here:

i. Rheological aging

ii. Residual stress relaxation.

All the listed possibility to the deviations are also applies to gluten gels will be further discussed in a more a in-depth manner in chapter 5.

The gel strength S and exponent n are fitted to the power law regime from the relaxation experiments and presented in Table 4.

Flour	S [Pa s^n]	n
Silo	15929	0.19
HRS	16360	0.21
OSRW	5298	0.19
TSRW	18910	0.19
HRW	12593	0.16
DF	22318	0.21
DS	9735	0.20
WWFA	53023	0.20
WWFB	63185	0.20

Table 4 Fitted parameters from stress relaxation test for all flours tested. $\gamma_0 = 10^{-3}, t_w = 1200s$. All doughs were mixed at 45% water content for 240s.

Transient extensional rheology at different strain rates

The extensional data were performed on an SER and were fitted to a simple exponential type behavior:

$$\Delta\sigma = F(\dot{\varepsilon})\exp(\alpha\varepsilon) \tag{4.34}$$

Samples were tested under strain rates from 0.003 to 30 s^{-1}. Results for OSRW are plotted in Figure 44.

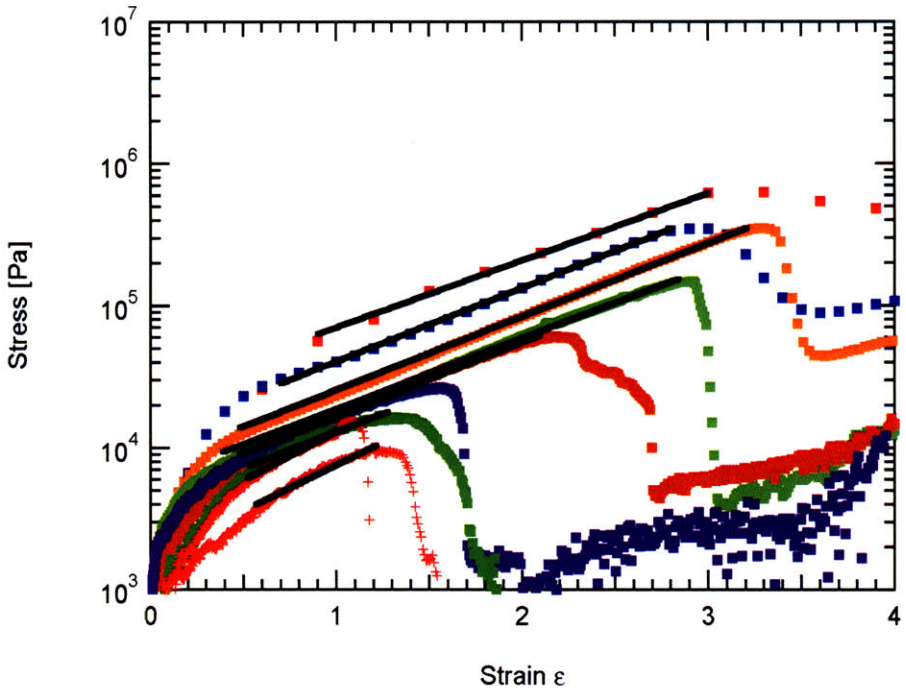

Figure 44 Extensional stress difference of OSRW flour dough mixed for 4 mins at 45% water content. Data for strain rates of 0.003, 0.01, 0.03, 0.1, 0.3, 1.0, 3.0, 10, 30 s^{-1} are presented. Solid lines represent best fit for equation (4.34) between strain of $\varepsilon \sim 0.5$ to rupture. In general, increasing rates resulted in increased stress in accordance with equation (4.37). The data was collected on the SER.

All samples showed a linear viscoelastic response at small strains ($\varepsilon < 0.5$):

$$\eta_{Ext} \rightarrow \frac{3S}{1-n} t^{1-n} \tag{4.35}$$

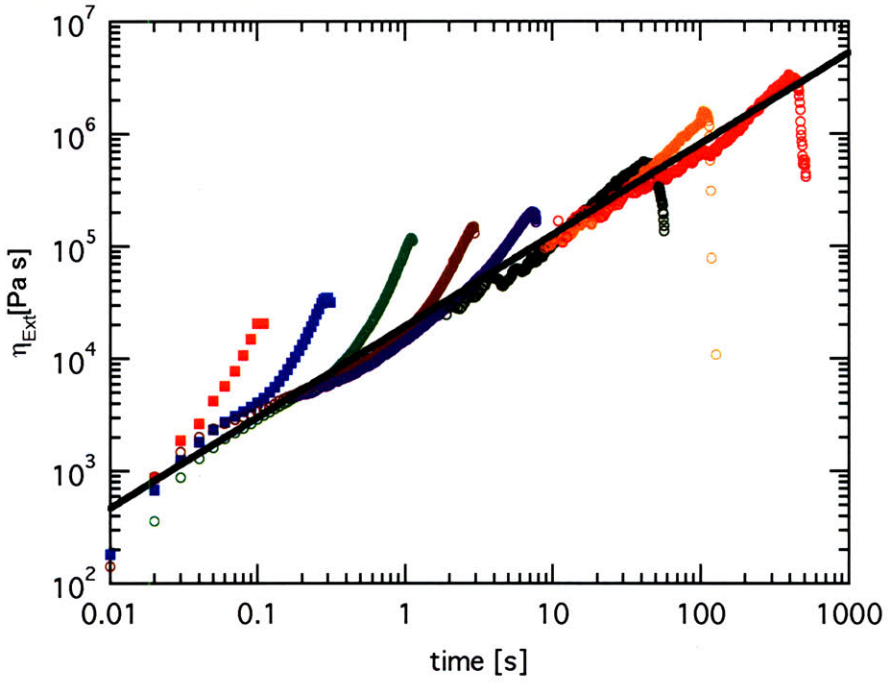

Figure 45 Extensional viscosity of OSRW flour dough mixed for 4 mins at 45% water content. Data for strain rates of 0.003, 0.01, 0.03, 0.1, 0.3, 1.0, 3.0, 10, 30 s^{-1} are presented. All data followed the linear viscoelastic limit (solid black line) at small strains predicted from step strain relaxation experiments.

Going back to Figure 44, for rates $\dot{\varepsilon} > \dot{\varepsilon}_{crit} = 0.01 s^{-1}$, an exponential stress growth can be seen. This exponent is roughly constant for a given flour type (Figure 46). At rates $\dot{\varepsilon} \leq \dot{\varepsilon}_{crit}$, the exponent appears to suddenly increase. However, this is an artifact from assuming that the shape of the stress strain curves resembles an exponential. Examining the stress strain curves, we see that the shapes at these low rates are "concave" and it is difficult to assign a consistent value for an exponent. It is unclear whether this shape is a true material function or if it is merely due to non-uniform deformation. For convenience, we define an alternative description of the transient extensional stress through an offset powelaw function:

$$\Delta\sigma_{Ext}^{+} \simeq H(\dot{\varepsilon}) + G(\dot{\varepsilon})\varepsilon^{c(\dot{\varepsilon})} \tag{4.36}$$

This material function is not frame invariant, but will be useful in comparing the extensional behavior.

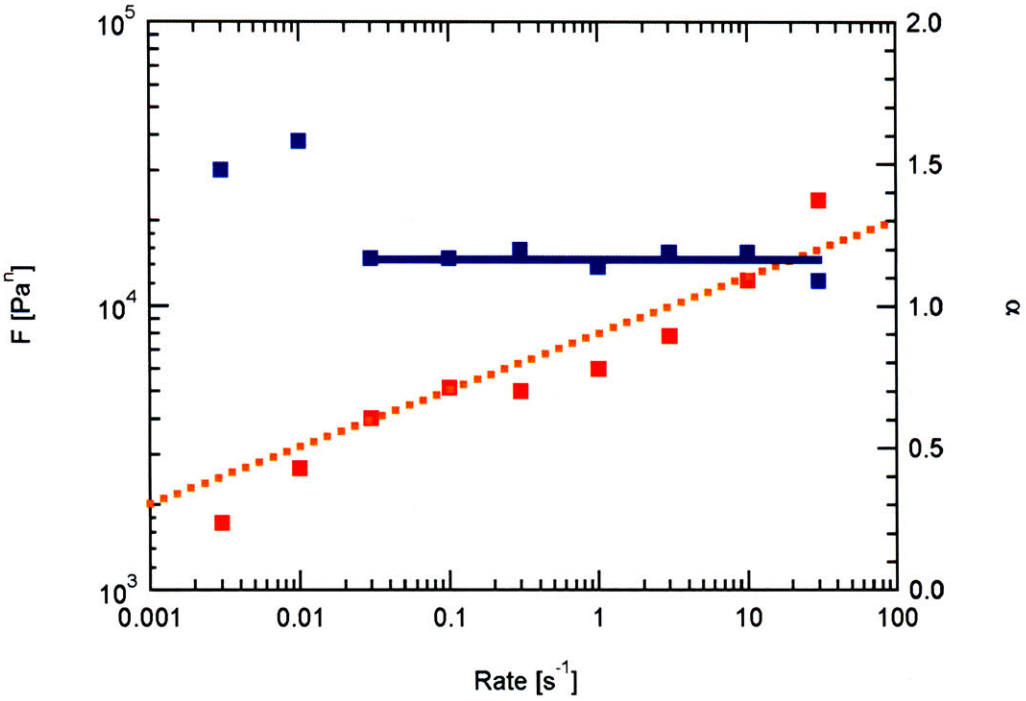

Figure 46 Extension parameters extracted from SER extensional tests performed on OSRW flour dough at 45% water content that has been pin mixed for 4 mins. Blue squares correspond to exponent α while red squares correspond to F.

In general, we expect the exponent α is dependent on the dough (i.e. flour type, mixing time). Above $\dot{\varepsilon}_{crit}$, the behavior is well described by equation (4.34), and from (4.15)the constitutive equation analysis [126], we expect:

$$F(\dot{\varepsilon}) \propto S\dot{\varepsilon}^n \tag{4.37}$$

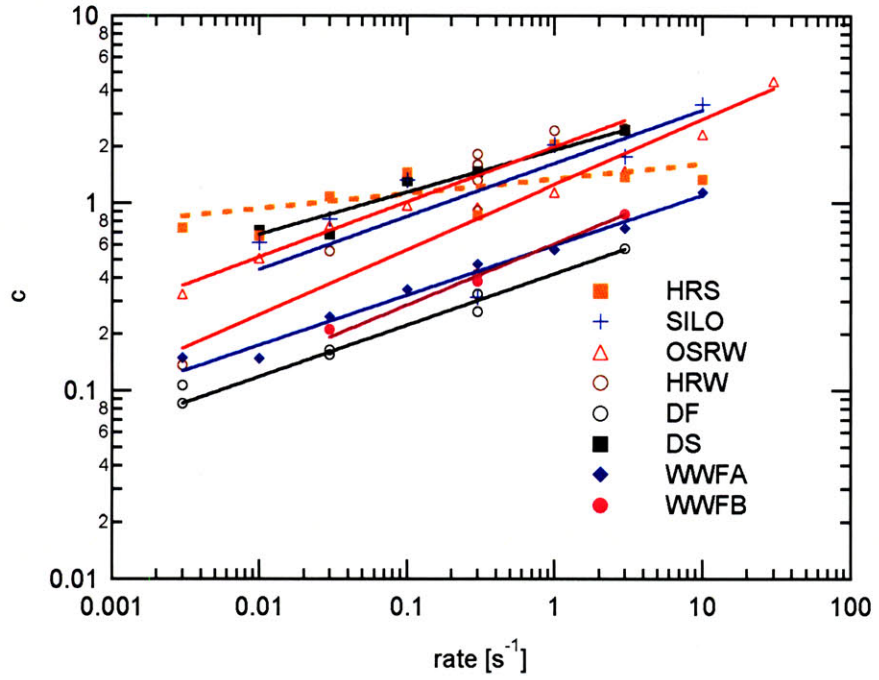

Figure 47 Rate sensitivity of various flour type doughs $c(\dot{\varepsilon}) = F / S$ (Gel strength S obtained through step strain relaxation experiments.. Most flours showed a power law increase in rate as predicted by equation (4.37) with n ~ 0.22. OSRW (0.25) and WWFB (0.26) showed a slightly steeper slope. While HRS exhibited a shallow slope corresponding to n = 0.12. Results obtained from dough at 45% water content mixed for 240s and stretched on the SER.

The rate dependence of the doughs were small and appear to vary almost universally because all the doughs tested have similar values of n. We plot $c(\dot{\varepsilon})$ (equation (4.36)) against strain rate (Figure 47). Despite the variable nature of the doughs leading to significant spread, the trend is clear in that stress increases with the strain rate raised to the power $n \approx 0.22$. This is consistent with the exponent values measured through stress relaxation.

The failure behavior of the various flour type doughs were also investigated. The ultimate failure strain for the various strain rates and doughs are illustrated in Figure 48.

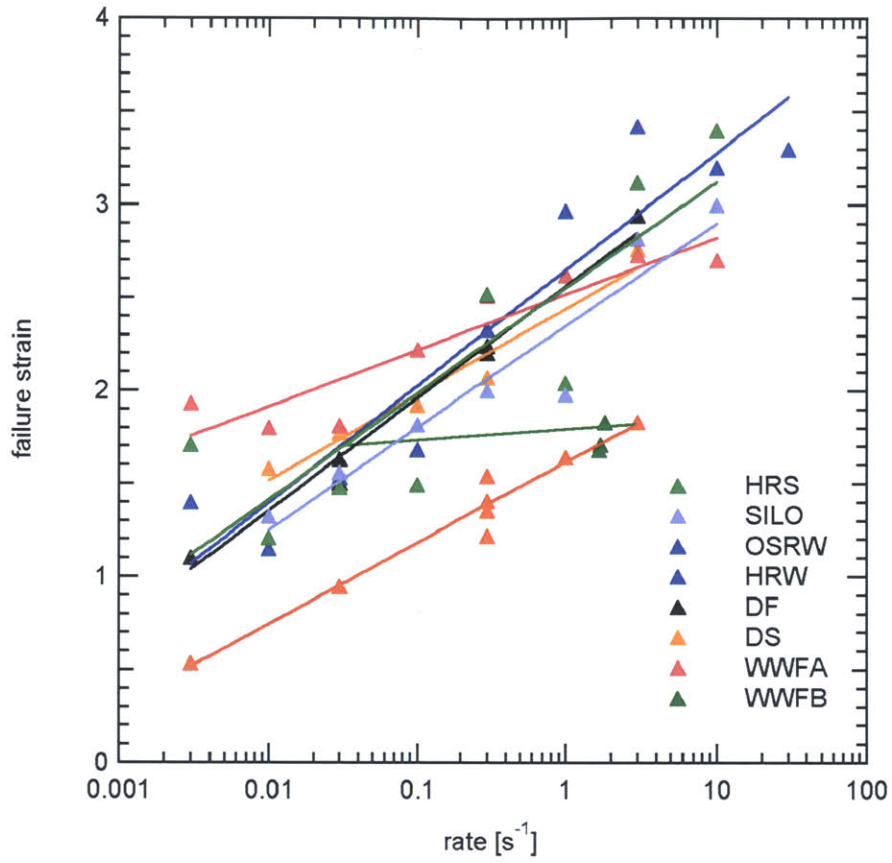

Figure 48 Ultimate failure strain of various doughs at 45% water content mixed for 240 as a function of strain rate. Data sets were collected on the SER.

We can quantify the failure behavior by assuming it takes the form:

$$\varepsilon_{fail} = A\log(\dot{\varepsilon}) + B \tag{4.38}$$

The quantities A and B are a measure of rate sensitivity and characteristic failure strain respectively and are summarized with the rest of the relevant material parameters in Table 4.

Flour	α	$\dot{\varepsilon}_{crit}$	A	B
DF	1.05	0.03	0.6	2.56
WWFB	1.13	0.01	0.06	1.18
DS	1.16	0.03	0.46	2.44
OSRW	1.16	0.01	0.63	2.65
WWFA	1.2	0.01	0.3	2.52
SILO	1.32	0.01	0.55	2.35
HRS	1.38	0.01	0.57	2.56
HRW	1.5	1.0	0.43	1.61

Table 5 Failure parameters for various flour type doughs. All doughs mixed to 45% water content for 240s. Results correspond to data collected on the SER presented in the appendix.

Conclusions

In this section we provided a brief overview of the rheological behavior of dough mixed from different flour types. We have tabulated the material parameters as characterized by the generalized gel model (S, n and α), and also a few other candidates functions ($\dot{\varepsilon}_{crit}, \varepsilon_{fail}$). However, similar to the water content study of the previous section, it is difficult to draw conclusions due to the inherent variability when dealing with dough. As warned in the introduction, it is difficult to form a general picture or comprehensive understanding of the different rheological phenomena measured over such a wide variety of parameters. Thus pursuing this line of research alone is insufficient, and we turn our attention to more fundamental questions on the source of these rheological properties in the next few chapters.

5. Power Law and Gluten Gels at Finite Strains

5.1. Introduction

Materials showing power-law relaxation behavior are often encountered in rheology. Examples include many foodstuffs [130, 131], biopolymer networks [132], nanocomposites [133, 134] and some liquid crystals [135]. Frequently these systems involve interacting microstructural features over multiple length scales. In terms of soft glassy dynamics, power-law material functions are predicted for certain effective temperatures [128, 136], while in the field of cellular mechanics, the term power-law rheology is often used to describe the frequency response of protein networks [137, 138]. As another example, both the Rouse [139] and Zimm [140] models will show power-law behavior under time scales that are longer than the segmental relaxation time but shorter than the longest relaxation time ($\lambda_{seg} \leq t \leq \lambda_1$). In general, polymeric systems with a large degree of polydispersity or an extremely broad relaxation spectrum will also exhibit power law relaxation over a significant span of time scales. One subset of materials that falls under the broad umbrella of power-law rheology and which has been studied relatively well is the *critical gel* first described by Winter and Chambon [74, 76]. Linear viscoelastic measurements show that in critical gels both the storage and the loss moduli scale as $G', G'' \sim \omega^n$ and the loss tangent is constant over a wide range of frequencies. Theoretical models show that this power law scaling can arise from the fractal nature of a flocculated gel [71, 72]. At the critical gel point, the material forms a percolated, sample-spanning structure that exhibits power-law frequency dependence in the dynamic moduli.

The linear viscoelastic functions of a critical gel have been discussed in detail by Chambon and Winter [74, 76] and by Larson [141]. Winter provides an excellent review of these systems that are near the liquid-solid transition [77]. However, there have been very few systematic investigation of such materials under finite strain deformations. Venkataraman and Winter [75] adopted the Lodge rubber-like liquid formulation originally suggested by Chambon and Winter [74] to analyze the non-linear large strain behavior of PDMS gels during start-up of

steady shear and creep experiments. They noticed a stress overshoot at shear strains of $\gamma^* \sim 2$ and a subsequent yield at $\gamma^P \sim 4$. Watanabe et al also studied the non-linear rheology of a polyvinyl chloride critical gel. To the best of the present authors' knowledge, no such study exists for critical gels under uniaxial extension.

Finding a suitable material is not easy. Firstly, critical gels are hard to formulate. One needs a reliable and reproducible method to bring the material to the critical gel point and then quench it to prevent additional percolation. Secondly, the percolated structure of gels can collapse under large deformations which will be manifested as strain-softening in rheometric tests. The specific form of the non-linear material response exhibited by a particular critical gel (for example strain-softening or stiffening) provides an additional rheological signature about the microstructure beyond the simple linear response [104, 126]. We first begin by identifying a suitable candidate material to serve as a model critical gel system that shows relatively simple non-linear behavior.

Curiously, many foodstuffs show power-law/critical gel like behavior [70, 78, 79]. Of particular interest here, are wheat flour-water doughs. Despite these numerous early observations of power-law like frequency response in the linear viscoelastic moduli [15, 19, 61, 68], Gabriele and co-workers [69] were the first to use the concept of a critical gel and a power-law relaxation modulus to describe the rheological behavior of dough. This descriptive framework has also been used recently [126, 142] to explore other types of deformation including creep relaxation, uniaxial and biaxial extension. This so-called 'weak gel model' [69] is extremely attractive because of its relative functional simplicity. Material functions in the linear viscoelastic regime can be well described by only two parameters.

In simple terms, dough may be described in the following way: a viscoelastic matrix of gluten (a branched polymer) filled with hydrated starch particles. In many aspects, the resulting composite is analogous to a carbon-black filled elastomer. The interactions between the polymeric and filler constituents lead to severe non-linearities and complex response [14, 143]. The precise microstructure

of the gluten forming the matrix is still poorly understood due to its high molecular weight and the high degree of chain branching, both of which result in poor solubility characteristics. Opinions can be broadly classified into two schools of thought. One school maintains that gluten, though a high molecular weight compound, takes the shape of a tight globule - neighboring protein molecules aggregate to form a network through hydrogen bonds and hydrophobic interactions [50, 51, 55, 58]. In this article, we refer to this idea as the particulate gel model. The other school believes that the gluten molecule is sufficiently swollen that it forms an entangled matrix or polymeric network with flexible chains spanning between junction points [48, 49, 53]; we refer to this picture as the polymeric gel model.

Despite the ease of formulating flour-water doughs, obtaining repeatable measurements and understanding the material rheology is difficult due to the strong time-dependent and non-linear softening effects observed in doughs [80]. Comprehensive studies on these systems, which can lead to insight into the microstructure, are hampered by the difficulty in collecting reproducible data. In our laboratory, we observe day-to-day variations of up to ±50% in modulus just by simply varying the mixing and testing schedule.

Eliminating the starch fillers to focus exclusively on the rubbery gluten network removes at least one level of complexity. The rheology of gluten doughs had been investigated by various workers [51, 55, 107, 144, 145]. Uthayakumaran et al reported shear and extension data for gluten gels that has been mixed with different amount of starch (0-100% starch weight content) and contrasted these results with tests performed on wheat flour doughs. They observed an exponential decrease in the limiting strain of linear viscoelastic behavior with increasing starch content; Lefebvre and co-workers investigated the linear viscoelastic behavior in the long time-scale terminal regime [52]. Critical-gel–like behavior in gluten doughs has also been observed: Letang et al [47] showed that the dynamic moduli both follow a power-law behavior with $n \simeq 0.3$ (see equation (5.12) in section 0), they also noted that gluten doughs possess a larger linear range when compared to wheat flour doughs.

To prepare critical gels with a well-defined and reproducible power-law linear viscoelastic response, we follow these earlier studies and isolate the viscoelastic response of the biopolymeric matrix forming the dough. In addition to being a 'model' system with a power-law relaxation spectrum, developing a quantitative understanding of the rheology of gluten is also of great practical interest. Despite the relatively small weight proportion of gluten in a typical flour (5-20%), the viscoelasticity of a wheat flour-water dough is largely determined by this protein phase [99] and it is widely believed that the bread-making qualities of a wheat flour dough are strongly linked to its mechanical properties [6, 27]. In particular, the large strain rheology of the dough has an impact on the texture and distribution of gas cells in the bread [8, 9, 46]. The most commonly-cited relationships are those between final loaf volume, dough extensibility and gluten quantity: beginning from the work of Bailey and others in the first half of the 20th century [2, 3, 146] to more recent studies such as those by Sliwinski et al [5, 147], Weegels et al [148] and Dobraszcyk et al [4, 7, 43]. An accurate constitutive and microstructural model will aid in documenting differences between wheat-flour doughs of different gluten content and 'functionality' – which are the key mechanical properties relevant to breadmaking. A robust rheological equation of state is also a good starting point for cereal scientists who would like to investigate systematically the effects of other components (e.g. starch, water content etc...), with the aim of increasing the complexity level until ultimately arriving at a real dough system.

There are three primary objectives of this paper. The first is to demonstrate that a gluten dough exhibits the rheological characteristics of a critical gel with relatively-well controlled material properties (i.e. a variability in modulus of less than 10%). We report rheological data for gluten doughs using both shear and extensional deformations that span the linear to non-linear regimes. The second objective is to identify a constitutive model that can provide a description of the stresses arising in non-linear deformations in terms of well-defined material functions which can be measured directly in the linear viscoelastic range. Finally, using the rheological evidence collected, we infer certain aspects regarding the microstructure of the gluten gel.

5.2. *Gluten dough preparation*

Gluten dough was prepared by placing 10g of vital gluten (Arrowhead Mills - ~ 12% moisture content) in a mixograph bowl with 14g of water (total dough moisture content = 63% by weight). The mixture is then stirred, stretched and folded through the action of the mixograph pins for 12 minutes [85]. Mixing over this length of time allows the dough to become 'fully developed', the appearance of the dough changes from dry and lumpy to a smooth, sticky and elastic paste. No significant changes to the dough properties could be observed when the mixing time was increased. We use a customized mixograph which has been digitally instrumented to record both the rapid temporal fluctuations and longer time variations in the mixograph torque output. Representative data for mixing of a vital gluten gel are shown in Figure 49. The torque signal shows a rise towards a steady plateau after approximately 11 minutes. The magnitude of the short time scale fluctuations (corresponding to stretching of material elements between interacting pairs of pins in the bowl) also remains constant. The dough is removed from the mixing bowl after 12 minutes (720s) of mixing and then allowed to rest for 1 hour at 22° C, before testing.

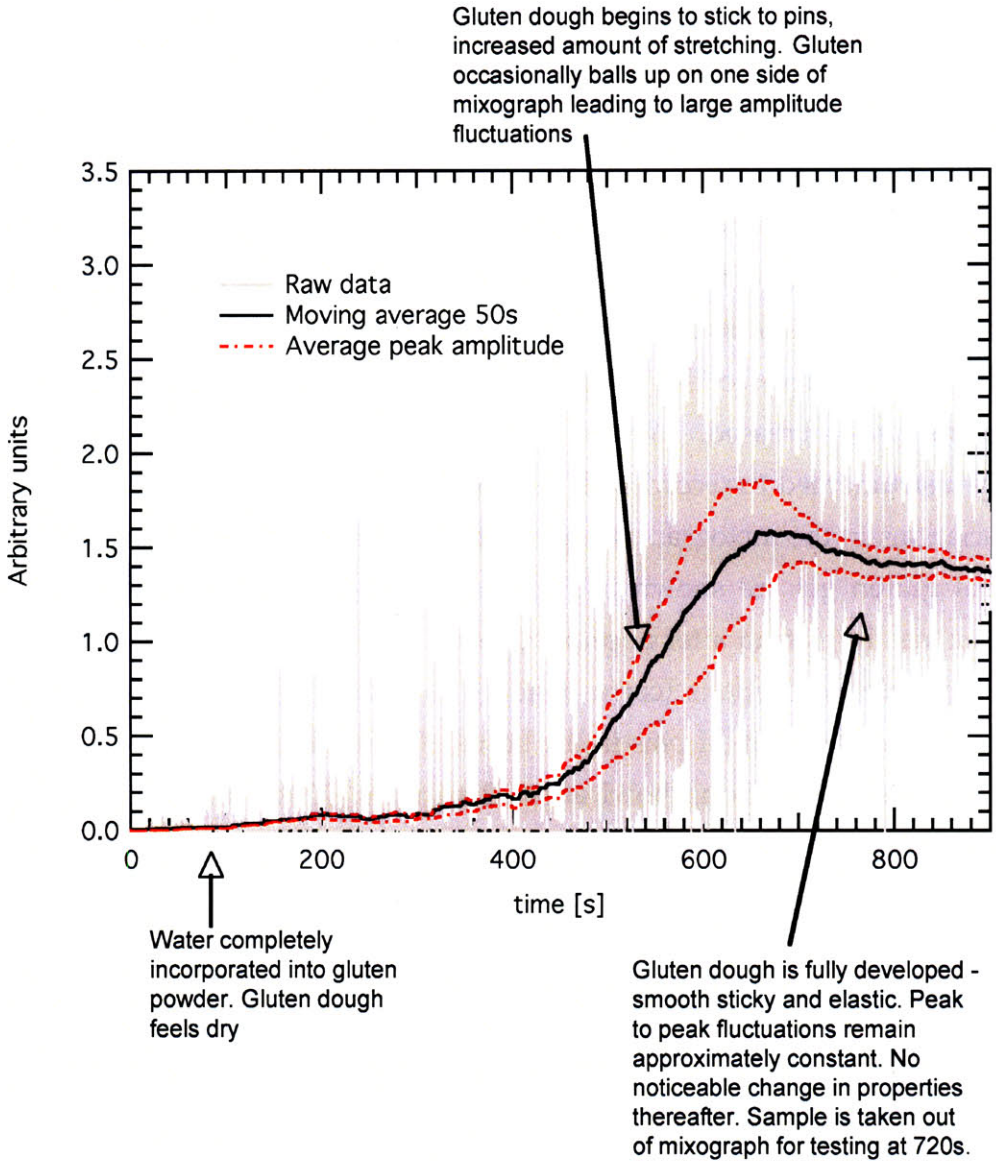

Figure 49 Mixograph output for 24g of gluten dough at 63% moisture content by weight. After the gluten dough has been fully developed, it is removed from the mixograph at 720s.

The window of practical moisture content for preparing a homogeneous gluten gel sample is surprisingly small as compared to a wheat flour dough. At moisture contents of less than 60%, the dough appears to be too dry and some

gluten powder around the edge of the mixing bowl remains unincorporated. By contrast if the moisture content exceeds 65%, the dough appears wet, with unincorporated water pooled at the bottom of the bowl.

5.3. Rheometry

Shear rheometry are performed under controlled strain mode on the ARES rheometer and under controlled stress mode on the AR-G2 rheometer (TA instruments). A Peltier plate and a 25mm parallel plate fixture at 1mm separation were used. Approximately 2 g of gluten dough was placed on the Peltier plate, and the upper plate was then brought down to compress the sample to the specified thickness. Excess dough was trimmed with a razor blade. The Peltier plate was held at a fixed temperature of 22°C, to approximate typical room temperature. Slip was eliminated by applying adhesive-backed sandpaper (600 grit McMaster Carr 47185A51) to the surfaces of both the Peltier plate and the parallel plate tool. Drying of the sample was minimized by painting the exposed surface of the dough with a low-viscosity silicone oil.

Measurements of the transient extensional stress growth were made on a wind-up drum type rheometer (the Sentmanat Extensional Rheometer or SER fixture) which was used in conjunction with the ARES rheometer [121]. Samples of 2 x 25mm were formed by pressing the gluten dough to a thickness of 2 mm, then cutting to shape using a Guillotine cutter. A thin film of silicone oil was painted onto the sample before mounting on the SER fixture to minimize drying.

5.4. Linear Viscoelasticity

We first investigate the linear viscoelastic response of the gluten gel. This enables us to compare and contrast our measurements with previously published data on gluten gels [47, 52, 107] and other critical gels [74-77, 149]. From these experiments, we extract two key constitutive parameters; the power-law exponent n and the gel strength S of the critical gel.

Step Strain Relaxation

Under linear viscoelastic conditions a critical gel will exhibit a power-law behavior in its material functions [74, 76]. For example, following an infinitesimal step strain of amplitude γ_0 at time t =0, the modulus decays like:

$$\frac{\sigma_{xy}}{\gamma_0} \equiv G_{gel}(t) = St^{-n} \tag{5.1}$$

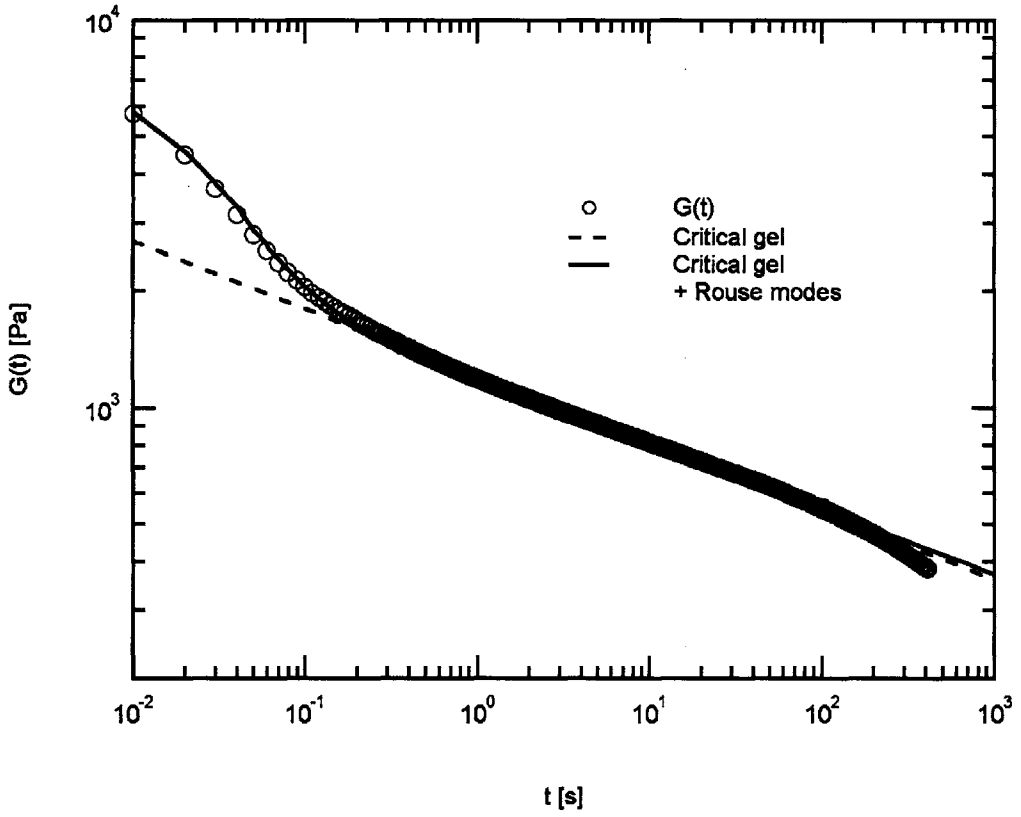

Figure 50 Stress relaxation behavior of a gluten gel. The relaxation modulus approaches a power-law as expected for a critical gel with $S = 1260 \pm 50\ Pas^n$, $n = 0.175 \pm 0.005$ over a wide range of time $0.2 \leq t \leq 100s$. At short times, an additional Rouse relaxation regime can be observed, with $G_R \simeq 803\ Pa$ and $\lambda_R = 0.05\ s$.

In Figure 50 we show the extent of power-law relaxation for a typical gluten-water dough. We find that the relaxation can be well described by equation (5.1) with $S = 1260 \pm 50\ Pas^n$, $n = 0.175 \pm 0.005$ for approximately three decades of elapsed time $0.2 < t < 100$s. At short times (t < 0.05 s), an additional Rouse-like response can also be observed. The overall response of the system can be accurately described by the following expression:

$$G(t) = G_{gel}(t) + G_{Rouse}(t) = St^{-n} + G_R \sum_{k=1}^{\infty} \exp\left(-tk^2/\lambda_R\right) \tag{5.2}$$

Where $G_R \simeq 803\,Pa$ and $\lambda_R = 0.05\,s$ are the modulus and relaxation time of the Rouse modes. The existence of this short time scale regime is consistent with the generic rheology of polymeric gels described by Winter [77]: the Rouse modes characterize the "molecular building blocks" of the critical gel, i.e. they represent the response of the segmental structure size within the gluten network. This segment length scale estimated from network theory $\ell \sim \left(k_B T/G_R\right)^{1/3} \approx 20\text{nm}$ is close to the typical structural sizes observed with transmission electron microscope [150], but is far smaller than the diameter of gluten gel particles ($D \sim 10\mu\text{m}$) seen through confocal microscope observations of gluten dispersed with SDS [51].

Departure from the power-law regime at long times (t > 100s) has often been attributed to a long time terminal relaxation and appears to be sensitive to the amount of rest time the sample is allowed before testing [151, 152]. The fact that dough properties appear to change if left to rest is also well-known to bakers, they refer to this effect as "slackening" [151]. We find that it is in fact related to residual relaxation from the initial mounting and compression of the sample in the test geometry. This particular sample was rested for 1 hour before testing. It was found that by increasing the rest time, the upper temporal limit of the power-law relaxation could be extended; however it is difficult to extract a simple relationship between rest time and onset of this residual relaxation, in part because the specific material history of the loading deformation is unknown.

To help comprehend this behavior, we consider the characteristic or 'mean' relaxation time of a viscoelastic material. A power law relaxation modulus with $0 < n < 1$ will imply a characteristic relaxation time that diverges:

$$\lambda_{char} = \frac{\int_0^{\infty} rG(r)dr}{\int_0^{\infty} G(r)dr} = \frac{\int_0^{\infty} Sr^{-n+1}dr}{\int_0^{\infty} Sr^{-n}dr} \to \infty \tag{5.3}$$

where $r = t - t'$ is the elapsed time.

Material functions at fully equilibrated initial conditions are therefore difficult to obtain for such systems with power-law relaxation. Unless the material sample was constituted on the rheometer plates, any residual stress from loading will require an infinite amount of time to relax away.

When a sample is first loaded onto the rheometer, the gluten gel is typically compressed from an irregular shape to a flat disc, then cut to shape. Of course, the deformations accumulated in this process are far from simple shear, and will most likely be unevenly distributed throughout the sample. During a typical loading event the compression process in which the sample is squeezed from a thickness of $h_0 = 20\,\text{mm}$ to $h_1 = 1\,\text{mm}$, we find $\gamma_0 \sim \ln(h_0/h_1) \sim 3$. This strain is significantly larger than the typical step shear strains applied in the stress relaxation tests, therefore residual stress relaxation will be significant. As an illustration, we consider experimentally the situation depicted in the inset of Figure 51. We impose a large uniform torsional shearing strain γ_0 on the sample in the θ-direction at $t = -t_w$ to emulate the effects of sample compression. The material is then allowed to relax for a waiting time t_w before the actual stress relaxation test in which a step strain of γ_a is applied in the same direction at $t = 0$. Assuming that the material response is linear in strain, the stress response measured from $t = 0$, will consist of a superposition of relaxation due to both the initial 'loading' strain γ_0 and the subsequent 'test' strain γ_a:

$$\sigma_{xy} = S\left[\gamma_a t^{-n} + \gamma_0 (t + t_w)^{-n}\right] \quad \text{for } t \geq 0 \tag{5.4}$$

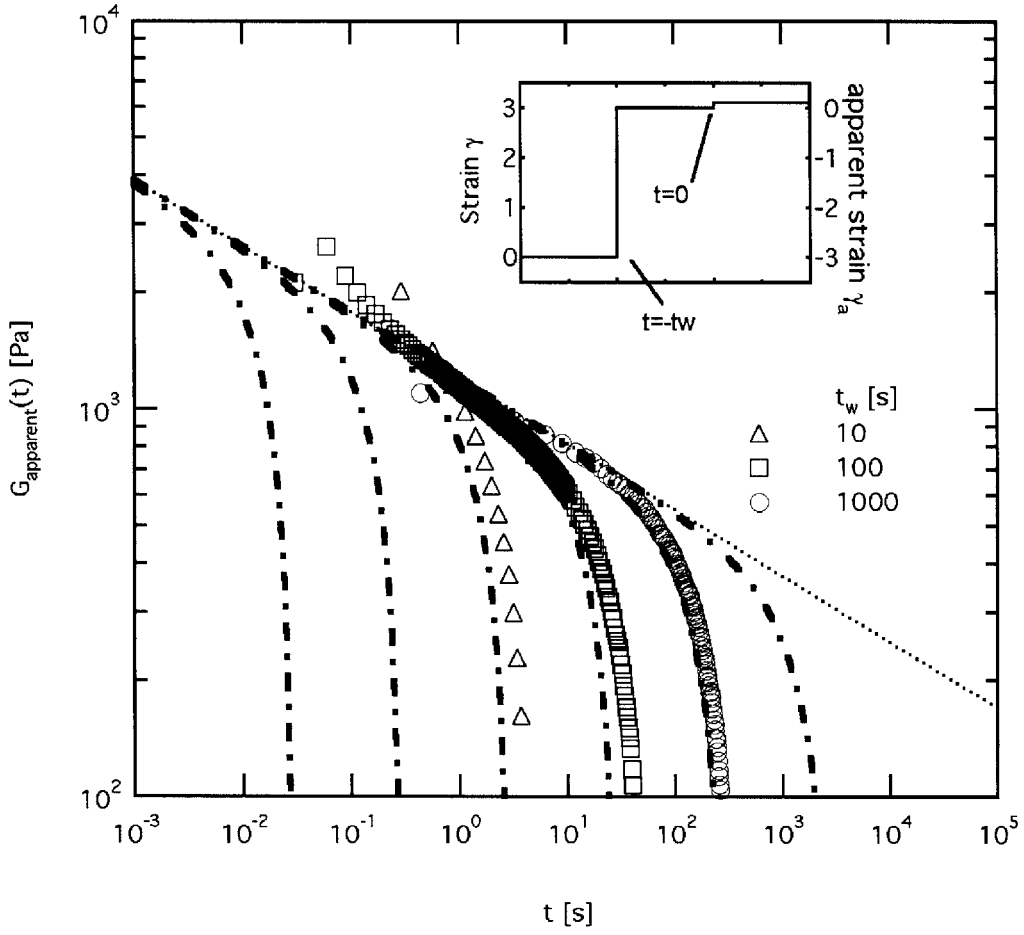

Figure 51 Deviations from power-law relaxation due to the effects of loading history for various values of sample rest time. Dashed lines represent predictions from the critical gel equation for the apparent modulus (equation (5.5)) with t_w = 0.1, 1, 10 ,100, 1000, 10000 s and $t_w \to \infty$ (dotted line). Open symbols are measured data for gluten gels with t_w = 10 ,100, 1000 s. Inset illustrates the strain protocol imposed on the sample during the experiment. Note that the rheometer resets or 'zeroes' the stress at $t = 0$.

For many conventional rheometers, such as the ARES used in these experiments, any residual stress values are automatically "zeroed out" at the beginning of the experiment: as a result, the apparent modulus will be smaller than the true value by an offset $G_{offset} = St_w^{-n}\gamma_0/\gamma_a$. The apparent or measured response is thus:

$$G_{apparent}(t) = \frac{\sigma_{xy}(t)}{\gamma_1} - G_{offset} = S\left[t^{-n} + \frac{\gamma_0}{\gamma_a}\left\{(t+t_w)^{-n} - t_w^{-n}\right\}\right] \tag{5.5}$$

The resulting decay in the apparent modulus of a critical gel is plotted in Figure 51 for $\gamma_0 = 3$, $\gamma_a = 0.1$ using a range of values for t_w. We also compare the predictions of the gel equation with measured data obtained in gluten samples with various waiting times ($t_w = 10, 100, 1000$ s). A rapid decay in the apparent modulus occurs at time $t \sim O(t_w)$ due to the subtraction of the residual relaxing stresses and this is captured qualitatively by equation (5.5).

Very long time scale processes such as the power-law stress relaxation in Figure 50 are therefore difficult to probe because the relative contribution of residual relaxation from initial loading histories will always become significant at long times $t \gtrsim t_w$. From an experimentalist's point of view, this means that in systems showing power-law relaxation, one can only access time scales that are significantly shorter than the amount of rest time provided to the sample.

Continuous and discrete relaxation spectrum

For materials with relaxation processes spanning a wide range of time scales, such as the critical gel, it is sometimes more convenient to express the material properties as a continuous relaxation spectrum over a logarithmic time scale [77, 81]:

$$G(t) = \int_{-\infty}^{\infty} \tilde{H}(\lambda)\exp\left(-\frac{t}{\lambda}\right) d\ln\lambda$$
$$\tilde{H}(\lambda) = \frac{S}{\Gamma(n)}\lambda^{-n} \tag{5.6}$$

Where $\tilde{H}(\lambda)$ is the continuous relaxation spectrum of a critical gel and λ is the range of relaxation time scales. Alternatively, it is common for numerical simulations to seek a suitable description of the relaxation modulus in terms of a

set of discrete Maxwell relaxation modes with moduli G_k and relaxation times λ_k [104, 153, 154]. As Dealy (2007) notes, this decomposition is, in general, ad hoc and non-unique; in the case of power-law relaxation, there exists a very elegant relationship between each successive relaxation mode which can be written in the following way [155]:

$$G(t) = \sum_{k=0}^{\infty} G \exp\left(-\frac{t}{\lambda_k}\right)$$
$$\lambda_k = \frac{\lambda_0}{k^{\alpha}} \tag{5.7}$$

Where $G_k = G$ sets the scale of the modulus for each mode and α characterizes the rate of relaxation. Relaxation spectra of the form in equation (5.7) can be converted into an integral form through the Euler Maclaurin series:

$$\sum_{k=0}^{K} f(k) = \int_0^K f(s)ds + \frac{1}{2}\left[f(K) + f(0)\right] + \ldots \tag{5.8}$$

Where K is the desired range of the summation. Substituting equation (5.7) into equation (5.8) gives:

$$\sum_0^{\infty} G \exp\left(-\frac{tk^{\alpha}}{\lambda_0}\right) \simeq \int_0^{\infty} G_0 \exp\left(-\frac{ts^{\alpha}}{\lambda_0}\right) ds + \frac{G_0}{2} \tag{5.9}$$

After performing the integral and rearranging we obtain:

$$\frac{G_0 \lambda_0^{1/\alpha}}{\alpha} \Gamma(1/\alpha) t^{-1/\alpha} = \frac{G_0}{2} + \sum_{k=1}^{\infty} G_0 \exp\left(-\frac{tk^{\alpha}}{\lambda_0}\right) \tag{5.10}$$

Comparing the final result to equation (5.1), it is clear that the power law relaxation modulus of a critical gel can be approximated by a series of discrete relaxation modes in the form of equation (5.10) with

$$\begin{aligned} \alpha &= 1/n \\ \lambda_k &= \lambda_0 k^{-1/n} \\ G_0 &= \frac{S}{n\Gamma(n)\lambda_0^n} \end{aligned} \tag{5.11}$$

A relationship of this form for the single specific case $n = 1/2$ was first noted by Winter et al [76].

This discrete relaxation spectrum starts from an arbitrary or user-specified maximum time scale λ_0 (which we may expect from Section 0 to scale as $\lambda_0 \sim O(t_w)$). Although an infinite summation is indicated in (5.10), in practice only a finite series of terms $0 \le k \le K$ need be considered. Since $n \le 1$ and $\alpha \ge 1$, the series converges smoothly.

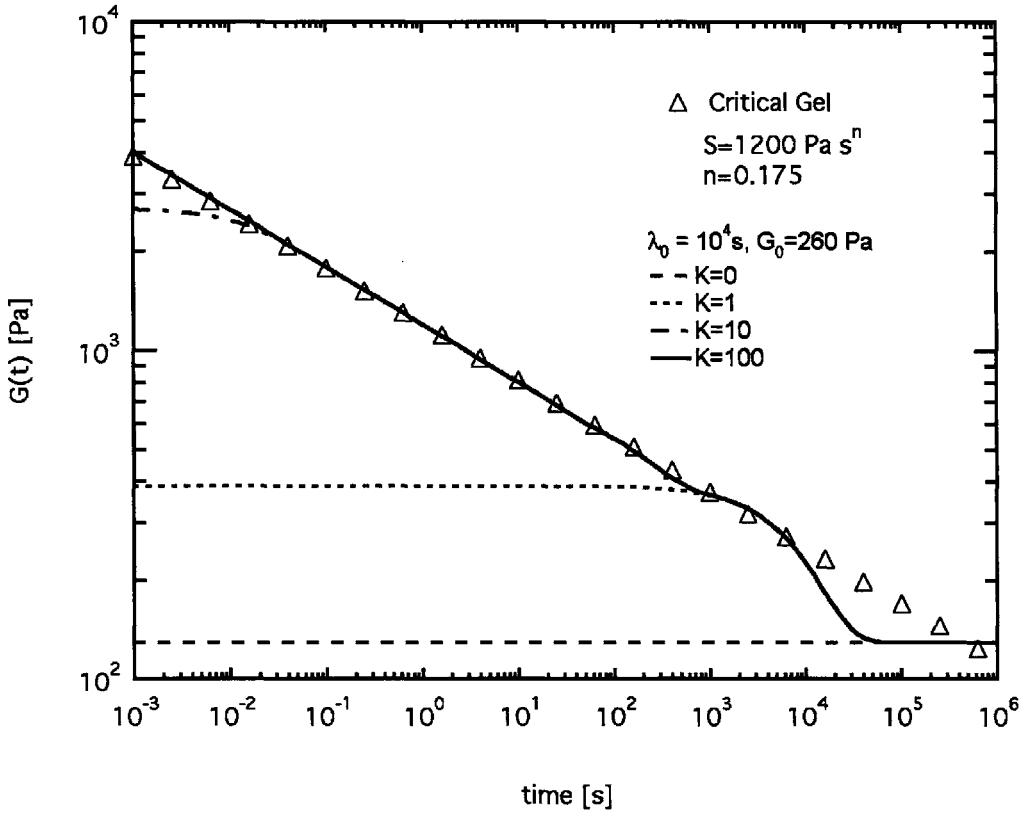

Figure 52. Expressing the power-law relaxation of a critical gel as a series of Maxwell modes. Deviations can be seen at either end of the spectrum corresponding to the longest λ_0 and shortest $\lambda_K = \lambda_0 K^{-1/n}$ time scales of the summation.

In Figure 52, we compare the predicted relaxation modulus of a critical gel (with properties close to that of gluten) as computed with a range of discrete Maxwell modes to the true power-law response. The discrete spectrum of relaxation modes accurately describes the relaxation modulus over a finite time span from a minimum time $\lambda_{min} = \lambda_0 / K^{1/n}$ to a maximum time $\lambda_{max} = \lambda_0$. Beyond this range the relaxation modulus given by (5.7) rolls off to asymptotic values of $G_{min} = G_0/2$ and $G_{max} = (K+1/2)G_0$ respectively. Reconsidering the experimental data in Figure 50, it is clear that we would need at least

$K \simeq \left(\lambda_{max}/\lambda_{min}\right)^n = \left(t_w/\lambda_R\right)^n \simeq 7$ discrete relaxation modes (14 model parameters) to approximately describe the relaxation modulus of a gluten gel. The economy of the two parameter description in equation (5.1) for timescales greater than the Rouse time λ_R and less than the rest time t_w is apparent.

Conceptually, expressing the relaxation spectrum in the forms described in this section reconciles the observed power-law relaxation with the traditional view of exponential stress decay. These spectra represent the range of length-scales present in a fractal network: successive exponential relaxation processes at longer times occur revealing the contributions from progressively longer length scales.

Small Amplitude Oscillatory Shear Flow

For a critical gel undergoing small amplitude oscillatory shear flow, the storage and loss moduli will also show power-law behavior. The dynamic moduli can be evaluated by Fourier-transforming equation (5.1) to obtain [76]:

$$G'_{gel}(\omega) = \frac{G''_{gel}(\omega)}{\tan(n\pi/2)} = \Gamma(1-n)\cos\left(\frac{n\pi}{2}\right)S\omega^n \tag{5.12}$$

In addition to having dynamic moduli that follow the same power-law exponent n, another distinguishing feature of the critical gel model is the relationship between the loss tangent $\tan\delta$ and n:

$$\tan\delta = \frac{G'_{gel}}{G''_{gel}} = \tan\left(\frac{n\pi}{2}\right) \tag{5.13}$$

This ratio is unique and independent of ω and S, in contrast to some other power-law models and takes on a different value to that of the SGR model [156].

Of course, the relaxation processes in the Rouse regime can be similarly transformed:

$$G'_R = G_R \sum_{k=1}^{\infty} \frac{(\lambda_k \omega)^2}{1+(\lambda_k \omega)^2}, \qquad G''_R = G_R \sum_{k=1}^{\infty} \frac{(\lambda_k \omega)}{1+(\lambda_k \omega)^2} \tag{5.14}$$

where $\lambda_k = \lambda_R / k^2$.

The dynamic moduli obtained from small amplitude controlled stress experiments at a stress amplitude of $\sigma_0 = 50\,\text{Pa}$ are plotted in Figure 53. The experimental data are in excellent agreement with predictions from the Fourier transformation of the step-strain relaxation response ($G' = G'_{gel} + G'_R, G'' = G''_{gel} + G''_R$ indicated by solid lines). The Rouse-like regime dominates at high frequencies ($\omega \geq 1/\lambda_R$), while at low frequencies some small deviation from a perfect power-law response can be detected, and we attribute this to the residual relaxation described in the previous section.

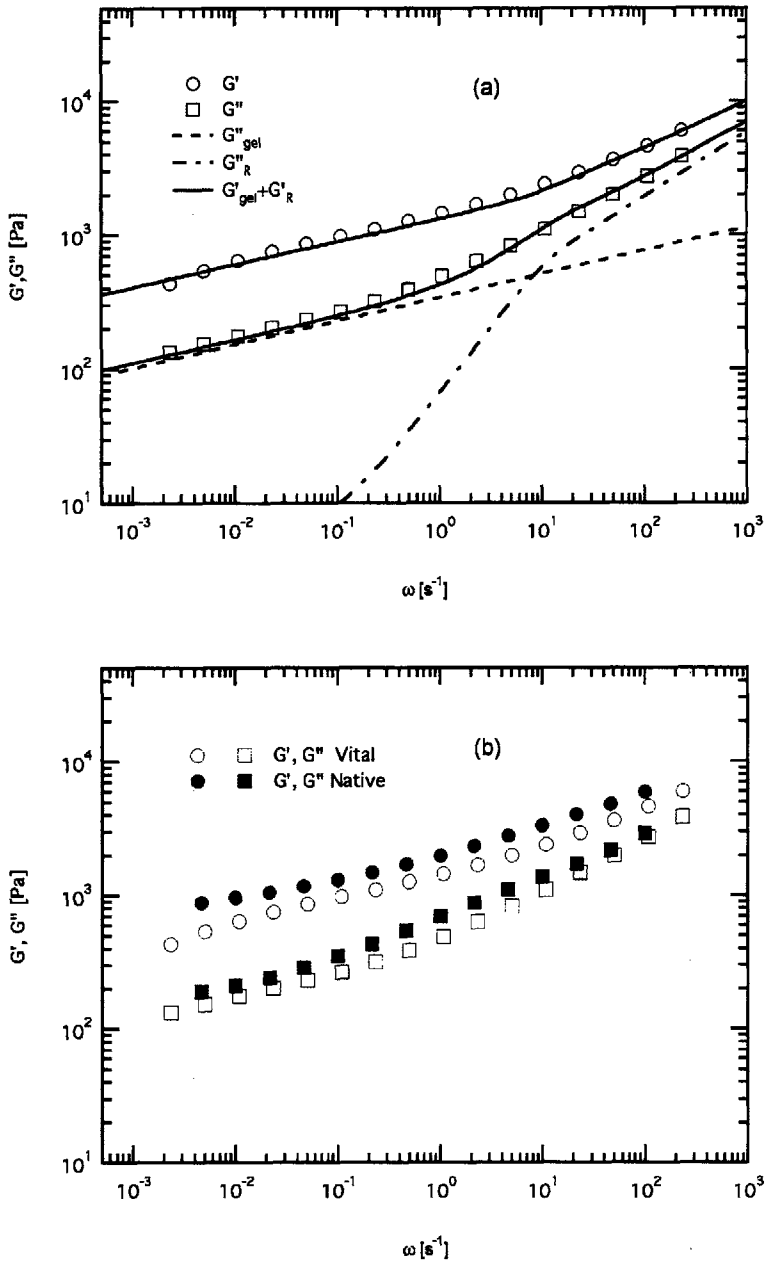

Figure 53 a) Storage and loss moduli measured in small amplitude oscillation. Solid lines represent predictions from equation (5.12) and incorporating Rouse modes: $S = 1260\ \mathrm{Pa s}^n$, $n = 0.17$, $G_R = 803\mathrm{Pa}$, $\lambda_R = 0.05\mathrm{s}$. These parameters were obtained from independent measurements of the relaxation modulus $G(t)$. b) Comparison between dynamic moduli of vital gluten and native (i.e. 'washed') gluten doughs, showing strong qualitative similarities in the frequency response.

We return here briefly to consider the relevance of using doughs formulated from vital gluten powder. The production of vital gluten involves drying and milling which may irreversibly damage or alter the 'functionality' of the network that is formed upon hydration. Ideally, the rheology of a gluten network directly washed-out from wheat flour doughs should be investigated. Unfortunately, the mechanical properties of native gluten networks are difficult to control: the washing process involves gently massaging the dough under running water; it is difficult to maintain consistent mechanical work input and ultimate water content. In Figure 53b, we compare the dynamic moduli of the vital gluten dough with those measured in a gluten network that has been washed out from a freshly mixed wheat flour. Both doughs show viscoelastic moduli of similar magnitudes and the segmental relaxation at high frequencies can also be observed in the native gluten dough. This regime transitions smoothly at $\omega \sim \lambda_R^{-1} \approx 20s^{-1}$ to gel-like behavior at low frequencies in the same manner as the vital gluten dough. Similarities in the low frequency power-law regime are partially masked by the greater variability in the native dough. However the close correspondence between the two sets of linear viscoelastic material functions are sufficient to validate the use of vital gluten doughs as a basis for discussing the role of gluten rheology to realistic breadmaking processes.

Creep

Measuring the creep compliance of soft solids and weak gels has certain advantages, and some of the difficulties encountered in directly measuring the relaxation modulus can be bypassed. Most significantly, while the measured forces decays to diminishingly small values at long times in a relaxation test and become obscured by residual relaxation processes (discussed in section 0), the applied stress is constant in a creep test and the resulting strain grows in time. Consequently, long time scale processes are often better characterized through creep [52].

Creep experiments are performed by incrementing the shear stress from zero to σ_0 such that $\sigma_{xy} = \sigma_0 \hat{H}(t)$, where $\hat{H}(t)$ is the Heaviside step function. From the resulting increase in strain with time $\gamma_{xy}(t)$, we define the creep compliance in the following manner:

$$J(t) = \frac{\gamma_{xy}(t)}{\sigma_0} \tag{5.15}$$

We can also consider the theoretical predictions of creep compliance for a critical gel. The compliance must satisfy the well known relationship given by Ferry [81]:

$$t = \int_0^t G(t-t')J(t')dt' \tag{5.16}$$

Thus with the relaxation modulus of equation (5.1) we can calculate the theoretical compliance [75] through the following expression:

$$J(t) = \frac{1}{S\Gamma(1-n)\Gamma(1+n)} t^n \tag{5.17}$$

Once again, the material function predicted shows a power-law dependence: strain and compliance grow without bound in time as t^n, and no steady state flow viscosity can be measured even as $t \to \infty$.

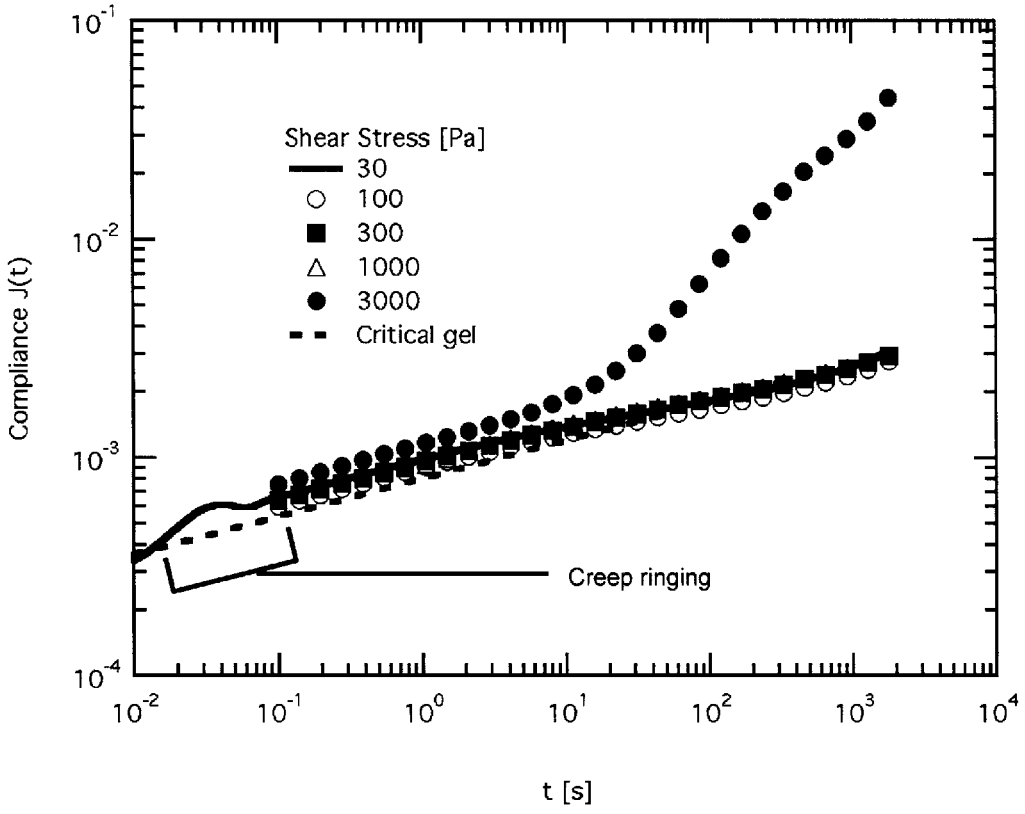

Figure 54 Creep compliance of a gluten gel. Dashed line represents predictions of the critical gel model from equation (5.17) with gel strength $S = 1280$ Pa s^n and gel exponent $n = 0.175$: these parameters are obtained independently from step strain relaxation experiments. Data at $t < 0.1$ s for $\sigma_0 = 30$ Pa are included to illustrate the observed "creep ringing".

In Figure 54, we compare the measured creep compliance of a gluten gel evaluated using equation (5.15) with the response of an ideal critical gel given by equation (5.17). The values of the gel strength $S = 1280$ Pa and gel exponent $n = 0.175$ used in equation (5.17) are obtained independently from step strain relaxation experiments.

One cycle of "damped oscillation" in strain is observed at short times ($t < 0.1$s). This is a consequence of the coupling between instrument inertia and sample elasticity [157], therefore only data from $t > 0.1$s are included in the analysis.

For an applied stress below 3000 Pa, the gluten gel exhibits a linear behavior, i.e. the compliance is independent of applied stress. The qualitative and quantitative agreement with the critical gel model is excellent: the compliance grows as a power-law with exponent $n = 0.175$ over four orders of magnitude in time ($0.1 < t < 2000s$).

For the case in which a shear stress of $\sigma_0 = 3000$ Pa is applied, the material shows an initial power-law increase. This continues up to a shear strain of $\gamma^* \simeq 5$ ($t = 12s$) when the gluten gel yields abruptly, and this is manifested as a rapid increase in strain and compliance. This is followed by an instability at large strain $\gamma \sim 10$ of the same form depicted in Figure 57. The nature of this "yield" event and progression into non-linearity is explored in greater detail in section 5.5 using controlled strain experiments.

Over the duration of the experiments, no steady state was observed for any of the shear stresses tested, this feature of gluten and dough rheology has also been discussed in detail by Lefebvre and co-workers [30, 52].

General Linear Viscoelastic Response

We have demonstrated through small amplitude oscillations, stress relaxation and creep measurements that gluten doughs exhibit a linear viscoelastic response that is strongly reminiscent of a polymeric critical gel. We now conclude this section by considering the linear viscoelastic stress response to an arbitrary deformation together with a brief summary of the historical development of the gel equations.

Using the Boltzmann superposition principle, we can write an integral constitutive equation for an arbitrary deformation history:

$$\sigma(t) = \int_0^t S(t-t')^{-n} \dot{\gamma}(t') dt' \tag{5.18}$$

where $\dot{\gamma}(t) = \nabla v + (\nabla v)^T$ is the infinitesimal strain rate tensor [60]. However, it must be stressed that this equation is only valid for infinitesimally small deformations. The response under finite strains is the subject of the following section.

The relaxation function of a critical gel (equation (5.1)) is also known as the Nutting's equation [158] and has long been used as an empirical approximation of material functions. Well before the concept of a critical gel was proposed, Scott Blair [159] generalized Nutting's equation by adopting the framework of fractional calculus [160] and arrived at the differential form of equation (5.18) given in the following expression:

$$\sigma(t) = \frac{S}{\Gamma(1-n)} \frac{\partial^n}{\partial t^n} \gamma(t) \tag{5.19}$$

Equation (5.19) can be considered to be a generalization of the mechanical analogs of springs ($n = 0$) dashpots ($n = 1$) and is often referred to as a Scott Blair element [161]. Scott Blair himself described the material parameters S and n as *quasi-properties* [159], he suggested that the non-integer exponents are a consequence of a "non-Newtonian equilibrium" and are closely correlated with perceptions of texture and firmness. Friedrich and Heymann [162] recognized this link between fractional calculus models and the critical gel, they generalized the stress relaxation function to include the post- and pre-gel states that exists near the solid-liquid transition.

Despite the sharp conceptual difference with traditional models that show exponentially decaying stress, these fractional calculus models have proven to be of great practical utility because they allow engineers to accurately model damping properties for many viscoelastic polymers with a minimum number of parameters. Winter and Mours noted that the damping properties (characterized by the loss tangent) is independent of temperature and frequency [77]; however,

a critical gel can still undergo dynamic oscillations at a characteristic frequency when coupled with a free mass. A convenient example is the viscoelastic ringing already encountered during the initial transient response of creep experiments depicted in Figure 54. We can write the equation of angular motion for the instrument coupled with the viscoelasticity of the sample as:

$$I\ddot{\phi} + b\frac{S}{\Gamma(1-n)}\frac{\partial^n \phi}{\partial t^n} = \mathrm{P}(t) \tag{5.20}$$

Where I is the instrument moment of inertia, b is the geometry factor, ϕ[rad] is the angle of plate rotation and P [Nm] is the instrument-applied torque. For our experiments shown in Figure 54 we have:

$$\begin{aligned} I &= 21.04 \times 10^{-6}\ \mathrm{Nms}^{-2} \\ b &= \pi \mathrm{R}^4/(2h) = 3.9\times10^{-5}\mathrm{m}^3 \\ R &= \text{ plate radius} = 12.5\times10^{-3}\mathrm{m} \\ h &= \text{ sample thickness} = 1\times10^{-3}\mathrm{m} \end{aligned} \tag{5.21}$$

The ringing frequency is given by the minima of the (complex) characteristic equation:

$$-\omega^2 I + b\frac{S}{\Gamma(1-n)}(i\omega)^n = 0 \tag{5.22}$$

This frequency can be evaluated numerically and is found to be 68.5 rad s^{-1} ($t^* = 0.09$ s) which is in good agreement with the heavily damped ringing frequency observed in creep experiments. Such excellent agreement is perhaps surprising, since the fixture response during the initial transients should also be influenced by the Rouse modes of the system ($t \sim \lambda_R = 0.05$ s).

5.5. *Critical gel response under finite strain*

We have examined the linear viscoelasticity of a critical gel and showed that for time-scales greater than the segmental relaxation time λ_R, the rheology can be economically described by two parameters, the gel strength S, and the gel

exponent n. As mentioned in the introduction, characterizing the non-linear deformation of a critical gel is essential in many applications. For example, in adhesives applications [77], information on the strain to failure can be useful. In bread and gluten dough, researchers have found little or no correlation between linear viscoelastic material functions and baking qualities. This of course should not be surprising, because non-linear deformation (kneading, proofing, baking etc...) feature prominently in the process of breadmaking [4, 6, 7, 44, 147].

Large Step Strain Relaxation

We begin probing the non-linear deformation of the gluten gels by simply increasing the amplitude γ_0 of the step strain relaxation tests discussed in section 0. The results are plotted in Figure 55a.

Qualitatively, the relaxation modulus at large strain amplitude is observed to be a function of both time and strain $G = G(t, \gamma_0)$. Both the Rouse segmental relaxation and power-law gel regimes are still clearly visible. Since it is the power-law/critical gel region that we are most interested, we can gain insight into this non-linear behavior by seeking a function that will collapse the data in this regime onto a single curve. The power-law exponent of the relaxation remains approximately constant despite the increase in strain, therefore a simple vertical shift factor – or damping function – suffices to collapse the data. In other words, the data can be taken to be time-strain separable in the power-law regime:

$$G(t, \gamma_0) = G(t)h(\gamma_0) = St^{-n}h(\gamma_0) \tag{5.23}$$

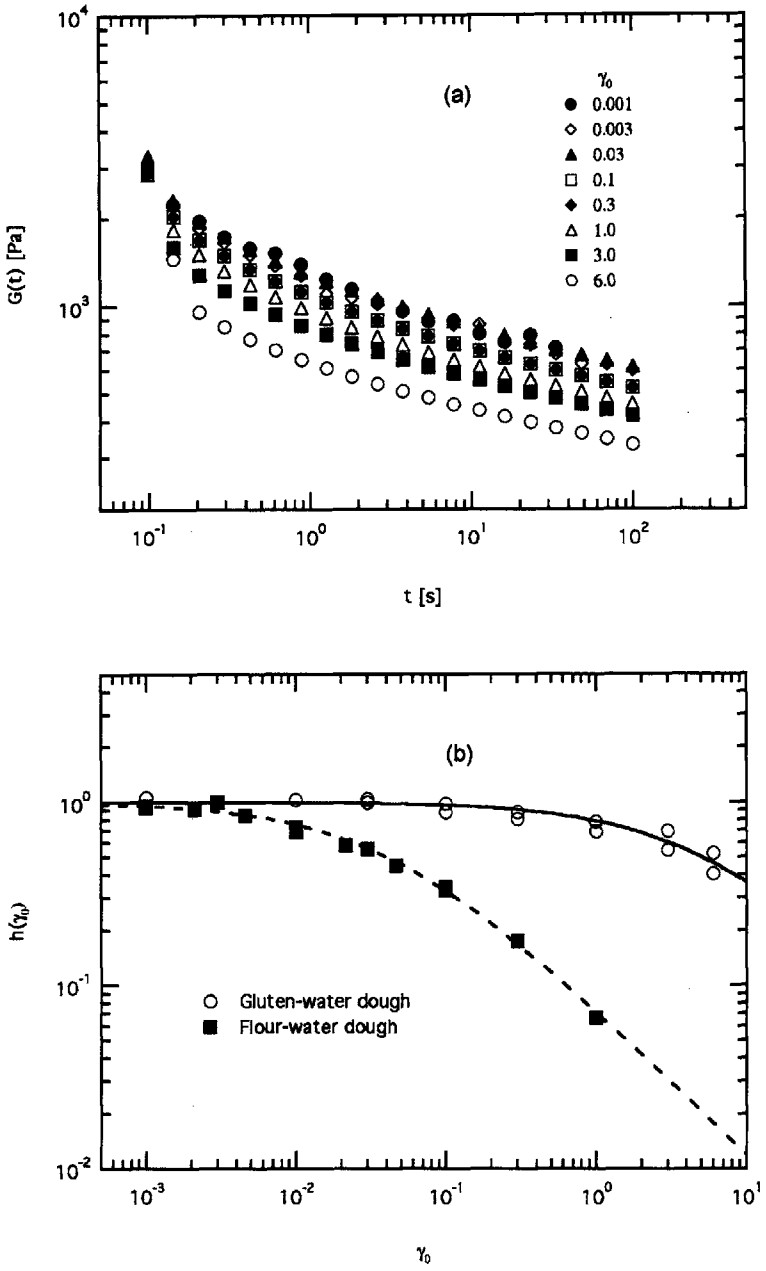

Figure 55 a) Stress relaxation function $G(t)$ of gluten dough for a range of finite step shear strains with magnitude γ_0. b) Damping function for finite strain amplitude stress relaxation experiments. Lines correspond to algebraic fit to the data set, $h(\gamma)=1/\left(1+(q\gamma_0)^{2k}\right)$. Unfilled gluten dough ($q=0.2, k=0.4$) shows substantially reduced damping compared to highly-filled wheat flour-water dough systems ($q=25, k=0.4$).

The resulting damping function is plotted in Figure 55b. The strain softening effect in the gluten gel is relatively weak, especially when compared to the highly-filled wheat flour systems, in which non-linearity begins at extremely small strains [163]. To quantitatively compare the two sets of data, they are fitted to a simple algebraic function that is motivated by the form commonly used to describe strain-softening in entangled melts $h(\gamma) = 1/\left(1+(q\gamma)^{2k}\right)$ [126]. The rate of softening $k = 0.4$ is the same for both systems; the onset of non-linear behavior corresponding to a critical strain $\gamma_0^* \sim q^{-1}$ occurs at $\gamma_0^* \sim 0.04$ for wheat flour dough but not until $\gamma_0^* \sim 5$ for gluten systems.

The weak damping characteristic of gluten dough is consistent with critical gels that are formed from randomly cross-linked networks of flexible polymeric strands. Even though particulate gels can also form self-similar fractal structures that exhibit power-law rheology in their linear viscoelastic material functions, they are typically "brittle". Non-linear behavior of particulate gels are commonly characterized by rapid softening or yielding at strains that are seldom greater than unity i.e. $\gamma^*_{Particulate} < 1$ [141, 164].

In fact, the behavior seen here is very similar to the damping function for critical gels polyvinylchloride in dioctyl phthlate (PVC-DOP) reported by Watanabe et al [149]. They argue that in contrast to highly entangled systems which show reptation dynamics, the recovery of polymer chains to their equilibrium length occurs at the same rate as orientation rearrangements in fractal networks; thus resulting in a damping function that is close to unity. The similar lack of reptation dynamics or a distinct yielding process observed in the present work strongly suggests that gluten gels should also be viewed as a polymeric network rather than a particulate gel or highly entangled melt.

The large range of linear response also suggests that gluten doughs can be treated up to moderately large strains approximately as a quasi-linear elastic material [60]. If we are to express the constitutive equation for the gluten gel as an integral model of the factorized Rivlin-Sawyer form, a simplification to the

strain-dependent function can be made, such that $h(\gamma) \simeq 1$; the non-linearity in the constitutive equation associated with large strains is then contained exclusively in the deformation tensors. This leads to greatly simplified constitutive equations and analytical solutions are possible for a wide variety of flow conditions. The construction of such a constitutive model will be the subject of the following section.

Transient Experiments

For quasi-linear models under finite deformation, the infinitesimal strain rate tensor $\dot{\gamma}$ in equation (5.18) must be replaced by a finite strain rate tensor $\frac{\partial}{\partial t'}C^{-1}(t,t')$ to preserve frame invariance [60]. $C^{-1}(t,t')$ is the Finger strain tensor. We can write a frame invariant constitutive equation [77] by considering a linear superposition of stress relaxation modes associated with this finite rate of strain $\frac{\partial}{\partial t'}C^{-1}(t,t')$:

$$\begin{aligned}\boldsymbol{\sigma}(t) &= -\int_0^t G(t-t')\frac{\partial}{\partial t'}C^{-1}(t,t')\,dt' \\ &= -\int_0^t S(t-t')^{-n}\frac{\partial}{\partial t'}C^{-1}(t,t')\,dt' \quad \text{for the gel equation}\end{aligned} \tag{5.24}$$

This form of constitutive equation (with an unspecified form of $G(t-t')$) is generically referred to as a Lodge rubber-like network model [165]. We refer to the particular constitutive model in equation (5.24) with a power-law relaxation modulus as the *generalized gel model.*

By analogy to the discussion in the previous section, equation (5.24) can also be expressed in a differential form:

$$\boldsymbol{\sigma}(t) = -\frac{S}{\Gamma(1-n)}D^n\left[C^{-1}(t,t')\right] \tag{5.25}$$

where the fractional differential operator denoted D^n is the convected fractional derivative which satisfies material objectivity [166].

In the limits of infinitesimal strains, equations (5.24) and (5.25) reduce to (5.18) and (5.19) respectively. To explore the constitutive response of gluten gels at large strains, we now consider the form of $C^{-1}(t,t')$ and $\frac{\partial}{\partial t'}C^{-1}(t,t')$ for specific modes of deformation commonly used in rheometric testing and the resulting form of the stress tensor.

Start-up of Steady Shear

In a step shear rate experiment, in which the rate of shearing strain is incremented from zero to $\dot{\gamma}_0$, such that $\dot{\gamma}_{xy}(t)=\dot{\gamma}_0\hat{H}(t)$, the finite strain and rate tensor takes the form:

$$C^{-1}=\begin{bmatrix}1+\dot{\gamma}_0^2(t-t')^2 & \dot{\gamma}_0(t-t') & 0\\ \dot{\gamma}_0(t-t') & 1 & 0\\ 0 & 0 & 1\end{bmatrix} \text{ for } 0\le t'\le t$$
$$=\begin{bmatrix}\dot{\gamma}_0^2t^2 & \dot{\gamma}_0t & 0\\ \dot{\gamma}_0t & 0 & 0\\ 0 & 0 & 0\end{bmatrix} \text{ for } t'<0 \qquad (5.26)$$

$$\frac{\partial}{\partial t'}C^{-1}=\begin{bmatrix}-2\dot{\gamma}_0^2(t-t') & -\dot{\gamma}_0 & 0\\ -\dot{\gamma}_0 & 1 & 0\\ 0 & 0 & 1\end{bmatrix} \text{ for } 0\le t'\le t$$
$$=\quad 0 \qquad\qquad \text{for } t'<0 \qquad (5.27)$$

Inserting the respective components into equations (5.24) or (5.25) gives an expression for the transient growth in the shear stress:

$$\begin{aligned}\sigma_{xy} &= -\int_0^t S(t-t')^{-n}\left[-\dot{\gamma}_0\right]dt' \\ &= S\dot{\gamma}_0\int_0^t (t-t')^{-n}\,dt'\end{aligned} \tag{5.28}$$

Substituting $r = t - t'$ and integrating, we find:

$$\sigma_{xy}^{+} = S\dot{\gamma}_0\int_0^t r^{-n}dr = S\dot{\gamma}_0\left[\frac{r^{1-n}}{1-n}\right]_0^t = \frac{S\dot{\gamma}_0}{1-n}t^{1-n} \tag{5.29}$$

So that the shear stress in a critical gel grows in time without bound as a power-law with t^{1-n}. The total strain imposed is $\gamma = \int_0^t \dot{\gamma}_0\,dt' = \dot{\gamma}_0 t$. We also note that the response (5.28) is factorizable into shear-strain and shear-rate contributions:

$$\begin{aligned}\sigma_{xy}^{+}(\dot{\gamma}_0,\gamma) &= \frac{S}{1-n}\dot{\gamma}_0{}^{n}\gamma^{1-n} \quad \text{for } \gamma \geq 0 \\ &= S\,f(\dot{\gamma}_0)\Phi_{xy}(\gamma)\end{aligned} \tag{5.30}$$

Where $f(\dot{\gamma}_0) = \dot{\gamma}_0^n$ and $\Phi_{xy}(\dot{\gamma}_0) = \gamma^{1-n}/(1-n)$.

In Figure 56 we demonstrate the ability of this generalized gel equation to predict the growth in the shear stress of gluten gels during the start-up of steady shear flow. After an initial short time response ($t \leq 0.1s$) which is governed by the Rouse modes convoluted with the finite response function of the rheometer, the material functions increase as power laws (i.e. straight lines on a log-log scale). The shear stress increases with shear strain as γ^{1-n} (equation (5.30)) and the data can be collapsed onto a single power law strain function $\Phi_{xy}(\gamma)$ by factoring out the rate-dependent component, $f(\dot{\gamma}_0) = \dot{\gamma}_0^n$. All of the samples show slip and/or fracture at large strains $\gamma \sim 10$ despite our efforts to prevent slip (Section 5.2).

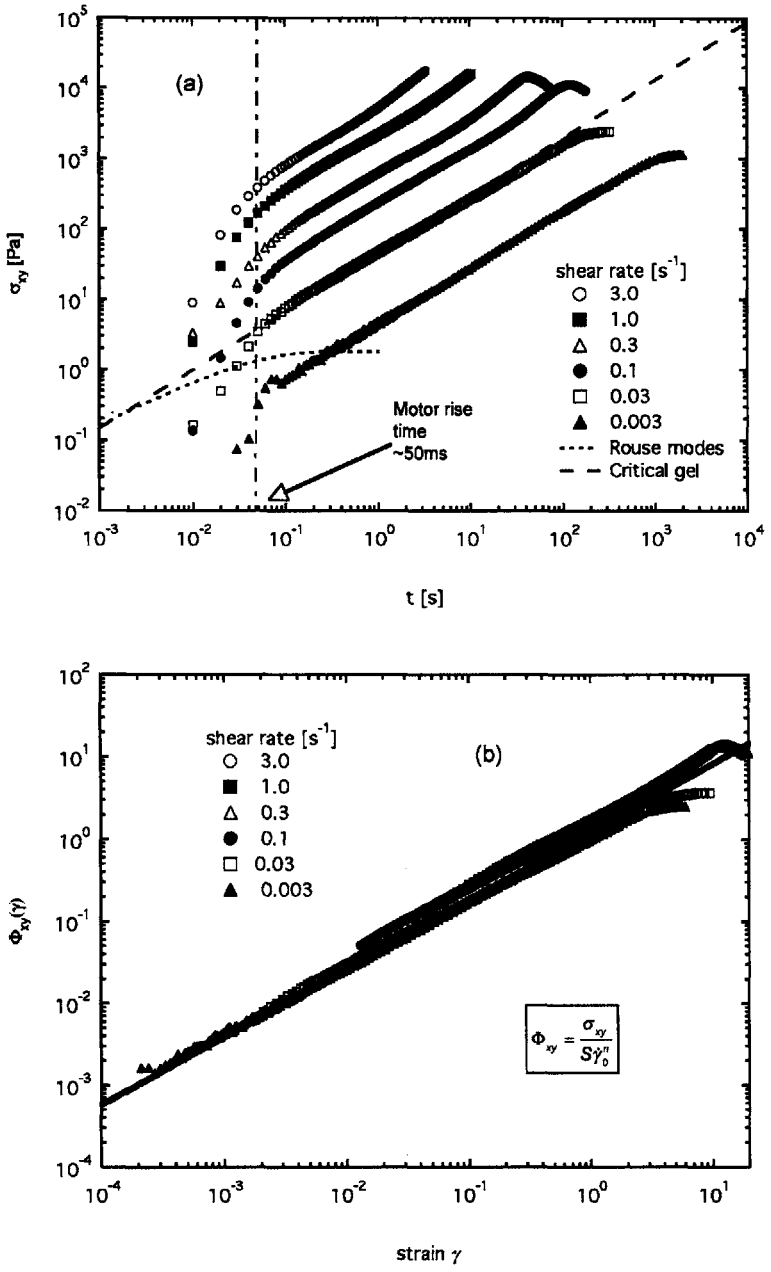

Figure 56 a) Transient shear stress during start-up of shear flow as a function of time measured for shear rates $0.003 \le \dot{\gamma}_0 \le 3.0\,\mathrm{s}^{-1}$. The calculated response from the critical gel component and Rouse modes for $\dot{\gamma}_0 = 0.03\,\mathrm{s}^{-1}$ are plotted as dashed lines. Deviation from equation (5.28) at $t \le 0.05$ s is a result of the finite rise time (~50 ms) of the motor. b) All curves can be collapsed onto a master strain function $\Phi_{xy}(\gamma) = \gamma^{1-n}/1-n$ (solid line) by factoring out the rate dependence $f(\dot{\gamma}_0) = \dot{\gamma}_0^n$.

At the highest strains and shear rates tested ($\gamma > 5, \dot{\gamma}_0 > 0.1s^{-1}$), the gluten gels exhibit a stress overshoot, in contrast to the softening observed in the previous section for step strain relaxation. The rheological significance of this overshoot remains unclear. Phan-Thien and coworkers [104] attempted to model the overshoot behavior through the use of a highly non-linear strain function that incorporates both strain stiffening and softening of the form:

$$\sigma_{PT}(\gamma) = G\Psi_{PT}(\gamma)\left(C^{-1} - aC\right)$$
$$\Psi_{PT}(\gamma) = \frac{1}{\left(1+\Gamma_1^2\gamma^2\right)^{(1-m)/2}}\exp\left(-\Gamma_2^4\gamma^4\right) \tag{5.31}$$

Where Γ_1, Γ_2, a and m are material constants, C is also known as the left-Cauchy-Green tensor. However in our experiments, we observed this phenomenon to be closely associated with a torsional elastic instability as depicted in Figure 57. This instability occurred shortly after the transient shear stress deviated from the predicted power-law form and becomes extremely severe at the point of stress softening: the sample rolls up and is ejected from the geometry gap. The flow is no longer viscometric at the onset of this instability and therefore we have made no attempts to model it constitutively.

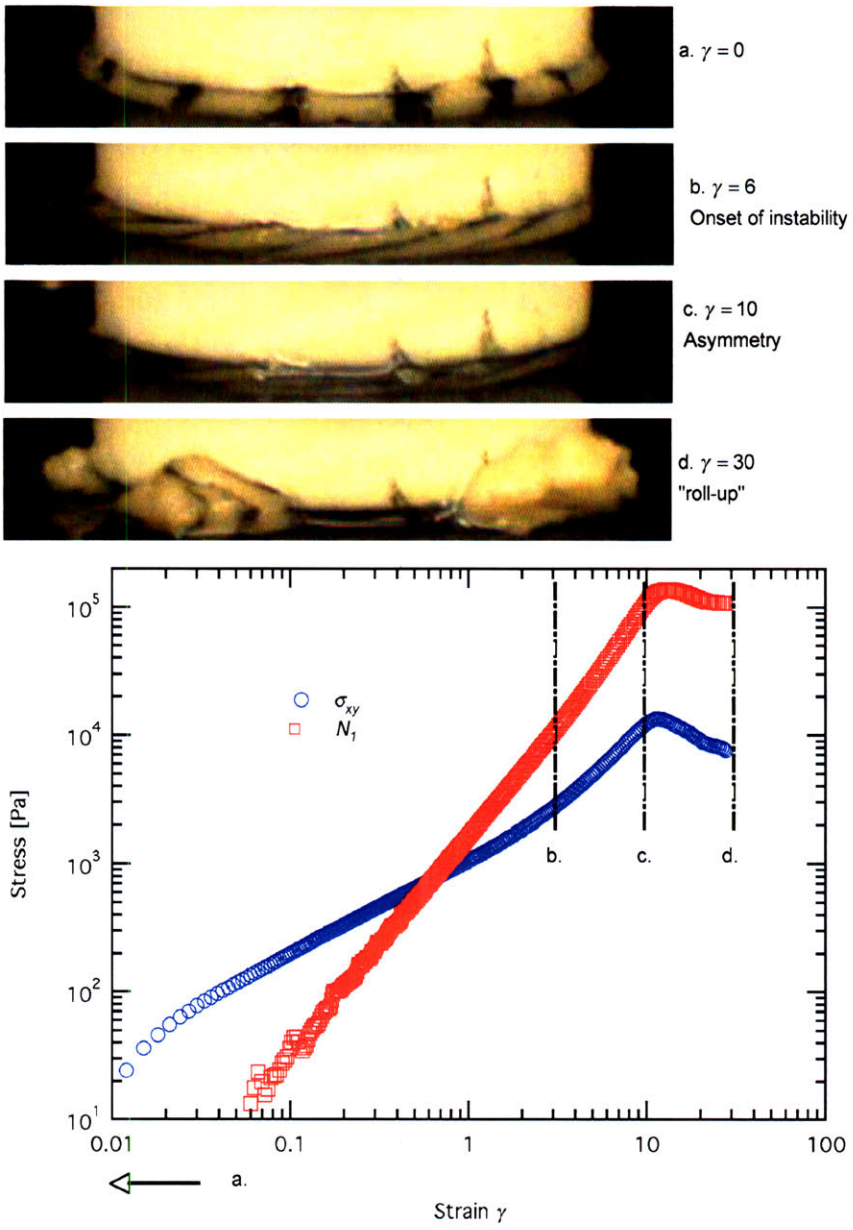

Figure 57 Torsional elastic instability at $\dot{\gamma}_0 = 1\ s^{-1}$. a. Initial conditions, b. Onset of instability; Initially vertical lines drawn on the sample with ink indicate uniform deformation up to this point; c. Sample becomes asymmetric and is retracted away from point of view while being ejected from the other side of the geometry, d. Sample rolls up and is ejected from rheometer.

Nevertheless, the fact that linear deformation persists without yield up to large strains is once again a strong indication that gluten doughs are polymeric gel networks consisting of flexible or semi-flexible filaments. This class of systems include many biopolymer gels that often exhibit extremely large linear range and has non-linear regimes that are typified by a stiffening behavior before yield [137, 167], in a manner very similar to the behavior of the gluten gel.

In fact the behavior of these gluten gels also bears a strong resemblance to the data reported by Venkataraman and Winter [75] on a synthetic critical gel. The PDMS they studied also forms a cross-linked polymeric network with flexible chains between junction points; they observed a relatively large linear range during start-up of steady shear flow ($\gamma^* \sim 2$) and a mild stress overshoot at large strains. However, the separability of the measured material response into rate-dependent and strain dependent functions cannot be checked in this previous study because data at only a single shear rate ($\dot{\gamma}_0 = 0.5\ s^{-1}$) was presented.

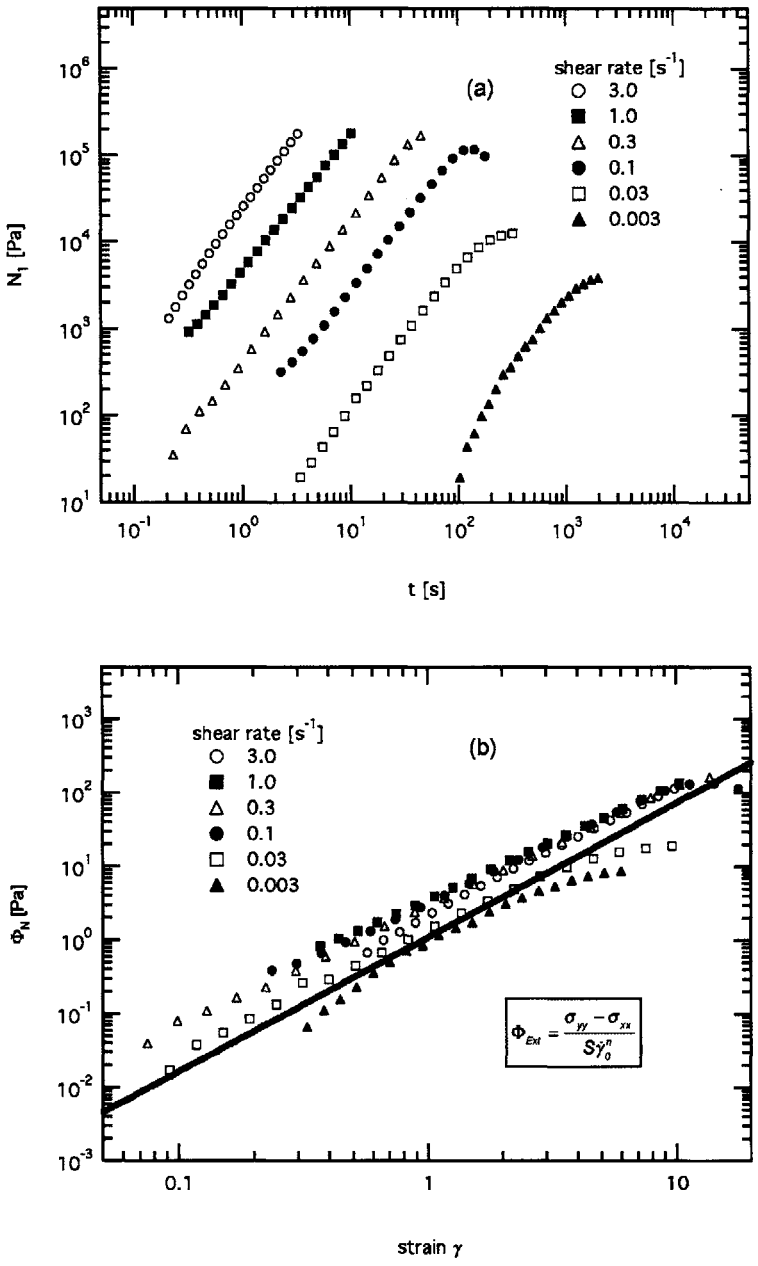

Figure 58. a) Power-law growth in the first normal stress difference as a function of time measured for shear rates $0.003 \le \dot{\gamma} \le 3.0\ s^{-1}$. b) All curves can be collapsed onto a master strain function $\Phi_N(\gamma)$ by factoring out the rate dependence $f(\dot{\gamma}_0) = \dot{\gamma}_0^n$. The solid line is the strain function $\Phi_N = 2\gamma^{2-n}/(2-n)$ given in equation (5.33) with $n = 0.175$ determined from linear viscoelastic measurements.

In these start-up experiments, we can also follow the evolution in the first normal stress difference of the gluten gels. From equation (5.24) we find:

$$\begin{aligned} N_1^+(\dot{\gamma}_0,t) \equiv \sigma_{xx}(t)-\sigma_{yy}(t) &= -\int_0^t S(t-t')^{-n}\left[-2\dot{\gamma}_0^2(t-t')\right]dt' \\ &= 2S\dot{\gamma}_0^2\int_0^t (t-t')^{1-n}dt' \\ &= 2S\dot{\gamma}_0^2\left[-\frac{1}{2-n}(t-t')^{2-n}\right]_0^t \\ &= \frac{2S}{(2-n)}\dot{\gamma}_0^2 t^{2-n} \\ &= \frac{2S}{(2-n)}\dot{\gamma}_0^n \gamma^{2-n} \end{aligned} \tag{5.32}$$

Notably, this result is again strain/strain-rate separable and can be written in the form:

$$\sigma_{xx}(t)-\sigma_{yy}(t) = Sf(\dot{\gamma})\Phi_N(\gamma) \tag{5.33}$$

Where, as in equation (5.30), the function $f(\dot{\gamma}_0)=\dot{\gamma}_0^n$ and the strain function for the normal stress difference is $\Phi_N = 2\gamma^{2-n}/(2-n)$.

In Figure 58 we show that the first normal stress difference measured in a gluten water dough system can also be described quite well by equation (5.32). The data shows a positive power-law increase in the normal stress difference with strain (typical of polymer networks) corresponding to an exponent of γ^{2-n}. The values of $S=1280\ Pa\,s^n$ and $n=0.175$ are consistent with those obtained from linear viscoelastic measurements. These curves can also be approximately collapsed onto a single curve by factoring out the rate-dependent component $f(\dot{\gamma})=\dot{\gamma}_0{}^n$. The normal force data show less perfect superposition when compared with the measured shear stress response. When the plates are brought together during loading and the sample is squeezed into a disc shape, the axial compressive

strain can result in substantial normal forces even when slow compression rates and long waiting times are employed, and this contributes to the observed variability at low deformation rates. The effect of this residual stress relaxation is analogous to that described in section 0. Nonetheless, the power-law growth in N_1 at large shear rates is very clear across several decades in stress. It is interesting to note that in the generalized gel equation, the ratio between transient shear stress and normal stress difference is given by $N_1/\sigma_{xy} = 2\gamma(1-n)/(2-n)$. For an ideal critical gel, this relationship is valid even in the limit of infinitely rapid deformations. This modified elastic response can be contrasted with that expected of typical viscoelastic materials which show purely elastic behavior at time shorter than the most rapid relaxation time: the Lodge-Meissner relationship [168] shows that the stress ratio approaches $N_1/\sigma_{xy} = \gamma$. The modified elastic behavior noted above is a distinguishing feature of a critical gel but might not be of practical utility in determining the gel point, especially for materials with small values of n. Furthermore, for gluten gels, the presence of a cut-off at the segmental relaxation time scale λ_R reported in the previous section will obscure the observation of this relationship at very high shear rates when $Wi_R = \lambda_R \dot{\gamma}_0 > 1$.

Start-up of Uniaxial Extensional Flow

Elongational deformations provide a litmus test for the robustness of the generalized gel equation. The applicability of a rheological constitutive equation such as the critical gel model is greatly increased if material parameters obtained from small amplitude shear experiments can be used to predict the rheological behavior under vastly different flow conditions such as those observed under large extensional strains.

In strong flows such as uniaxial elongation, the integral expression to be evaluated for the stress becomes slightly more involved because the components of the finite strain-rate tensor increase exponentially with strain rather than

polynomially. For extensional stress growth following inception of a uniaxial extensional flow at a finite constant strain rate, the Finger strain tensor $C^{-1}(t,t')$ and finite rate of strain tensor $\frac{\partial}{\partial t'}C^{-1}(t,t')$ are:

$$\begin{aligned} C^{-1} &= \begin{bmatrix} \exp\left[-\dot{\varepsilon}_0(t-t')\right] & 0 \\ 0 & \exp\left[2\dot{\varepsilon}_0(t-t')\right] \end{bmatrix} \text{ for } 0 \le t' \le t \\ &= \begin{bmatrix} \exp\left[-\dot{\varepsilon}_0(t')\right] & 0 \\ 0 & \exp\left[2\dot{\varepsilon}_0(t)\right] \end{bmatrix} \qquad \text{for } t' < 0 \end{aligned} \tag{5.34}$$

$$\begin{aligned} \frac{\partial}{\partial t'}C^{-1} &= \begin{bmatrix} \dot{\varepsilon}_0\exp\left[-\dot{\varepsilon}_0(t-t')\right] & 0 \\ 0 & -2\dot{\varepsilon}_0\exp\left[2\dot{\varepsilon}_0(t-t')\right] \end{bmatrix} \text{ for } 0 \le t' \le t \\ &= 0 \text{ for } t' < 0 \end{aligned}$$

The normal stress difference predicted by the generalized gel equation in steady uniaxial extension is then:

$$\sigma_{zz}(t) - \sigma_{rr}(t) = \int_0^t S(t-t')^{-n}\dot{\varepsilon}_0\left\{2\exp\left(2\dot{\varepsilon}_0[t'-t']\right) + \exp\left(-\dot{\varepsilon}_0[t-t']\right)\right\}dt' \tag{5.35}$$

We first perform a change of variable to recast the solution into a separable form composed of a rate-dependent term and a strain-dependent integral. Substituting for the Hencky strain $\varepsilon(t) = \dot{\varepsilon}_0 t$ and the strain difference $r = \dot{\varepsilon}_0(t-t')$, we obtain:

$$\Delta\sigma(\varepsilon) = S\dot{\varepsilon}_0^n\int_0^\varepsilon r^{-n}\left\{2\exp(2r) + \exp(-r)\right\}dr \tag{5.36}$$

The extensional stress growth in a critical gel can once again be written in terms of rate- and strain-dependent components by factorizing equation (5.36) to give:

$$\Delta\sigma(\dot{\varepsilon}_0,\varepsilon) = Sf(\dot{\varepsilon}_0)\Phi_{Ext}(\varepsilon) \tag{5.37}$$

where

$$f(\dot{\varepsilon}_0) = \dot{\varepsilon}_0^n$$
$$\Phi_{Ext} = \int_0^{\varepsilon} r^{-n}\left\{2\exp(2r) + \exp(-r)\right\}dr \tag{5.38}$$

The integral for the strain dependent function can be integrated repeatedly by parts to yield a solution in the form of a summation. However, this approach is rather cumbersome and the result converges slowly. It is more convenient to consider approximations to the expression at large and small strain limits.

For small strains (i.e. $\varepsilon \ll 1$), equation (5.37) approaches the linear viscoelastic limit:

$$\Delta\sigma(\dot{\varepsilon}_0, \varepsilon) \to \frac{3S}{1-n}\dot{\varepsilon}_0^n \varepsilon^{1-n}, \text{ as } \varepsilon \to 0$$
$$\Phi_{Ext} \simeq \frac{3\varepsilon^{1-n}}{1-n} \tag{5.39}$$

The corresponding Trouton ratio approaches:

$$Tr^+ = \frac{\sigma_{Ext}(\dot{\varepsilon}_0, \varepsilon)}{\sigma_{xy}(\dot{\gamma}_0, \gamma)} \to 3, \text{ for } \varepsilon \ll 1 \tag{5.40}$$

where $\dot{\gamma}_0 = \sqrt{3}\dot{\varepsilon}_0$ and $\gamma = \sqrt{3}\varepsilon$ is used in evaluating the ratio.

At large strains (i.e. $\varepsilon \gg 1$), an asymptotic approximation can be made such that:

$$\Delta\sigma \simeq S\dot{\varepsilon}_0^n \varepsilon^{-n}\exp(2\varepsilon)$$
$$\Phi_{Ext} \simeq \varepsilon^{-n}\exp(2\varepsilon) \tag{5.41}$$
$$Tr^+ \simeq (1-n)\varepsilon^{-1}\exp(2\varepsilon)$$

An approximation is made to equation (5.38) by considering a function that smoothly connects the two limits (equation (5.39) and (5.41):

$$\Delta\sigma^{+}_{Ext} \simeq S\dot{\varepsilon}_0^{n}\varepsilon^{-n}\left[\exp(2\varepsilon)+\frac{(1+2n)}{1-n}\varepsilon-1\right]$$
$$\Phi^{+}_{Ext} \simeq \varepsilon^{-n}\left[\exp(2\varepsilon)+\frac{(1+2n)}{1-n}\varepsilon-1\right] \qquad (5.42)$$
$$Tr^{+} \simeq \frac{(1-n)}{\varepsilon}\left[\exp(2\varepsilon)-1\right]+(1+2n)$$

Equations in (5.42) are a surprisingly accurate approximation and is barely distinguishable from the true solution over the range of strains discussed in this article.

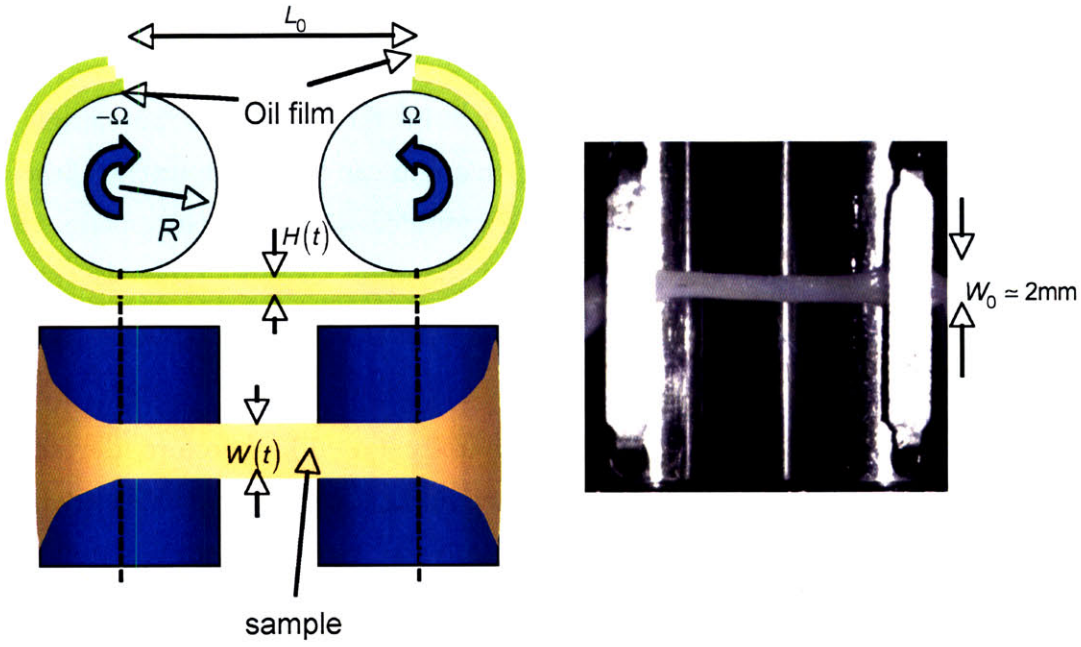

Figure 59 Schematic of the Sentmanat Extensional Rheometer (SER). The sample of initial cross-section area $W_0 \times H_0$ and gage length L_0 is stretched between two counter-rotating cylindrical drums.

We examine the response of gluten gels experimentally under uniaxial extension using a wind-up drum type rheometer. The geometry is shown in Figure 59. A Sentmanat Extensional Rheometer (SER) fixture [122] is mounted onto the ARES

rheometer. Samples of gluten gel ($L_0 = 12.5\text{mm}, H_0 = W_0 \simeq 2\text{mm}$) are held in place between two cylinders by clamps and then stretched uniaxially as the cylinders are rotated by the drive system of the rheometer. The resulting torque and sample deformation are measured independently through the ARES torque transducer and digital video imaging respectively. Figure 60 illustrates the measurements obtained during a typical experiment.

The counter rotating cylinders apply a nominal strain rate of:

$$\dot{E} = \frac{2\Omega R}{L_0} \tag{5.43}$$

However, the true strain rate in the sample is also independently measured from video images. A thin film of oil is painted onto the surface of the sample to eliminate evaporation and sample drying, this film can also inadvertently lead to slip in the contact area with the rotating cylinders [126]. Measurements with polyisoprene have shown that if the sample aspect ratio is small, i.e. $\Lambda = H/W \ll 1$, the deformation will deviate from uniform uniaxial stretching [169] and approaches the planar limit instead as $\Lambda \to 0$. In the present experiments, the aspect ratio is close to unity ($\Lambda \sim 1$), therefore the actual deformation can be well approximated by homogeneous uniaxial stretching. Video imaging at 100 frames/sec. confirms the assumptions of uniform uniaxial deformation and no-slip at the cylinder-sample interface. The strain rate calculated from lateral contraction of the sample $\dot{\varepsilon}(t)$ is identical to the imposed longitudinal strain $\dot{E}(t)$, and the width $W(t)$ of the sample thus decays as a simple exponential:

$$\begin{aligned} \dot{\varepsilon} &= -\frac{2}{W(t)}\frac{dW(t)}{dt} \simeq \dot{E} \\ W(t) &\simeq W_0 \exp\left(-\dot{E}t/2\right) \end{aligned} \tag{5.44}$$

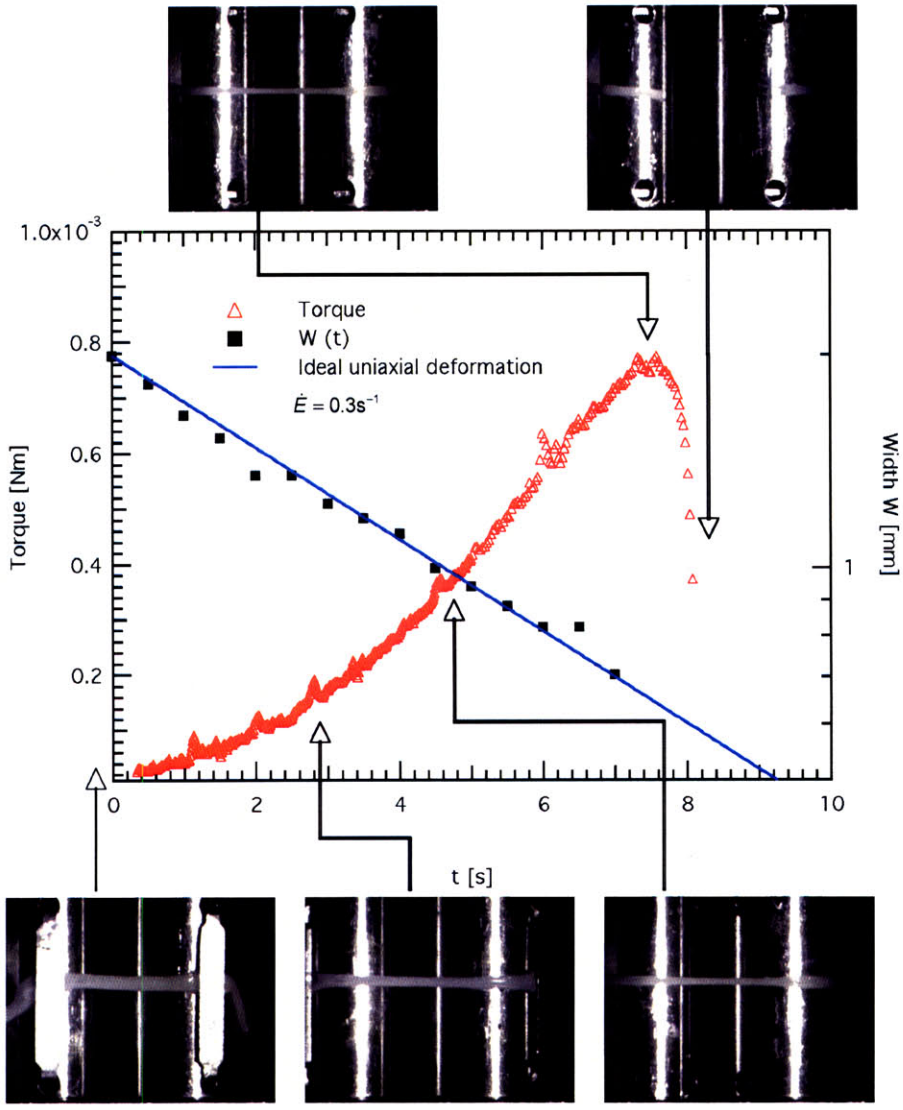

Figure 60 Wind-up drum rheometry of a gluten gel using the SER fixture. Deformation and torque measurements were provided by the host ARES rheometer while true strain measurements were made by studying images collected with high-speed digital videography (at 100 frames/sec). Initial width of sample is $W_0 = 2$ mm. Solid line is the calculated variation in width under ideal uniaxial elongation given by equation (5.44)

From the torque P(t) and sample width $W(t)$ measurements collected, it is straight forward to calculate the true evolution in the normal stress difference during uniaxial elongation:

$$\sigma_{zz}(t)-\sigma_{xx}(t)=\frac{\mathrm{P}(t)}{2RH_0W_0}\exp\left(+\varepsilon(t)\right) \tag{5.45}$$

The results from three different strain rates $\dot{\varepsilon}_0 = 0.03, 0.3, 3.0\,\mathrm{s}^{-1}$ are plotted in Figure 61a. The experiments for each strain rate were repeated to confirm their reproducibility; because of sample-to-sample variability such reproducibility is not often achieved in typical dough systems [80, 126]. Deviations between individual experiments at the same strain rate are only discernible at small strains. These differences can be attributed to slightly different preloads associated with the backlash inherent to the SER gearing system, and the torque signal for data collected at strains $\varepsilon < 0.1$ have been omitted for analysis purposes. The samples were stretched at constant strain rates till they ruptured, usually around total Hencky strains of $\varepsilon \sim 2-3$, corresponding to the point when the torque measurement drops rapidly. Some fluctuations are apparent at low stresses, however these only occur below the stated resolution of the torque transducer; $\Delta\sigma_{\min} = \left(\mathrm{P}_{\min}\right)/\left(2RH_0W_0\right)$. For typical values of sample dimensions $H_0 = 2\mathrm{mm}$, $W_0 = 2\mathrm{mm}$ and cylinder radius $R = 5.25\,\mathrm{mm}$, we find the minimum resolvable stress to be approximately $\Delta\sigma_{\min} = 5\times10^3\ \mathrm{Pa}$.

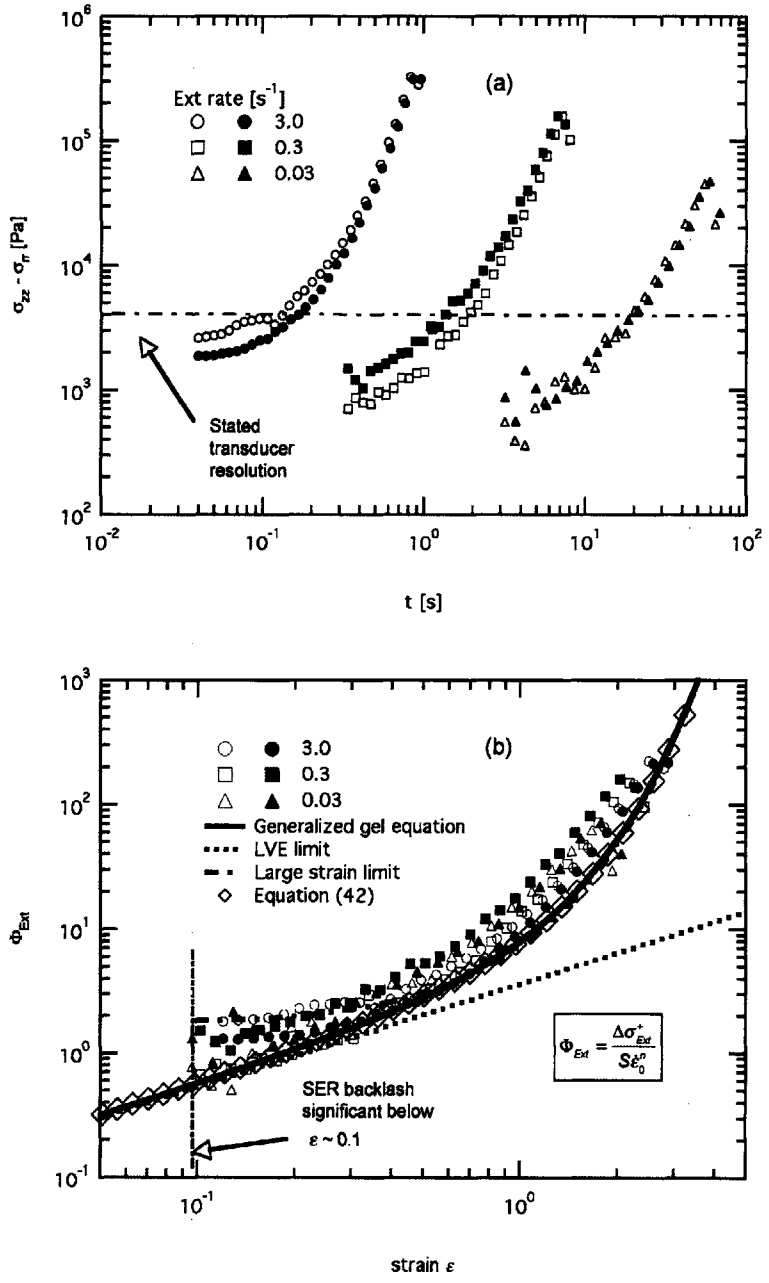

Figure 61 a) Tensile stress difference in gluten gels during transient uniaxial elongation at rates of $\dot{\varepsilon}_0 = 0.03, 0.3, 3.0\,s^{-1}$. At least two runs were performed at each strain rate to ensure reproducibility. b) Scaled stress function plotted against Hencky strain showing power-law growth at small strains and exponential growth at large strains.

Once again we can separate the rate- and strain-dependent contributions by using equation (5.37). The tensile stress growth data can be collapsed onto a single master curve of the strain function by dividing the tensile stress difference by $f(\dot{\varepsilon}_0) = \dot{\varepsilon}_0^n$ as shown in Figure 61b. The strain function $\Phi_{Ext}(\varepsilon)$ is well described by equation (5.38), and the gel parameters used to collapse the data at different rates are obtained through the linear viscoelastic step-strain relaxation experiments discussed in section 0 ($S = 1260\ Pa\ s^n$ and $n = 0.175$) i.e. we do not refit the material properties and there are no adjustable parameters.

As we also noted in equation (5.3), the effective characteristic time constant for a critical gel diverges ($\lambda_{char} \to \infty$), therefore the effective Deborah number in a critical gel also approaches infinity and nonlinear elastic effects always become important. As a result, the tensile stress growth measured at all strain rates will deviate from the linear viscoelastic power-law response $\Phi_{Ext} = 3\varepsilon^{1-n}/(1-n)$ at moderate strains $\varepsilon > 1$. At large Hencky strains, the stress response approaches the asymptotic approximation of the form $\Delta\sigma_{Ext}^{+} \simeq St^{-n}\exp(2\varepsilon)$. This large strain behavior highlights the fact that a critical gel does indeed lie on the point of solid-liquid transition: the material exhibits both neo-Hookean–like affine network deformation $\Delta\sigma_{Ext}^{+} \sim f(x_1) = \exp(2\varepsilon) = x_1^{\,2}$ (where $x_1 = (W/W_0)^{-2}$ is the principal stretch in the SER device) as well as fading memory dependence in time, $\Delta\sigma_{Ext}^{+} \propto t^{-n}$.

We observe no need to incorporate additional strain-dependent damping in the gluten gel which would lead to non-affine deformation in Figure 61b. This is in contrast to analogous measurements with wheat flour doughs which show exponential, but sub-affine, stress growth at large strains [126]. These differences are consistent with our step shear strain measurements in Figure 55. The gluten gels rupture at Hencky strains of $\varepsilon \sim 3$ before such non-linearities would become important.

As a final confirmation that gluten gels should be considered as flexible elastic networks, we note that few (if any) particulate gels can withstand such large stretch ratios ($x_1 = (W/W_0)^{-2} \simeq 20$) without yield or rupture. by contrast such behavior is rather common for crosslinked polymeric networks such as rubber elastomers, collagen etc...

5.6. Conclusions

In this paper we have demonstrated that a vital gluten dough exhibits a power-law relaxation modulus characteristic of that observed in polymeric networks at the liquid-solid transition i.e. the response of a critical gel. We applied the *generalized gel equation* by incorporating the well-known relaxation modulus for a critical gel into the Lodge rubber-like-liquid formulation. We performed a comprehensive set of experiments on a gluten dough and showed that the generalized gel equation provides an accurate description of the rheological response in flow situations ranging from linear to non-linear deformations in both shear and extension. We also demonstrated the implications for these slowly-relaxing systems of residual stress relaxation from deformation incurred during sample loading. The power-law decay in relaxation modulus $G(t) = St^{-n}$ at long times was found to be substantially affected by the waiting time t_w.

The linear viscoelasticity of gluten doughs can be well-characterized by the two-parameter critical gel model over a wide range of timescales and this is an indication of the self similarity in the polymeric network comprising the gluten gel. At very short length scales $l \sim 20$ nm, this self similarity breaks down as the structure of individual strands in the network become important and is reflected by the Rouse regime observed at short time scales $t \sim \lambda_R = 0.05$ s.

At large strains, the gluten gel only shows a very weak damping behavior which is consistent with the idea of strong physical crosslinks in a fractal polymeric network. We contrast this observation with examples of entangled and particulate gel systems that have strong damping functions due, respectively, to

either the mismatch in the rotation/stretch relaxation times or to plastic yielding events between neighboring particles.

In start-up of steady shear flow, power-law growth in both the shear stress and the normal stress difference are observed, and these are in good agreement with the generalized gel equation up to $\gamma^* \sim 5$. Beyond this critical strain, the shear stress exhibits an overshoot and attains a peak value at $\gamma^P \sim 12$. Just before the point of peak stress, the gluten gel undergoes an edge instability that eventually leads to the sample being ejected from the geometry at $\gamma^E \sim 30$. In uniaxial extension, the transient response of the tensile stress difference progressively changes from power-law growth in the linear viscoelastic regime to an exponential increase in agreement with the constitutive prediction of the generalized gel equation. This exponential growth can be observed for a wide range of deformation rates ($0.03 \leq \dot{\varepsilon}_0 \leq 3\,s^{-1}$) up to the point of rupture at Hencky strains of $\varepsilon_{rupture} \sim 3$.

We can compare these observations with earlier experiments performed on critical gels of cross-linked polydimethylsiloxane. In start-up of steady shear flow, Venkataraman and Winter [75] observed a similar departure from linearity at $\gamma^* \sim 2$ followed shortly by an overshoot and a peak in shear stress at $\gamma^P \sim 4$. The rheological signatures of the PDMS and gluten gels are qualitatively similar; but evidently, the gluten system has a significantly larger range of quasi-linearity. The percolated gel structure of the gluten remains intact even under large deformations pointing to significant tensile strength of the gluten backbone and strong interchain binding at network junctions.

The strain/rate factorization observed in the present experiments (in both shearing and extensional flow) strongly supports the extension of the simple linear viscoelastic gel model to large strains by application of the Lodge rubber-like network formulation. Finally, we note that because of the power-law dependence of the relaxation modulus, critical gels exhibit a special form of viscoelastic behavior: They will show characteristics akin to those of ideal elastic

networks, with increasingly affine deformation of the form $\Delta\sigma^{+}_{Ext} \sim \exp(2\varepsilon)$ observed up to large Hencky strains $\varepsilon \sim 3$ in uniaxial elongation; however, at the same time, they also exhibit nonlinear viscous characteristics with a fading power-law dependence in time $\Delta\sigma^{+}_{Ext} \propto t^{-n}$. In addition to the measurements presented here, we have also performed large amplitude oscillatory shear (LAOS) tests to further assess the predictions of the proposed rheological equation of state, these results will be discussed in a later publication.

To summarize, the rheological evidence provides a compelling indication that the gluten gel is a polymeric network consisting of flexible or semi-flexible filaments between network junctions. This is not necessarily incompatible with the particulate microgel structure sometimes observed under confocal microscopy [170]. These observable length scales might lie beyond those that can be practically probed by rheological measurements within a reasonable time window. Exactly what individual roles di-sulphide bonds, hydrogen bonds and physical entanglements play in the resulting gel structure is still hotly debated [8, 47-49, 51, 55]. Future rheological tests to progressively large strains may be able to shed light on the individual contributions of each type of crosslink; preliminary experiments on disrupting the network structure by dissolving the gluten gels in sodium dodecyl sulphate (SDS) or in concentrated urea solution indicate that hydrogen bonding plays a central role in the formation of networks structure.

The ability of such a simple two parameter constitutive model to predict quantitatively the material functions for vital gluten doughs over several orders of magnitude in stress and time scales is both surprising and encouraging. Food stuffs are notorious for being "hopelessly non-model" [171]; and soft solids or wheat flour doughs are considered one of the worst offenders [80]. The model behavior of gluten gels may prove to be invaluable in providing a framework or foundation from which more complex models that fully capture the functionality of a realistic flour-water dough formulation can be constructed. For example, it provides a natural framework for incorporating a damping function to capture more complex non-linear behavior [126].

Moving forward, the logical step to take next is to reintroduce these additional non-linear effects through the addition of a well-characterized filler. Obviously in real bread doughs the filler of interest consists of the starch particles. Unfortunately, simply mixing wheat starch, vital gluten powder and water already reintroduces excessive complexity. The rheology of the resulting dough changes significantly with time and it is challenging to obtain reproducible data [126]; this is due to the gradual swelling and strong interactions between starch particles. An alternative route may be to separate the effects of the filler; for example, by first asking what is the effect of filling the gluten gel with non-reactive hard spheres such as glass beads [143]? Preliminary rheological data collected on such a system in our laboratory suggests that many of the characteristic differences between a critical gluten gel and real dough systems, e.g. non-linear strain softening, can indeed be explained by the interactions of the elastic network with these hard particles and this will form the subject of future work.

6. Power Law and Gluten Gels in Large Amplitude Oscillatory Shear

6.1. *Introduction*

The rheology of biopolymer networks exhibit an intriguing variety of non-linear phenomena. Commonly observed features include non-linear softening/stiffening , reversibility and thixotropy... etc. Currently, there exist a wide variety of measurement techniques and a range of constitutive models have been developed towards understanding these systems [132, 137, 167, 172]. In this article, we will illustrate some of these features observed in a biopolymer gel formed by a hydrated gluten network.

Gluten is the generic name given to the insoluble proteins present in wheat flour. It is widely believed that the mechanical properties of this hydrated network state are intrinsically linked to the quality of the bread dough formed when the flour is mixed with water [6, 8, 13, 48, 49, 99, 173]. The discussion here will be based around the molecular structure of gluten gels proposed in an earlier publication [174]. Rheological behavior under small amplitude oscillations and large deformations in both shear and extension have demonstrated that the gluten gel should be considered as flexible/semi-flexible segments that are interconnected as a gel network. The interstitial spaces are filled with water but have little contribution to the rheology as little or no solvent viscosity can be detected. We also demonstrated that over time scales that are greater than the Rouse relaxation time, the quasi-linear behavior extends up to large strains and can be well-described by the generalized gel equation:

$$\sigma(t) = -\int_0^t S(t-t')^{-n} \frac{\partial}{\partial t} C^{-1}(t,t')dt' \tag{6.1}$$

where C^{-1} is the finger strain tensor. The expression can also be rewritten in terms of the finite strain rate tensor in the following way:

$$\sigma(t) = \int_0^t S(t-t')^{-n} \gamma_{[1]} dt' \tag{6.2}$$

where $\gamma_{[1]} = -\frac{\partial}{\partial t'} C^{-1}$.

In start-up of steady shear tests, both transient shear stress and normal stress showed power-law growth up to a critical strain $\gamma^* \sim 5$ at which non-linear stress growth becomes significant and is followed rapidly by a viscometric instability leading to sample roll-up and ejection from the rheometer. The quasi-linear behavior before the instability is given by equation (6.1) and can be integrated to give:

$$\sigma_{xy}^+(\dot{\gamma}_0, \gamma) = \frac{S}{1-n} \dot{\gamma}_0^{\,n} \gamma^{1-n} \tag{6.3}$$

While the transient extensional stress difference in strips of gluten undergoing uniaxial elongation also closely followed the predicted behavior up to the point of rupture:

$$\Delta\sigma(\varepsilon) = S\dot{\varepsilon}_0^n \int_0^{\varepsilon} r^{-n} \left\{ 2\exp(2r) + \exp(-r) \right\} dr \tag{6.4}$$

In general, the material functions up to the onset of non-linearity for these start-up tests can be shown to be of a time-strain factorizable form in which the stress response is separated into a power-law rate dependent component multiplied by a master strain function:

$$\sigma(t) = S\dot{\gamma}^n \Phi(\gamma) \tag{6.5}$$

Because of the difficulty in maintaining viscometric flow at large strains, the details of this progression into non-linear behavior are still not well understood. Nevertheless, there are clear hints of strain-hardening in the network, however this large additional stress growth leads to sample disruption (either by ejection from gap in shear or cohesive rupture in extension).

Unlike deformations in the linear viscoelastic regime, there exists no standard non-linear rheological test that will provide all the parameters that characterize a material's non-linear rheological behavior. Typically, different tests are required to probe different aspects of the non-linearity. Large amplitude oscillatory shear (LAOS) flows are one of the more common methods used [175], but unfortunately, the interpretation of the measured response is far from obvious.

The experimental and analytical techniques of LAOS and Fourier transforms was neatly summarized by Wilhelm [176]. Due to the conceptual familiarity of Fourier transforms, this framework of collecting and analyzing data is the most widely adopted. An alternative to Fourier analysis have been proposed by Cho [177]. The method is based on symmetry arguments that decompose Lissajous curves into non-linear elastic and viscous components. While more recently, Ewoldt et al [109, 110] also suggested some alternative measure of moduli that captures the physical features observed in Lissajous figures, they were able to generate a rheological fingerprint for pedal mucus collected from snails and slugs.

To our best knowledge, the only published study in which gluten gels were subjected to large amplitude oscillations was performed by Uthayakumaran et al [107]. Their experiments consisted essentially of a strain sweep at fixed frequency in which the strain amplitude was gradually increased and the corresponding dynamic moduli were reported. The data show a gradual decrease in moduli for increasing strains that they interpreted as a strain-softening behavior. As we shall discuss later, simply reporting the dynamic moduli is insufficient because a simple harmonic analysis cannot adequately capture the response of the system [176] if it is not discussed in context with the Lissajous curves or a more detailed Fourier decomposition of the stress-strain response during an oscillation cycle.

Lefebvre [30] studied the Lissajous figures of the more complex wheat flour dough. The experiments were performed on a controlled stress rheometer, in which the stress amplitude was gradually increased. Lefebvre analyzed the corresponding strain response in terms of a Fourier series and he suggested that the relative magnitude of the higher harmonics could be considered to be a measure of the non-linearity. Though this Fourier decomposition approach is

complete and mathematically consistent [176], it is difficult to obtain a physical interpretation of these higher harmonic components. Furthermore, the controlled stress nature of these experiments makes it extremely awkward to compare data against candidate constitutive equations that typically have material stress written as a non-linear function of input strain or strain rate. Nevertheless, the Lissajous figures presented by Lefebvre do indeed show distinct non-linear behavior, the most prominent being the dramatic distortion from the elliptical shapes observed from moderate stresses (i.e. $\sigma_0 < 100\,\text{Pa}$) and small strains ($\gamma_0 \sim 0.05$).

Phan-Thien et al [178] on the other hand performed large amplitude oscillations on a wheat flour dough using a controlled strain approach. As a result, they were able to propose a constitutive equation that described the extreme softening behavior observed when the dough is subject to large strains. The resulting constitutive model [104, 178] is essentially a linear viscoelastic response multiplied by an empirical softening function that is dependent on the strain.

We conclude this section by summarizing our objectives: we will study the non-linear rheological behavior of a model biopolymer network of hydrated gluten. Following the earlier work performed by Lefebvre [30] and Phan-Thien [178], we analyze the resulting Lissajous figures of the gluten gel under various amplitudes of oscillations. The experimental data collected will lead us to a constitutive model that can describe all the non-linear phenomena observed. This model will be based on the transient network ideas described in our earlier work [174] and we will explain how such rheological features can arise from underlying changes in microstructure.

6.2. *Gluten dough preparation*

Gluten dough was prepared by placing 10g of vital gluten (Arrowhead Mills - ~ 12% moisture content) in a mixograph bowl with 14g of water (total dough moisture content = 63% by weight). The mixture is then stirred, stretched and folded through the action of the mixograph pins for 12 minutes [85]. The torque exerted by the mixing action is monitored on an instrumented mixograph. In

Figure 62 (a), we plot the typical torque signal as a function of mixing time. Frequently, a moving average signal corresponding to the slow variation of torque is cited to be indicative of dough development [6]. The various stages of development can be summarized by the following:

i. 0 – 500 s. Under-developed dough – mixing torque is low. The sample is dry and lumpy.

ii. 500-600 s. Dough development – both moving average torque signal and amplitude of fluctuations rise rapidly. Sample begins to form a cohesive dough that is stretched around the mixograph pins.

iii. 600-900 s. Fully developed dough – average signal and fluctuations reach a plateau. Gluten samples harvested at this stage give consistent results under rheometric tests. The detailed fluctuations of the signal is plotted in Figure 62 (b).

iv. > 900 s. Over developed dough – gradual decrease of torque signal. Dough samples collected at this stage are believed to have weak "functionality" [6].

In fact, the mixing motion can be thought of as a series of large amplitude oscillatory tests. The epitrochoidal motion of the mixograph pins are given in Cartesian coordinates with origin at the center of the mixing bowl by the following equations [85]:

$$\begin{aligned} x &= r_1 \cos(\theta + \theta_i) + r_2 \cos\left\{\left(1 + \frac{n}{m}\right)\theta + \phi_i\right\} \\ y &= r_1 \sin(\theta + \theta_i) + r_2 \sin\left\{\left(1 + \frac{n}{m}\right)\theta + \phi_i\right\} \end{aligned} \tag{6.6}$$

where r_1 = 1.78cm, r_2 = 0.89cm are the geometric parameters of the mixograph with four moving pins positioned at (θ_i, ϕ_i) = (0,0), (0,π), (π, 1/4π), (π, 5/4π) respectively. The resulting epitrochoidal deformation imposed on the dough by the four moving pins whirling around the three stationary pins is extremely complicated, and we plot the power spectrum of this motion in Figure 62 (c). The power spectrum is calculated from the kinematic function that describes the

distances between each of the moving pins with respect to the stationary pins. Few of the peaks are clearly identifiable in the corresponding power spectrum calculated from the torque response.

The transfer function that transforms the kinematic spectrum of the rotating pins into the measured torque spectrum must therefore be solely a function of the dough properties. It is this rheological response that we ultimately seek to characterize.

Because of the complex harmonic content of this deformation we seek to decompose the response into contributions that depend on the strain amplitude and deformation frequency using the ideas of large amplitude oscillatory shear flow (LAOS).

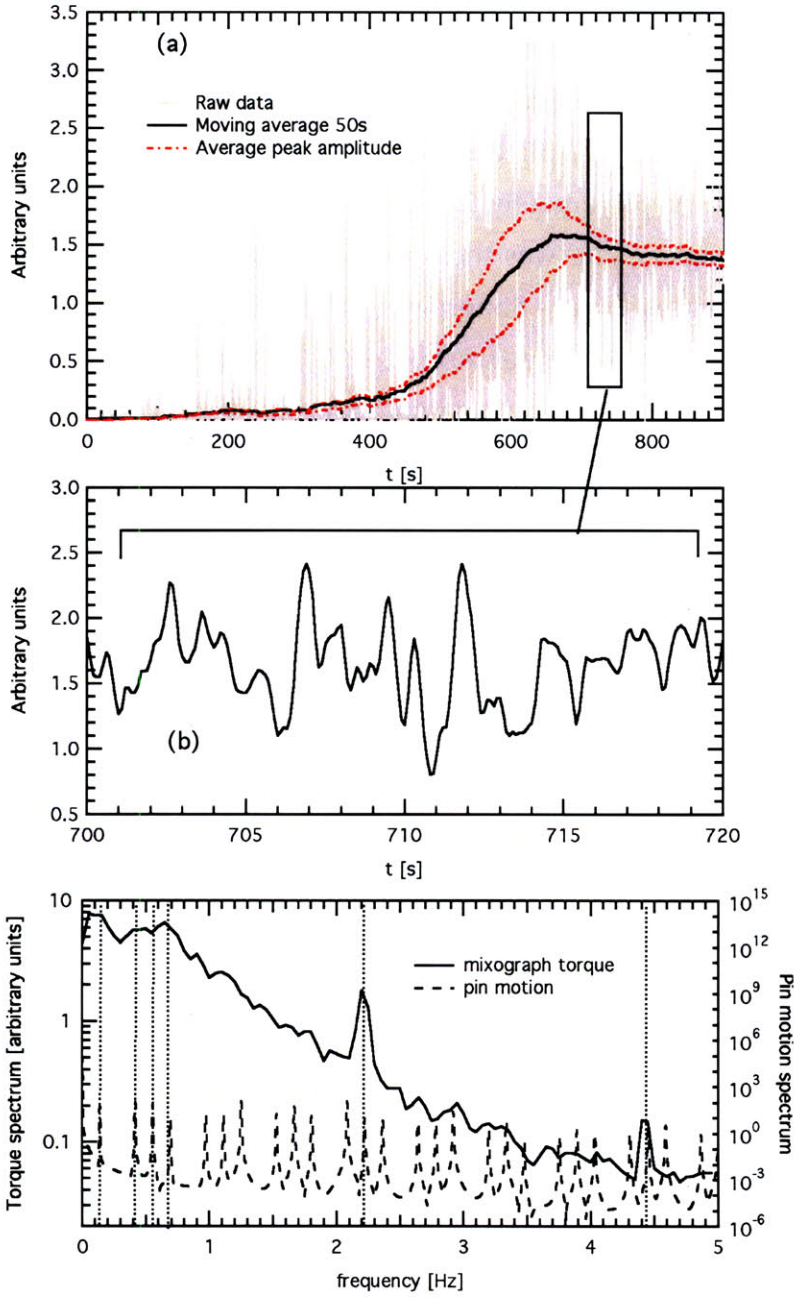

Figure 62 (a) Measured mixograph output (torque in arbitrary units) vs. mixing time for a typical gluten dough. (b) Detail of temporal oscillations in the torque due to the periodic motion of the pins from 700-720s. (c) Power spectrum of the measured mixograph torque from 700-800s. Peaks correspond to harmonics calculated from the motion of moving pins in relation to stationary pins.

6.3. Rheometry

Shear rheometry experiments are performed under controlled strain conditions on the ARES rheometer and under controlled stress mode on the AR-G2 rheometer (TA instruments). A Peltier plate and a 25mm parallel plate fixture at 1mm separation were used. Approximately 2 g of gluten dough was placed on the Peltier plate, and the upper plate was then brought down to compress the sample to the specified thickness. Excess dough was trimmed with a razor blade. The Peltier plate was held at a fixed temperature of 22°C, to approximate typical room temperature. Slip was eliminated by applying adhesive-backed sandpaper (600 grit McMaster Carr 47185A51) to the surfaces of both the Peltier plate and the parallel plate tool. Drying of the sample was minimized by painting the exposed surface of the dough with a low-viscosity silicone oil.

6.4. linear viscoelasticity and network structure of gluten gels

We begin by outlining the important concepts discussed in the previous publication [174]. In this study we showed that the gluten gel forms a polydisperse network of macromolecular strands held between junction points. This polydispersity is reflected in the power-law like relaxation function which can be thought of as a series of Maxwell modes capturing the response of the fractal gel at different length and time scales. In terms of material functions we showed the basic response could be categorized by two regimes. For the dynamic moduli plotted in Figure 52b, at low frequencies ($\omega < 20\ s^{-1}$), the gluten dough exhibits a critical-gel–like behavior [74, 76, 77], in which both dynamic moduli are power-law functions of the frequencies and are related by the following expression:

$$G'_{gel}(\omega) = \frac{G''_{gel}(\omega)}{\tan(n\pi/2)} = \Gamma(1-n)\cos\left(\frac{n\pi}{2}\right)S\omega^n \qquad (6.7)$$

where S is the gel strength and n is the gel index/exponent.

We can draw upon the idea that this power-law behavior is a summation of contributions from structures of varying length scales, and express it neatly as a summation over a finite range of time ($t_{min} < t < t_{max}$):

$$G'_{gel} = \frac{G_0}{2} + G_0 \sum_{k=1}^{K} \frac{(\lambda_k \omega)^2}{1+(\lambda_k \omega)^2}, \qquad G''_{gel} = G_0 \sum_{k=1}^{K} \frac{(\lambda_k \omega)}{1+(\lambda_k \omega)^2} \tag{6.8}$$

where $\lambda_1 = t_{max}$, $\lambda_K = t_{min}$ and the individual relaxation modes are connected by a recursion relationship $\lambda_k = \lambda_1 k^{-1/n}$. The modulus scale for each relaxation mode is set by the expression:

$$G_0 = \frac{S}{n\Gamma(n)\lambda_1^n} \tag{6.9}$$

Under high frequency excitation, the gel also exhibits a Rouse-like regime that reflects the response of network segments within the gel [77]. The additional contributions to the dynamic moduli under this regime can be expressed as:

$$G'_R = G_R \sum_{k=1}^{\infty} \frac{(\lambda_k \omega)^2}{1+(\lambda_k \omega)^2}, \qquad G''_R = G_R \sum_{k=1}^{\infty} \frac{(\lambda_k \omega)}{1+(\lambda_k \omega)^2} \tag{6.10}$$

where $\lambda_k = \lambda_R / k^2$, and λ_R, G_R are the relaxation time and modulus of the Rouse segments.

Therefore, in general, we can write the total dynamic moduli as:

$$\begin{aligned} G'(\omega) &= G'_{gel}(\omega) + G'_R(\omega) \\ G''(\omega) &= G''_{gel}(\omega) + G''_R(\omega) \end{aligned} \tag{6.11}$$

The dynamic moduli obtained from small amplitude controlled stress experiments at stress amplitude of $\sigma_0 = 50$ Pa are plotted in Figure 63. The experimental data are in excellent agreement with equation (5.12) to (6.11) and the linear viscoelastic parameters (S = 1300 ± 100 Pa, n = 0.175, G_R = 803 Pa, λ_R = 0.05s) are consistent with data obtained through other small strain measurements

such as step strain relaxation and creep [174]. From the Rouse relaxation modulus, we estimate the segment length between junction points in the network to be $l \sim \left(k_B T / G_R\right)^{1/3} = 20$ nm.

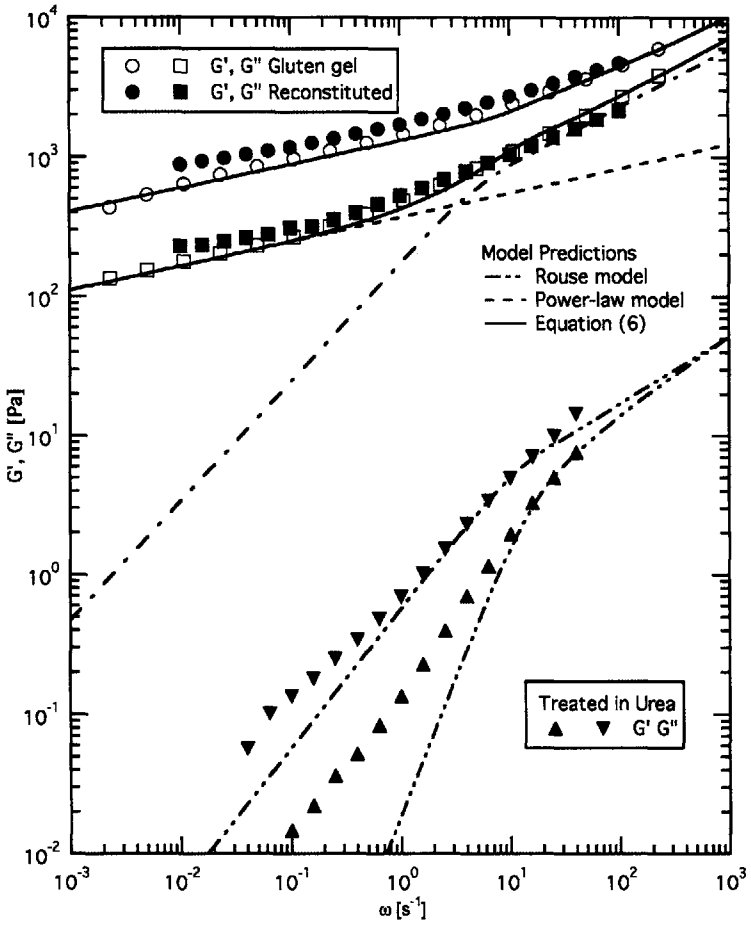

Figure 63 Storage and loss moduli of a gluten gel measured in small amplitude oscillation (hollow symbols) at T = 22° C. Solid lines represent predictions from equation (5.12) to (6.11): $S = 1260$ Pas^n, $n = 0.17$, $G_R = 803$Pa, $\lambda_R = 0.05$s. The response of a gluten gel dissolved in 8M Urea solution (triangles) and the corresponding reconstituted dough (solid symbols) are also shown. The dissolved gluten show a viscoelastic fluid-like behavior with significantly lower moduli. The gluten gel reformed by diluting the solution with water to wash out the Urea is almost identical to the original sample.

Figure 63 also illustrates the physical/chemical nature of these cross-links. Though the gluten gel is formed by hydration in water, it is not soluble in water: introducing more water during the process of mixing does not "dilute" the gel,

instead the excess water forms a pool at the bottom of the mixing bowl [174]. However, it is possible to breakdown the network structure by diluting the gluten gel in 8M Urea solution (5 g gluten in 35 ml of 8M Urea solution). The resulting mixture exhibits a viscoelastic fluid response, evident from the relative magnitudes of the storage and loss moduli. Draining this solution through a 30 μm sieve leaves no significant residues. The diluted solution still shows a viscoelastic response that suggests structures below Rouse network size (20 nm) are still present. This indicates the original gel network to be predominantly held together by physical interactions at junction points such as hydrogen bonds or possibly hydrophobic interactions [179, 180], while the macromolecular backbone is not significantly affected by the Urea treatment.

Furthermore, the screening effect of the Urea is reversible, if the mixture is poured into a large beaker of water, filaments will appear which coagulate rapidly into a dough. The linear viscoelastic properties of the dough harvested from this reforming process are also plotted in. The gel shows a complete recovery to the original moduli indicating the physical interactions at junction points are reversibly disrupted by the presence of Urea. These observations are consistent with the proposed structural model of Letang et al [47]; hydrogen bonds or hydrophobic interactions allow structure elements composed of gluten molecules to percolate and form a sample spanning network structure.

We can highlight some features of gluten gels and many other biopolymer networks in general by comparing and contrasting the results from this set of experiments to a familiar substance: vulcanized rubber consists of polymer strands that have been cross-linked at network junctions [181]. Due to the permanence of the covalent cross-links, rubbers display strong elasticity with little dissipation. However, beyond a typical yield strain or stress, the *intra-molecular* bonds within the macromolecular strands can rupture, causing the network to be irreversibly damaged; this event is manifested macroscopically as strain-softening or cohesive failure. In the case of gluten gels, these permanent cross-links are replaced by hydrogen bonds and hydrophobic interactions. Since the strength of these junctions are typically weaker than those in covalently bonded systems, the tensile force accumulated under large strains within the

intra-molecular strands can be released by yielding of these *inter-molecular* junction points, thus avoiding severe rupture of the network segments. Furthermore, these transient junction points have the potential to reform if the material is returned to a state of lower stress, allowing the network to regain its strength.

Thus as an alternate approach to disrupting the junction point interactions through chemical means, we can also explore the possibility of breaking these bonds through mechanical methods, i.e. through the application of large stresses and strains. We should expect a decrease in modulus as the applied strain is increased because the tensile force carried by individual network segments will also correspondingly increase, thus leading to a greater probability of breakage [182]. This phenomenon has already been observed in gluten gels as the strain-softening presented by Uthayakumaran et al [107], and we wish to be able to model such observations in the context of the change in microstructure described above.

But up to this point, we have only presented data on the linear viscoelastic response of the gluten gel, the strain amplitude of the oscillation was largest for the data at the lowest frequency $\omega = 0.003\ s^{-1}$, $\gamma_0 = 0.125$, and was still well within the linear regime: the linear viscoelastic moduli are independent of strain amplitude and the corresponding Lissajous figures [183, 184] are found to be elliptical for all frequencies.

Under these linear viscoelastic conditions, the output signal (strain in this case) is sinusoidal; the two dynamic moduli G' and G'' are clearly defined as the in-phase and out-of-phase component with respect to the input signal. Unfortunately, for high molecular weight polymeric materials, this simple way of decomposing the data is insufficient as the strain is increased because the output signal deviates from a purely sinusoidal form [108, 110]. From another point of view, measuring this deviation can be thought of as a technique to highlight the distinguishing features of a given material, especially if one has the means to quantitatively describe it. The modeling and quantifying of these non-linear features will be the subject of the following sections.

6.5. *Non-linear deformation of gluten gel*

In this section, we first describe and quantify the features exhibited by a gluten gel under large amplitude oscillatory shear (LAOS). Next we construct a constitutive model based on the network structure of the gel and demonstrate how this formulation is able to predict a range of non-linear rheological phenomena observed in gluten gels.

Large amplitude oscillations provide a number of advantages. First of all, since the amplitude of oscillation can be gradually increased, we can probe deformation ranges close to the point of viscometric instabilities (e.g. the ejection of samples from the gap at large strains). The measurements are taken under quasi-steady state (the oscillations are continued till any initial transient response has decayed and the shape of the Lissajous curves remain time invariant), therefore the accuracy and repeatability are greatly improved when compared against transient start-up tests. Also, since the tests are performed on conventional rotational rheometers, the experimental protocols are simpler and more convenient compared to non-linear tests involving large extensional deformations such as filament stretching or wind-up tests [126].

Large Amplitude Oscillatory Shear

In contrast to linear viscoelastic experiments, for large amplitude oscillations, the material parameters are formally treated as functions of the oscillation frequency and strain amplitude rather than just frequency alone. The most common method to express this idea is through the use of Fourier decomposition [176] in which the departure from linear (sinusoidal) response is contained in the higher Fourier harmonics:

$$\frac{\sigma}{\gamma_0} = G^*\left(t;\omega,\gamma_0\right) = \sum_{n=1}^{N} G'_n\left(\omega,\gamma_0\right)\sin(n\omega t) + G''_i\left(\omega,\gamma_0\right)\cos\left(n\omega t\right) \qquad (6.12)$$

In the linear viscoelastic domain ($\gamma_0 \to 0$), we require the contribution from these higher harmonics to tend to zero such that the simple sinusoidal response is recovered.

$$\frac{\sigma}{\gamma_0} \rightarrow G^*(t;\gamma_0)\Big|_{\gamma_0 \rightarrow 0} = G'_1(\omega)\sin\omega t + G''_1(\omega)\cos\omega t \qquad (6.13)$$

In this framework, each experiment can be thought of as the material response at a particular point in the two-dimensional parameter space with frequency ω on one axis and strain amplitude γ_0 on the other. This is often referred to as the the Pipkin space of an experiment matrix [185]. Ewoldt et al. [109] described a systematic process to analyse behavior in this Pipkin space, and we will adopt this framework here.

The shapes of these Lissajous figures for a range of strain amplitudes ($0.02 < \gamma_0 < 6.0$) at $\omega = 1.0$ $s^{-1}$are plotted in Figure 64. At small strains ($\gamma_0 < 1$), the Lissajous figures are essentially elliptical and are consistent with the linear viscoelastic regime described by equation (5.12) through (6.11). The shapes of the ellipses and the moduli are only a function of frequency and are independent of strain amplitude. Equation (6.13) can be rewritten to eliminate the time dependence:

$$\sigma^2 - 2\sigma\gamma G' + \gamma^2\left(G'^2 + G''^2\right) = G''^2\gamma_0^2 \qquad (6.14)$$

As the strain amplitude is increased, the response and shape deviate significantly from this simple behavior. A number of visually distinguished features can be observed: Firstly a gradual softening indicated by the rotation of the major axis towards the x-axis. Secondly, a distinct stiffening indicated by the "upturn" of the shear stress is observed at large strains. The magnitude of the enclosed area also increases with increasing frequency.

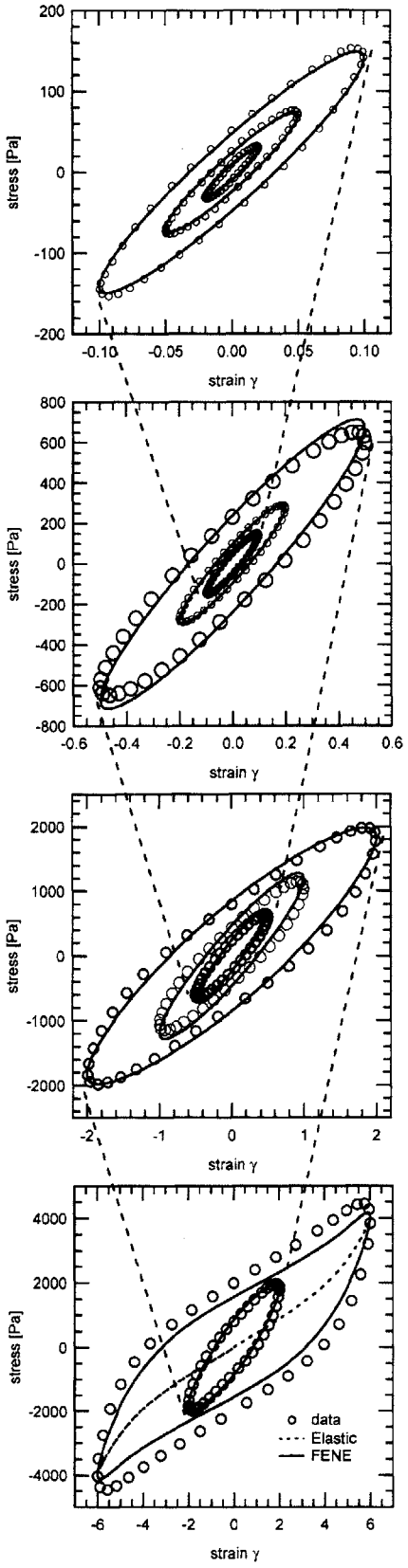

Figure 64 Lissajous curves after 12 cycles for $\gamma_0 = 0.02, 0.05, 0.10, 0.20, 0.50, 1.00, 2.00$ and 6.00 at fixed frequency $\omega = 1.0\ s^{-1}$. Experimental data are plotted as open symbols. The decomposed elastic stresses are plotted as a dotted line for $\gamma_0 = 6$.

It is evident that this wealth of non-linear features cannot be fully captured by simply reporting the dynamic moduli G' and G'' familiar from linear viscoelasticity. To illustrate this, we plot three different measures of the elastic moduli as a function of strain in Figure 65.

The parameters G_1' and G_3' are the first and third in-phase (real) Fourier coefficient of the output signal (equation (6.12)). The first coefficient $G_1'(\omega)$ is the typical method of calculating storage moduli for rheometer software. For strain sweep experiments, frequently only the values G_1' and G_1'' are reported, this is often justified by the fact that the higher harmonics are small (i.e. G_3' is less than 12% in this case) [19, 186]. But simply inspecting these linear viscoelastic material functions will not reveal the dramatic changes observed in the Lissajous curves of Figure 64.

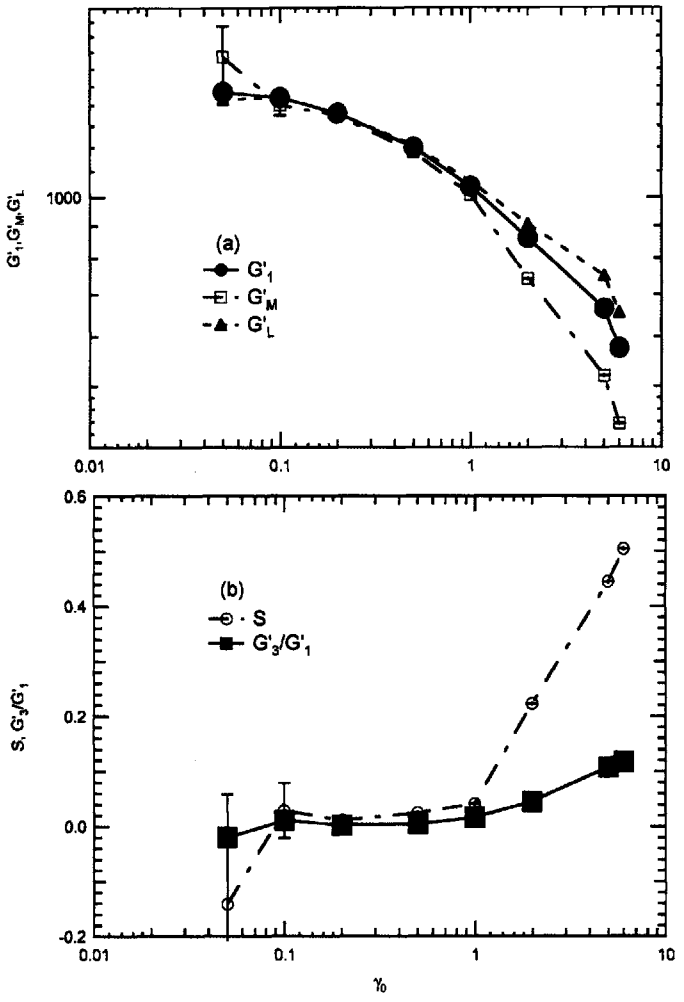

Figure 65 Dynamic moduli of gluten gel undergoing strain-sweep (ARES rheometer, controlled strain mode) at $\omega = 1.0\ s^{-1}$. G_1' and G_3' are the first and third in-phase Fourier coefficient of the output signal, G_1' is typically quoted as the storage modulus. G_M' and G_L' are the small and large strain modulus respectively. S is the stiffening ratio defined in equation (6.19).

Instead, we use the definitions proposed by Ewoldt et al [110] as a simple yet practical method of quantifying these features through the use of some complimentary definitions of elastic moduli: G_M' is the small strain dynamic modulus, it is defined as the slope of the Lissajous curve as it crosses through zero strain.

$$G'_M = \left.\frac{\partial\sigma}{\partial\gamma}\right|_{\gamma=0} \tag{6.15}$$

Similarly, G_L' is the large strain modulus and is defined as the secant or slope of the line connecting the origin to the point at maximum strain.

$$G'_L = \left.\frac{\sigma}{\gamma_0}\right|_{\gamma=\gamma_0} \tag{6.16}$$

In the linear viscoelastic regime, we show that G_1', G_M' and G_L' are all mathematically equivalent measures of the dynamic modulus by substituting these definitions into equation (6.14). For G'_L we calculate the stress at the maximum strain σ_{max}:

$$\begin{aligned} \sigma_{max}^2 - 2\sigma_{max}\gamma_0 G' + \gamma_0^2\left(G'^2 + G''^2\right) &= G''^2\gamma_0^2 \\ \sigma_{max} &= \gamma_0 G' \\ G_L' &= \frac{\sigma_{max}}{\gamma_0} = G' \end{aligned} \tag{6.17}$$

And similarly for G'_M, we calculate the rate of change of the stress at $\gamma = 0$.

$$\begin{aligned} \frac{\partial}{\partial\gamma}\left[\sigma^2 - 2\sigma\gamma G' + \gamma^2\left(G'^2 + G''^2\right) = G''^2\gamma_0^2\right]\Big|_{\gamma=0} & \\ 2\left.\frac{\partial\sigma}{\partial\gamma}\right|_{\gamma=0} - 2G' = 0 & \\ G_M' = \left.\frac{\partial\sigma}{\partial\gamma}\right|_{\gamma=0} = G' & \end{aligned} \tag{6.18}$$

As the strain amplitude is increased, G_M' does not remain constant, instead we see a gradual decrease that corresponds to the observed softening or clockwise rotation of the ellipse. The absolute value of G_L' also decreases, however, this decrease is less "severe" compared to that of G_M'. These features can be interpreted in conjunction as the stiffening at large strains observed in the

Lissajous figures and can be unambiguously parameterized by defining the ratio between these two moduli.

$$S = \frac{G_L' - G_M'}{G_M'} \tag{6.19}$$

The ratio S may be referred to as the stiffening ratio [110]. For an ideal linear viscoelastic system $S = 0$. A positive stiffening ratio implies stiffening of the viscoelastic network at large strains as is observed in the Lissajous plots.

Alternatively, we can visualize the elastic component by considering the method of decomposition described by Cho et al [108]. This method utilizes symmetry to define an elastic and viscous component that are purely odd functions of strain and strain rate respectively:

$$\sigma = \sigma' + \sigma'' \tag{6.20}$$

in which σ' is the elastic component calculated through the following expression:

$$\sigma' = \frac{\sigma(\gamma, \dot{\gamma}/\omega) - \sigma(-\gamma, \dot{\gamma}/\omega)}{2} \tag{6.21}$$

where $\gamma = \gamma_0 \sin \omega t$ and $\dot{\gamma} = \gamma_0 \omega \cos \omega t$. The normalized elastic components are plotted in Figure 66.

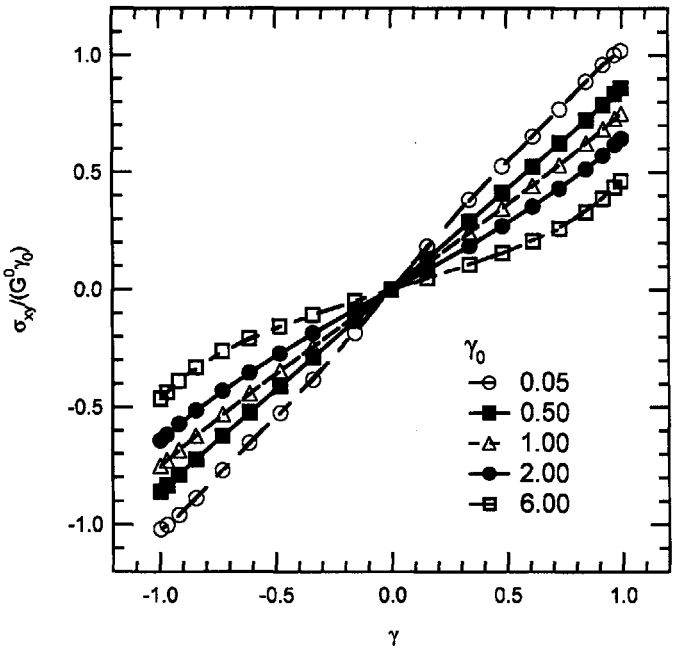

Figure 66 Normalized elastic stress of the Lissajous curves for $\gamma_0 = 0.03, 0.1, 0.3, 1.0, 3.0, 6.0$ at $\omega = 1.0\ s^{-1}$ and T = 22° C.

The normalized stress is calculated by dividing the stress by the "zero strain" modulus $G^0 = G'_1(\gamma_0 \to 0)$ and strain amplitude γ_0, the value is calculated from small strain experiments and is found to be 1400 Pa for this gluten gel. The clockwise rotation and non-linear stiffening of the elastic stress as the strain amplitude is increased are both clearly demonstrated through this technique.

To summarize, the rheological fingerprint [110] of the gluten gel in this Pipkin space is illustrated in Figure 67. Each Lissajous curve represents the stress strain response over a single oscillation cycle after the initial transient response has decayed and reached a quasi-steady state, or in other words, the shapes of the curves is time invariant for successive cycles. Typically, this requires a minimum of 4 cycles. Presenting the data in this manner gives a qualitative overview of the salient features as the material response changes from the linear to non-linear regime over the range of strain amplitude and oscillation frequency.

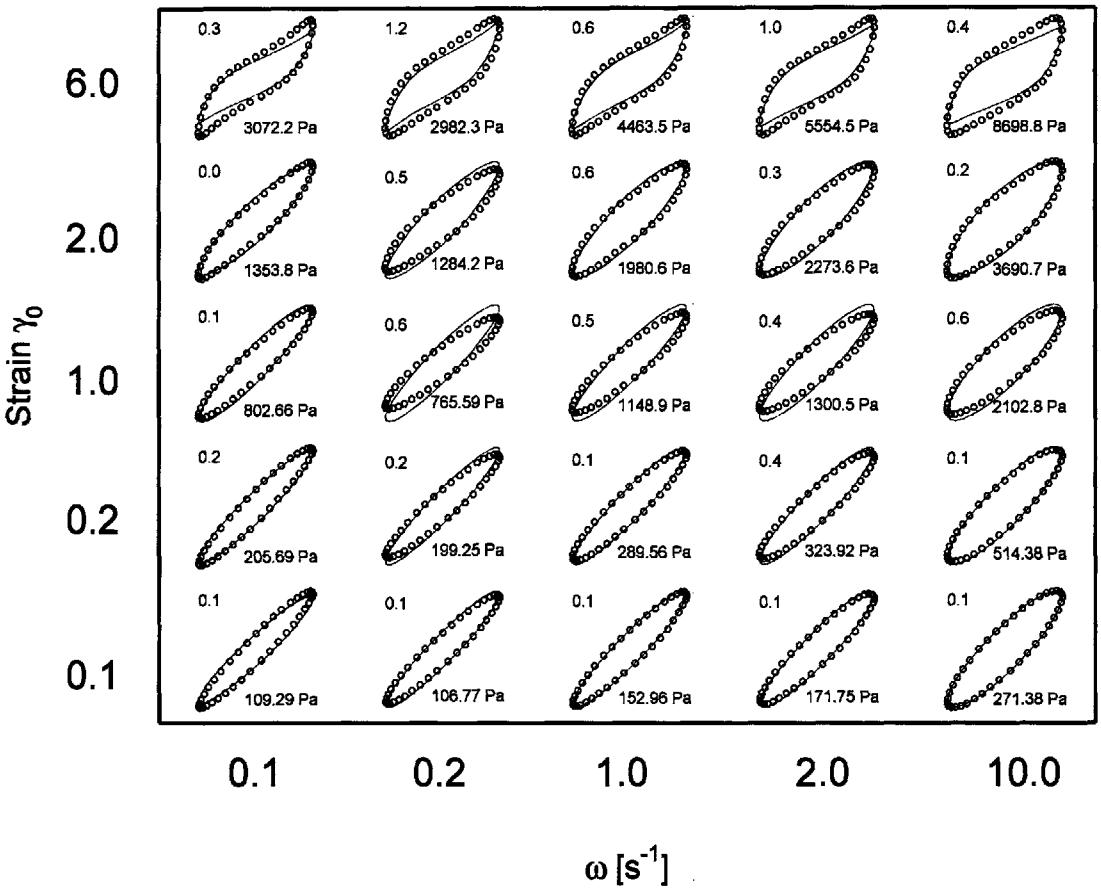

Figure 67. Rheological fingerprint of a gluten gel in Large Amplitude Oscillation Shear Flow. The shapes and maximum stress amplitude are presented over the Pipkin space $0.10 < \omega < 10\ s^{-1}$, $0.10 < \gamma_0 < 6.00$. In each case, the data represents the sixth cycle of the oscillation and there are at least 80 data points in each cycle. The relative error ξ (defined in equation (6.33)) is given on the top right of each figure, while the maximum stress is plotted on the bottom left. Solid lines represent the predictions from the FENE network model of equation (6.24).

6.6. *Network Model*

We have discussed the non-linear features exhibited by a well-mixed gluten-water system under oscillatory shear qualitatively and introduced quantitative measures that highlight their physical significance. In the next part of this paper,

we consider how such features can arise from the microstructural behavior of the gluten gel. In terms of constitutive modeling, we will choose a level of complexity that is sufficient to explain the observed features, but yet simple enough so that we are not overwhelmed by a large number of material parameters and equations.

In our previous work [174] and in section 6.4, we have shown that the rheology of gluten can be well represented by an elastic network response, therefore we begin by modeling the gluten gel as a transient network of interacting filaments. The basic concepts underlying such network theories are succinctly outlined in Bird et al [187]. The gel is idealized as an affinely deforming network and we refer to the filaments spanning junction points as elastic segments. These segments are assumed to have a distribution of end-to-end vectors Q_k.

The total stress tensor $\boldsymbol{\pi}_k$ resulting from the distribution of chain stretch and orientation can be written as:

$$\boldsymbol{\pi}_k = n_k H f(Q_k)\langle Q_k Q_k \rangle \tag{6.22}$$

Where $\langle Q_k Q_k \rangle$ is the ensemble average of the second order tensor $Q_k Q_k$, n_k is the number density of segments in the network, H is the Hookean spring constant of an elastic segment and $f(Q_k)$ represents the non-linearity of the elastic restoring force as the stretch of the segment is increased. The transient nature of the network is reflected in a continuous dissociation of network junctions characterized by a rate of destruction $\lambda^{-1}(Q_k, t)$, and a rebirth of junctions that are in the equilibrium state at a constant rate L. Hence the evolution equation of the second order tensor $\langle Q_k Q_k \rangle$ can be written in the following way:

$$\langle Q_k Q_k \rangle_{(1)} = L_k Q_{k,eq}^2 \boldsymbol{I} - \frac{\langle Q_k Q_k \rangle}{\lambda(Q_k)} \tag{6.23}$$

Equations (6.22) and (6.23) can be expressed in terms of the dimensionless microstructural tensor A_k:

$$\begin{aligned} \boldsymbol{\pi}_k &= G_k\left[f(\boldsymbol{A}_k)\boldsymbol{A}_k\right] \\ \boldsymbol{A}_{k(1)} &= L_k\boldsymbol{I} - \frac{\boldsymbol{A}_k}{\lambda(\boldsymbol{A}_k)} \end{aligned} \tag{6.24}$$

Where $\boldsymbol{A}_k = \langle \boldsymbol{Q}_k \boldsymbol{Q}_k \rangle / Q_{k,eq}^2$ and $G_k = n_k H Q_{k,eq}^2$.

To capture the stiffening effect, we consider a commonly used non-linear spring law of the *FENE-P* form:

$$f(\boldsymbol{A}_k) = \frac{1}{1 - Tr(\boldsymbol{A}_k)/b} \tag{6.25}$$

where $Tr(\boldsymbol{A}_k) = A_{k,11} + A_{k,22} + A_{k,33}$ is the trace operator and b is the FENE parameter that characterizes the limit of extensibility of a polymer strand. The functional form of equation (6.25) is illustrated in Figure 68 (b).

Next we turn our attention to the term describing the rate of destruction λ_k^{-1}. For a viscoelastic material composed of transient network at equilibrium, by definition, the rate of creation of network junctions has to be exactly balanced by the rate of destruction. However, under increased deformation, as individual filaments become increasingly stretched, the probability of them breaking off from the neighboring strands increases and thus the corresponding rate of destruction should also increase. In effect, the average "magnitude" of $\langle \boldsymbol{Q}_k \boldsymbol{Q}_k \rangle$ is reduced for increasing oscillation amplitudes, leading to a softening that is manifested in the Lissajous figures as an apparent clockwise rotation of the major axis. We model this effect by assuming an empirical first order network destruction rate as a function of the magnitude of microstructural stretch $\boldsymbol{A}_k$:

$$\lambda_k^{-1} = \lambda_{k,eq}^{-1}\left(1 + C_1\left[Tr(\boldsymbol{A}_k) - 3\right]\right) \tag{6.26}$$

where C_1 is a constant to be determined, it characterizes this increased rate of network breakage. $\lambda_{k,eq}$ is the linear viscoelastic the relaxation time, i.e.

characteristic structural relaxation time under infinitesimal microstructural deformation ($Tr(\boldsymbol{A}_k) \to 3$).

Furthermore, we require the rate of network destruction to become increasingly rapid as the tension in the network filaments diverges near the finite extensibility limit (in that $Tr(\boldsymbol{A}_k) \to b$). Once more, we express this as a FENE like term:

$$\lambda_k^{-1} \sim \frac{1}{1 - Tr(\boldsymbol{A}_k)/b} \tag{6.27}$$

We combine equations (6.26) and (6.27) to write a non-linear rate of network destruction that captures these two physical ideas:

$$\lambda_k^{-1}(\boldsymbol{A}_k) = \lambda_{k,0}^{-1} \frac{1 + C_1(Tr(\boldsymbol{A}_k) - 3)}{1 - Tr(\boldsymbol{A}_k)/b} \tag{6.28}$$

The corresponding rate of creation required to maintain steady state at equilibrium conditions ($\boldsymbol{A}_{k,eq} = \boldsymbol{I}$) is then:

$$L_k = \lambda_{k,0}^{-1} \frac{1}{(1 - 3/b)} = \lambda_{k,eq}^{-1} \tag{6.29}$$

The deviatoric stress tensor $\boldsymbol{\sigma}_k$ can then be written as:

$$\begin{aligned} \boldsymbol{\sigma}_k &= \boldsymbol{\pi}_k - p\boldsymbol{I} \\ &= \boldsymbol{\pi}_k - \boldsymbol{\pi}_{eq} \\ &= G\left(f(\boldsymbol{A}_k)\boldsymbol{A}_k - f_{eq}\boldsymbol{I}\right) \end{aligned} \tag{6.30}$$

where $Gf_{eq} = G(1 - 3/b)^{-1}$ is the equilibrium isotropic pressure.

Finally, we recall that the linear viscoelastic network response of the gluten gel can be represented as a summation of individual modes such that:

$$\begin{aligned}\sigma &= \int_0^t G(t-t')\dot{\gamma}\,dt' \\ &= \sum_k^K \int_0^t G_{k,gel}(t-t')\dot{\gamma}\,dt' + \sum_m^M \int_0^t G_{m,R}(t-t')\dot{\gamma}\,dt'\end{aligned} \tag{6.31}$$

Various techniques towards obtaining the linear viscoelastic parameters that characterize these modes were outlined by Ng and McKinley [174]. Here, we extend the idea and represent the non-linear response as a series of non-linear network modes like equation (6.30) such that:

$$\boldsymbol{\sigma} = \sum_k^K \boldsymbol{\sigma}_k \tag{6.32}$$

In this form, the network model will give linear viscoelastic response that is identical to equation (5.12) through (6.11) and yet still allow for the non-linear features to become apparent at large strains.

We summarize the construction of this model in Figure 68. The linear viscoelastic parameters of the model S =1400 Pa s^n, n = 0.175, G_R = 803 Pa and λ_R = 0.05 s are obtained by fitting equations (5.12) through (6.11) to the small amplitude oscillatory shear (SAOS) data or other equivalent linear viscoelastic measurements. The gel parameters S and n are then combined with λ_1 (an arbitrarily chosen maximum time scale) and K (total number of gel modes to span the relevant time scale) to generate a series of discrete modal relaxation times $\lambda_k = \lambda_1 k^{-1/n}$ with zeroth order modulus $G_0 = S/\left(n\Gamma(n)\lambda_1^n\right)$. This conversion is illustrated in Figure 68 (a). This series of gel modes $\left(G_{gel}(t) = \frac{G_0}{2} + G_0\sum_{k=1}^{K}\exp(-t/\lambda_k)\right)$ together with the Rouse modes $\left(G_{Rouse}(t) = G_R\sum_{m=1}^{M}\exp\left(-tm^2/\lambda_R\right)\right)$ give the entire spectrum of discrete modes.

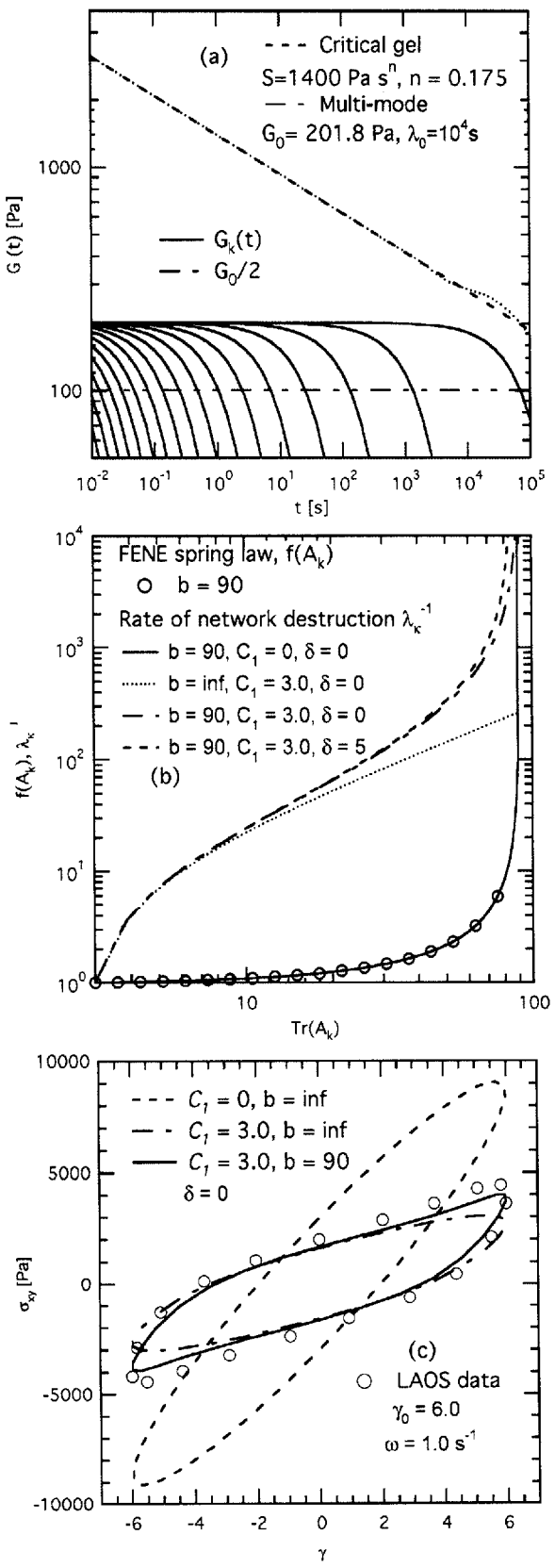

Figure 68. Summary of constitutive parameters in the FENE network model.

(a) The critical gel-like behavior in linear viscoelasticity is approximated by a series of Maxwell relaxation modes. $G_{gel}(t) = St^{-n} \simeq G_0/2 + \sum G_k(t)$. The total relaxation modulus is given by $G(t) = G_{gel}(t) + G_R(t)$.

(b) Non linear functions in the network model. A FENE type spring law is used as the non linear modulus $f(A_k)$ and is characterized by the finite extensibility limit b. The rate of junction destruction λ_k^{-1}, is characterized by two additional parameters. C_1 describes an increase in network destruction rate at intermediate microstructure deformation, δ modifies the FENE function by allowing the junction points to be destroyed close to but before the finite extensibility limit b is reached.

(c) Lissajous figures for $\gamma_0 = 6$. Quasi-linear formulation with C_1 = 0 and b = inf grossly over predicts the stress. Inclusion of C_1 gives strain softening (clockwise rotation of ellipse). The strain-stiffening is apparent at large strain when non-linear FENE spring law is introduced.

The non-linear model parameters $C_1 = 3.0$ and $b = 90$ are obtained by a manual fitting process to the large amplitude oscillatory shear (LAOS) data. For the sake of simplicity, the same values for C_1 and b are used for all modes. The respective contributions from each of these non-linear parameters are illustrated in Figure 68 (c). This value of b is within the range of typical reported values of finite extensibility ($10 < b < 1000$) [187] and corresponds to a stretching of the network segment through approximately 10 times its original length.

We now return to the Lissajous curves presented in Figure 64 and Figure 67, we compare them with the predictions of the FENE network model that are also plotted on the same figure. Overall, the network model is able to capture both the rotation and stiffening of the measured data with reasonable quantitative agreement. An estimate of the relative R.M.S. error is also given on the plot. The relative error is calculated from N data points through the following definition:

$$\xi = \frac{\sqrt{\sum_{n=1}^{N}\left(\frac{\sigma_{FENE}(n)-\sigma_{data}(n)}{\sigma_{data}(n)}\right)^2}}{N} \tag{6.33}$$

The deviations are most apparent at intermediate to large strains ($1.0 < \gamma_0$). This presumably is due to an over-simplification of the softening function used in equation (6.26). Further improvements to this function are discussed in the section 6.7.

Frequency Dependence of Lissajous Figures

Returning once more to the Lissajous fingerprint of Figure 67, we see that the qualitative effect of increasing strains are similar at all frequencies. As already noted in the figure and equation (6.14), at small strains $\gamma_0 < 1$, the Lissajous curves are elliptical and the resulting frequency response is well predicted by the integral and differential forms of critical gel and Rouse modes presented in

section 6.4 or by the linear viscoelastic limit of the multi-mode FENE network model.

Instead, in Figure 69, we focus on the comparison between the network predictions and the measured Lissajous curves of varying frequencies at large strains. The model gives excellent qualitative agreement, the changes in shape and enclosed area of the Lissajous curves are captured by the network model while other salient features such as the clockwise rotation and local strain hardening are also present in the predicted response. Further improvements to the quantitative accuracy of the model are discussed briefly in the conclusion section.

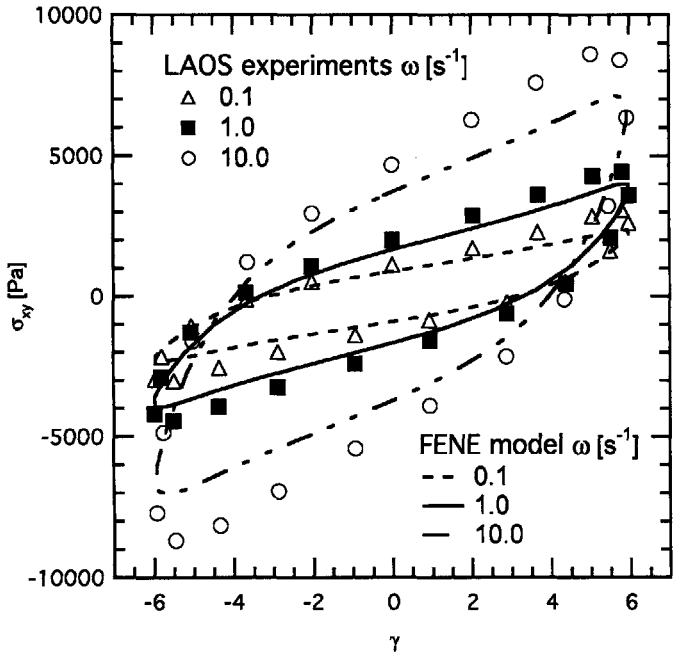

Figure 69 Lissajous curves of a gluten gel performed at large amplitude for a range of frequency ω = 0.1, 1,0 and 10 s^{-1} at $\gamma_0 = 6$. The FENE network model correctly predicts the trends and magnitude of stress over the frequency range.

Transient Response

The progressive change in network structure as the network junctions are broken and reformed following the inception of deformation can be considered as a form of thixotropy. The transient behavior arising from these changes is conceptually different from linear viscoelastic transients that involve the stress response to infinitesimal changes to microstructure.

We illustrate these differences by considering a situation in which the amplitude of oscillation is suddenly changed while we monitor the transient changes to the oscillatory stress amplitude. This is realized experimentally by changing the amplitude of oscillation from $\gamma_0 = 0.10$ to $\gamma_1 = 3.0$, then back to $\gamma_0 = 0.10$ again. The transient stress response is plotted in Figure 70 a and b.

In Figure 70 c, we plot the transient modulus defined as:

$$G_A(t) = \frac{\sigma_{xy}(t)}{\gamma_0}$$
$$\gamma_0^{\{t\}} = 3.0 \text{ for } 106.8 < t < 169.6 \text{ s} \qquad (6.34)$$
$$= 0.1 \text{ otherwise}$$

The experimental data clearly shows a pronounced transient during the first five cycles after the increase in oscillation amplitude. During this time the material is progressively softened as indicated by a decrease of the transient modulus by as much as ~40% (from 1300 Pa to 800 Pa). Quasi-linear or linear viscoelastic constitutive models of the form:

$$\sigma_{xy} = \int_0^t G(t-t')\gamma_0\omega\cos(\omega t)dt' \qquad (6.35)$$

will in fact predict an increasing stress amplitude that converges rapidly to the linear viscoelastic modulus with a response of the form $\sim 1 - e^{-\frac{t}{\lambda}}$. This is plotted in Figure 70 as a dotted line.

Instead, this transient softening or thixotropy is almost perfectly captured by the inclusion of finite-extensibility and strain-dependent network destruction terms as shown by the solid line in Figure 70. These lines represent the response of the constitutive model given by equations (6.24) to (6.32). We emphasize that there are no adjustable parameters here; S and n are determined from linear viscoelastic experiments, the corresponding discrete spectrum for the linear response is given by equation (6.10). The nonlinear response is given by integrating equations (6.24) to (6.32) with $b = 90$, and $C_1 = 3.0$ (determined by fitting to the data in Figure 64). Furthermore, the predicted complete recovery to the small amplitude modulus is also observed experimentally. This can be understood in context of the experiments conducted by "breaking" the network structure through dilution with Urea and the subsequent reconstitution by washing out the Urea with water. In large amplitude oscillations, the hydrogen bonds at network junctions are reversibly broken through application of large strains on the network. Thus upon cessation of large deformations, the reversible nature of hydrogen bonding events means that the material is able to reform its network structure. Both mechanical and chemical treatment have negligible effect on the covalent interactions within the filaments thus allowing complete recovery of the network modulus when the "interruptions" are removed. This complete recovery contrasts with the incomplete recovery of wheat flour doughs in which additional bonding interactions between chains and starch particles must be considered. These latter interactions can be described by damage functions [127] in which the network changes are permanent and irreversible.

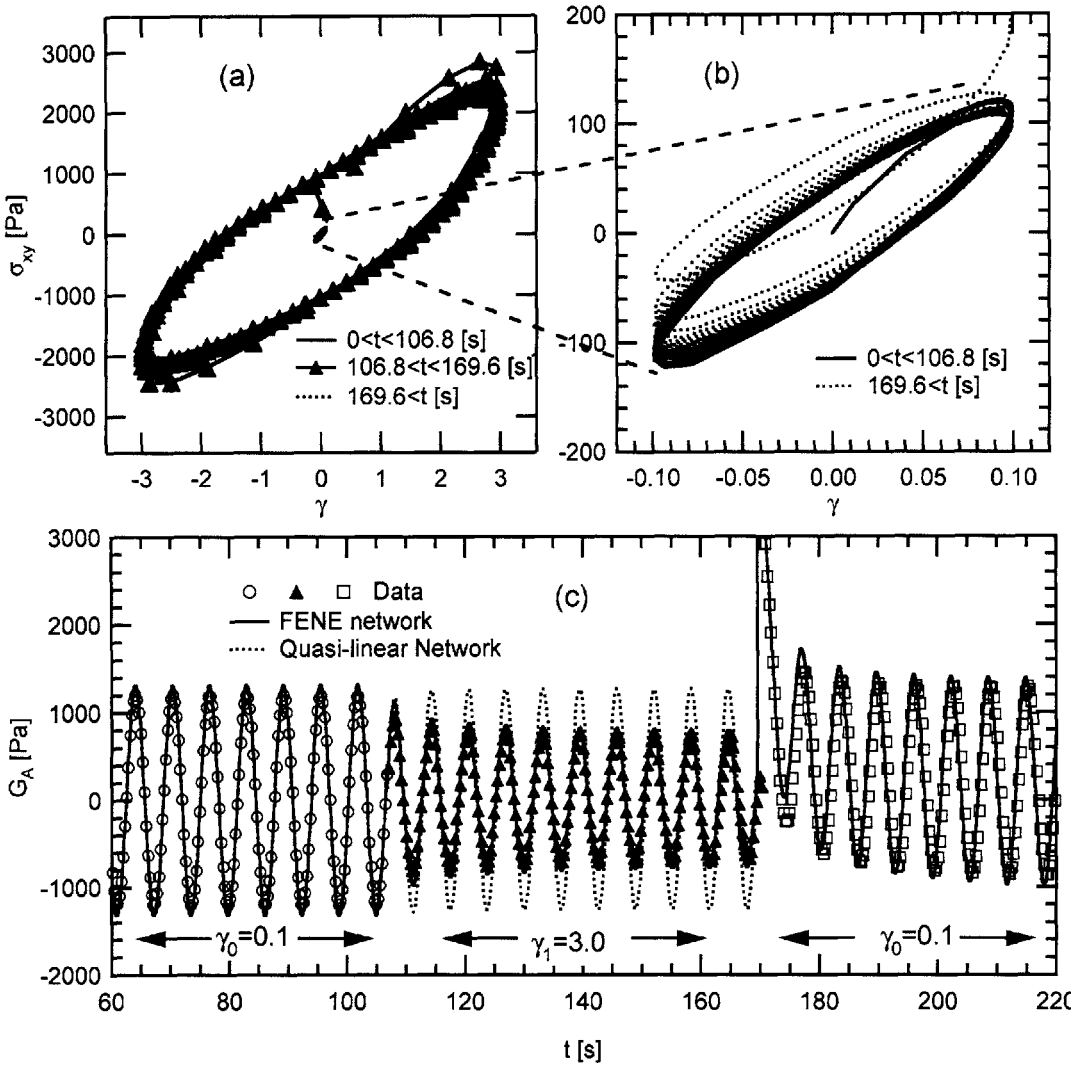

Figure 70 Transient behavior of gluten gel. a). Lissajous figures depicting material response when the strain amplitude of oscillation is increased from $\gamma_0 = 0.10$ to $\gamma_0 = 3.0$, then back to $\gamma_0 = 0.10$ again at a fixed frequency of ω = 1.0 s^{-1}. b). Stress response against time illustrating the transient nature of the network. The FENE network correctly predicts the transient stress growth and complete recovery of the gluten gel.

Comparison with other non-linear deformations

So far we have focused solely on the mechanical response under large amplitude oscillatory deformations, next we address briefly the rheological implications of the finitely extensible network model in the start up of transient deformations.

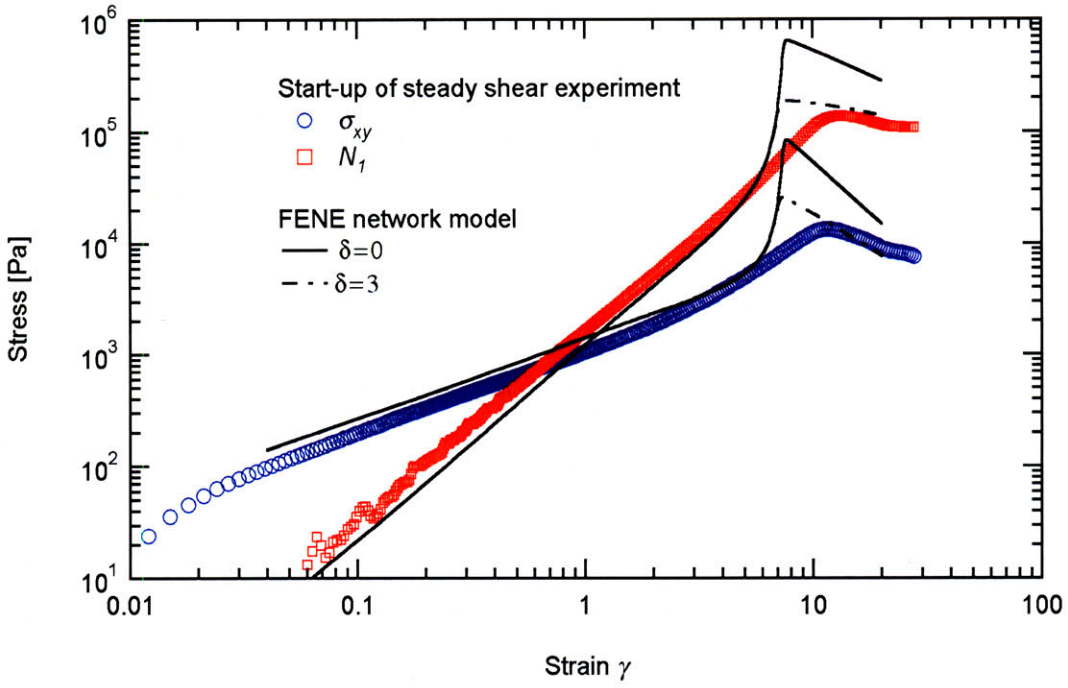

Figure 71 Start-up of steady shear flow at $\dot{\gamma}_0 = 1.0\ s^{-1}$. Power-law growth in shear stress and normal stress difference is well predicted by the FENE network model up to $\gamma^* = 5$, after which the non-linearity of the model overpredicts the stress over-shoot. Improvements to the predictions can be made by using the modified network model. However, accurate constitutive modeling at large strains is difficult because the sample deformation deviates substantially from viscometric flow at $\gamma \sim 9$.

We first compare the model predictions to the transient growth in the shear stress during the start up of steady shear. The model and data show good agreement in the power-law regime $\gamma^* \leq 5$ in which:

$$\begin{aligned} \sigma_{xy}^{+} &\sim t^{n} \\ N_1^{+} &\sim t^{2n} \end{aligned} \tag{6.36}$$

Deviations from power law growth and time-strain factorizablity discussed in equation (6.5) begin to be discernible when the strain-stiffening effect becomes significant. In fact the stress overshoot is grossly over predicted by the FENE network model. It is possible to capture the apparent stress overshoot empirically by using an extremely non-linear elastic term [104] that bounds the stress at very large strains.

Here we will discuss the causes of this apparent overshoot. Firstly, as discussed in our previous work [174], video imaging shows that the sample begins to undergo an instability shortly after the onset of strain-stiffening ($\gamma^* \sim 5$). This instability ultimately leads to the sample being ejected from the gap. The deformation in the gluten gel is no longer viscometric from the point of instability onwards and thus we do not expect the constitutive equation to give accurate predictions unless the full dynamic equations are solved.

Secondly, we attribute part of this discrepancy once again to the over-simplistic evolution equation. The proposed form of equation (6.27) relates to the fact that the probability for the breaking of a junction point should increase as the tension in the stretched filament is increased. Upon further consideration, though reasonable, there is no reason to suppose the rate of breakage should only diverge when the chains reach the finite extensible limit (i.e. $Tr(\boldsymbol{A}_k) \to b$), i.e. the ultimate tensile strength of a junction point can be a finite value or in other words, the probability of survival of a junction point can tend to zero when a critical but finite value of tension is sustained by a elastic segment. Therefore we consider improvements to the model by allowing the junctions to be completely destroyed slightly before the FENE limit. The modified rate of destruction can then be written as:

$$\lambda_k^{-1}(\boldsymbol{A}_k) = \lambda_{k,0}^{-1} \frac{1 + C_1\left(Tr(\boldsymbol{A}_k) - 3\right)}{1 - Tr(\boldsymbol{A}_k)/(b - \delta)} \tag{6.37}$$

The resulting stress response of this modified network model is essentially the same as equation (6.27) through (6.32), but the stress overshoots are slightly

tempered. In figure Figure 71 we show that the predicted magnitude of the overshoot is much more reasonable for the chosen value of $\delta = 5$.

Finally, the use of FENE-P type models with closure approximations are known to result in over-prediction of transient stress growth [188]. The reason being that the Peterlin closure approximation cannot accurately capture the statistical distribution of segment lengths at intermediate deformations near the point of finite extensibility and instead predicts a fraction of the filaments to be deformed beyond the maximum allowable length. More accurate simulations utilizing Brownian dynamics will reveal a much weaker overshoot behavior.

The qualitative behavior is similar for start-up of uni-axial extension flow as depicted in Figure 72. The data are collected on a wind-up drum type rheometer that has been discussed in detail in a previous publication [174]. The FENE network over-predicts the magnitude of the stress difference that occurs just before the sample ruptures, while the modified network model gives more reasonable stress growth functions. The fact that the point of rupture occurs extremely close to the finite extensibility plateau should not be surprising, since the mass rupturing of network junctions dramatically reduces the rate of stress growth in the system and can lead to tearing or necking as implied in the Considère criterion [126, 189-191].

Significantly, the extensibility of dough is often quoted as a measure of its quality [6, 8, 9, 27, 43, 147, 173], and this is the first piece of direct evidence that shows how the extensibility (defined as the maximum strain achieved before rupture) of a dough can be linked to molecular phenomena, and and be predicted or at least estimated by performing shear experiments at large amplitude oscillations: a reasonable estimate of the extensibility of a dough like material can be inferred if the linear viscoelastic relaxation function $G(t-t')$ and finite extensibility parameter b are known. The magnitude of the stress may be over predicted (as shown in Figure 71) without additional experiments but this does not affect the critical strains.

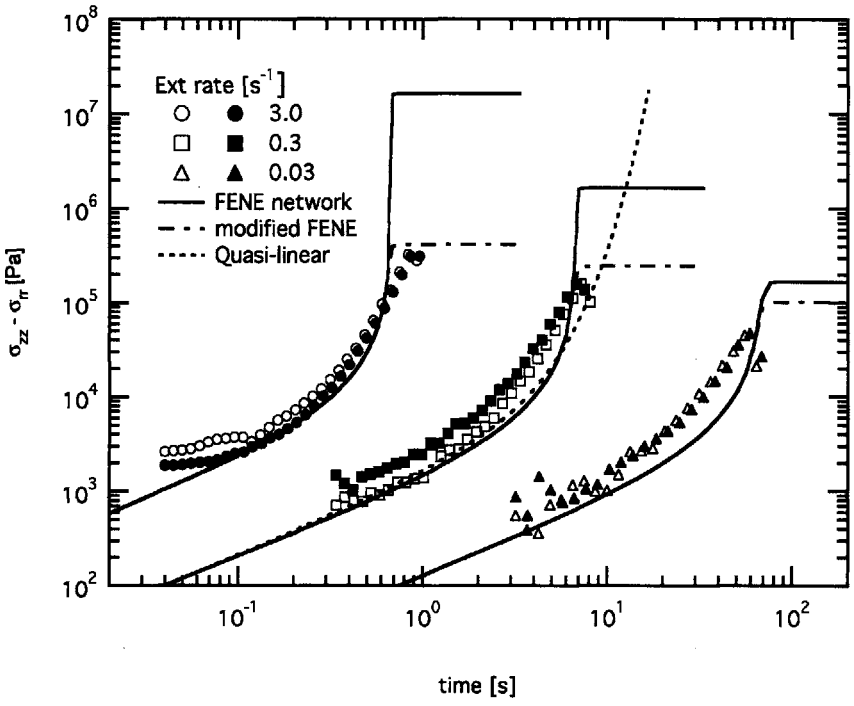

Figure 72 Transient extensional stress difference upon inception of uni-axial elongation for deformation $0.03 < \dot{\varepsilon}_0 < 3.0$ s^{-1}. The FENE network over predicts the magnitude of stress, this can be remedied by including a modification term δ. However, the strain and time to rupture corresponds closely to that predicted by the finite extensibility limit determined from LAOS with $b = 90$ and $\delta = 5$.

6.7. *Conclusions*

In this article, we investigated the mechanical properties of a gluten gel through large amplitude oscillatory shear (LAOS). This experimental technique allowed us to study the rheological response over a range of strain amplitudes γ_0 and frequencies ω with good accuracy and repeatability up to the point of viscometric instability without destroying the sample. From the data, we are able to generate a rheological fingerprint of the gluten gel that in turn forms the basis for devising a constitutive equation.

We have built upon the critical gel-like response documented in our earlier work to construct this constitutive model that illustrates the origin of the non-linear behavior in a gluten gel. The non-linearity of the constitutive equation is encapsulated in two simple functions, namely a FENE spring law that captures the strain-stiffening and a non-linear network destruction term that reflects the observed softening behavior at intermediate strains. We have demonstrated how using a relatively low level of complexity in the constitutive model is sufficient to capture the important non-linear features observed in both shear and extension, while further improvements to the quantitative agreement between experiment and model can be made by fine tuning these non-linear functions and will be the subject of future work. We briefly describe some of the possible modifications here.

Perhaps most importantly, we have based our model on the multi-mode approach described in equation (6.8). Because of the frequency independence of the Lissajous fingerprint in Figure 67, we have assumed all the modes to have the same non-linear behavior (i.e. same b, δ and C_1) in order to minimize the number of adjustable model parameters. This allowed us to concentrate on the essential features of these non-linearities and highlight their respective relationships to physical material properties. We compared the model predictions to experimental observations and showed that indeed using just four linear (S, n, G_R and λ_R) and three non-linear (b, δ and C_1) viscoelastic parameters are sufficient to capture the rheological behavior of this complex cross-linked gel to a surprising degree of accuracy over a wide range of strains γ_0 and frequencies ω. We could of course relax this assumption and allow each of these modes (which represent network structures at different length scales) to exhibit different non-linear behavior. To map out these effects thoroughly, a detailed sweep of the Pipkin space shown in Figure 67 would be required to find the corresponding modal parameters (b_k, δ_k and C_{1k}).

We have also, perhaps naively, assumed an extremely simple form for describing the non-linear softening (equation (6.28)). One can easily imagine more

sophisticated functions to describe the complex energy landscape. For example, we can increase the order of the polynomial such that:

$$\lambda_k^{-1} \sim \lambda_{k,eq}^{-1}\left(1+C_1\left[Tr\left(\boldsymbol{A}_k\right)-3\right]+C_2\left[Tr\left(\boldsymbol{A}_k\right)-3\right]^2\right) \tag{6.38}$$

Alternatively, other functions such as exponential, hyperbolic or even functions that include the rate of strain can be adopted. Rather than the empirical approach, Evans and Ritchie [182] suggested a bond dissociation model with an energy landscape that has a single energy barrier. The characteristic of this barrier is determined by both the magnitude and rate of loading of the tensile force in the elastic segments.

Finally, we will like to mention that more complex spring laws can be used to better approximate the semi-flexible nature of the network segments [192]. A possible candidate is the Worm-like chain law (WLC) that has been used with reasonable success in describing bioipolymer gel networks [167]. Evans and Ritchie [182] also investigated the force extension behavior of a WLC when it is coupled with their non-linear network destruction equation; the resulting rate of network dissociation is of an exponential form.

Currently, there exists no strong evidence to prefer one function over another and this seemingly endless list of possible modifications merely illustrates the flexibility of the transient network approach [193].

To conclude, we note the strong similarities between the gluten gel and other bio-polymer networks in terms of the strain-stiffening observed and the ability to regain the equilibrium strength even after severe deformations and softening [137]. The latter feature also bears strong resemblance to the so called reversible polymer networks that are held together by hydrogen bonding at the network junctions [194]. These junctions can yield before the macromolecular strands are irreversibly ruptured due to the application of external strain and are reformed when the material is returned to its equilibrium state. This idea can be simply demonstrated by the fact that if a gluten dough is cut into halves, the two halves can be recombined by simply holding them together. An analogous method is to disrupt the hydrogen bonds chemically with 8M urea solution; The gel can then

be reconstituted by simply reintroducing water to wash out the Urea. Such similarities suggest that the multiple mode finitely extensible network model developed here can find applications in a much a wider context.

6.8. *Apendix - Measuring nonlinear rheological properties using parallel plates geometry with large amplitude oscillatory shear (LAOS)*

Conceptually, rectilinear shear flow is most easily visualized. Velocity and its gradient can be simply expressed in the Cartesian system. Unfortunately, the presence of boundaries limits the range of strain accessible, costly linear drive systems have to be used to motivate these deformations. Also the idealized situation for which material functions are truly independent of position can never be attained; a boundary layer has to be present at the end interfaces.

In view of these limits, most commercially available rheometers utilize rotational drive systems and axi-symmetric geometries. The Couette cell and the cone-plate geometries are examples of systems of this kind. In a Couette cell, a cylindrical bob is driven within a concentric cup, the local flow between the bob and the cup closely approximates that of a rectilinear shear flow provided the gap between the two fixtures is small compared to the overall radius. In a cone-plate geometry, the cone is aligned so that its axis of symmetry is perpendicular to the plane of a flat plate, and the vertex of the cone lies on the plane. The local shearing motion generated between the cone and the plate once again closely approximates that of a rectilinear shear flow and can be considered as uniform within the swept volume along the axis of symmetry between the cone and the plate.

The recent interest in complex materials such as biopolymer gels, yield stress and shear thickening materials has led to difficulties when testing samples with high bulk viscosities; slip is frequently observed at the sample geometry interface. Slip can be eliminated by using roughened surfaces that increase the traction between the sample and the geometries. The most common and convenient method of introducing roughened surfaces is by simply applying a layer of adhesive backed sandpaper onto the surfaces. Cleaning is minimized since used samples can be

simply peeled off along with the adhesive backed sandpaper. Care must be taken when applying the sandpaper to ensure that it lies flat on the surface of the geometries with no "wrinkles". This turns out to be extremely difficult for both the Couette cell and the cone-plate geometries; it is difficult to coax the stiff sandpaper to conform to the radius of curvature of the said geometries. A very precise shape of sandpaper also has to be pre-cut so that the edges of the sand paper closes upon itself without introducing too much irregularity.

Under these circumstances, the parallel-plates geometry becomes far more attractive. Simple circular sheets of sandpaper can be simply attached to the flat surfaces of the parallel-plates geometry. But this convenience comes at a cost: the shear flow between the parallel plates is not homogeneous. In a well-made pair of parallel plates, the gap h between the two plates is constant. From the axial-symmetry of the geometry, we find that the velocity V of the rotating plate increases linearly with the distance r from the axis of symmetry. Thus the shear rate at a distance r can be written as:

$$\dot{\gamma} = \frac{V}{h} = \frac{\Omega r}{h} \tag{6.39}$$

We can see from the expression that it also increases linearly with r.

Though the flow is inhomogeneous, the strain field is still largely independent of material properties provided the gap is small compared to the radius of the plates and inertial effects are negligible. It is convention to cite the shear rate at the edge of the plate ($r = R$) as the characteristic rate of the geometry, i.e.:

$$\dot{\gamma}_E = \frac{\Omega R}{h} \tag{6.40}$$

The corresponding shear stress σ_R is then calculated by the rheometer from the measured torque Γ by assuming a linear relation between shear stress and r:

$$\Gamma = 2\pi \int_0^R \sigma(r) r^2 \, dr$$

$$\Gamma = 2\pi \int_0^R \sigma_R \frac{r^3}{R} dr \qquad (6.41)$$

$$\Gamma = \frac{\pi \sigma_R R^3}{2}$$

$$\sigma_R = \frac{2\Gamma}{\pi R^3}$$

The assumption of linear relationship is of course valid for linear viscoelastic systems; stress is linearly proportional to strain and its time derivatives. In this short article, we discuss the limits for calculating this characteristic "edge" stress for material that exhibit nonlinear viscoelastic behavior.

Example of nonlinear material behavior and the calculated edge shear stress

To illustrate the shortfalls of the above-mentioned linearized analysis, we take a FENE-P model that exhibits cyclic weakening and strong stiffening at finite strains. The model can be succinctly expressed by a differential equation that describes the evolution of the microstructure:

$$\boldsymbol{A}_{(1)} = -\frac{1}{\lambda}\left[f(TrA)\boldsymbol{A} - f_{eq}\boldsymbol{I} \right] \qquad (6.42)$$

where the function $f = 1/(1 - TrA/b)$, $f_{eq} = 1/(1 - 3/b)$ and the finite extensibility parameter b describe the nonlinearity of the system. $\boldsymbol{A}$ can be thought of as a finger strain tensor of the microstructure and λ is a characteristic relaxation time.

A nonlinear spring law is then used to convert the state of microstructure deformation to a resulting state of stress:

$$\boldsymbol{\sigma} = G\left(f(TrA)\boldsymbol{A} - f_{eq}\boldsymbol{I} \right) \qquad (6.43)$$

The Lissajous figures calculated for a FENE model (with λ - 5.0 s, G = 1200 and b = 2) under dynamic oscillatory shear at ω = 1.0 s^{-1} after 6 cycles are plotted in

Figure 73. The model, shows typical viscoelastic behavior at small strains. At intermediate strains, the Lissajous figures exhibit mild inter-cycle softening (overall rotation of major axis of Lissajous curves). At large strain amplitude due to the relatively large Deborah number ($De = \lambda\omega = 5.0$), it shows both dramatic intra-cycle stiffening as indicated by the distortion of the Lissajous curves and inter-cyclic stiffening (maximum stress increases more rapid than linearly with strain).

Lissajous curves for both the true edge shear stress and the simulated rheometer output stress (equation (6.41) for parallel-plate geometry) are plotted in the figure for comparison. In the intermediate strain softening regime, σ_R slightly overpredicts the true edge stress σ_E. While at large strains, the true stress and degree of stiffening can be grossly underpredicted. Not unexpectedly, the largest differences are for instances in which material functions are strongly nonlinear i.e. in the region of dramatic intra-cyclic stiffening as the finite extensibility limit is approached.

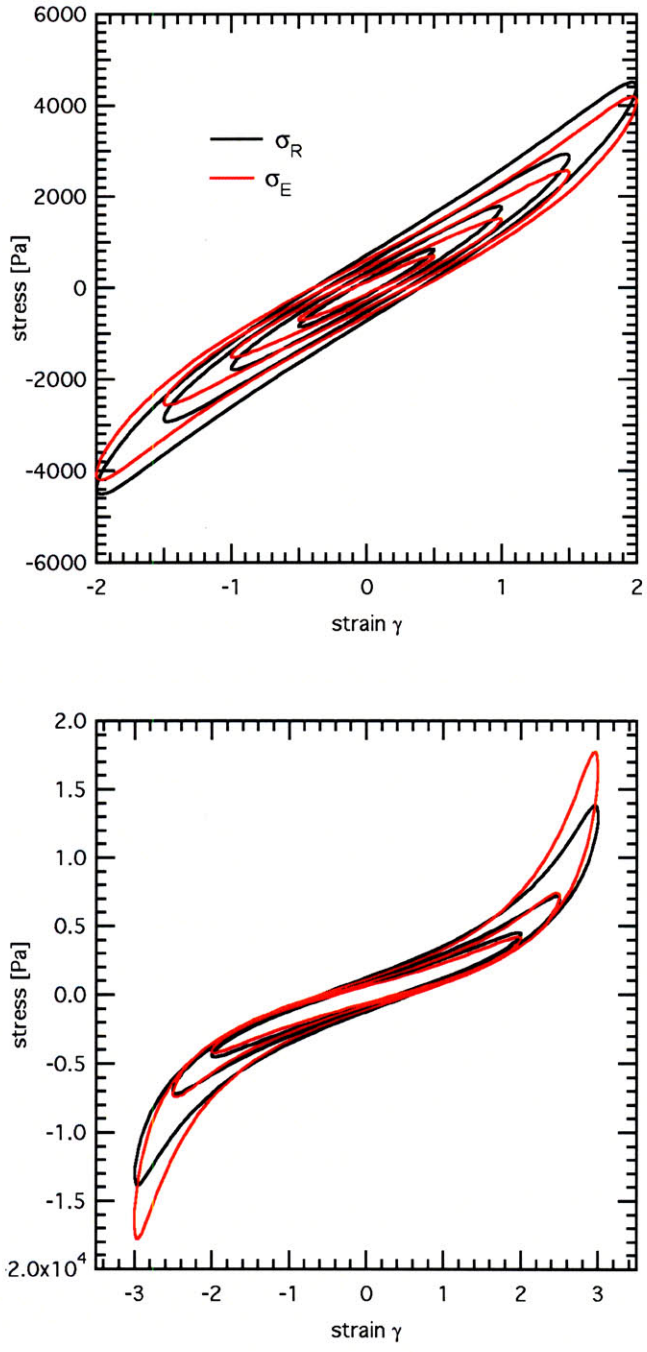

Figure 73 Lissajous figures plotted for idealized homogeneous stress and strain for FENE-P model under a range of strain amplitude as red lines. Also plotted as black lines are the simulated Lissajous figures of rheometer output stress for the same material under equivalent edge shear strain.

Possible corrections

Despite the large potential errors arising from using equation (6.41), currently there exists no general method for correction. However, there does exist a correction commonly used for calculating true steady state edge viscosities [60], and Parker et al have also introduced a correction for dynamic moduli in axial-Couette geometries. In this section we introduce some general methods for calculating the true edge stress σ_E in parallel-plates geometry under oscillatory shear. The method can be generalized to arbitrary controlled strain deformations; oscillatory and steady shear are special cases of the general correction.

Method of plate size variation

A simple correction is to consider the difference between experiments performed on parallel plates of two different sizes (R_1 and R_2). In the two experiments (case 1 and case 2), the oscillation frequency is kept constant, but the oscillation amplitude is modified such that for $r < R_1$, the deformation and thus the stresses are identical i.e. both experiments are performed at the same angular displacement amplitude. Provided the edge effects are negligible, the difference in torque between the two measurements must be the contribution from the annular material of the larger plate between $R_1 < R \le R_2$. If the difference in plate sizes are small ($R_2 - R_1 = \delta$), the edge shear stress can then be approximated by:

$$\begin{aligned} \Gamma_2 - \Gamma_1 &= 2\pi R^3 \sigma_{2,E} \delta \\ \sigma_{2,E} &= \frac{\Gamma_2 - \Gamma_1}{2\pi R^3 \delta} \end{aligned} \tag{6.44}$$

Method of strain amplitude variation

Perhaps a more elegant work around is to consider the differences between two separate experiments performed at the same frequency (case 1 and case 2) for which the oscillation amplitude is related by $\gamma_2 = k\gamma_1$ and $\dot{\gamma}_2 = k\dot{\gamma}_1$ (recall that

even though the deformation is inhomogeneous, the velocity field can still be easily calculated and is independent of the material functions). The torque measured in the quasi-steady oscillation cycles of the two cases can be written as:

$$\begin{aligned}\Gamma_1 &= 2\pi\int_0^R \sigma_1(r)r^2\,dr \\ \Gamma_2 &= 2\pi\int_0^R \sigma_2(r)r^2\,dr\end{aligned} \tag{6.45}$$

We define a radius R' as the distance from the axis of symmetry for which the strain and strain rate of case 2 is identical to the edge strain and strain rate of case 1. i.e. $\gamma_2(R') = \gamma_1(R)$ and $\dot{\gamma}_2(R') = \dot{\gamma}_1(R)$. The condition for this to be satisfied is $kR' = R$.

The torque measured in case 2 can be decomposed into two parts, one resulting from the contribution of material that has coordinates $r > R'$ and a second part that comes from material within $r \geq R'$:

$$\Gamma_2 = 2\pi\int_{R'}^R \sigma_2(r)r^2\,dr + 2\pi\int_0^{R'} \sigma_2(r)r^2\,dr \tag{6.46}$$

The material in the second part experience stress that varies from zero at $r = 0$ to $\sigma_2 = \sigma_2(R') = \sigma_1(R)$ at $r = R'$. Upon further inspection, this portion of material can be considered to be dynamically similar to the stress state in case 1, or in other words, deformations of the same strain history within $r > R'$ can be mapped onto case 1:

$$\sigma_2(r) = \sigma_1(kr) \tag{6.47}$$

Thus rewriting the expression for the torque in case 2:

$$\begin{aligned}\Gamma_2 &= 2\pi\int_{R'}^R \sigma_2(r)r^2\,dr + 2\pi\int_0^{R'} \sigma_1(kr)r^2\,dr \quad \text{let } kr = r' \\ \Gamma_2 &= 2\pi\int_{R'}^R \sigma_2(r)r^2\,dr + \frac{2\pi}{k^3}\int_0^R \sigma_1(r')r'^2\,dr'\end{aligned} \tag{6.48}$$

It is now clear the second integral can be expressed in terms of the torque in case 1:

$$\Gamma_2 = 2\pi \int_{R'}^{R} \sigma_2(r) r^2 \, dr + \frac{\Gamma_1}{k^3} \tag{6.49}$$

For two cases with strain amplitude that are sufficiently similar, we can substitute $k = 1 + \delta$, where δ is the small fractional difference between the two strain rates. The first integral can then be rewritten in terms of the edge stress of case 2:

$$\Gamma_2 \simeq 2\pi R^3 \sigma_{2,E} \delta + \frac{\Gamma_1}{(1+\delta)^3} \tag{6.50}$$

This expression can be linearized and rearranged to give the edge shear stress in terms of the torque difference and δ:

$$\sigma_{2,E} = \frac{1}{2\pi R^3}\left[\frac{\Gamma_2 - \Gamma_1(1-3\delta)}{\delta}\right] \tag{6.51}$$

To check the validity of this analysis, we consider a linear viscoelastic material, for which torque is proportional to the applied strain amplitude, i.e. $\Gamma_2 = k\Gamma_1 = \Gamma(1+\delta)$. The expression yields a result that is consistent with equation (6.41):

$$\begin{aligned} \sigma_E &= \frac{\Gamma_1}{2\pi R^3}\left[\frac{1+\delta-1+3\delta}{\delta}\right] \\ &= \frac{2\Gamma_1}{\pi R^3} \end{aligned} \tag{6.52}$$

Finally, we consider equation (6.51) for vanishingly small changes to the strain amplitude (i.e. $\delta \to 0$):

$$\sigma_E \to \frac{1}{2\pi R^3}\left[\frac{\Gamma+\Delta\Gamma-\Gamma(1-3\delta)}{\delta}\right] = \frac{\Gamma}{2\pi R^3}\left[\frac{\Delta\Gamma/\Gamma+3\delta}{\delta}\right] \tag{6.53}$$

We recall that $\Delta\gamma_0 = \delta\gamma_0$. Subsituting this into equation (6.53) we find:

$$\begin{aligned}\sigma_E &= \frac{\Gamma}{2\pi R^3}\left[3+\frac{\Delta\Gamma/\Gamma}{\delta}\right] \\ &= \frac{\Gamma}{2\pi R^3}\left[3+\frac{\Delta\Gamma/\Gamma}{\Delta\gamma_0/\gamma_0}\right] \\ &= \frac{\Gamma}{2\pi R^3}\left[3+\frac{\gamma_0}{\Gamma}\frac{\partial\Gamma}{\partial\gamma_0}\right] \text{ or } \frac{\Gamma}{2\pi R^3}\left[3+\frac{\partial \ln\Gamma}{\partial \ln\gamma_0}\right]\end{aligned} \tag{6.54}$$

It is sometimes more convenient to write equation (6.54) in terms of the rheometer output stress σ_R calculated from equation (6.41):

$$\sigma_E = \frac{\sigma_R}{4}\left[3+\frac{\gamma_0}{\sigma_R}\frac{\partial\sigma_R}{\partial\gamma_0}\right] \tag{6.55}$$

This result agrees with the calculations performed on the model FENE-P simulation in which inter-cyclic stiffening results in σ_R underpredicting the true edge stress σ_E and vice-versa for the case of inter-cyclic weakening.

We demonstrate the ideas discussed in this article by considering some large amplitude oscillatory shear (LAOS) experiments performed on gluten gels in the nonlinear regime. Results from three sets of data collected at γ_0 = 4.0, 5.0, 6.0 and ω = 1.0 s^{-1} are illustrated in Figure 74. The nonlinearity is evident from the wave shapes of the cycle, a linear viscoelastic material will exhibit sinusoidal response when excited by a sinusoidal strain input. We apply a centered difference method to calculate the correction factor in equation (6.55). Note that the correction factor is a function of time, i.e. it is different during different parts of the cycle.

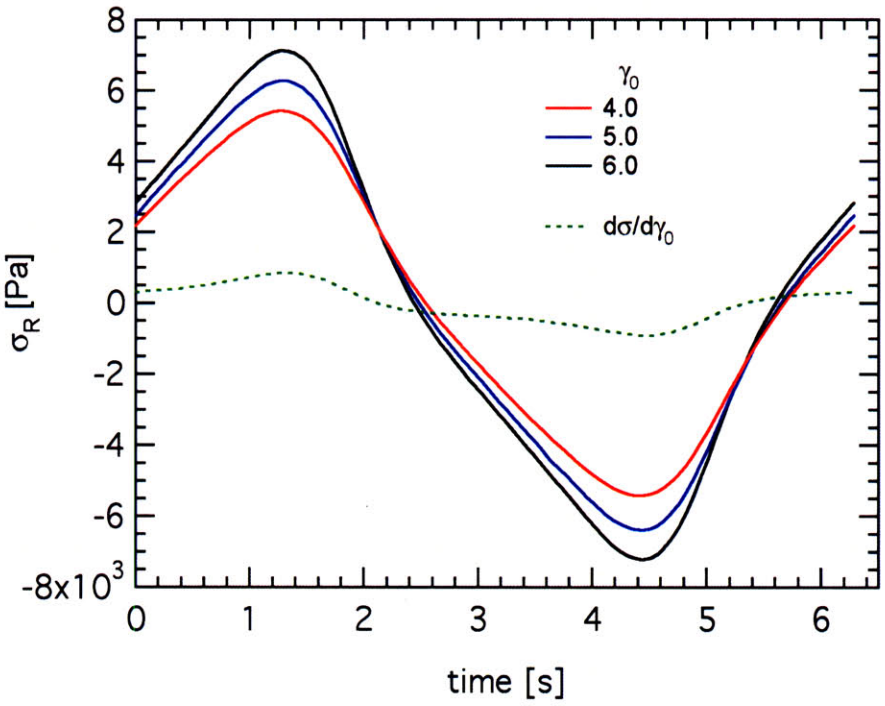

Figure 74 Rheometer calculated stress as a function of time for gluten gels deformed under a range of oscillatory strain amplitudes γ_0 = 4.0, 5.0, 6.0 at ω = 1.0 s^{-1}. The data are collected at quasi-steady state, i.e. the cycles remain invariant in time. Also plotted is the rate of change of calculated stress w.r.t. strain amplitude as a function of time calculated from the centered difference of the three sets of data.

In Figure 75, we compare the rheometer output stress to the true corrected edge stress. Over most of the cycle, σ_R is slightly greater than σ_E due to the overall softening.

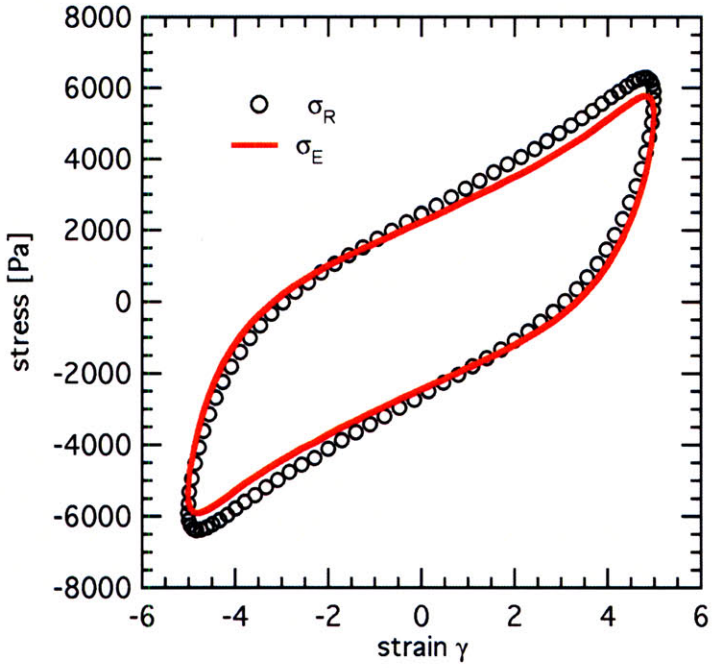

Figure 75 Quasi-steady state Lissajous curves of large amplitude oscillatory shear experiments performed on gluten gels at $\gamma_0 = 5.0$ and $\omega = 1.0\ s^{-1}$. The rheometer output stress is plotted as open circles, while the true corrected stress is plotted as a solid red line. The shapes of the curves are similar. The strain softening (decrease in modulus for increasing strain) leads to rheometer calculated stress that is slightly greater than the true corrected edge stress.

The calculation of this correction is not trivial since it is a function of the time. However, for strongly elastic materials for which variation in loss angle is small, a rough estimate for the overall fractional error ζ incurred by using equation (6.41) instead of (6.54) can be calculated by considering the change in dynamic modulus G^*:

$$\zeta \approx \frac{1}{4}\frac{\partial \ln G^*}{\partial \ln \gamma_0} \tag{6.56}$$

It must be stressed that this is only an overall estimate on the errors in the magnitude of the stress, the shape of the Lissajous figures can be dramatically altered for samples that show strong variation in loss angle

Due to the weakly softening nature of the gluten gels in the range of tested strains, the overall errors are small. For this particular set of experiments, $\zeta \simeq -0.2$ Using the rheometer output stress is a reasonable approximation to the true behavior of the material. However for other strongly nonlinear materials such as biopolymer gels comprising of semi-flexible filaments [167], the inter-cyclic stiffening can be extremely large (1 – 2 orders of magnitude per decade increase in strain) and it is extremely important to consider the correction factors described here.

Finally, we note that the analysis can be generalized to arbitrary deformations for which the edge strain on the parallel plate is specified by $\gamma_E(t,t')$ such as start-up of steady shear and step strain relaxation. The inclusion of t' in the function denotes the strain history of the deformation. The strain field within the parallel plate can then be written as $\gamma(t,t',r)=\gamma_E(t,t')r/R$ and the stress resulting from a deformation of this strain history is then $\sigma(\gamma(t,t'),r)=\sigma(\gamma_E(t,t')r/R)$. Note that the dependence in strain rates and other higher derivatives are included in the history of the deformation. Without any loss of generality, we once again put down the expression for the torque exerted by the sample between the parallel plate:

$$\begin{aligned}\Gamma &= 2\pi\int_0^R \sigma(\gamma(t,t'),r)r^2\,dr \\ &= 2\pi\int_0^R \sigma\left(\gamma_E\frac{r}{R}\right)r^2\,dr\end{aligned} \tag{6.57}$$

Analogous to the development for the special case of oscillatory shear flows, we perform a change of variables to the integration $k=\gamma_E r/R$:

$$\Gamma = \frac{2\pi R^3}{\gamma_E^3}\int_0^{\gamma_E} \sigma(k)k^2\,dk \tag{6.58}$$

The expression is then differentiated with respect to γ_E using the Leibniz formula:

$$\begin{aligned}\frac{\partial\Gamma}{\partial\gamma_E} &= \frac{\partial}{\partial\gamma_E}\left[\frac{2\pi R^3}{\gamma_E^3}\int_0^{\gamma_E}\sigma(k)k^2\,dk\right] \\ &= 2\pi R^3\left[\frac{\partial}{\partial\gamma_E}\left(\frac{1}{\gamma_E^3}\right)\int_0^{\gamma_E}\sigma(k)k^2\,dk+\frac{1}{\gamma_E^3}\frac{\partial}{\partial\gamma_E}\int_0^{\gamma_E}\sigma(k)k^2\,dk\right] \\ &= 2\pi R^3\left[-\frac{3}{\gamma_E^4}\int_0^{\gamma_E}\sigma(k)k^2\,dk+\frac{1}{\gamma_E}\sigma(\gamma_E)\right]\end{aligned} \tag{6.59}$$

The last expression can be rearranged in terms of the edge shear stress $\sigma_E = \sigma\left(\gamma_E(t,t')\right)$:

$$\begin{aligned}\frac{\partial\Gamma}{\partial\gamma_E} &= \frac{2\pi R^3}{\gamma_E}\left[-\frac{3}{\gamma_E^3}\int_0^{\gamma_E}\sigma(k)k^2\,dk+\sigma(\gamma_E)\right] \\ \frac{\partial\Gamma}{\partial\gamma_E} &= -\frac{3}{\gamma_E}\Gamma+\frac{2\pi R^3}{\gamma_E}\sigma_E \\ \sigma_E &= \frac{\gamma_E}{2\pi R^3}\left[3\Gamma+\frac{\partial\Gamma}{\partial\gamma_E}\right] \\ \sigma_E &= \frac{\Gamma}{2\pi R^3}\left[3+\frac{\gamma_E}{\Gamma}\frac{\partial\Gamma}{\partial\gamma_E}\right]\end{aligned} \tag{6.60}$$

and the corresponding equation for rheometer output stress:

$$\sigma_E = \frac{\sigma_R}{4}\left[3+\frac{\gamma_E}{\sigma_R}\frac{\partial\sigma_R}{\partial\gamma_E}\right] \tag{6.61}$$

For the special case of calculating steady state viscosities where $\sigma = \sigma\left(\gamma(t,t')\right) = \sigma(\dot{\gamma}t)$, the expression reduces to the well-known correction function [60]:

$$\begin{aligned}\eta_E = \frac{\sigma_E}{\dot{\gamma}_E} &= \frac{\Gamma}{2\pi R^3\dot{\gamma}_E}\left[3+\frac{\dot{\gamma}_E}{\Gamma}\frac{\partial\Gamma}{\partial\dot{\gamma}_E}\right] \\ &= \frac{\Gamma}{2\pi R^3\dot{\gamma}_E}\left[3+\frac{\partial\ln\Gamma}{\partial\ln\dot{\gamma}_E}\right]\end{aligned} \tag{6.62}$$

7. Highly Filled 'Glassy' Gels

7.1. Introduction

In the previous chapters, we explored the origins of the distinct rheological behavior of flour-water-dough by first considering the mechanical properties of the gluten gel alone. Through this simplified system, we showed that many of the features exhibited by flour water dough, such as power-law rheology and time–strain separability, stem from the rheology of the gluten macromolecules. We then refined our model to capture additional nonlinear rheological features such as that are exhibited by gluten gels.

In this chapter, we refocus our attention to more realistic systems by reintroducing the presence of filler particles. Wheat-flour–water doughs can be usefully considered as a highly filled gluten gel. The filler in this case consists of starch particles which absorb water from the hydrated gluten matrix over time leading to significant changes in their size and stiffness. Thus their rheological response is typically extremely complex with the effects of thixotropy and rheological aging convoluted into the measured data. As a result, most constitutive models concerning these systems have been largely empirical; it is difficult to associate individual elements within the constitutive equation to real physical processes occurring in the material.

We bypass the difficulties involved when dealing with starch-filled systems by first asking the question: what is the most pronounced effect of filling a gluten gel with starch? We do this by substituting the starch particles with spherical, inert, glass spheres of similar size (Potters Industries Speriglass A3000). The visual similarity between a real flour-water dough and a glass filled gluten gel is illustrated in Figure 76.

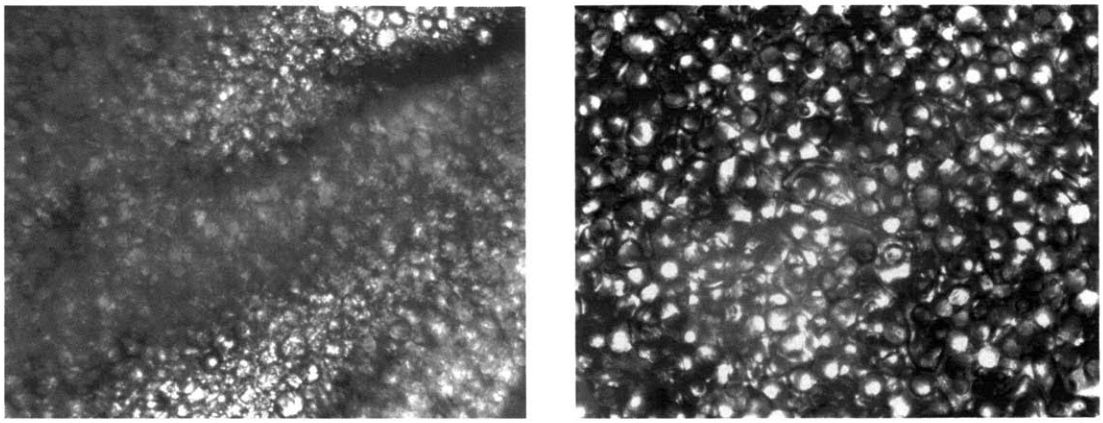

Figure 76 Micrographs of (a) flour-water-dough (average starch granule size ~30 μm). (b) glass filled gluten gels (average glass bead size ~50 μm).

Surprisingly, the relationship between filler content and rheology has scarcely been investigated for gluten gels. Edwards et al [143] also used glass beads as a replacement for starch particles. They illustrated the change in linear viscoelastic properties of dough as an increasing portion of the starch volume is substituted by an equivalent volume of glass beads filler. They showed a gradual weakening of the dynamic moduli as the starch is replaced suggesting that protein-starch bonding plays an important role in the rheology of the dough. They also altered the surface property of the starch granules by coating it with bovine serum albumin (BSA) which decreases the degree of adhesion of the fillers (both starch and glass beads) and found a decrease in viscoelastic moduli measured in small strain dynamic oscillations. However, the suggested explanation for the observed rheology is incomplete. Edwards et al assumed that the surface adhesion property of gluten on glass is weaker than on starch granules, this is inconsistent with the fact that while starch granules can be easily washed out of a dough by gently massaging it in running water, the same procedure will not wash out the glass beads from a filled gluten gel; which in turn suggest the bonding between glass and gluten gel is in fact much stronger than the starch-gluten interactions.

Uthayakumaran et al [107] performed a series of experiments to investigate the small to large strain rheological properties of a gluten gel with a range of starch content (0-100% gluten-starch weight ratio). They concluded the starch decreased

the range of strain amplitude for which linear viscoelastic approximation is valid for dough, but has a complex effect on the large strain rheology.

Overall, studies that involve starch are difficult to interpret, because of the competing effects between the gluten gel and starch particles for the water present in the system. Simply changing the amount of starch present can have a complicated effect on the gluten gel. Therefore, the results from these studies are often inconclusive.

On the other hand, the progressive increase in viscosity for a Newtonian matrix fluid with particles suspended within has been a subject of study since the beginning of the century. Other than simple mixture rules, Einstein[4] [196, 197] was the first to calculate the increase in viscosity of a fluid comprising of a dilute suspension of hard spherical particles. He considered the increase in rate of viscous energy dissipation of the system due to the presence of the spheres and concluded that the effective (or bulk) viscosity should increase with volume fraction according to the following formula:

$$\eta = \eta_{matrix}\left(1+\frac{5}{2}\phi\right) \tag{7.1}$$

where η_{matrix} is the viscosity of the base matrix and ϕ is the volume fraction of particles..

Einstein has based his approach by first assuming the viscosity to have a polynomial dependence on the volume fraction:

$$\eta = \eta_{solvent}\left(1+B_1\phi+B_2\phi^2+...\right) \tag{7.2}$$

---

[4] Einstein's derivation was in fact rather complex. The current author is still struggling with some of the ideas involved and takes solace in the fact that even the brilliant scientist who laid down the laws of relativity and quantum physics made an error in the initial publication and were corrected in a subsequent paper 195. Einstein, A., Correction to my paper: "A New Determination of Molecular Dimension". Annalen der Physik, 1911. 34: p. 591..

And there has been many subsequent efforts to calculate the higher order terms. Batchelor [198] gave a solution that includes the effects of two-body interactions:

$$\eta = \eta_{solvent}\left(1+\frac{5}{2}\phi+6.2\phi^2\right) \tag{7.3}$$

The problem concerning the increase in modulus due to the presence of filler particles in a viscoelastic medium is mathematically similar to that of the increase in viscosity of a fluid. In an earlier paper [199], Batchelor also gives an expression for the case in which a dispersion of identical hard spheres are embedded in an elastic medium of shear modulus G_{medium}:

$$G = G_{medium}\left(1+2.5\phi+5.2\phi^2\right) \tag{7.4}$$

Guth, Simha and Gold [200] also introduced terms that allow for interactions between particles and found that up to moderate volume fractions ($\phi < 0.30$), the following expression can be used to describe the increase in modulus:

$$G = G_{medium}\left(1+2.5\phi+14.1\phi^2\right) \tag{7.5}$$

In theory, this type of formulation can be further extended by considering interactions of increasing numbers of particles and calculating the higher order coefficients. However, they are only valid for systems in the dilute or semi-dilute regime. At higher concentrations, the rheology becomes strongly dominated by the short-length scales between particles and an alternative approach such as that suggested by Krieger and Dougherty [201] (equation (7.16)) is required.

Many of these theories are originally developed for the rubber industry in which carbon black fillers are routinely added to reinforce the strength of the crosslinked synthetic polybutadiene or natural rubber networks. Unfortunately, the typically small carbon black particles (~30 nm) are colloidal in nature and tend to aggregate to form complex fractal structures during the processing that are difficult to model, let alone predict the changes in properties [200]. However, the relatively large length scales of starch and glass particles and the high modulus and viscosity of gluten means that colloidal interactions can probably

be safely neglected in dough systems and glass-filled gluten gels, thus increasing the range of validity of these models.

Now, to summarize the objectives of this chapter: We will investigate the rheological properties of gluten gels with a range of filler volume fraction. We use inert, spherical, glass beads as the filler to avoid the complex behavior encountered when dealing with starch-filled systems. By understanding the prominent rheological features of this hard inert filler, we hope to elucidate the principal role of the starch particles by comparing the results with data obtained on a real flour-water–dough.

7.2. Methods

Gluten dough preparation

Gluten dough was prepared by placing 10g of vital gluten (Arrowhead Mills - ~ 12% moisture content) in a mixograph bowl with 14g of water (total dough moisture content = 63% by weight ratio to gluten solids) and the appropriate amount of glass beads to give the desired volume fraction. The mixture is then stirred, stretched and folded through the action of the mixograph pins for 12 minutes [85].

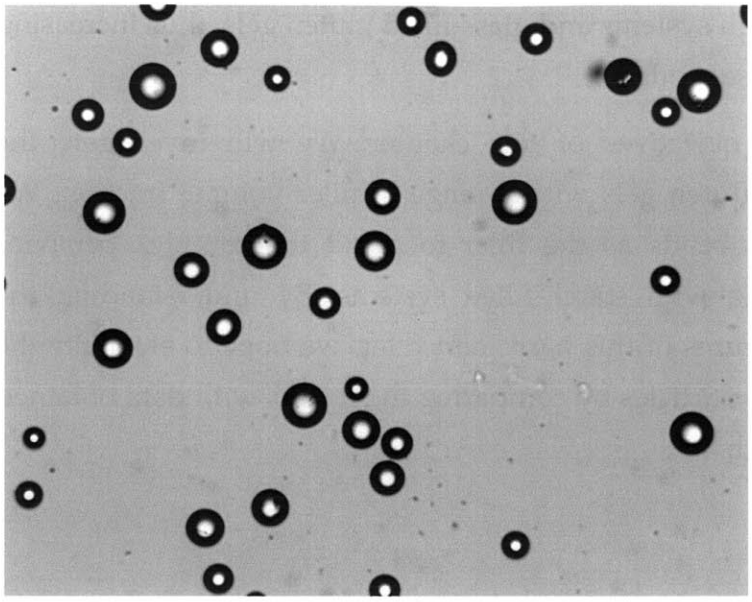

Figure 77 Glass beads with average diameter 50 μm.

The glass beads (~50 μm diameter Potters Industries Speriglass A3000) are chosen to approximate starch particles (~30 μm diameter) in terms of size and distribution. The resemblance to a flour-water-dough when viewed under a microscope is striking (Figure 76).

Volume fraction measurement

To calculate the volume fraction, we have to know the density of the gluten portion. We do this by first weighing a piece of gluten dough, then submerging it in a bath of silicon oil to find the volume displaced by it. The density is simply calculated as the ratio between the weight and volume found through the two procedures, assuming the gas cell content is negligible. Silicon oil is used instead of water for the displacement measurement because water will soak into the dough.

An average was taken from the calculation done on three different pieces of dough and the density was found to be $\rho_{gel} = 1.1 \pm 0.1 \times 10^3$ kgm^{-3}. The density of the beads are given by the manufacturer to be $\rho_{beads} = 2.5 \times 10^3$ kgm^{-3} which is

typical of glass. Thus the volume of gluten and glass beads can be calculated by the following formulas:

$$V_{gel} = \frac{\left(m_{water} + m_{gluten}\right)}{\rho_{gel}}$$
$$V_{beads} = \frac{m_{beads}}{\rho_{beads}} \tag{7.6}$$

and the volume fraction ϕ used throughout this chapter is simply the ratio between V_{beads} and the total volume:

$$\phi = \frac{V_{beads}}{V_{beads} + V_{gel}}$$
$$= \frac{m_{beads}}{\left(m_{water} + m_{gluten}\right)\rho_{beads}/\rho_{gel} + m_{beads}} \tag{7.7}$$

Rheometry

Shear rheometry experiments are performed under controlled strain conditions on the ARES rheometer and under controlled stress mode on the AR-G2 rheometer (TA instruments). A Peltier plate and a 25mm parallel plate fixture with 1mm separation were used. Approximately 2 g of gluten dough was placed on the Peltier plate, and the upper plate was then brought down to compress the sample to the specified thickness. Excess dough was trimmed with a razor blade. The Peltier plate was held at a fixed temperature of 22°C, to approximate typical room temperature. Slip was eliminated by applying adhesive-backed sandpaper (600 grit McMaster Carr 47185A51) to the surfaces of both the Peltier plate and the parallel plate tool. Drying of the sample was minimized by painting the exposed surface of the dough with a low-viscosity silicone oil.

7.3. *Rheology of filled gluten gels*

Under linear viscoelastic conditions, gluten gels show dynamic moduli that can be considered to be composed of two distinct regimes (see chapter 5). Firstly, at low frequencies ($\omega < 20\ s^{-1}$), a powerlaw regime that arise from the structural rearrangement of the fractal gluten gel. The dynamic moduli in this regime can be described by the expression below [74]:

$$G'_{gel}(\omega) = \frac{G''_{gel}(\omega)}{\tan(n\pi/2)} = \Gamma(1-n)\cos\left(\frac{n\pi}{2}\right)S\omega^n \tag{7.8}$$

where S = 1300 Pa s^n is the typical gel strength and n = 0.175 is the gel index/exponent for the gluten gel formed from the protocol described in the previous section.

At shorter time scales ($\omega > 20\ s^{-1}$), the dominant mode of relaxation is through the configuration rearrangement of polymer segments between network junctions. The rheological behavior in this regime can be described by a Rouse-like distribution of Maxwell modes:

$$G'_{Rouse} = G_R\sum_{k=1}^{\infty}\frac{(\lambda_k\omega)^2}{1+(\lambda_k\omega)^2}, \quad G''_{Rouse} = G_R\sum_{k=1}^{\infty}\frac{(\lambda_k\omega)}{1+(\lambda_k\omega)^2} \tag{7.9}$$

where $\lambda_k = \lambda_R/k^2$, and λ_R, G_R are the relaxation time and modulus of the Rouse segments.

The overall dynamic moduli can be written as a sum of the contributions from these two regimes:

$$\begin{aligned} G'(\omega) &= G'_{gel}(\omega) + G'_{Rouse}(\omega) \\ G''(\omega) &= G''_{gel}(\omega) + G''_{Rouse}(\omega) \end{aligned} \tag{7.10}$$

In Figure 78, we plot the storage modulus of unfilled gluten gels (solid circles) under small amplitude oscillatiory shear (SAOS). The same data is also presented in Figure 79 along with the loss modulus (hollow circles). We compare equations (7.8) to (7.10) (G_1' solid line, G_1'' dashed line) to the data obtained with the

unfilled gluten gels system and show that they are indeed an apt description of the rheological behavior of this network gel.

Also plotted in Figure 78 are storage modulus G_1' of filled gluten gels for a range of filler volume ($0.2 < \phi < 0.48$). Qualitatively, the shapes of the curve remain similar, and both power law gel regime and Rouse regime are still discernible at increased volume fractions. However, there is an increase in the modulus for increasing volume fractions.

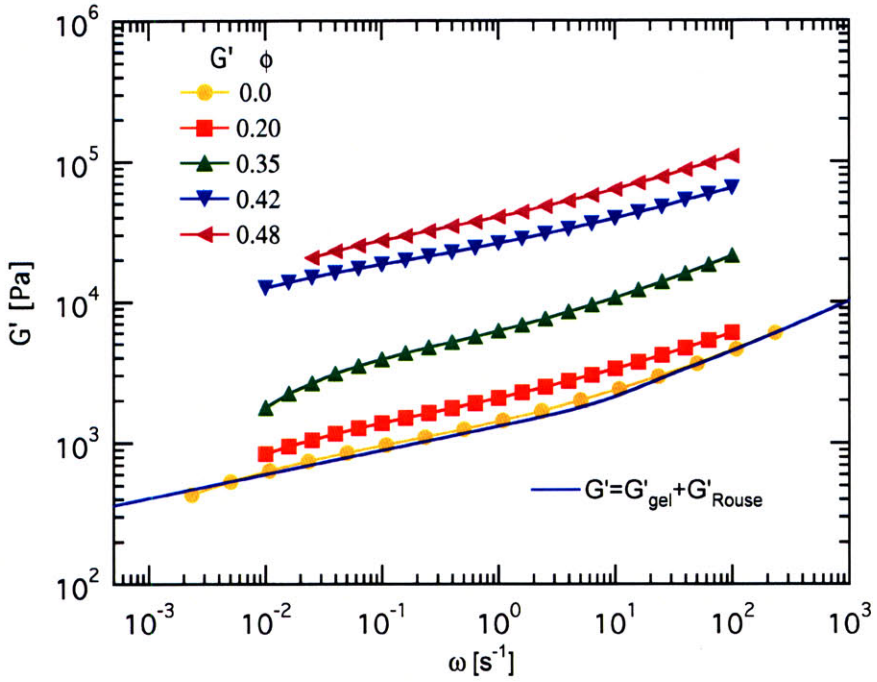

Figure 78 Storage modulus G' of gluten gels filled with glass beads for a range of filler volume fraction, $\phi = 0.0, 0.20, 0.35, 0.42, 0.48$. The storage modulus in each system show a similar powerlaw and Rouse-like variation over the frequency range i.e. see equation (7.8) : $G'_{gel}(\omega) = \Gamma(1-n)\cos(n\pi/2)S\omega^n$. All samples show similar values of n ~ 0.175 ± 0.15, however the magnitude of the moduli increases with volume fraction.

In Figure 79, we show the dynamic moduli of gluten gels with a range of filler volume fraction that have been shifted vertically to lie on the data for the unfilled system and the prediction of equation (7.10). Presenting the data in this manner reinforces the idea that the dynamic moduli at small strains are of essentially the

same shape, thus adding suspended particles to the gluten gel does not change the distribution of relaxation time scales, it simply serves to rescale the magnitude of the modulus (or stiffness) of the system.

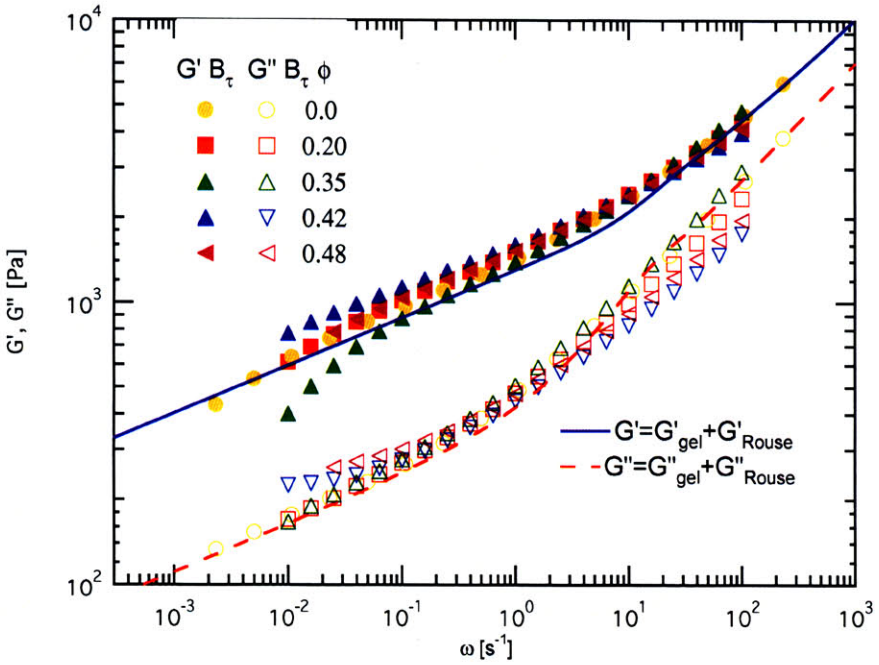

Figure 79 Dynamic moduli. G', G'' shifted vertically through the application of shift factors in the manner of equations (7.11) and (7.12). The dynamic moduli are of essentially the same shape, thus adding suspended particles to the gluten gel do not change the distribution of relaxation time scales.

We can understand this modification to the rheology by considering the theory of strain amplification suggested by Mullins et al [202].

Since the particles (glass in this case) are chemically inert; and we assume that they do not cause any significant changes (through changes to the mixing conditions) to the mechanical properties of the gluten gel medium; changes to the strain field within the gluten must be the source of the modification to the rheological behavior. At the simplest, we can consider an amplification factor [202] for strain B_τ such that:

$$\gamma_{local} = B_\tau \gamma_{macro} \tag{7.11}$$

where γ_{local} is the effective strain actually experienced by the gluten medium due to the presence of the filler, and γ_{macro} is the apparent or macroscopic strain that is measured by the rheometer. We illustrate how this amplification in strain is equivalent to an increase in the linear modulus by considering the stress generated in a linearly elastic material (with unfilled modulus G_u) by a macroscopic deformation of magnitude γ_{macro}:

$$\sigma_{xy} = G_u \gamma_{local} \tag{7.12}$$

The external or effective modulus is defined as the measured stress divided by the applied macroscopic strain i.e.:

$$G \equiv \frac{\sigma_{xy}}{\gamma_{macro}} = G_u \frac{\gamma_{local}}{\gamma_{macro}} = G_u B_\tau \tag{7.13}$$

Thus from the Guth Simha Gold theory [200], we have $B_\tau = 1 + \frac{5}{2}\phi + 14.1\phi^2$.

We can also deduce a possible functional form of B_τ at higher volume fractions by considering the situation where the volume fraction ϕ is close to the maximum packing ratio $\phi_{\max}$. We denote the average diameter of the particles to be D and the average gap between adjacent particles to be h. The parameters can be related through geometric considerations and written as:

$$\left(\frac{h+D}{D}\right)^3 = \left(\frac{\phi}{\phi_{\max}}\right)^{-1} \tag{7.14}$$

The value of the maximum packing ratio $\phi_{\max}$ for a random distribution of hard spheres was calculated by Onoda and Liniger $\phi_{\max} \sim 0.55\text{-}0.65$ [203].

In Figure 80, we illustrate how during shearing deformation, since the particles are assumed to be hard (cannot be deformed), they have to displace vertically as they pass over one another. Thus an amplification to the local strain sustained by the elastic medium is required in order to satisfy the (assumed) no-slip boundary

conditions on the particle surfaces. This increase in strain will be the of the order $(h+D)/h$ for closely packed systems, and can be found by rearranging equation (7.14):

$$B_\tau = \frac{h+D}{h} = \frac{\phi_{max}^{1/3}}{\phi_{max}^{1/3} - \phi^{1/3}} = \frac{1}{1-(\phi/\phi_{max})^{1/3}} \tag{7.15}$$

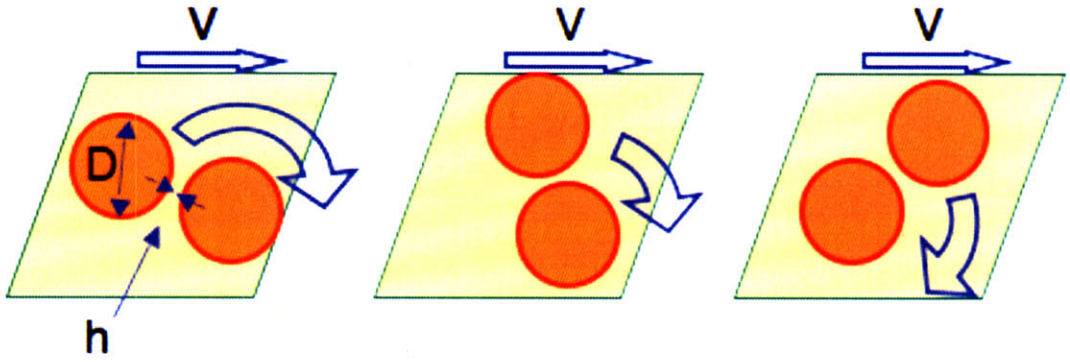

Figure 80 Schematic of strain magnification

A more established theory is in the form of the Krieger-Dougherty relationship [201]:

$$B_\tau = \left(1 - \frac{\phi}{\phi_{max}}\right)^{-x\phi_{max}} \tag{7.16}$$

This is a general expression for the strain amplification in concentrated suspensions of particles in a variety of shapes and stiffness. Krieger et al arrived at this expression by considering the viscosity increment due to adding particles to a suspension already containing particles. x takes the value of 2.5 for hard spherical particles:

$$B_\tau = \left(1 - \frac{\phi}{\phi_{max}}\right)^{-2.5\phi_{max}} \tag{7.17}$$

The expression reduces to the Einstein relationship in equation (7.1) at the limit of low volume fractions.

Alternatively, the form of this strain amplification factor can also be found through finite element simulations. Hwang et al calculated the change in bulk viscosity of a viscoelastic material with different volume fraction of hard fillers [204]. They simplified their calculations by only considering the effects of circular discs in a two-dimensional geometry but reasoned that the qualitative features are invariant for spheres in three-dimensional geometries.

Stickel and Powell [25] have recently reviewed other possible candidates for the shift functions. Bergstrom and Boyce [205] also provides an excellent review of the typical shift factors used in the field of solid mechanics such as the Mori-Tanaka estimate [206] and the Govindjee Simo model [207] .

The shift factors B_τ are plotted in Figure 81. At low volume fraction ($\phi < 0.4$), the magnitude of amplification observed experimentally is consistent with the theory of Einstein, Guth, Simha and Gold (equation (7.5)), but the range of validity is greater than that originally suggested by Guth ($\phi < 0.2$). As hinted in the introduction, this presumably is due to the fact that colloidal structures are not formed in this system. At higher volume fractions ($\phi > 0.4$), as we expected, the rheology is dominated by the decreased length scales between the particles and the data diverges and follows the trend suggested by equation (7.15) instead. The formula suggested by Krieger and Dougherty (equation (7.17)) is able to smoothly span these two regimes.

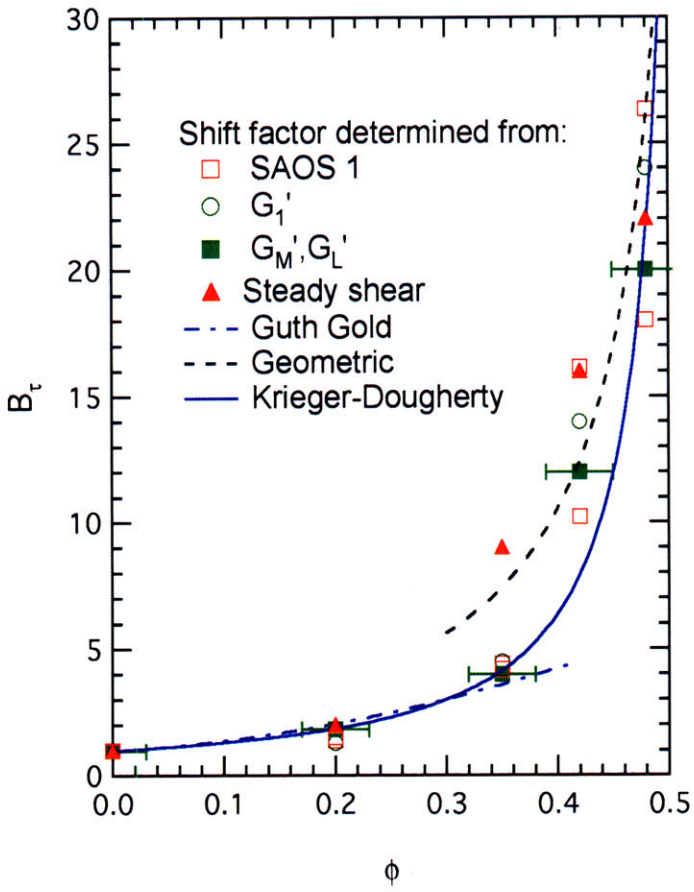

Figure 81 Strain amplification factors calculated from different experiments. Compared with predictions from different theories. The shift factors are compared to Guth-Gold's formula (equation (7.5)), a geometric scaling (equation (7.15)) with $\phi_{max} = 0.55$ and the Krieger-Dougherty relation with x =2.5 and $\phi_{max} = 0.55$.

Thus we show that the data are consistent with the gel network model of equations (7.8) to (7.10), but with magnitude of the modulus simply shifted due to this increase in local strain amplitude. Even though mathematically equivalent in the linear viscoelastic regime (where stress is proportional to strain and its higher order derivatives), there is an important conceptual difference between a direct increase of modulus and an amplification of local strain. This is especially apparent when we consider nonlinear deformations.

Unfortunately, in the nonlinear regime, there is no single viscoelastic parameter that can sufficiently describe the features on the Lissajous figures and underlying

changes in microstructure. Amongst the variety of typical measures in the nonlinear regime, the most commonly used is the first coefficient in the Fourier transformation G_1' and G_1'' introduced in the previous chapter. We plot the variation of G_1' as a function of strain amplitude for gluten gels with a range of filler volume fraction in Figure 82.

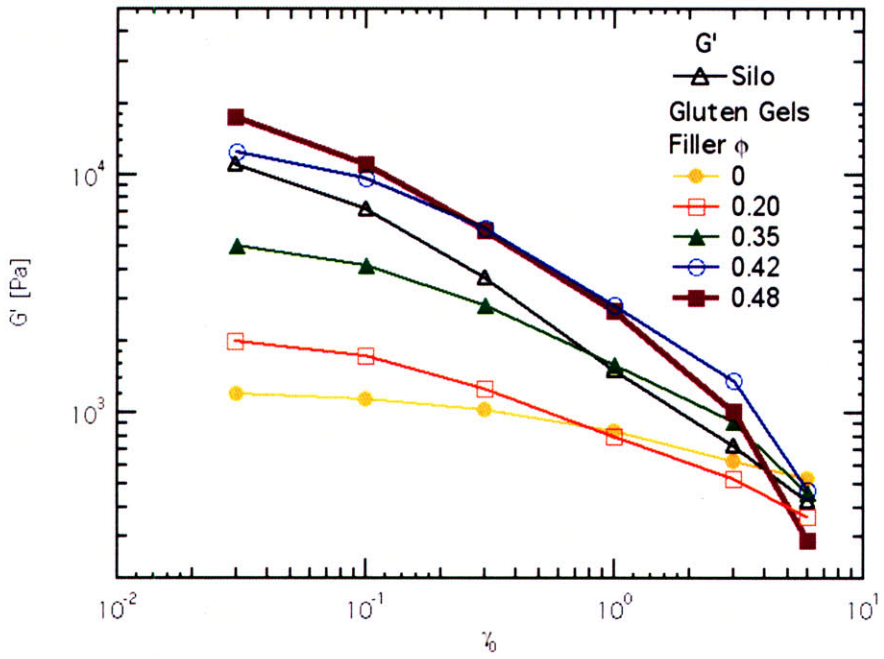

Figure 82 Magnitude of the in phase (i.e. real) component of the first Fourier coefficient G_1' at increasing strain amplitude for gluten gel systems with a range of filler volume fraction $\phi = 0.0, 0.20, 0.35, 0.42, 0.48$.

From the figure, we can see that G_1' decreases with strain amplitude. The gluten gels shows a larger region of linear viscoelasticity in which modulus is approximately constant for a range of strain amplitudes before it begins to decrease as a weak function of strain amplitude. The domain of this linear viscoelasticity decreases in range for increasing filler volume fractions, such that for the highest volume fraction tested, the modulus begins to decrease even at the smallest strains investigated i.e. no data could be obtained within the linear viscoelastic range.

Once again, we turn to the idea of strain amplification to interpret these observations. In Figure 82 we show that the data can be collapsed in a similar

fashion onto a master "softening" curve. The scaling argument is essentially the same as that given in equation (7.13). The modulus is scaled by the small strain, unfilled limit of G_1': $G^0 = G_1'(\gamma \to 0, \phi = 0) =$ 1208 Pa, and since it is calculated from the stress amplitude divided by the strain amplitude the strain amplification factor B_τ. The strain on the x-axis is also scaled by B_τ.

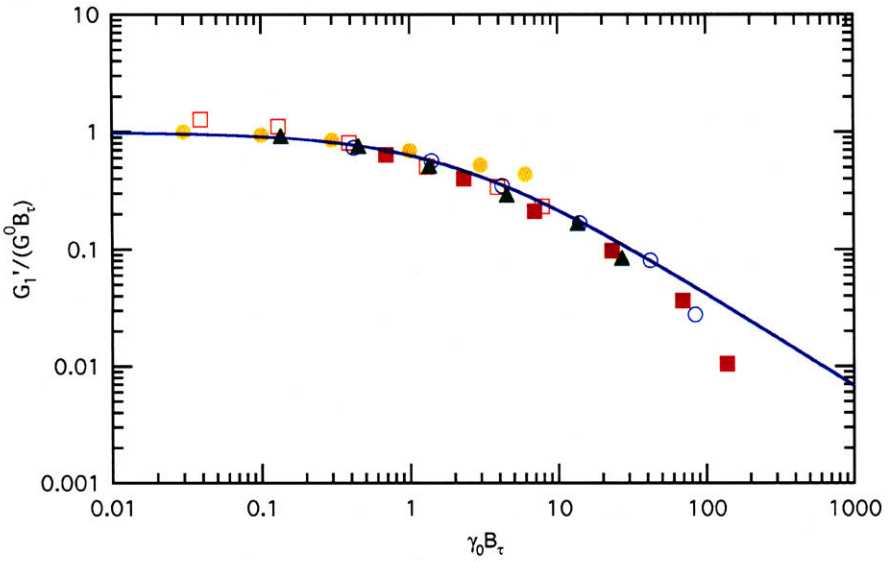

Figure 83 First in-phase Fourier coefficient G_1' for a range of volume fractions ϕ = 0.0, 0.20, 0.35, 0.42, 0.48 can be shifted onto a master curve by application of strain amplification factor B_τ.

The extreme softening of wheat flour dough was also noted by Uthayakumaran et al. [107]. They compared the values of storage moduli obtained through a strain sweep experiment to those of a gluten gel under the same procedure. They showed a decrease in the storage modulus for both of these materials as the amplitude of oscillation is increased. However, the onset of this non-linearity occurs at much smaller strains for the wheat-flour-water-dough system. Encouragingly, this is consistent with the idea that the local strain experienced by the gluten network is amplified by the presence of filler particles (starch in Uthayakumaran's case and glass beads in the current work).

Further insight to the rheological behavior and strain amplification of the glass filled gluten gels can be gained by considering the shapes of the Lissajous curves corresponding to the data presented in Figure 82.

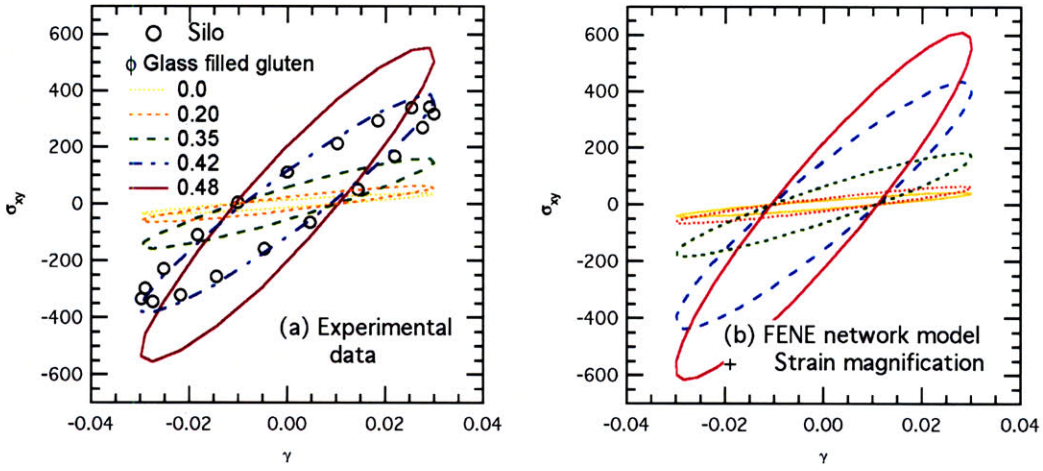

Figure 84 Lissajous curves at small strains. $\gamma_0 = 0.03$, $\omega = 1.0\ s^{-1}$. (a) Experimental data on gluten gels with a range of volume fraction $\phi = 0.0, 0.20, 0.35, 0.42, 0.48$. Data for a typical flour-water-dough are also plotted as open circles. (b) Theoretical predictions obtained by integrating the FENE gel network model with imposed γ_0 replaced by the rescaled amplitude $\gamma_{local} = \gamma_0 B_\tau$.

At small oscillation amplitudes, the curves are elliptical. The increase in modulus due to the increase in filler volume fraction is reflected by the anti-clockwise rotation of the ellipses.

We can also compare the Lissajous curves obtained through these experiments to predictions of the FENE network model[5]. Details of the model and its parameters

---

[5] A smaller number of nodes was used in the discrete representation of gel modes to improve the time integration stability: $\lambda_{max} = 5000, K = 20$ compared to $\lambda_{max} = 100000, K = 50$ used in the previous chapter. This simplification leads to slightly reduced stiffening at large strains, but does not affect the general trends/change in shape of the Lissajous figures generated as ϕ is increased.

can be found in the previous chapter. The model is integrated with values of macroscopic strain γ_{macro} replaced by the local strain $\gamma_{local} = \gamma_{macro} B_\tau$, i.e. $\sigma_{filled}(\gamma_{macro}) = \sigma_{gluten}(B_\tau(\phi)\gamma_{macro})$ Since we are plotting stress rather than a modulus, the y-axis does not need to be rescaled.

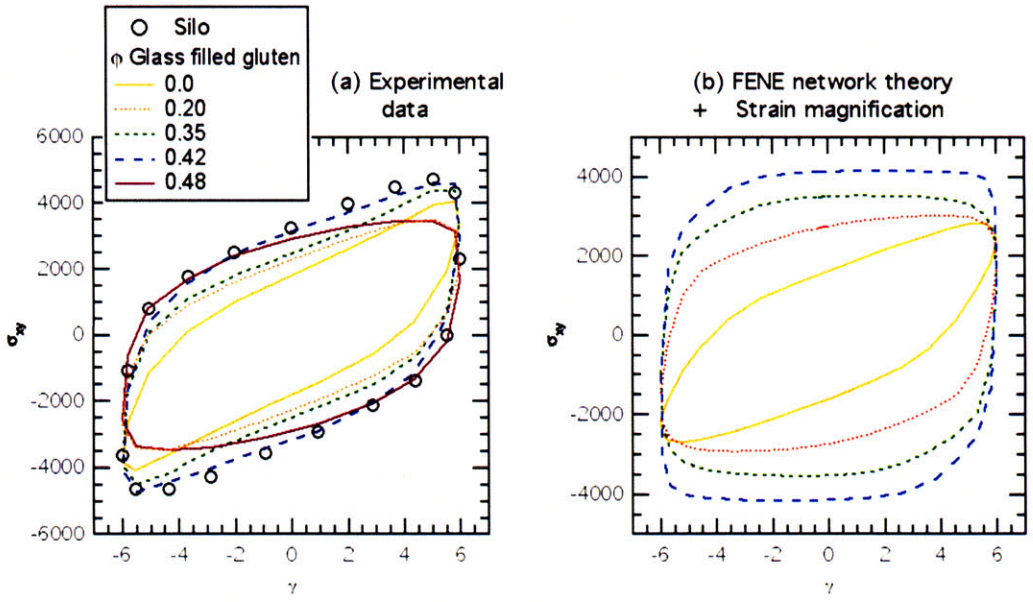

Figure 85 Experimental and computed Lissajous curves at large strain γ_0 = 6.0, ω = 1.0 s^{-1}.

At large strains, the nonlinear features become apparent in both the experimental data and the FENE model. Firstly, the area enclosed within the Lissajous curves is equivalent to the energy dissipated per unit volume of the material (see chapter 6). This area increases for systems with a greater filler volume fraction. For the unfilled system, there is also a significant strain-stiffening at large strain, indicated by the upturn in stress at the extremes of the Lissajous curves. As the filler fraction is increased, the strain stiffening becomes progressively reduced. This reduction is so severe at the highest filler volume fraction that the stresses for $\phi = 0.48$ are lower than $\phi = 0.42$ (the Lissajous curve for $\phi = 0.48$ lies on top of

that recorded for $\phi = 0.42$ in the small strain region. The reduction in stiffening is apparent at large strains, at which the higher volume fraction shows lower stress levels).

These observations can be described quantitatively by considering the physical quantifiers of small and large strain elastic moduli introduced in the previous chapter. G'_M is the tangent modulus at the point of zero strain, while G'_L is the secant modulus defined by the line joining the origin to the stress at maximum strain. Figure 86 and Figure 87 illustrates how these nonlinear moduli can be shifted onto a master curve by considering the effects of strain amplification. The shift factors are plotted in Figure 81. They follow the same trend as those found through shifting the first Fourier coefficient. The Krieger-Dougherty relation provides a reasonable estimate of the values.

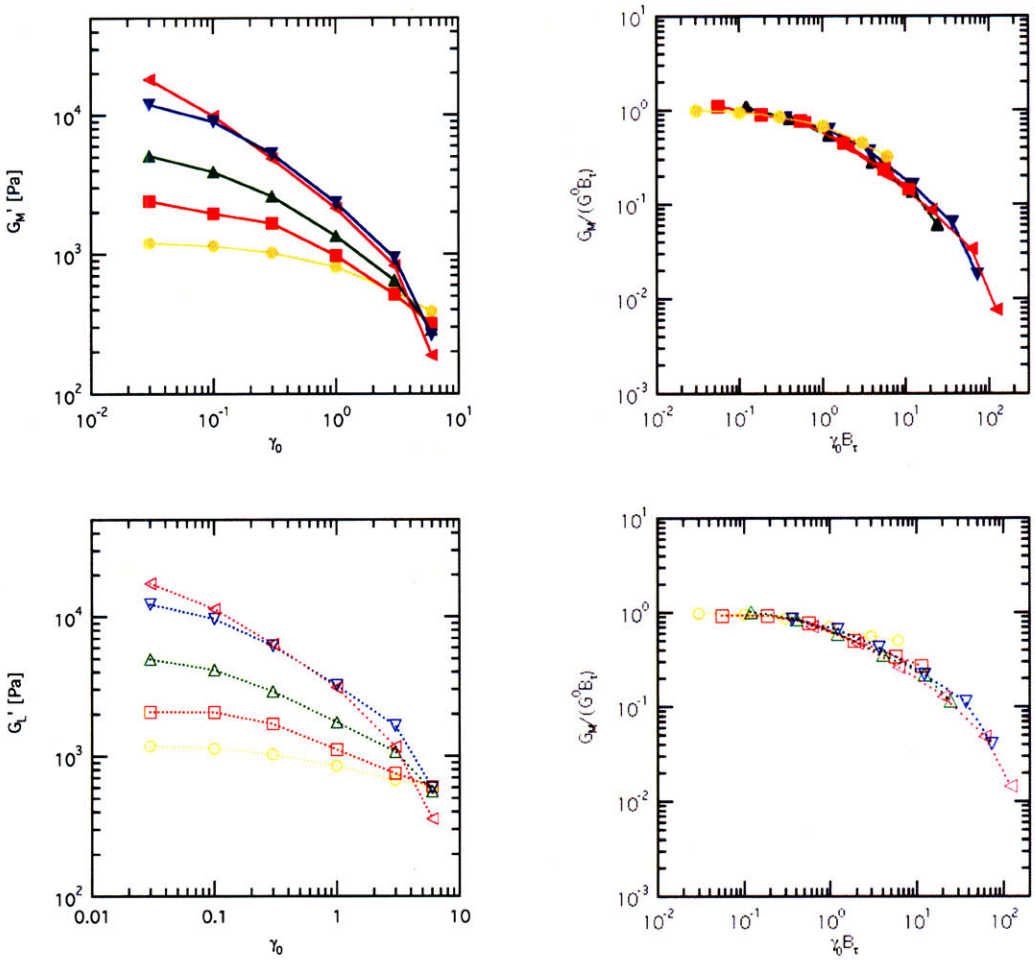

Figure 86 Nonlinear physical quantifiers G'_M and . Both moduli can be shifted onto a master curve by applying the idea of strain amplification equations (7.11) to (7.13).

As we discussed in the previous chapter, the amount of stiffening can be characterized by a ratio between the small and large strain moduli (G_M' and G_L'). We denote the stiffening ratio as S and plot the ratio for each filled system in Figure 87. We note that in Figure 86 the nonlinear moduli themselves can be shifted onto their respective master curves, but S, the ratio of them, when plotted on a linear scale in Figure 87 can show some significant differences when plotted on a linear scale. It is clear from the range of volume fraction presented, that the onset of this stiffening occurs at progressively smaller strains as the volume fraction of the filler is increased.

In Figure 87 (b) we attempt to collapse the data using the Krieger-Dougherty relationship (equation (7.17)). The figure shows that a reasonable level of agreement is achieved for all volume fractions up to an effective or local strain of $\gamma_0 B_\tau \sim 10$. For the lowest filler fraction, the shifted data suggests that it lies on the same master curve as the unfilled gluten for all levels of effective strains investigated. We refer to this curve as the "master stiffening curve" of the gluten gel. It also agrees surprisingly well with the predictions from the FENE network model and can be approximated by an exponential function in effective strain:

$$S \simeq \exp\left(\frac{\gamma_0 B_\tau}{C}\right) \tag{7.18}$$

$C = 2$ is the characteristic effective strain at which nonlinearity in S becomes significant and is related to C_1 and b introduced through the FENE network model. Deviations from this master stiffening curve begin at progressively smaller strains as the volume fraction is increased; the degree of stiffening S at a particular effective strain also decreases. Instead of increasing monotonously, S for the filled systems reaches a maximum and decreases for increasing strain amplitudes thereafter. We recall that this can also be observed in the Lissajous figures in Figure 85: the curve for the highest volume fraction at the largest strain shows dramatically less stiffening compared to curves at lower volume fractions.

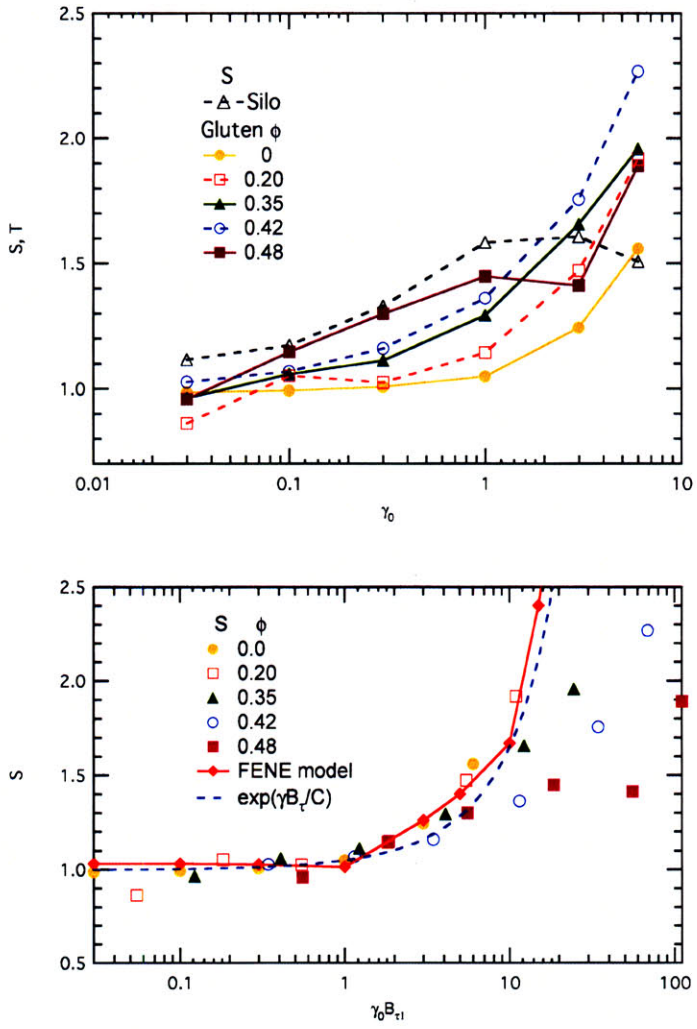

Figure 87 Strain stiffening ratio S. The unfilled gluten gel shows a clear region ($\gamma_0 < 1$) for which the stiffening ratio is close to unity. Strain amplitude greater than $\gamma_0 > 1$ shows stiffening ($S > 1$). Increasing filler volume fraction clearly decreases the strain amplitude that this nonlinear stiffening occurs at. All curves can be shifted onto the master curve of unfilled pure gluten gel up to small effective/local strains ($\gamma_0 B_\tau < 10$). The behavior of high filler volume fractions deviate from the master curve at large strains ($\gamma_0 B_\tau > 10$).

The deviation from the master stiffening curve is probably due to the fact that significant tensile stresses have built up around the surface of the glass beads along the principle axes of the deformation and the gluten gels begins to detach

from the glass beads at these large strains. Parsons [208] suggested a method to account for this debonding. He calculated the level of tensile stress normal to the filler particle surface by considering only the secant modulus of the matrix. Debonding was assumed to occur if the level of this stress rises above a critical value S_0. Experimentally they found that the debonding takes place over a range of macroscopic stresses/strains and a cumulative fraction of debonded particles can be specified by a Weibull distribution as a function of the maximum principal stress in the particles:

$$c_d = 1 - \exp\left[-\left(\frac{\hat{\sigma}_{\max}}{S_0}\right)^{m_0}\right] \tag{7.19}$$

where c_d is the fraction of debonded particles, $\hat{\sigma}_{\max}$ is the maximum principal stress, and m_0 is a constant that describes the distribution of stresses over which debonding occurs.

Applying this idea to our framework, we assume that once the filler has debonded, it has no further effect in strain amplification. The fraction of remaining active filler is thus:

$$\phi_a = \phi c_d = \phi \exp\left[-\left(\frac{\hat{\sigma}_{\max}}{S_0}\right)^{m_0}\right] \tag{7.20}$$

and the strain amplification factor should then be only a function of this active filler volume fraction, i.e.(2.1):

$$B_\tau = B_\tau(\phi_a) \tag{7.21}$$

Using this modified strain amplification factor in the FENE network model integration will be able to reconcile some of the differences between the predicted behavior and the actual measured data in Figure 92. We expect the reduction of effective strain amplification at high stress levels of the highly filled systems ($\phi > 0.35$) will reduce the energy dissipated since fewer modes are

extended beyond the finite extensibility limit and the Lissajous curves will be more similar in shape to the unfilled gluten gel.

We also expect the values of S_0 and m_0 to be a function of dough conditions and can be experimentally increased by the method described by Edwards et al (i.e. coating with BSA) or reduced by a coating of fluorinated (teflon-like) chlorosilane molecules which are extremely hydrophobic and will not bond well with the hydrophilic/hydrogen bonds of the gluten matrix. We shall see in the next chapter that they are also a function of flour-type and water content, i.e. debonding (maximum in stiffening ratio S) occurs at different stress/strain levels for different flour types and water content.

Before moving on, we also note the similarities between the flour-water-dough system and the glass filled systems at high volume fractions $\phi \sim 0.42 - 0.48$ in Figure 84 and Figure 85. The Lissajous figures of these two systems are almost identical, with similar values of small strain modulus, energy dissipation, intermediate softening (clockwise rotation of curves when the strain is increased), and large strain stiffening (shape distortion of Lissajous curves). Furthermore, the gluten gel filled to $\phi = 0.48$ also show the maximum in stiffening ratio S exhibited by the flour-water dough i.e. filler-matrix debonding.

Transient start-up of steady shear

In addition to large amplitude oscillations, we also show that the framework of strain amplification can be used to interpret data collected during the transient start up of steady simple shear flow. Equation (7.16) is applied equivalently to the data presented in Figure 88 (a) by once again considering the relationship between local and macroscopic strain [209]:

$$\dot{\gamma}_{local} t = \dot{\gamma}_{macro} t B_\tau \tag{7.22}$$

and thus the data can be collapsed by multiplying the elapsed time by the shift factor :

$$t_{shifted} = t B_\tau \tag{7.23}$$

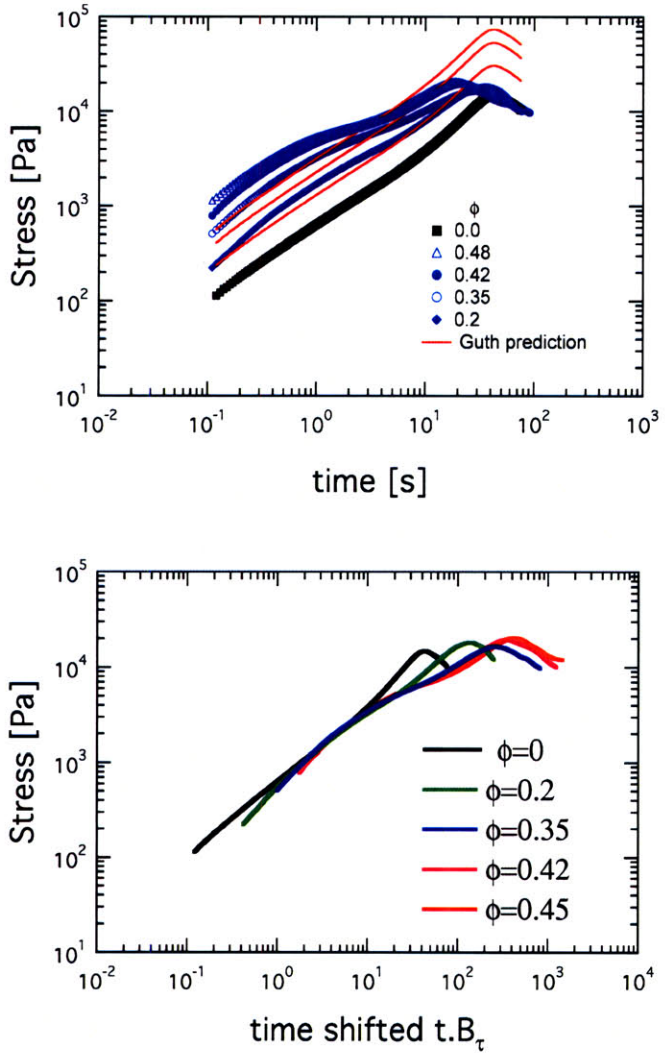

Figure 88 Transient start-up of steady shear of filled gluten gels at $\dot{\gamma}_0 = 0.3\ s^{-1}$. (a) Transient growth of shear stress. (b) Transient growth of shear stress reduced by application of strain amplification.

The shifted data is replotted on Figure 88 (b). The experiments performed on the different volume fractions show a similar initial powerlaw increase ~ t^{1-n}. But they begin to deviate from one another at increasing strains, with the samples with higher volume fractions deviating at progressively lower strains. Once again, we find the shift factors to be consistent with those collected through the

various measures in oscillation experiments. The large strain deviations are consistently lower than the simply shifted curves. These deviations are consistent with the idea of matrix debonding: the release from the no-slip restriction at the particle-matrix interface reduces the effect of strain amplification, therefore the actual local strain will be at a lower level compared to the case of no debonding.; the corresponding stress will thus be lower.

7.4. Conclusions

The similarity between the flour-water dough and the highly filled gluten gels are certainly encouraging. A large part of this thesis was spent discussing model systems and idealization in order to reduce the complexity of flour-water dough to a level that can be understood on a structural component basis. In some sense, it feels that we have rounded a corner; through this series of experiments and modeling, we have taken another step towards more realistic formulations. We have once again built upon the critical gel and the FENE network model. On these ideas, we have added another layer of complexity in the form of "strain amplification" which allow us to extend the existing theories for continuum viscoelasticity to filled systems that more closely approximate the starch filled systems of dough. In many senses, we feel that we have captured a large part of the key rheological features exhibited by wheat flour dough through these model systems.

Spherical, inert, glass beads were selected as a replacement for starch granules due to the strong time-dependent swelling effects of the latter. Now that we have outlined the rheological properties of the gluten gels filled with glass beads, we will be able to separate the effects caused simply by the presence of inert particles from other chemical, colloidal or time dependent interactions that the starch might have with the gluten [94]. In the final chapter, we will further discuss how these various levels of idealization can help us further understand the mechanical properties and perhaps predict the baking qualities of a real dough system. For example, we can start explaining some of the rheological features recorded in the earlier chapters of the thesis: What happens when we increase the water content of a dough? Does the extra water get absorbed into the

starch granules, causing it to swell and effectively increase the filler volume fraction? Or does it cause the gluten gel that forms the matrix to swell more thus decreasing the filler volume fraction instead? These are all interesting questions that we are now in a position to investigate.

8. Conclusion

Since bread is such a large part of the world's diet, it's been a popular research topic since the 1930s. Despite this long history, the complexity of bread baking and the difficulty of working with gooey dough and its unstable nature has limited research. In the literature review, we summarized the important works conducted in the field. The roots of the subject are traced to the seminal work of Schofield and Scott Blair in the 1930s [10-13]. They outlined the importance of good experimental technique, strongly nonlinear and time dependent nature of dough, and the basis of the gluten network. A large portion of the subsequent was performed on wheat flour dough of different formulations. Researchers varied each component (water content, flour type, deformation conditions etc...) individually and measured the subsequent change in rheology.

In the first part of this thesis, we followed this line of investigation, and tested a range of wheat flour dough over a range of conditions. But before attempting to measure the rheological properties of a dough, we must first identify the appropriate techniques and protocols, a brief survey on some of the existing techniques are given in Chapter 3. Standard shear rheometry protocols are similar to those employed by polymer scientist and can be performed on most rheometers, but the handling and preparation can vary from lab to lab. Most published results will include some method to prevent drying. A solvent trap is insufficient, and a thin film (or bath) of paraffin or silicone oil is usually used as a barrier to evaporation.

To these standard techniques, we added filament stretching (FISER), wind-up drum rheometry (SER) and Large Amplitude Oscillatory Shear (LAOS). We provide a detail record of the required corrections and procedures to give good reproducible results.

With these techniques, we go on to show how the critical gel model can be used as an appropriate description of the dough under linear viscoelastic deformation ($\gamma < 10^{-3}$). We extended the result to larger deformations by using a Lodge-rubber-like liquid formulation and the inclusion of a nonlinear damping function

and arrived at the generalized gel equation. We showed that this equation is able to describe the rheological behavior of dough with good accuracy with a minimal number of parameters (i.e. Linear viscoelastic gel strength S and gel index n, damping factors q and k). This is a huge improvement compared to more complex formulations such as the Phan-Thien model that requires more than 20 parameters.

Having set down a suitable mathematical description of the dough, we next investigate and tabulate how each of these gel and damping parameters vary with different dough conditions (i.e. mixing time, water content, flour type etc...).

Of course there already exists a vast amount of work published on the rheology of wheat flour dough, but unfortunately there are an even larger number of variations possible. Wheat flours from the same farm grown in different years can have different rheological properties [210]. While obvious factors such as water content, mixing time and additives can all have dramatic influence on the final property of the dough. Thus work along this line without some deeper understanding of the physical origins of these variations can really only be considered as case studies. It is extremely easy to lose oneself in this mountain of literature without ever gaining an overall picture of the behavior of the system.

To rectify this, we follow another line of investigation and consider the origins of these properties in the second part of the thesis. It is believed that these properties primarily arise from the protein content of the flour; and within the protein contents, the large molecular weight non-soluble proteins known as gluten are the prime suspects. Armed with this belief and with encouragement from Professor Windhab from ETH, we began to pursue the rheological properties of a simplified system, namely, gluten gel. Effectively, we are moving down in length scale and simplifying the problem by considering the microstructure and rheology of the gluten phase only.

The critical gel model discussed in the context of dough rheology has an unusual powerlaw like relaxation that is significantly different to the conventional exponential relaxation predicted by simple models. The origin of this unusual

behavior lies in the multiple length scale present in the gluten fraction of the dough.

The first order of business is to identify an appropriate physical model for this gluten phase that can explain the unusual rheology of dough and gluten. In the literature survey, we presented a number of candidate models that have been put forth to describe the microstructure of gluten, but there are none that also show conclusive rheological evidence that supports the proposed molecular picture. Hence we performed some detailed investigation on the linear and non-linear rheometric behavior of our gluten gels to show that in terms of mechanical proeprties, it should be best described as a viscoelastic polymeric network: material functions show a powerlaw regime that arise from the fractal nature of the network, and a Rouse regime that reflects the segmental building blocks of the network. The rheological behavior is incompatible with the particulate gel (significant elasticity and extensibility) or reptation models (weak damping function). We also show (through chemical decomposition and reconstitution) this network to be held together at junction points by hydrogen bonds and/or hydrophobic interactions.

With this picture in mind, we explored in greater detail the linear to nonlinear rheology of the gluten gel through the use of LAOS. We proposed a constitutive model that models the nonlinear rate of detachment of junction point under strain and the effect of finite extensibility of the network.

The predictions of this network was compared to experimental data obtained in small to large amplitude oscillatory shear and were found to be consistent both qualitatively and quantitatively.

Model	Linear behavior	Nonlinear softening	Nonlinear stiffening	Transient	Physical Interpretation	# of parameters
U.C.M.	2	0	2	0	2	2 per mode
Weak gel	8	0	0	0	7	2
Pom-Pom	3	3	5	3	5	4 per mode
Reptation	5	3	3	N/A	2	2 per mode
Phan-Thien	10	6	8	0	4	20+
Damage functions	8	7	3	5	7	4
FENE network	8	8	8	9	9	4

Table 6 A survey of some proposed constitutive models for gluten/bread dough. A subjective score (out of 10) are given for each category.

In Table 6, we show that this constitutive model has two outstanding features that ranks it above other models that have been proposed. Firstly, each component of the model can be attached to its physical origins. Secondly it is able to describe the linear to nonlinear features with only four parameters (i.e. two linear viscoelastic parameters gel strength S and gel index n, and two nonlinear parameters C_1 that describes the intermediate softening and b the finite extensibility parameter).

At this point, we have grasped the basics of gluten gel rheology: we have come to understand the physical origins of the rheological features and have successfully modeled the behavior quantitatively these behavior. Encouraged by this, we felt ready to reintroduce the next layer of complexity and explored a dough at a length scale/idealization in which the composite nature of the dough is apparent, i.e. we explored the effect of the starch filler. Unfortunately, the

presence of wheat starch gives rise to all sorts of nonlinear time dependent effects which are difficult to independently investigate.

As a first order approximation, we isolate the possible roles of the starch filler, and consider them as inert fillers. We modeled this idealized dough by mixing the gluten gel with various volume fraction of spherical glass beads that are of similar size and distribution to starch granules. In doing this we show that it is possible to "synthesize" a dough that closely approximates one that is mixed from a real flour.

We also show how the idea that the dominant contribution to the rheology of the starch phase is through the strain amplification effect of an inert filler. That is not to say the other properties of the starch phase such as surface conditions etc are not important. But rather, the most prominent features exhibited in the rheological measurements can be understood through this model. Considering the deviations from this idealization can then highlight other properties that are relevant.

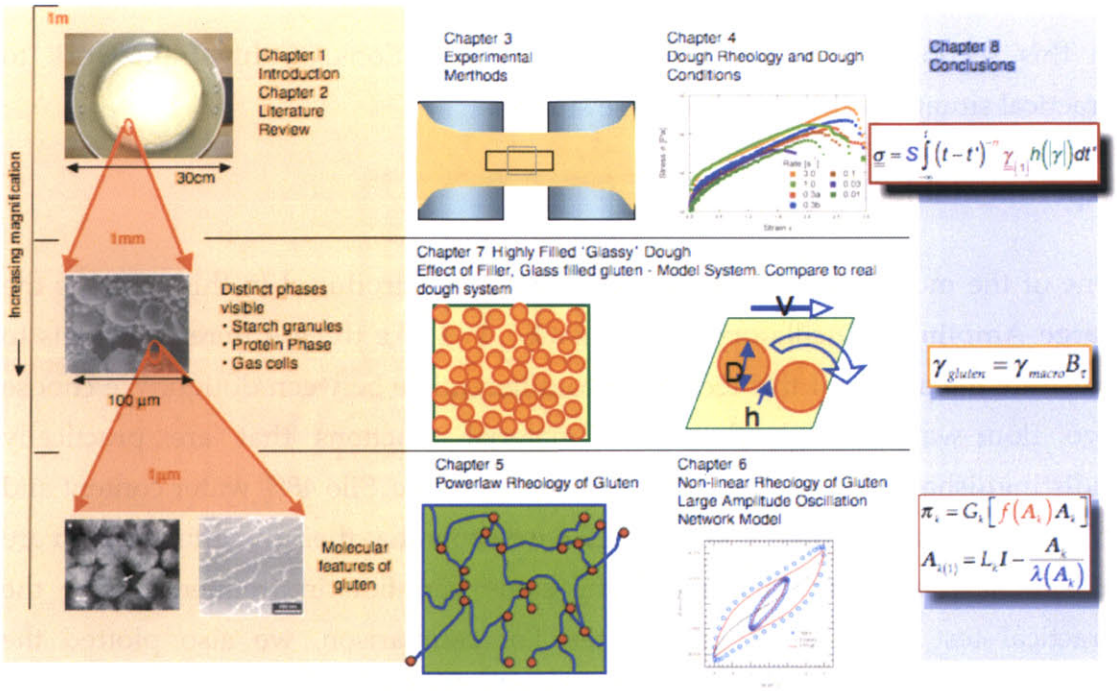

Figure 89 Summary of thesis

We summarize the work presented in this thesis in Figure 89. Spatially, the left most column represents the length-scales present in dough. And each row represents the conceptual abstraction, experimental tests and modeling performed at each level, and is finally condensed in the last column as a mathematical equation.

In terms of this outline, most of the work in the literature review concerns the topmost row, representing data done with a wide variety of dough, but nonetheless dough without much consideration for the microstructure. While there also exists some work that proposes candidate microstructure but without much consideration of the rheological behavior. Our work is intended to fill up the large space in between these two lines of investigation in order to gain a more complete picture of the whole system.

8.1. Applications

In this section, we briefly outline some applications of this framework to practical situations in a couple of case studies.

Experimental technique

One of the most useful experimental techniques introduced in this thesis is the Large Amplitude Oscillatory Shear (LAOS). We take three different systems to illustrate the ability of this technique to differentiate between dough. We choose two flour-water dough that have material functions that are practically indistinguishable in the linear viscoelastic regime (i.e. Silo 48% water content and WWF3 44% water content). In Figure 90, we show that their dynamic moduli are of similar magnitudes and show the same variation in frequency over the practical test range of the rheometer. For comparison, we also plotted the dynamic moduli of an unfilled gluten gel (63% water content). Flour-water dough are typically stiffer than gluten gels due to the effect of strain amplification of the starch filler (chapter 7).

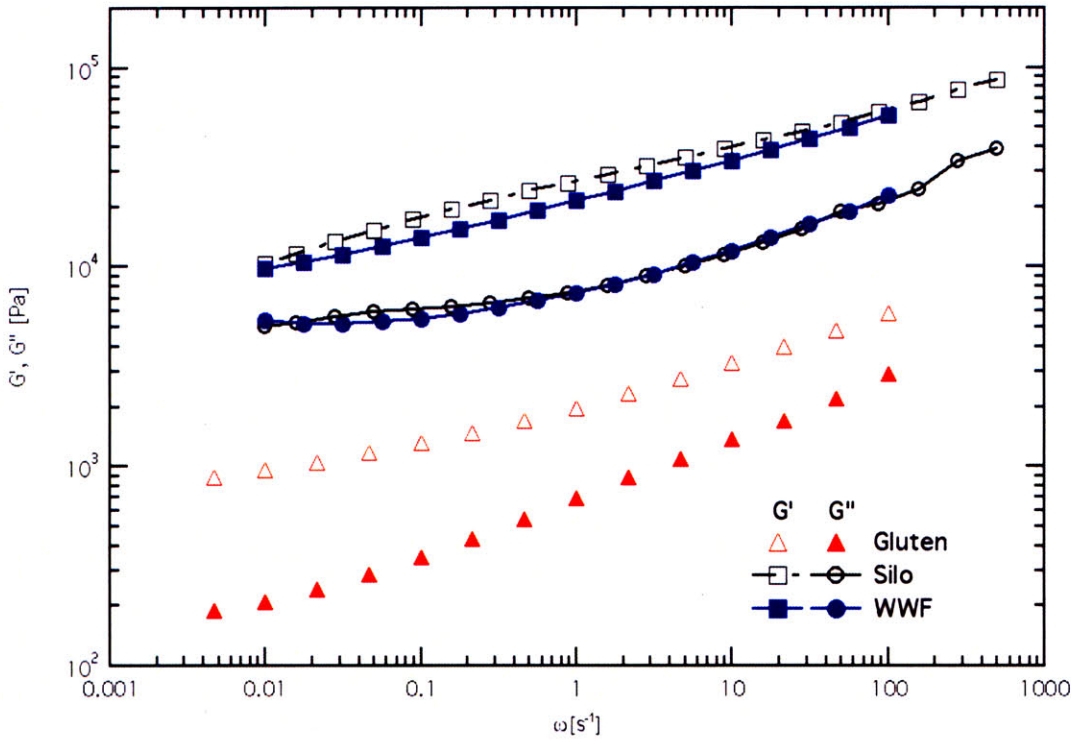

Figure 90 Dynamic moduli of two different flour-water dough and a gluten-water gel. The material functions of these two flour-water dough are practically indistinguishable in linear viscoelastic experiments. Typically, unfilled gluten gels are much softer in the linear viscoelastic regime.

A closer look at the Lissajous figure plotted in Figure 91 collected at ω =1.0 s^{-1} yields the same observations. All the curves are elliptical in shape indicating they are within (or very close to) the linear viscoelastic range. The two flour-water dough show similar moduli (slope of the major axis) and similar elliptical shapes.

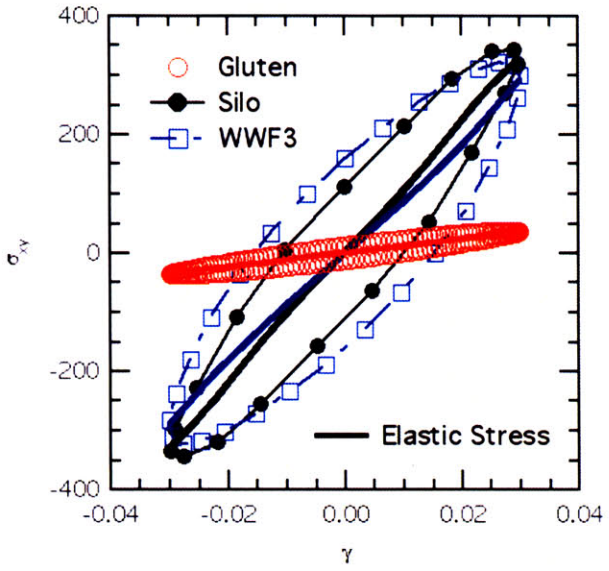

Figure 91 Lissajous figure of three different dough system at ω =1.0 s^{-1} and $\gamma = 0.03$. All curves are approximately elliptical indicating that they are taken within the linear viscoelastic range.

However, if we allow the amplitude of the oscillation to increase, the differences between these systems can be extracted. Like the unfilled gluten gels described in chapter 6, both flour-water dough show intermediate strain softening (rotation of major axis of Lissajour curves) and local stiffening (upturn distortion from the initial elliptical curve shape). However, these effects occur at much smaller strains when compared to the gluten gel. This is once again expected: flour-water dough should be considered as highly filled systems and the effect of strain amplification is strong (chapter 7). The two flours can be qualitatively distinguished by the fact that Silo shows a stronger strain stiffening character at large strains when compared to WWF3. At $\gamma_0 = 6$, the strain stiffening is almost imperceptible in WWF3, and the Lissajous figure resembles that of a yield stress material (abrupt decrease of stress at strain extremes, rectangular shape of Lissajous figure).

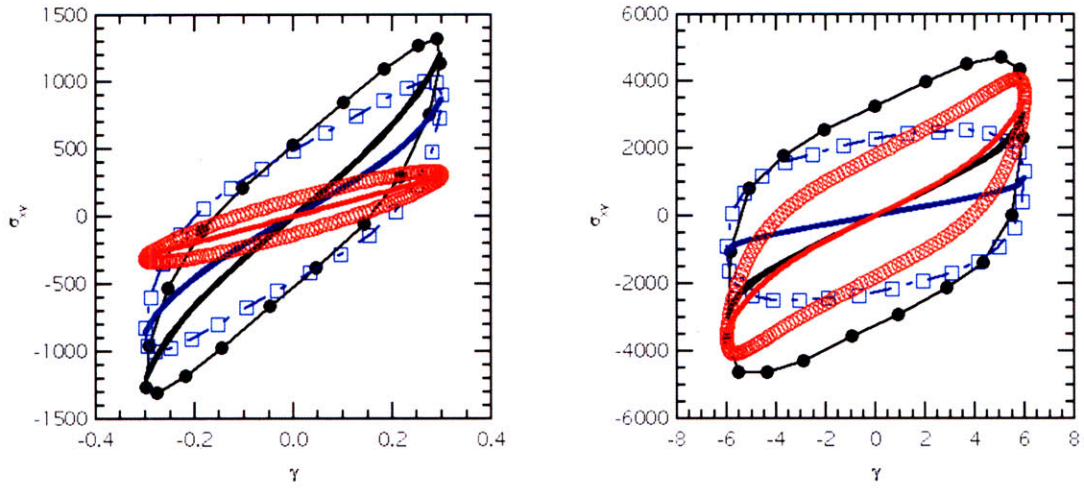

Figure 92 Medium and large amplitude oscillatory experiments performed on three different dough systems. Flour-water dough exhibit the same the softening and local stiffening observed in the unfilled gluten gel (Chapter 6) at relatively small strains. The Silo exhibits a strong degree of stiffening while WWF3 exhibited an strong shear thinning/yield stress-like behavior at large strains.

We can quantitatively represent these differences by plotting the different nonlinear measures introduced in chapter 6. These are shown in Figure 93 (a) – (c). Both the (a) conventional dynamic moduli (first order Fourier coefficient expansion of the Lissajous figures) and (b) small-large strain moduli alone does not show any conclusive differences between the flour-water dough: both dough show a similar softening behavior. However, the stiffening ratio (defined as the ratio between large and small strain moduli) is most able to clearly illustrate the differences in behavior. Both show a departure from linear behavior at small strains ($S > 1$ at $\gamma \sim 0.05$) indicating a high filler volume fraction ($\phi \sim 0.42$ in chapter 7). But the WWF3 reached a maximum in stiffening ratio S at a smaller strain ($\gamma \sim 1.0$) compared to SILO ($\gamma \sim 2.5$). This agrees with our earlier observation that WWF3 shows less stiffening qualities at large strains.

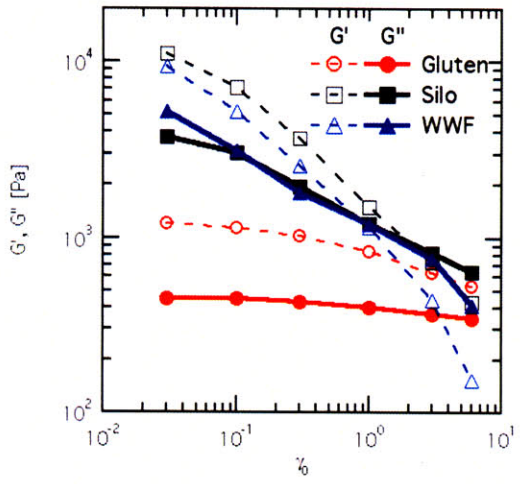

a.

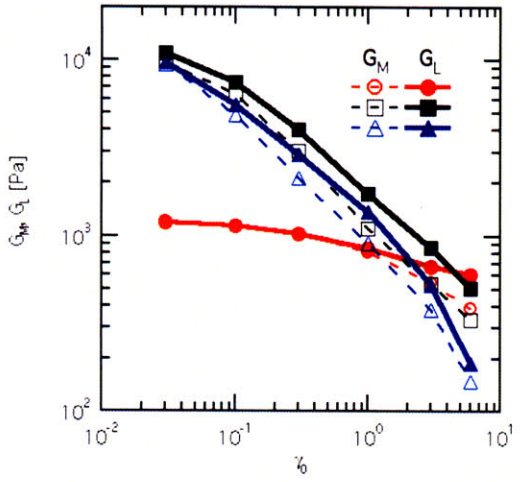

b.

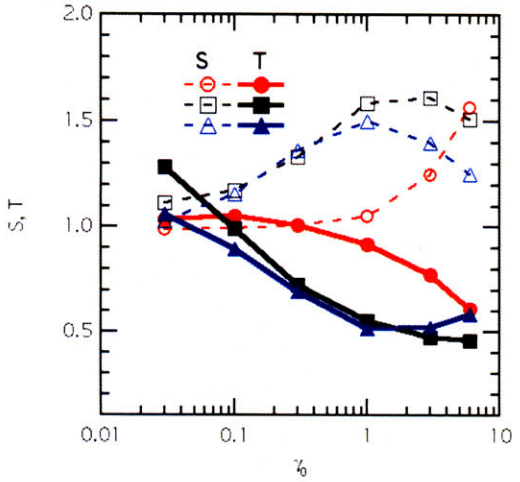

c.

Figure 93 Using physical quantifiers to describe and distinguish between doughs.

(a) Conventional dynamic moduli. This is equivalent to the first order in-phase (G′) and out-of-phase (G″) coefficient of the Fourier expansion of the Lissajous figures. A comparison using this measure does not show significant differences between the two flour-water dough.

(c) shows the ratio between the small and large strain moduli plotted in (b). The difference in stiffening behavior is most clearly illustrated through this measure. The stiffening behavior of WWF3 is much weaker at large strains.

Through this example, we have showed how the methodology of LAOS can be used to distinguish between two flour-water doughs. We demonstrated that both flours have a similar filler volume fraction but different stiffening behavior at large strains. The physical reason behind this difference is unclear. As hinted in the previous chapter, we suspect the maximum in stiffening ratio corresponds to the point when the large stresses built up at the interface between filler and medium causes one to debond from the other and it is our belief that understanding the surface properties and behavior of this interface to be the next important step towards understanding the rheology of flour-water dough.

Water content revisited

In chapter 4, we discussed the change in rheology when the water content of a dough is varied. In linear viscoelasticity, we noted the gel strength decreases with increasing water content. On the other hand, from our gluten mixing experiments in chapter 5, we find that gluten admits only a small range of water content. So even though increasing the water content of gluten can lead to a decrease in the modulus, the effect is some what limited. This implies that the additional water is possibly taken up by the starch. If we naively assume the starch to swell due to this additional water, we should expect exhibit an increase in gel strength due to the increase in filler volume fraction. This of course, is contrary to our observations, and the resulting change is more complex and will be affected by the decrease in stiffness of the starch particles. Another possibility is that the excess water exists as a separate phase. We will briefly discuss how the technique of LAOS can help us understand these effects.

We first consider the change in storage moduli as a function of strain for doughs of different water content. The experimental data is plotted in Figure 94. Even though the magnitude of the moduli decreases dramatically with increasing water content, the general shapes of the curves on a log-log plot are similar. In other words, the softening behavior seems to be independent of the water content.

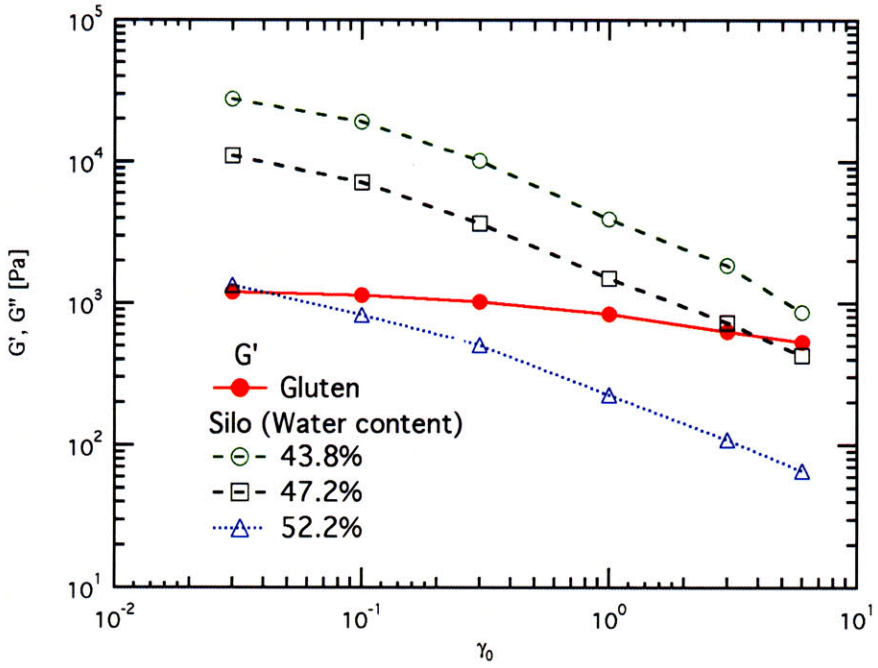

Figure 94 Storage moduli vs strain for a Silo flour dough mixed to different levels of water content. Water content moduli thingy appears to be valid.

However, water content does have an effect on the degree of large strain stiffening. This idea is illustrated in Figure 95. The curve for stiffening ratio of the flour-water dough at the highest water content (52.2%) shows a slightly more rapid increase with strain. Using the idea of strain amplification discussed in chapter 7, we expect higher volume fractions to show a more rapid increase in stiffening ratio, and can therefore conclude that the hypothesis of starch swelling leading to a slight increase in volume fraction is indeed consistent. This is effect, is rather mild, the change in volume fraction (estimated by comparing to the experiments with glass beads gluten gel) is only about 3% (42 to 45%).

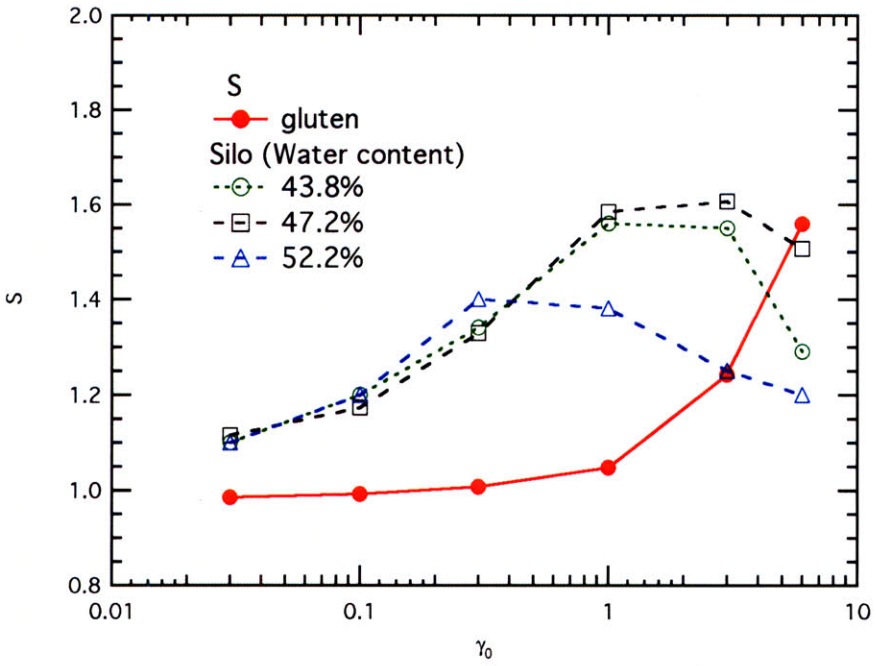

Figure 95 Change in stiffening ratio S for different water content. Dough at highest water content show a more rapid increase in stiffening ratio at small strain amplitudes. Though the strain at which maximum in the stiffening ratio occurs is not monotonous with water content.

Furthermore, there is also a change in the large strain amplitude behavior. From the baseline case of 47.2% water content, the maximum of S occurs at a lower strain for both increasing and decreasing water content. This change can be likely attributed to a modification to the surface properties. An investigation on the details of this phenomenon can be the basis of a possible future work.

8.2. *Future work and recommendations*

Through these two examples, we briefly illustrated how some of the ideas presented in this thesis, can be used in practical situations. However, there remains a lot to be learnt about the mechanical properties of dough. We outline two areas which we feel are the natural steps to take next.

Starch properties

In chapter 7, we studied a simplified system in which the filler material is assumed to be indeformable. We also modeled the system by assuming a no-slip

boundary condition at the surface of the filler. This we showed to be a reasonable approximation and a large part of the rheology of a flour-water dough can be understood by considering such an idealized situation. On the other hand, the water content experiments mentioned in the previous section and chapter 4 suggests that the truth is rather more complex than this idealized system, and the properties of the starch granules probably have an important role especially at large strains.

Specifically, we showed that the strength of the bond between matrix and filler can be an important factor especially at large strains. The large stresses generated at these strains can lead to detachment between the matrix and filler. A possible way to account for the effect of detachment is an analysis along the lines of void formations can provide the link between these apparent differences [211]. This along with the effect of filler stiffness will form an interesting line of investigation.

Mixing revisited

At its simplest, dough is formed by simply mixing flour and water. Mechanical energy is supplied to disperse the ingredients and develop the gluten structure through stretching and folding. A method that estimates the relevant rheological parameters during this mixing process is of great practical utility. One can imagine a production line in which ingredient ratios and mixing intensity can be varied "on the fly" in order to achieve a required dough consistency.

The most common method of doing this is already described in chapter 3. The long time variation (averaged over 1mins) is usually reported as the mixing characteristic of a particular dough [27]. In a separate document [129], we have discussed how this pseudo-material function only describes the intermediate strain behavior of a dough and can give misleading information regarding the full constitutive behavior.

The mixing process can be considered as a form of oscillatory deformation and we suggested in chapter 6 that more detailed information on the rheological properties can be extracted from the torque signal by considering its Fourier spectrum.

In a separate document [212], we proposed an alternative non-dimensional measure that considers the ratio between the rapidly varying component and this slowly varying component. We refer to this measure as the mixing number:

$$Mn = \frac{\text{Rapidly varying component}}{\text{Slowly varying component}} \tag{9.1}$$

In Figure 96, we show that this measure showed some universal correlation with the rheological properties (characterized by c, a stiffening index obtained by fitting curves of extensional stress difference vs strain by $\Delta\sigma^{+}_{Ext} = H + G\varepsilon^{c}$) of different doughs in the overmixed regime when viscous effects are significant.

A line of investigation that seeks to understand the relation between these different pseudo material functions measured from mixing will be of invaluable use to the bread-making industry. To start with, we suggest using the more robust material functions proposed in this thesis such as the stiffening ratio S and b the finite extensibility parameter to establish more definite correlations with the mixing functions.

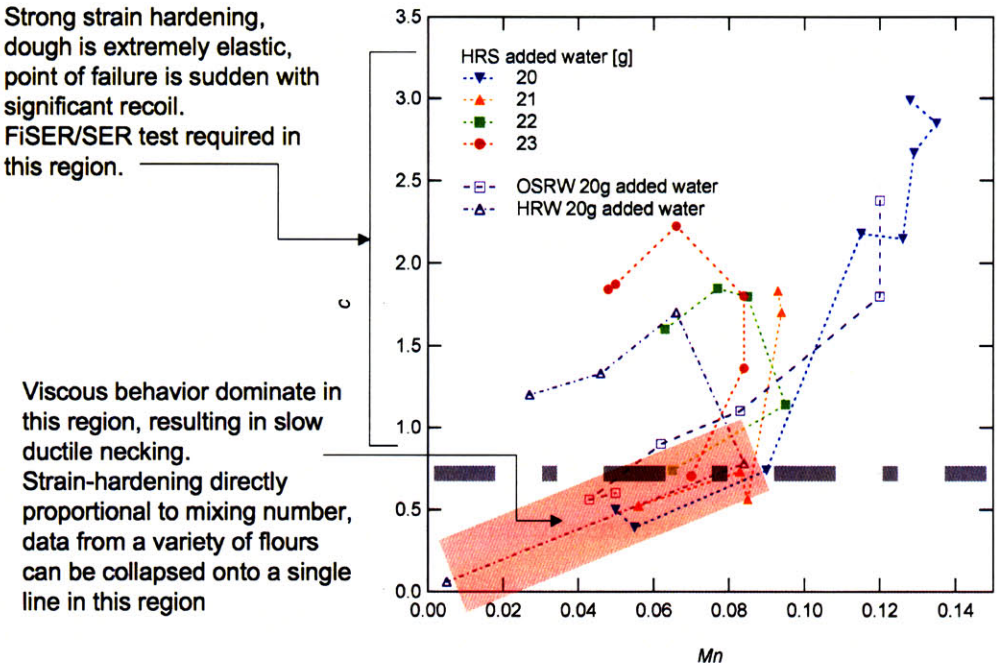

Figure 96 Mixing number vs strain stiffening index of a range of dough.

8.3. *Final words*

In this thesis, we presented a comprehensive treatment of the rheological properties of dough. The aim is to provide a conceptually clear basis from which to launch analysis and to facilitate the understanding of specific case studies often encountered in this field.

The most striking idea we hope to leave the reader with is the strong analogy between the starch-filled-gluten-dough systems with carbon-black filled rubber networks. In fact, throughout the thesis, we have borrowed heavily from the ideas established in polymer science and applied them to this unusual food system. In doing so, we arrived at a scientific framework for studying dough and

its constituents. We hope to have convinced the reader that this rheological approach to understanding dough rheology is useful and appropriate.

9. Bibliography

1. Faubion, J. and H. Faridi, Dough rheology and baked product texture. 1990, New York: Van Nostrand Reinhold.

2. Aitken, T.R. and W.F. Geddes, Relation between protein content and strength of gluten enriched flours. Cereal Chemistry, 1939. 16: p. 223-231.

3. Bailey, C.H., Relation of the composition of flour to baking quality. Can. Miller and Cerealist, 1913. 15: p. 181-196.

4. Dobraszczyk, B.J. and M.P. Morgenstern, Rheology and the breadmaking process. Journal of Cereal Science, 2003. 38(3): p. 229-245.

5. Sliwinski, E.L., P. Kolster, A. Prins, and T. van Vliet, On the relationship between gluten protein composition of wheat flours and large-deformation properties of their doughs. Journal of Cereal Science, 2004. 39(2): p. 247-264.

6. Bloksma, A.H., Rheology of the Breadmaking Process. Cereal Food World, 1990. 35(2).

7. Dobraszczyk, B.J. and C.A. Roberts, Strain-Hardening and Dough Gas Cell-Wall Failure in Biaxial Extension. Journal of Cereal Science, 1994. 20(3): p. 265-274.

8. Ewart, J.A.D., Hypothesis for how linear glutenin holds gas in dough. Food Chemistry, 1989. 32(2): p. 135-150.

9. van Vliet, T., A.M. Janssen, A.H. Bloksma, and P. Walstra, Strain hardening of doughs as a requirement for gas retention. Journal of Texture Studies, 1992. 23: p. 439-460.

10. Schofield, R.K. and G.W. Scott Blair, The Relationship between Viscosity, Elasticity and Plastic Strength of Soft Materials as Illustrated by Some Mechanical Properties of Flour Doughs, I. Proceedings of the Royal Society of London. Series A, Containing Papers of a Mathematical and Physical Character, 1932. 138(836): p. 707-718.

11. Schofield, R.K. and G.W. Scott Blair, The Relationship between Viscosity, Elasticity and Plastic Strength of a Soft Material as Illustrated by Some Mechanical Properties of Flour Dough. ii. Proceedings of the Royal Society of London. Series A, Containing Papers of a Mathematical and Physical Character, 1933. 139(839): p. 557-566.

12. Schofield, R.K. and G.W. Scott Blair, The Relationship between Viscosity, Elasticity and Plastic Strength of a Soft Material as Illustrated by Some Mechanical Properties of Flour Dough. III. Proceedings of the Royal Society of London. Series A, Containing Papers of a Mathematical and Physical Character, 1933. 141(843): p. 72-85.

13. Schofield, R.K. and G.W. Scott Blair, The Relationship between Viscosity, Elasticity and Plastic Strength of a Soft Material as Illustrated by Some Mechanical Properties of Flour Dough. IV. The Separate Contributions of Gluten and Starch. Proceedings of the Royal Society of London. Series A, Mathematical and Physical Sciences, 1937. 160(900): p. 87-94.

14. Hibberd, G.E., Dynamic viscoelastic behaviour of wheat flour doughs. Part III: The influence of starch granules. Rheol. Acta, 1970. 9: p. 501-505.

15. Hibberd, G.E., Dynamic viscoelastic behaviour of wheat flour doughs. Part II effects of water content on the linear region. Rheol. Acta, 1970. 9: p. 497-500.

16. Hibberd, G.E. and N.S. Parker, Dynamic Viscoelastic Behavior Of Wheat-Flour Doughs.4. Nonlinear Behavior. Rheologica Acta, 1975. 14(2): p. 151-157.

17. Hibberd, G.E. and W.J. Wallace, Dynamic Viscoelastic Behaviour of Wheat Flour Doughs. Part I. Linear aspects. Rheol. Acta, 1966. 5(3): p. 193-198.

18. Safari-Ardi, M. and N. Phan-Thien, Stress relaxation and oscillatory tests to distinguish between doughs prepared from wheat flours of different varietal origin. Cereal Chemistry, 1998. 75(1): p. 80-84.

19. Smith, J.R., T.L. Smith, and N.W. Tschoegl, Rheological properties of wheat flour doughs III. Dynamic shear modulus and its dependence on

amplitude, frequency, and dough composition. Rheologica Acta, 1970. 9(2): p. 239-252.

20. Smith, T.L. and Tschoegl N. W., Rheological properties of wheat flour doughs IV. Creep and creep recovery in simple tension. Rheologica Acta, 1970. 9(3): p. 339-344.

21. Tschoegl, N.W., J.A. Rinde, and T.L. Smith, Rheological Properties of Wheat Flour Doughs I. Method for determining the large deformation and rupture properties in simple tension. J. Sci. Fd Agric, 1970. 21: p. 65-70.

22. Tschoegl, N.W., J.A. Rinde, and T.L. Smith, Rheological properties of wheat flour doughs II. Dependence of large deformation and rupture properties in simple tension on time, temperature, and water absorption. Rheol. Acta, 1970. 9: p. 223-238.

23. Becarri, J.B., De Frumento. De Bononiensi Scientarium et Artium. De Bononiensi Scientarium et Artium. Instituto atque Academia Commentarii. Bologna, 1745. 2: p. 122-127.

24. Barnes, H.A., Shear-Thickening ("Dilatancy") in Suspensions od Nonaggregating Solid Particles Dispersed in Newtonian Liquids. Journal of Rheology, 1989. 33(2): p. 329-366.

25. Stickel, J.J. and R.L. Powell, Fluid Mechanics and Rheology of Dense Suspensions. Annual Review of Fluid Mechanics, 2005. 37: p. 129-149.

26. Sasaki, T. and J. Matsuki, Effect of Wheat Starch Structure on Swelling Power. Cereal Chemistry, 1998. 75(4): p. 525-529.

27. Bloksma, A.H., Dough Structure, Dough Rheology and Baking Quality. Cereal Foods World, 1990. 35(2): p. 237-244.

28. Eliasson, A.-C. and K. Larsson, Cereals in Breadmaking. A molecular colloidal approach. 1993, New York: Marcel Dekker.

29. Martinez-Anaya, M.A. and T. Jiménez, Functionality of enzymes that hydolyse starch and non-starch polysaccharide in breadmaking. Zeitschrift fur Lebensmittel-Untersuchung und -Forschung, 1997. 205: p. 209-214.

30. Lefebvre, J., An outline of the non-linear viscoelastic behavior of wheat flour dough in shear. Rheologica Acta, 2006. 45(4): p. 525-538.

31. Wrigley, C.W., Giant proteins with flour power. Nature, 2002. 381: p. 738-739.

32. Osborne, T.B., The vegetable proteins. 1924, London: Longmans Green and Co.

33. Feeney, K.A., N. Wellner, S.M. Gilbert, N.G. Halford, A.S. Tatham, P.R. Shewry, and P.S. Belton, Molecular structures and interactions of repetitive peptides based on wheat glutenin subunits depend on chain length. Biopolymers, 2003. 72(2): p. 123-131.

34. Alberti, E., S.M. Gilbert, A.S. Tatham, P.R. Shewry, A. Naito, K. Okuda, H. Saito, and A.M. Gil, Study of wheat high molecular weight 1Dx5 subunit by C-13 and H-1 solid-state NMR. II. Roles of nonrepetitive terminal domains and length of repetitive domain. Biopolymers, 2002. 65(2): p. 158-168.

35. Alberti, E., S.M. Gilert, A.S. Tatham, P.R. Shewry, and A.M. Gil, Study of high molecular weight wheat glutenin subunit 1Dx5 by C-13 and H-1 solid-state NMR spectroscopy. I. Role of covalent crosslinking. Biopolymers, 2002. 67(6): p. 487-498.

36. Humphris, A.D.L., T.J. McMaster, M.J. Miles, S.M. Gilbert, P.R. Shewry, and A.S. Tatham, Atomic force microscopy (AFM) study of interactions of HMW subunits of wheat glutenin. Cereal Chemistry, 2000. 77(2): p. 107-110.

37. Southan, M. and F. MacRitchie, Molecular weight distribution of wheat proteins. Cereal Chemistry, 1999. 76(6): p. 827-836.

38. Thomson, N.H., M.J. Miles, Y. Popineau, J. Harries, P. Shewry, and A.S. Tatham, Small angle X-ray scattering of wheat seed-storage proteins: alpha-, gamma- and omega-gliadins and the high molecular weight (HMW) subunits of glutenin. Biochimica Et Biophysica Acta-Protein Structure And Molecular Enzymology, 1999. 1430(2): p. 359-366.

39. Egorov, T.A., T.I. Odintsova, P.R. Shewry, and A.S. Tatham, Characterisation of high M-r wheat glutenin polymers by agarose gel

electrophoresis and dynamic light scattering. Febs Letters, 1998. 434(1-2): p. 215-217.

40. Stevenson, S.G. and K.R. Preston, Flow field-flow fractionation of wheat proteins. Journal Of Cereal Science, 1996. 23(2): p. 121-131.

41. Field, J.M., A.S. Tatham, and P.R. Shewry, The Structure Of A High-Mr Subunit Of Durum-Wheat (Triticum-Durum) Gluten. Biochemical Journal, 1987. 247(1): p. 215-221.

42. Fan, J., J.R. Mitchell, and J.M.V. Blanshard, A model for the oven rise of dough during baking. Journal of Food Engineering, 1999. 41(2): p. 69-77.

43. Dobraszczyk, B.J., The physics of baking: rheological and polymer molecular structure-function relationships in breadmaking. Journal of Non-Newtonian Fluid Mechanics, 2004. 124(1-3): p. 61.

44. Sliwinski, E.L., P. Kolster, and T. van Vliet, Large-deformation properties of wheat dough in uni- and biaxial extension. Part I. Flour dough. Rheologica Acta, 2004. 43(4): p. 306-320.

45. Sliwinski, E.L., F. van der Hoef, P. Kolster, and T. van Vliet, Large-deformation properties of wheat dough in uni- and biaxial extension. Part II. Gluten dough. Rheologica Acta, 2004. 43(4): p. 321-332.

46. van Vliet, T. and J.J. Kokelaar. Biaxial strain hardening in relation to foam formation and stability towards disproportionation. in Progress and Trends in Rheology IV, Proceedings of the 4th European Rheology Congress. 1994.

47. Letang, C., M. Piau, and C. Verdier, Characterization of wheat flour-water doughs. Part I: Rheometry and microstructure. Journal of Food Engineering, 1999. 41(2): p. 121-132.

48. Belton, P.S., On the elasticity of wheat gluten. Journal Of Cereal Science, 1999. 29(2): p. 103-107.

49. Singh, H. and F. MacRitchie, Application of Polymer Science to Properties of Gluten. Journal of Cereal Science, 2001. 33(3): p. 231.

50. Don, C., W.J. Lichtendonk, J.J. Plijter, and R.J. Hamer, Understanding the link between GMP and dough: from glutenin particles in flour towards developmed dough. Journal of Cereal Science, 2003. 38: p. 157-165.

51. Don, C., W.J. Lichtendonk, J.J. Plijter, and R.J. Hamer, Glutenin Macropolymer: A gel formed by glutenin particles. Journal of Cereal Science, 2003. 37: p. 1-7.

52. Lefebvre, J., A. Pruska-Kedzior, Z. Kedzior, and L. L., A phenomological analysis of wheat gluten viscoelastic response in retardation and in dynamic experiments over large time scale. Journal of Cereal Science, 2003. 38: p. 257-267.

53. Belton, P.S. and B.J. Dobraszczyk, Letter to the editor. Journal of Cereal Science, 2006. 43: p. 258.

54. Don, C., W.J. Lichtendonk, J.J. Plijter, and R.J. Hamer, Understanding the link between GMP and dough: from glutenin particles in flour towards developed dough. Journal of Cereal Science, 2003. 38(2): p. 157-165.

55. Domenek, S., L. Brendel, M.H. Morel, and S. Guilbert, Swelling Behavior and structural characteristics of wheat gluten polypeptide films. Biomacromolecules, 2004. 5(3): p. 1002-1008.

56. Flory, P.J., Principles of Polymer Chemistry. 1953, Ithaca, New York: Cornell University Press.

57. Djabourov, M., J.P. Lechaire, and F. Gaill, Structure And Rheology Of Gelatin And Collagen Gels. Biorheology, 1993. 30(3-4): p. 191-205.

58. Hamer, R.J., T. van Vliet, and J. Lefebvre, Letter to the editor. Journal of Cereal Science, 2005. 42: p. 344-345.

59. Bagley, E.B., D.D. Christianson, and J.A. Martindale, Uniaxial Compression of a Hard Wheat-Flour Dough - Data-Analysis Using the Upper Convected Maxwell Model. Journal of Texture Studies, 1988. 19(3): p. 289-305.

60. Bird, R.B., R.C. Armstrong, and O. Hassager, Dynamics of polymeric liquids - Fluid Mechanics. 2nd Edition ed. Vol. Volume 1. 1987, New York: Wiley.

61. Phan-Thien, N. and M. Safari-Ardi, Linear viscoelastic properties of flour-water doughs at different water concentrations. Journal of Non-Newtonian Fluid Mechanics, 1998. 74(1-3): p. 137.

62. Rock, K., Rheological modelling of bi-axial inflation of bread dough, in Department of Mechanical Engineering. 2002, Massachusetts Institute of Technology: Cambridge.

63. Blackwell, R.J., T.C.B. McLeish, and O.G. Harlen, Molecular drag-strain coupling in branched polymer melts. Journal of Rheology, 2000. 44(1): p. 121-136.

64. Larson, R.G., T. Sridhar, L.G. Leal, G.H. McKinley, A.E. Likhtman, and T.C.B. McLeish, Definitions of entanglement spacing and time constants in the tube model. Journal of Rheology, 2003. 47(3): p. 809-818.

65. Doi, M. and S.F. Edwards, The Theory of Polymer Dynamics. 1986: Oxford University Press.

66. Bagley, E.B. and D.D. Christianson, Stress-Relaxation Of Chemically Leavened Dough - Data Reduction Using The Bkz Elastic Fluid Theory. Journal Of Rheology, 1987. 31(5): p. 405-413.

67. Dus, S.J. and J.L. Kokini, Prediction of the Nonlinear Viscoelastic Properties of a Hard Wheat-Flour Dough Using the Bird-Carreau Constitutive Model. Journal of Rheology, 1990. 34(7): p. 1069-1084.

68. Berland, S. and B. Launay, Rheological Properties Of Wheat-Flour Doughs In Steady And Dynamic Shear - Effect Of Water-Content And Some Additives. Cereal Chemistry, 1995. 72(1): p. 48-52.

69. Gabriele, D., B. de Cindio, and P. D'Antona, A weak gel model for foods. Rheologica Acta, 2001. 40(2): p. 120.

70. Cordobés, F., P. Partal, and A. Guerrero, Rheology and microstructure of heat induced egg yolk gels. Rheological Acta, 2004. 43: p. 184-195.

71. Muthukumar, M., Dynamics of polymer fractals. Journal of physical chemistry, 1985. 8(6): p. 3161-3168.

72. Muthukumar, M., Screening effect on viscoelasticity near the gel point. Macromolecules, 1989. 22(12): p. 4658-4660.

73. Stein, J., The Perfect Egg, in Time. 2007.

74. Chambon, F. and H.H. Winter, Linear Viscoelasticity At The Gel Point Of A Cross-Linking PDMS With Imbalanced Stoichiometry. Journal Of Rheology, 1987. 31(8): p. 683-697.

75. Venkataraman, S.K. and H.H. Winter, Finite shear strain behavior of a crosslinking polydimethylsiloxane near its gel point. Rheological Acta, 1990. 29(5): p. 423-432.

76. Winter, H.H. and F. Chambon, Analysis Of Linear Viscoelasticity Of A Cross-Linking Polymer At The Gel Point. Journal Of Rheology, 1986. 30(2): p. 367-382.

77. Winter, H.H. and M. Mours, Rheology of polymers near liquid-solid transitions. Advances in Polymer Science, 1997. 134: p. 165-233.

78. Hossain, K.S., K. Miyanaga, H. Maeda, and N. Nemoto, Sol-gel transition behavior of pure i-carrageenan in both salt-free and added salt states. Biomacromolecules, 2001. 2: p. 442-449.

79. Muliawan, E.B. and S.G. Hatzikiriakos. Rheology of cheese: comparison of results from four different rheometers PP9. in Society of Rheology: 78th Annual Meeting. 2006. Portland, Maine.

80. Bagley, E.B., F.R. Dintzis, and S. Chakrabarti, Experimental and conceptual problems in the rheological characterization of wheat flour doughs. Rheologica Acta, 1998. 37(6): p. 556-565.

81. Ferry, J.D., Viscoelastic properties of polymers. 1980: John Wiley and Sons Inc.

82. Macosko, C.W., Rheology: Principles, Measurements and Applications. 1994, New York: VCH.

83. Ng, T.S.K., Extensional Rheology of Bread Dough, in Mechanical Engineering. 2005, Massachusetts Institute of Technology: Cambridge.

84. Buchholz, R.H., An epitrochoidal mixer. The Mathematical Scientist, 1990. 15: p. 7-14.

85. Gras, P.W., H.C. Carpenter, and R.S. Anderssen, Modelling the Developmental Rheology of Wheat-Flour Dough using Extension Tests. Journal of Cereal Science, 2000. 31(1): p. 1-13.

86. Anderssen, R.S., P.W. Gras., and F. MacRitchie, The Rate-Independence of the Mixing of Wheat Flour Dough to Peak Dough Development. Journal of Cereal Science, 1998. 27(2): p. 167-177.

87. Ross, K.A., L.J. Pyrak-Nolte, and C.O. H., The use of ultrasound and shear oscillatory tests to characterize the effect of mixing time on the rheological properties of dough. Food Research International, 2004. 27: p. 567.

88. Suchy, J., O.M. Lukow, and M.E. Ingelin, Dough Microextensibility Method Using a 2-g Mixograph and a Texture Analyzer. Cereal Chemistry, 2000. 77(1): p. 39-43.

89. Faergestad, E.M., E.M. Magnus, S. Sahlstrom, and T. Naes, Influenceof Flour Quality and Baking Process on Hearth Bread Characteristic Made Using Gentle Mixing. Journal of Cereal Science, 1999. 30: p. 61-70.

90. Kilborn, R.H. and K.H. Tipples, Factors Affecting the Mechanical Dough Development. I. Effect of Mixing Intensity and Work Input. Cereal Chemistry, 1972. 49: p. 34-47.

91. Martinani, J.P., Y. Nicolas, A. Bouguennec, P. Y., L. Saulnier, and G. Branlard, Relationship between Mixograph Parameters and Indices of Wheat Grain Quality. Journal of Cereal Science, 1998. 27: p. 179-189.

92. Khatkar, B.S., R.J. Fido, T.A. S., and S.J. D., Functional Properties of Wheat Gliadins. I. Effects on Charactersitics and Bread Making Quality. Journal of Cereal Science, 2002. 35: p. 299-306.

93. Weegels, P.L., R.J. Hamer, and J.D. Schofield, Depolymerisation and Re-polymerisation of Wheat Glutenin During Dough Processing. II. Changes in Composition. Journal of Cereal Science, 1997. 25(2): p. 155-163.

94. Goesaert, H., K. Brijs, W.S. Veraverbeke, C.M. Courtin, K. Gebruers, and J.A. Delcour, Wheat flour constituents: how they impact bread quality, and how to impact their functionality. Trends in Food Science & Technology, 2005. In Press, Corrected Proof.

95. Lee, L. and P.K.W. Ng, Relationship Between Rheological Properties and MIcrostructural Characteristics of Nondeveloped, Partially Developed and Developed Doughs. Cereal Chemistry, 2001. 78(4): p. 447-452.

96. Tronsmo, K.M., E.M. Faergestad, A. Longva, S.J. D., and E.M. Magnus, A Study on how Size Distribution of Gluten Proteins, Surface Properties of Gluten and Mixing Properties Relate to Baking Properties of Wheat Flours. Journal of Cereal Science, 2002. 35: p. 201-214.

97. Rasper, F.V., The Extensigraph Handbook. 1991: American Association of Cereal Chemists.

98. Faridi, H. and F.V. Rasper, The Alveograph Handbook. 1987: American Association of Cereal Chemists.

99. Uthayakumaran, S., M. Newberry, M. Keentok, F.L. Stoddard, and F. Bekes, Basic rheology of bread dough with modified protein content and glutenin-to-gliadin ratios. Cereal Chemistry, 2000. 77(6): p. 744-749.

100. Bloksma, A.H., A calculation of the shape of the Alveograms of some model rheological substances. Cereal Chemistry, 1957. 34: p. 126-136.

101. Charalambides, M.N., L. Wanigasooriya, J.G. Williams, and S. Chakrabarti, Biaxial deformation of dough using the bubble inflation technique. I. Experimental. Rheologica Acta, 2002. 41(6): p. 532-540.

102. Charalambides, M.N., L. Wanigasooriya, and J.G. Williams, Biaxial deformation of dough using the bubble inflation technique. II. Numerical modelling. Rheologica Acta, 2002. 41(6): p. 541-548.

103. Hlynka, I. and H.W. Barth, Chopin Alveograph studies. I. Dough resistance at constant sample deformation. Cereal Chemistry, 1955. 32(6): p. 463-471.

104. Phan-Thien, N., M. Safari-Ardi, and A. Morales-Patino, Oscillatory and simple shear flows of a flour-water dough: A constitutive model. Rheologica Acta, 1997. 36(1): p. 38-48.

105. Gleissle, W., Fluids, in Rheology, G. Astarita, G. Marucci, and L. Nicolais, Editors. 1980, Plenum Press: New York. p. 457-462.

106. Liao, H.-J., J. Tattiyakul, and M.A. Rao, Superposition of complex viscosity curves during gelatinzation of starch dispersion and dough. Journal of Food Process Engineering, 1999. 22(3): p. 215-234.

107. Uthayakumaran, S., M. Newberry, N. Phan-Thien, and R. Tanner, Small and large strain rheology of wheat gluten. Rheologica Acta, 2002. 41: p. 162-172.

108. Cho, K.S., K. Hyun, K.H. Ahn, and S.J. Lee, A geometrical Interpretation of large amplitude oscillatory shear response. Journal Of Rheology, 2005. 49(3): p. 747-758.

109. Ewoldt, R.H., C. Clasen, A.E. Hosoi, and G.H. McKinley, Rheological fingerprinting of gastropod pedal mucus and synthetic complex fluids for biomimicking locomotion. Soft Matter, 2007. 3: p. 634-643.

110. Ewoldt, R.H., A.E. Hosoi, and G.H. McKinley. Rheological fingerprinting of terrestrial gastropods (snails and slugs) using large amplitude oscillatory shear (LAOS) experiments #BS9. in Society of Rheology: 78th Annual Meeting. 2006. Portland, Maine.

111. Kreyszig, E., Advanced Engineering Mathematics. 8th edition ed. 2005, Singapore: John Wiley and Sons, Inc.

112. Sharma, N., M.A. Hanna, and Y.R. Chen, Flow behavior of wheat flour-water dough using a capillary rheometer. I. Effect of capillary geometry. Cereal Chemistry, 1993. 70(1): p. 59-63.

113. Petrie, C.J.S., One hunderd years of extensional flow. Journal Of Non-Newtonian Fluid Mechanics, 2006. 137(1): p. 1-14.

114. Trouton, F.T., On the coefficient of viscous traction and its relation to that of viscosity. Proceedings of the Royal Society of London A, 1906. 77: p. 426-440.

115. Anna, S.L., Filament Stretching of Model Elastic Liquids, in Division of Engineering and Applied Sciences. 2000, Harvard University: Cambridge.

116. Anna, S.L., G.H. McKinley, D.A. Nguyen, T. Sridhar, S.J. Muller, J. Huang, and D.F. James, An interlaboratory comparison of measurements from filament-stretching rheometers using common test fluids. Journal Of Rheology, 2001. 45(1): p. 83-114.

117. McKinley, G.H. and T. Sridhar, Filament-stretching rheometry of complex fluids. Annual Review Of Fluid Mechanics, 2002. 34: p. 375-415.

118. Szabo, P., Transient filament stretching rheometer.1. Force balance analysis. Rheologica Acta, 1997. 36(3): p. 277-284.

119. Szabo, P. and G.H. McKinley, Filament stretching rheometer: inertia compensation revisited. Rheologica Acta, 2003. 42(3): p. 269-272.

120. Sentmanat, M., E.B. Muliawan, and S.G. Hatzikiriakos, Fingerprinting the processing behavior of polyethylenes from transient extensional flow and peel experiments in the melt state. Rheologica Acta, 2004. 44(1): p. 1-15.

121. Sentmanat, M., B.N. Wang, and G.H. McKinley, Measuring the transient extensional rheology of polyethylene melts using the SER universal testing platform. Journal Of Rheology, 2005. 49(3): p. 585-606.

122. Sentmanat, M.L., Miniature universal testing platform: from extensional melt rheology to solid-state deformation behavior. Rheologica Acta, 2004. 43(6): p. 657-669.

123. Meissner, J., Dhnungsverhalten von Polyathylen-Schmelzen. Rheologica Acta, 1971. 10(2): p. 230-242.

124. Schulze, J.S., T.P. Lodge, C.W. Macosko, J. Hepperle, H. Munstedt, H. Bastian, D. Ferri, D.J. Groves, Y.H. Kim, M. Lyon, T. Schweizer, T. Virkler, E. Wassner, and W. Zoetelief, A comparison of extensional viscosity measurements from various RME rheometers. Rheologica Acta, 2001. 40(5): p. 457-466.

125. Li, W., B.J. Dobraszczyk, and J.D. Schofield, Stress relaxation behavior of wheat dough, gluten, and gluten protein fractions. Cereal Chemistry, 2003. 80(3): p. 333-338.

126. Ng, T.S.K., M. Padmanabhan, and G.H. McKinley, Linear to non-linear rheology of wheat flour-water doughs. Applied Rheology, 2006. 16(5): p. 265-274.

127. Tanner, R.I., F. Qi, and S.-C. Dai, Bread Dough Rheology and Recoil I. Rheology. Journal of Non-Newtonian Fluid Mechanics, 2007. Accepted Manuscript.

128. Sollich, P., F. Lequeux, P. Hébraud, and M.E. Cates, Rheology of soft glassy materials. Physical Review Letters, 1997. 78(10): p. 2020-2023.

129. Ng, T.S.K. and G.H. McKinley, Kraft foods research report. 2004.

130. Gallegos, C., J.M. Franco, and P. Partal, Rheology of Food Dispersions. Rheology Reviews, 2004: p. 19-66.

131. Rao, M.A., Rheology of Fluid and Semisolid Foods - Principles and Applications, ed. G.V. Barbosa-Canovas. 1999: Springer-Verlag. 441.

132. Gittes, F. and F.C. MacKintosh, Dynamic shear modulus of a semiflexible polymer network. Physical Review E, 1998. 58(2): p. R1241-1244.

133. Hoffmann, B., C. Dietrich, R. Thomann, C. Friedrich, and R. Mülhaupt, Morphology and rheology of polystyrene nanocomposites based upon organoclay. Macromolecules Rapid Communication, 2000. 21(1): p. 57-61.

134. Krishnamoorti, R. and E.P. Giannelis, Rheology of End-Tethered Polymer Layered Silicate Nanocomposites. Macromolecules, 1997. 30(14): p. 4097-4102.

135. Kundu, S., Investigation of flow and microstructure in rheometric and processing flow conditions for liquid crystalline pitch, in Clemson University. 2006, Clemson University: Clemson.

136. Sollich, P., Rheological constitutive equation for a model of soft glassy materials. Physical Review E, 1998. 58(1): p. 738-792.

137. Chaudhuri, O., S.H. Parekh, and D.A. Fletcher, Reversible stress softening of actin networks. Nature, 2007. 445: p. 295-298.

138. Fabry, B., G.N. Maksym, J.P. Butler, M. Glogauer, D. Navajas, and J.J. Fredberg, Scaling the microrheology of living cells. Physical Review Letters, 2001. 87(14): p. 148102-1-4.

139. Rouse, P.E.J., A Theory of the Linear Viscoelastic Properties of Dilute Solutions of Coiling Polymers. Journal of Chemical Physics, 1953. 21(7): p. 1271-1280.

140. Zimm, B.H., Dynamics of Polymer Molecules in Dilute Solution: Viscoelasticity, Flow Birefringence and Dielectric Loss. Journal of Chemical Physics, 1956. 24(2): p. 269-278.

141. Larson, R.G., The structure and rheology of complex fluids. 1999: Oxford University Press.

142. Gabriele, D., M. Milgliori, and B. de Cindio. Bread dough characterization using oscillatory and biaxial extension technique. in 4th International Symposium on Food Rheology and Structure. 2006. ETH, Zurich.

143. Edwards, N.M., J.E. Dexter, and M.G. Scanlon, Starch participation in durum dough linear viscoelastic properties. Cereal Chemistry, 2002. 79(6): p. 850-856.

144. Redl, A., M.H. Morel, J. Bonicel, S. Guilbert, and B. Vergnes, Rheological properties of gluten plasticized with glycerol: dependence on temperature glycerol content and mixing conditions. Rheologica Acta, 1999. 38: p. 311-320.

145. Wang, C.F. and J.L. Kokini, Simulation of the Nonlinear Rheological Properties of Gluten Dough Using the Wagner Constitutive Model. Journal of Rheology, 1995. 39(6): p. 1465-1482.

146. Shollenberger, J.H., Protein and gluten in wheat and flour. U.S.D.A. grain investigations, Abs and Reg., 1923. 12: p. 16.

147. Sliwinski, E.L., P. Kolster, and T. van Vliet, On the relationship between large-deformation properties of wheat flour dough and baking quality. Journal of Cereal Science, 2004. 39(2): p. 231-245.

148. Weegels, P.L., R.J. Hamer, and J.D. Schofield, Functional Properties of Wheat Glutenin. Journal of Cereal Science, 1996. 23(1): p. 1-17.

149. Watanabe, H., T. Sato, K. Osaki, Y. Aoki, L. Li, M. Kakiuchi, and M.L. Yao, Rheological images of Poly(Vinyl Chloride) gels. 4. Nonlinear behavior in a critical gel state. Macromolecules, 1998. 31(13): p. 4198-4204.

150. Amend, T. and H.D. Belitz, Microstructural studies of gluten and a hypothesis on dough formation. Food structure, 1991. 10: p. 277-288.

151. Cunningham, J.R. and I. Hlynka, Relaxation time spectrum of dough and influence of temperature, rest and water content. Journal of Applied Physics, 1954. 25(9): p. 1075-1081.

152. Rao, D.H.S., K.V. Mulvaney, and J.E. Dexter, Rheological characterization of long and short mixing flours based on stress relaxation. Journal of Cereal Science, 2000. 31: p. 159-171.

153. Dealy, J., Questions about relaxation spectra submitted by a reader. Rheology Bulletin, 2007. 76(1): p. 14.

154. Charalambides, M., W. Xiao, and G. Williams. Rolling of wheat flour dough. in 4th International Symposium on Food Rheology and Structure. 2006. ETH, Zurich.

155. Spriggs, T.W., A four constant model for viscoelastic fluids. Chemical Engineering Science, 1965.

156. Fielding, S.M., P. Sollich, and M.E. Cates, Aging and rheology in soft materials. Journal of Rheology, 2000. 44(2): p. 323-369.

157. Ewoldt, R.H. and G.H. McKinley, Creep ringing in rheometry or How to deal with oft-discarded data in step stress tests! Rheology Bulletin, 2007. 76(1): p. 4.

158. Nutting, P.G., A new general law of deformation. Journal of the Franklin Institute, 1921. 191: p. 679-685.

159. Scott Blair, G.W., B.C. Veinoglou, and J.E. Caffyn, Limitations of the Newtonian Time Scale in Relation to Non-Equilibrium Rheological States and a Theory of Quasi-Properties. Proceedings of the Royal Society of London. Series A, Mathematical and Physical Sciences, 1947. 189(1016): p. 69-87.

160. Oldham, K.B. and J. Spanier, The Fractional Calculus. Mathematics in Science and Engineering, ed. R. Bellman. Vol. 111. 1974, New York and London: Academic Press.

161. Mainardi, F., Fractional calculus - Some basic problems in continuum and statistical mechanics, in Fractals and fractional calculus in continuum mechanics, A. Carpinteri and F. Mainardi, Editors. 1997, Springer Wien: New York.

162. Friedrich, C. and L. Heymann, Extension of a model for cross-linking polymer at the gel point. Journal of Rheology, 1988. 32(3): p. 235-241.

163. Sofou, S., E.B. Muliawan, S.G. Hatzikiriakos, and E. Mitsoulis, Rheological characterization and constitutive modelling of bread dough - Submitted. Rheologica Acta, 2007.

164. Buscall, R., P.D.A. Mills, J.W. Goodwin, and D.W. Lawson, Scaling behaviour of the rheology of aggregate networks formed from colloidal particles. Journal of the Chemical Society, Faraday Transactions 1. Physical Chemistry in Condensed Phases, 1988. 84(12): p. 4249-4260.

165. Lodge, A.S., Elastic liquids. 1964, New York: Academic Press. 389.

166. Drozdov, A.D., Fractional differential models in finite viscoelasticity. Acta Mechanica, 1997. 124: p. 155-180.

167. Storm, C., J.J. Pastore, F.C. MacKintosh, T.C. Lubensky, and P.A. Janmey, Nonlinear elasticity in biological gels. Letters to Nature, 2005. 435(7039): p. 191-194.

168. Larson, R.G., Constitutive equations for polymers melts and solutions. Butterworth's series in chemical engineering. 1988: Butterworth-Henneimann.

169. Nielsen, J.K., O. Hassager, and G.H. McKinley. Onset of chain stretch in a highly entangled polyisoprene melt observed using shear measurements and several extensional techniques EP11. in Society of Rheology, 78th Annual meeting. 2006. Portland, Maine.

170. Peighambardoust, S.H., Development of dough under shear flow, in Agrotechnology and Food Science Department. 2006, Wageningen University: Wageningen.

171. Fischer, P., M. Pollard, and I. Marti, From Saulus to Paulus: Becoming a Food Rheologist. Rheology Bulletin, 2006. 75(1): p. 6-12.

172. Janmey, P.A., A torsion pendulum for measurement of viscoelasticity of biopolymers and its application to polymer networks. Journal of Biochemical and Biophysical Methods, 1991. 22(1): p. 41-53.

173. Kokelaar, J.J., T. van Vliet, and A. Prins, Strain Hardening Properties and Extensibility of Flour and Gluten Doughs in Relation to Breadmaking Performance. Journal of Cereal Science, 1996. 24(3): p. 199-214.

174. Ng, T.S.K. and G.H. McKinley, Power-law gels at finite strains. Journal of Rheology, 2007: p. submitted April 2007.

175. Dealy, J.M., Rheometers for Molten Plastics: A Practical Guide to Testing and Property Measurement. 1982, New York: Van Nostrand Reinhold.

176. Wilhelm, M., Fourier Transform Rheology. Macromolecular Materials Engineering, 2002. 287(2): p. 83-105.

177. Cho, K.S., A geometrical interpretation of large amplitude oscillatory shear response. Journal of Rheology, 2005. 49(3): p. 747-758.

178. Phan-Thien, N., N. M., and R.I. Tanner, Non-linear oscillatory flow of a soft solid-like viscoelastic material. Journal of Non-Newtonian Fluid Mechanics, 2000. 92(1): p. 67-80.

179. Creeth, J.M., Constituents of Mucus and their Separation. British Medical Bulletin, 1978. 34(1): p. 17-24.

180. Zou, Z., S.M. Habermann-Rottinghaus, and K.P. Murphy, Urea effects on Protein Stability: Hydrogen Bonding and the Hydrophobic Effect. Proteins: Structure, Function, and Genetics, 1998. 31(2): p. 107-115.

181. Treloar, L.R.G., The Physics of Rubber Elasticity. Physical Sciences. 2005, Oxford: Oxford University Press.

182. Evans, E. and K. Ritchie, Strength of a Weak Bond Connecting Flexible Polymer Chains. Biophysical Journal, 1999. 76(5): p. 2439-2447.

183. Philippoff, W., Vibrational Measurements with Large Amplitudes. Transactions of the Society of Rheology, 1966. 10(1): p. 317-334.

184. Tee, T.-T. and J.M. Dealy, Nonlinear Viscoelasticity of Polymer Melts. Transactions of the Society of Rheology, 1975. 19(4): p. 595-615.

185. Pipkin, A.C., Lectures on Viscoelasticity Theory. Applied Mathematical Sciences. 1972, New York: Springer-Verlag.

186. Wyss, H.M., K. Miyazaki, J. Mattsson, Z. Hu, D.R. Reichman, and D.A. Weitz, Strain-Rate Frequency Superposition (SRFS) - A rheological probe of structural relaxation in soft materials. arXiv:cond-mat/0608151v1 [cond-mat.soft], 2006.

187. Bird, R.B., C.F. Curtiss, R.C. Armstrong, and O. Hassager, Dynamics of polymeric liquids - Kinetic Theory. 2nd Edition ed. Vol. Volume 2. 1987, New York: Wiley.

188. Keunings, R., On the Peterlin approximation for finitely extensible dumbbells. Journal of Non-Newtonian Fluid Mechanics, 1997. 68(1): p. 85-100.

189. Considère, M., Annales des Ponts Chausées, 1885. 9: p. 574.

190. McKinley, G.H. and O. Hassager, The Considere condition and rapid stretching of linear and branched polymer melts. Journal of Rheology, 1999. 43(5): p. 1195-1212.

191. Pearson, G.H. and R.W. Connelly, The Use Of Extensional Rheometry To Establish Operating Parameters For Stretching Processes. Journal Of Applied Polymer Science, 1982. 27(3): p. 969-981.

192. Van den Brule, V.H.A.A., Brownian dynamics simulation of finitely extensible bead-spring chains. Journal of Non-Newtonian Fluid Mechanics, 1993. 47: p. 357-378.

193. Hyun, K., S.H. Kim, K.H. Ahn, and S.J. Lee, Large amplitude oscillatory shear as a way to classify the complex fluids. Journal of Non-Newtonian Fluid Mechanics, 2002. 107(1-3): p. 51-65.

194. Sijbesma, R.P., F.H. Beijer, L. Brunsveld, B.J.B. Folmer, J.J.K.K. Hirschberg, R.F.M. Lange, J.K.L. Lowe, and E.W. Meijer, Reversible Polymers Formed from

the Self-Complimentary Monomers Using Quadruple Hydrogen Bonding. Science, 1997. 278(5343): p. 1601-1604.

195. Einstein, A., Correction to my paper: "A New Determination of Molecular Dimension". Annalen der Physik, 1911. 34: p. 591.

196. Einstein, A., A new determination of molecular dimensions. Annalen der Physik, 1906. 19: p. 289.

197. Einstein, A., Investigations on the theory of the Brownian Movement, ed. A.D. Cowper. 1956: Dover Publications.

198. Batchelor, G.K., The effect of Brownian motion on the bulk stress in a suspension of spherical particles. Journal of Fluid Mechanics, 1977. 83(1): p. 97-117.

199. Batchelor, G.K. and J.T. Green, The determination of bulk stress in a suspension of spherical particles to order c^2. Journal of Fluid Mechanics, 1972. 56(3): p. 401-427.

200. Guth, E., Theory of Filler Reinforcement. Journal of Applied Physics, 1945. 16: p. 20-25.

201. Krieger, I.M. and T.J. Dougherty, A Mechanism for Non-Newtonian Flow in Suspensions of Rigid Spheres. Transactions of the Society of Rheology, 1959. 3: p. 137-152.

202. Mullins, L. and N.R. Tobin, Stress Softening in Rubber Vulcanizates. Part I. Use of a Strain Amplification Factor to Describe the Elastic Behavior of Filler-Reinforced Vulcanized Rubber. Journal of Applied Polymer Science, 1965. 9(9): p. 2993-3009.

203. Onoda, G.Y. and E.G. Liniger, Random loose packings of uniform spheres and the dilatancy onset. Physical Review Letters, 1990. 64(22): p. 2727-2730.

204. Hwang, W.R., M.A. Hulsen, and H.E.H. Meijer, Direct simulations of particle suspensions in a viscoelastic fluid in sliding bi-periodic frames. Journal of Non-Newtonian Fluid Mechanics, 2004. 121(1): p. 15-33.

205. Bergstrom, J.S. and M.C. Boyce, Mechanical Behavior of Particle Filled Elastomers. Rubber Chemistry and Technology, 1999. 72(4): p. 779-806.

206. Mori, T. and K. Tanaka, Average Stress in Matrix and Average Elastic Energy of Materials with Misfitting Inclusions. Acta Metallurgica, 1973. 21: p. 571-574.

207. Govindjee, S. and J. Simo, A Micro-Mechanically Based Continuum Damage Model for Carbon-Black-Filled Rubbers Incorporating Mullins' Effect. Journal of Mechanics and Physics of Solids, 1991. 39(1): p. 87-112.

208. Parson, E.M., Mechanics of large strain deformation of particle-modified polymers, in Course 2 - Mechanical Engineering. 2006, Massachusetts Institute of Technology: Cambridge.

209. Ohl, N. and W. Gleissle, The characterization of steady-state shear and normal stress functions of highly concentrated suspensions formulated with viscoelastic liquids. Journal of Rheology, 1993. 37(2): p. 381-406.

210. Johansson, E., M.L. Prieto-Linde, G. Svensson, and J.O. Jönsson, Influences of cultivar, cultivar year and fertilizer rate on amount of protein groups and amount and size distribution of mono- polymeric proteins in wheat. Journal of Agricultural Sciences, 2003. 140(03): p. 275-284.

211. Boyce, M.C., Formation of voids in filled viscoelastic systems - Personal communication. 2007: Cambridge.

212. Ng, T.S.K. and G.H. McKinley, Kraft foods research report, M. Padmanabhan, Editor. 2005.